

Metal-Organic Framework Catalysis in the Upgrading of Ethanol for Advanced Biofuels



Harry Dylan Jepson

December 2023

Word Count: 53,030

**This thesis is presented for the degree of Doctor of
Philosophy**

Chemistry Catalysis CDT

Abstract

The work presented in this thesis focusses on the Guerbet reaction for the upgrading of ethanol to *n*-butanol, in particular researching heterogeneous catalytic routes for this transformation.

The use of metal-organic frameworks as heterogeneous Lewis acid catalysts for the aldol condensation of acetaldehyde in the Guerbet reaction of ethanol was initially explored, with homogeneous transfer hydrogenation catalysts. Reaction optimisation using UiO-66(Zr) as an aldol catalyst with $[\text{RuCl}_2(\text{dppm})_2]$ showed that this combination of catalysts were active for the synthesis of *n*-butanol from ethanol, while further study was conducted on changing the nature of the MOF, and the homogeneous ruthenium catalyst in the reaction. System recyclability experiments shows that over multiple cycles, the combination of UiO-66(Zr) and $[\text{RuCl}_2(\text{dppm})_2]$ evolved to give a catalyst mixture that was more active and selective for *n*-butanol synthesis from ethanol than the initial catalysts. A combination of these catalysts initially catalysed the conversion of ethanol to *n*-butanol to a 10.7 % yield of the desired product. Through subsequent recycling steps, where liquid product was removed from the reaction mixture under vacuum, the residual catalyst mixture demonstrated a significant improvement in activity over subsequent cycles, where *n*-butanol yield improved to 21.1 % after 6 cycles.

As UiO-66(Zr) was shown to be an active aldol catalyst in the upgrading of ethanol to *n*-butanol, attention turned to synthesising a single, heterogeneous catalyst for the upgrading of ethanol. Initially, the immobilisation of homogeneous complexes into the linkers of the zirconium derived UiO-67(Zr) was attempted in search of a heterogeneous Guerbet catalyst. The main body of this work consisted of the immobilisation of $[\text{RuCl}(\text{cymene})(\text{bipy-COOH})]\text{Cl}$ into the linkers of UiO-67. UiO-67(Zr) was demonstrated to be an active aldol catalyst in the Guerbet upgrading of ethanol, and under certain reaction conditions $[\text{RuCl}(\text{cymene})(\text{bipy-COOH})]\text{Cl}$ was demonstrated to be an active transfer hydrogenation catalyst. And while the immobilisation of $[\text{RuCl}(\text{cymene})(\text{bipy-COOH})]\text{Cl}$ in the linkers of UiO-67(Zr) was not demonstrated, the work conducted on this area forms a strong foundation for further research into immobilised catalysis in the

Guerbet reaction., Further preliminary work into the immobilisation of pincer complexes into zirconium MOFs was also conducted.

The concept of utilising etched derivatives of UiO-66(Zr) as a support for homogeneous transfer hydrogenation catalysts was explored. With primary work focused on the synthesis of new ruthenium complexes bearing ligands with pendant carboxylate groups, that could be used for complex immobilisation on the nodes of UiO-66(Zr). Different methods of synthesising complexes with this desired functionality were probed, and a detailed *in-situ* transfer hydrogenation catalyst formation study with phosphino azomethinylate ligands in the Guerbet reaction was conducted. Combinations of phosphino azomethinylate ligands with $[\text{RuCl}_2(\text{cymene})]_2$ were shown to be active hydrogenation catalyst precursors in the Guerbet upgrading of ethanol with sodium ethoxide, where the formation of both mono- and bischelate complexes were targeted. Further work into designing a catalytic system to utilise these transfer hydrogenation catalysts in combination with metal-organic frameworks is warranted,

Acknowledgments

I would initially like to thank my family for their consistent love and support throughout the four years of my PhD, and the entirety of my life. Although we're a small group, I couldn't ask for a better support network, and I wouldn't be where I am today without you.

I would like to extend a great deal of thanks to Professor Duncan Wass for allowing me to work on what has been a very exciting and interesting project. The guidance and support you have given me during my PhD have been incredibly valuable and I've learned a lot from you, which will no doubt help me in trying to make a successful career in science.

I also would like to thank Dr. Richard Wingad for time and effort he has contributed to helping me navigate my PhD. You have been a wonderful mentor, and an equally as wonderful friend to me through the entirety of my study in the Wass group.

The Wass group has grown over the years I've been present and most of the characters have changed, but to all Wass Group members new and old, I would like to thank you all for making my time in the lab so enjoyable and generating such a positive atmosphere in which to conduct research. Ashley and Alex Riley were key welcoming figures when I first joined the lab, and I want to thank them both for showing me the ropes and always being on hand to help when I first started ... no matter how silly the questions were. I don't think I've met or will meet a PhD student who is as big of a team player as Sam Bates, consistently coming up with exciting (sometimes bordering on insane) lab ideas, your companionship through my PhD has been invaluable. To Bala, I don't think I've become as close to someone in as short a period as we've known each other, throughout the back end of my PhD you've been a strong support and I thank you for all the advice both in and out of the lab you've given me. It would be remiss of me not to mention Jessie here, we've been on quite a journey, and you were an integral part of my time in Cardiff, and I am glad I leave it with you as a friend for life. And while I could write about all the Wass group individually, I would also like to thank: Josephine, Taha, Andres, Jamie, Kennedy, Prashant, Kieren, Alex Adshead, Osian, Ellie and Max.

I also want to thank the undergraduate students, Elliot and Jess, that I played a part in supervising. You both showed enthusiasm in the lab and a keenness to produce good research, and I thank you for the work you conducted.

To my housemates of 3+ years, Matt and Jack, I cannot imagine two better people to spend a lockdown with. I could not have asked for better housemates, and I'm glad to be leaving my time in Cardiff with you both as friends for life.

Finally, I would like to extend a special mention to my family cat, Alfie. My confidant and companion through the days of writing this thesis. You made it to the grand old age of 20 while this body of work was being produced, and while being occasionally slightly irritating (regarding constant pestering for food, milk and general attention), I have appreciated your company over these past months, and the majority of my life. I miss you terribly.

Table Of Contents

Abstract.....	i
Acknowledgements	iii
Table of Contents.....	v
List of Schemes.....	xiv
List of Figures.....	xviii
List of Tables.....	xxii
List of Abbreviations.....	xxiv
Chapter 1 – Introduction.....	1
1.1 Climate change and global warming	1
1.2 Renewable transportation fuels	2
1.2.1 Hydrogen.....	3
1.2.2 Biofuels	4
1.2.2.1 Biodiesel.....	5
1.2.2.2 Ethanol	5
1.3 Butanol as an alternative to ethanol	7
1.3.1 Petrochemical synthesis of butanol.....	8
1.3.1.1 Reppe synthesis and crotonaldehyde hydrogenation.....	8
1.3.1.2 The oxo process.....	8
1.3.2 Butanol synthesis by the ABE fermentation process	9
1.4 The Guerbet reaction	10
1.5 Guerbet synthesis of butanol.....	11

1.5.1 Heterogeneous catalysis for Guerbet synthesis of <i>n</i> -butanol from ethanol	11
1.5.1.1 Basic metal oxides	12
1.5.1.2 Hydroxyapatite	13
1.5.1.3 Transition metal catalysis	14
1.5.2 Homogeneous catalysis for Guerbet synthesis of butanol from ethanol.....	15
1.5.2.1 Iridium catalysis.....	15
1.5.2.2 Ruthenium catalysis	17
1.5.2.3 Limitations of current homogeneous systems	21
1.6 Alternative catalytic systems	23
1.7 Metal-organic frameworks (MOFs).....	23
1.8 MOF Catalysis.....	27
1.8.1 Catalysis by open metal sites	27
1.8.1.1 Aldol catalysis by MOFs	27
1.8.2 Catalysis by immobilised metals.....	29
1.8.2.1 MOF Transfer hydrogenation catalysis.....	33
1.8.3 MOFs in Guerbet catalysis	35
1.8.3.1 Limitations of current MOF Guerbet catalysts	38
1.9 Thesis scopes	39
1.10 References.....	42
Chapter 2 – Homogeneous/heterogeneous catalysed Guerbet upgrading of <i>n</i> -butanol	49
2.1 Homogeneous Lewis acid screen.....	49
2.2 UiO-(66)Zr and [RuCl ₂ (dppm) ₂] as heterogeneous and homogeneous catalysts in the Guerbet upgrading of ethanol.....	51

2.2.1 Reaction temperature screen	51
2.2.1.1 Effect of temperature optimised reaction conditions on the catalysts	56
2.2.2 Further reaction optimisation	59
2.2.3 Effect of water on the system	65
2.3 Changing the MOF	67
2.4 Changing the transfer hydrogenation catalyst	77
2.5 UiO-66(Zr) Recycling.....	83
2.6 Recyclability of entire catalytic system	85
2.7 Conclusions.....	91
2.8 Further work	92
2.9 References.....	95
Chapter 3 – Linker Immobilisation of Homogeneous Complexes.....	96
3.1 Background and preliminary study	96
3.2 UiO-67 as a heterogeneous aldol catalyst.....	105
3.3 Linker immobilisation of [RuCl(cymene)(bipy-COOH)]Cl in UiO-67(Zr)	109
3.3.1 Post-synthetic modification of UiO-67(Zr) – exchanging [RuCl(cymene)(bipy-COOH)]Cl with UiO-67(Zr) linkers	109
3.3.2 Immobilisation of [RuCl ₂ (cymene)] ₂ on the linkers of UiO-67(Zr)-Bipy.....	118
3.4 Immobilisation of pincer complexes in MOFs – preliminary study	126
3.5 Summary.....	131
3.6 Further work	133
3.7 References	136

Chapter 4 – Development of Homogeneous Ruthenium Complexes for Node-Immobilisation on MOFs.....	137
4.1 Background	137
4.2 Complexes based on $[\text{RuCl}_2(\text{dppEth})_2]$	139
4.2.1 Addition of amino acids across $[\text{RuCl}_2(\text{dppEth})_2]$	140
4.3 Phosphino azomethinylate ligands	147
4.3.1 Homogeneous catalyst synthesis	150
4.3.2 <i>In-situ</i> catalytic study – NaOEt base.....	158
4.3.3 <i>In-situ</i> catalytic study – UiO-66(Zr) aldol catalyst	166
4.4 Conclusions.....	172
4.5 Further work	175
4.5.1 $[\text{RuCl}_2(\text{dppEth})_2]$ work	176
4.5.2 Phosphino azomethinylates.....	177
4.5.3 Other further work	179
4.6 References	181
Chapter 5 – Final Conclusions	182
5.1 Conclusions.....	182
5.2 Key further work	184
Chapter 6 – Experimental.....	187
6.1 General experimental	187
6.1.1 General considerations	187
6.1.2 Guerbet reaction procedure.....	188
6.1.3 Post Guerbet reaction analysis.....	188

6.1.4 Guerbet reaction EtOH conversion and product selectivity calculation	189
6.2 Chapter 2 experimental	191
6.2.1 Homogeneous ruthenium complexes	191
6.2.1.1 [RuCl ₂ (dppm) ₂] Synthesis	191
6.2.2 MOF Synthesis	192
6.2.2.1 UiO-66(Zr) synthesis – acetic acid modulated – modified from Jiang <i>et al.</i> 2.1 (x = 14.4 mL), 2.3 (x = 7.2 mL), 2.4 (x = 28.8 mL)	192
6.2.2.2 UiO-66(Zr) (2.2) synthesis – non-modulated – modified from Xu <i>et al.</i>	192
6.2.2.3 UiO-66(Hf) (2.5) Synthesis	193
6.2.2.4 UiO-66(Zr)-NH ₂ (2.6) Synthesis	193
6.2.3 Guerbet reaction procedures – conditions screen	194
6.2.3.1 Homogeneous Lewis acid screen	194
6.2.3.2 Reaction temperature screen	194
6.2.3.3 Reaction duration screen	195
6.2.3.4 UiO-66(Zr) Loading screen	195
6.2.3.5 Stirring rate screen	195
6.2.3.6 Water loading screen	195
6.2.4 Guerbet reaction procedures – changing the MOF	196
6.2.4.1 UiO-66(Zr) modulation screen	196
6.2.4.2 UiO-66 analogue screen	196
6.2.5 Guerbet reaction procedures – changing the ruthenium catalyst	196
6.2.6 Guerbet reaction catalyst recycling studies	197
6.2.6.1 UiO-66(Zr) recycling procedure (Scheme 26)	197

6.2.6.2 UiO-66(Zr) and [RuCl ₂ (dppm) ₂] recycling procedure (Scheme 27).....	197
6.3 Chapter 3 experimental	198
6.3.1 Preliminary work (conducted by Elliot Rogers)	198
6.3.1.1 Homogeneous complex synthesis.....	198
6.3.1.1.1 Synthesis of [RuCl(cymene)(bipy)]Cl (3.3)	198
6.3.1.1.2 Synthesis of [RuCl(cymene)(phen)]Cl (3.4)	199
6.3.1.1.3 Synthesis of [RuCl(cymene)(bipy-COOH)]Cl (3.1)	199
6.3.1.2 Guerbet reactions – benchmarking homogeneous ruthenium catalysts	200
6.3.1.2.1 [RuCl(cymene)(bipy)]Cl and [RuCl(cymene)(phen)]Cl screen – with NaOEt	200
6.3.1.2.2 [RuCl(cymene)(bipy)]Cl and [RuCl(cymene)(phen)]Cl screen – with UiO- 66(Zr)	200
6.3.1.2.3 [RuCl(cymene)(bipy-COOH)]Cl screen.....	200
6.3.2 MOF synthesis	201
6.3.2.1 UiO-66(Zr) (3.5) synthesis – Prepared according to Katz <i>et al.</i>	201
6.3.2.2 UiO-66(Zr)-NH ₂ (3.6) synthesis – Prepared according to Katz <i>et al.</i>	201
6.3.2.3 UiO-67(Zr) (3.7) synthesis – Prepared according to Katz <i>et al.</i>	202
6.3.3 Guerbet reactions – benchmarking heterogeneous UiO-derived catalysts.....	202
6.3.3.1 UiO-Derived MOF screen	202
6.3.4 Post synthetic modification of UiO-67(Zr) - exchanging [RuCl(cymene)(bipy- COOH)] with UiO-67(Zr) linkers	203
6.3.4.1 Post synthetic exchange reaction - replacing biphenyl-4,4'-dicarboxylic acid with [RuCl(cymene)(bipy-COOH)] in UiO-67(Zr) – Modified from Liao <i>et al.</i> (3.8, 3.9, 3.10)	203

6.3.5 Post synthetic modification of UiO-67(Zr) – Immobilisation of [RuCl ₂ (cymene) on the linkers of UiO-67(Zr)-Bipy.....	203
6.3.5.1 Attempted synthesis of UiO-67(Zr)-Bipy (3.11).....	203
6.3.5.2 Attempted immobilisation of [RuCl ₂ (cymene)] ₂ on the assumed UiO-67(Zr)-Bipy (prepared according to Section 6.3.5.1) (3.12, 3.13, 3.14).....	203
6.3.6 Immobilisation of pincer complexes on MOFs – preliminary study.....	204
6.3.6.1 Synthesis of 3.19 – prepared according to Burgess <i>et al.</i>	204
6.3.6.2 Synthesis of 3.20 - prepared according to Burgess <i>et al.</i>	205
6.3.6.3 Synthesis of RuHCl(CO)(PCNCP- ^t Bu)] (3.21).....	205
6.3.6.4 Synthesis of [RuHCl(CO)(PCNCP-Ph)] (3.22).....	206
6.3.6.5 Guerbet reactions – screening [RuHCl(CO)(PCNCP- ^t Bu)] and [RuHCl(CO)(PCNCP-Ph)]	206
6.4 Chapter 4 experimental.....	207
6.4.1 [RuCl ₂ (dppEth) ₂] and attempted complexations in Section 4.2.1.....	207
6.4.1.1 Synthesis of [RuCl ₂ (cymene)] ₂	207
6.4.1.2 Synthesis of [RuCl ₂ (PPh ₃) ₃]	207
6.4.1.3 Synthesis of [RuCl ₂ (dppEth) ₂] (4.1) – prepared according to Barkley <i>et al.</i> .	207
6.4.2 Phosphino azomethinylate ligand synthesis – performed by Cole.....	208
6.4.2.1 Sodium 2-((2-(diphenylphosphaneyl)benzylidene)amino)acetate – adapted from Wencil <i>et al.</i> (4.8).....	208
6.4.2.2 Sodium 3-((2-(diphenylphosphaneyl)benzylidene)amino)propanoate – adapted from Wencil <i>et al.</i> (4.9).....	209
6.4.2.3 Sodium 4-((2-(diphenylphosphaneyl)benzylidene)amino)butanoate – adapted from Wencil <i>et al.</i> (4.10).....	210

6.4.2.4 Sodium 5-((2-(diphenylphosphaneyl)benzylidene)amino)pentanoate – adapted from Wencel <i>et al.</i> (4.11)	211
6.4.2.5 Sodium 6-((2-(diphenylphosphaneyl)benzylidene)amino)hexanoate – adapted from Wencel <i>et al.</i> (4.12)	211
6.4.3 Complexation reactions with ligands prepared in 6.4.2	212
6.4.3.1 Monochelate complex formation.....	212
6.4.3.2 Bis chelate complex formation.....	213
6.4.4 Guerbet reactions – forming transfer hydrogenation catalysts <i>in situ</i>	214
6.4.5 Reactions of ethanol under Guerbet conditions in absence of aldol catalyst....	215
6.5 References	216
Chapter 7 – Appendix.....	218
7.1 Chapter 3 appendix	218
7.1.1 Mass spectrum of [RuCl(cymene)(bipy-COOH)]Cl (3.1) synthesised by Elliot Rogers.....	218
7.1.2 PXRD pattern of UiO-66(Zr) (3.5)	219
7.1.3 PXRD pattern of UiO-66-(Zr)NH ₂ (3.6)	220
7.1.4 PXRD pattern of UiO-67(Zr) (3.7)	221
7.1.5 Elemental breakdown of EDX analysis of 3.10	222
7.1.6 Elemental breakdown of EDX analysis of 3.9	222
7.1.7 ³¹ P{ ¹ H} NMR Spectrum of 3.19	223
7.1.8 ³¹ P{ ¹ H} NMR Spectrum of 3.20	224
7.2 Chapter 4 appendix	225
7.2.1 Mass spectrum of the product mixture of the reaction between [RuCl ₂ (cymene)] ₂ and 4.8	225

7.2.2 Mass spectrum of the product mixture of the reaction between $[\text{RuCl}_2(\text{cymene})]_2$ and 4.9	226
7.2.3 Mass spectrum of the product mixture of the reaction between $[\text{RuCl}_2(\text{cymene})]_2$ and 4.10	227
7.2.4 $^{31}\text{P}\{^1\text{H}\}$ NMR spectrum of the product mixture of the reaction between 4.12 and $[\text{RuCl}_2(\text{PPh}_3)_3]$	228
7.2.5 $^{31}\text{P}\{^1\text{H}\}$ NMR spectrum of the product mixture of the reaction between 4.11 and $[\text{RuCl}_2(\text{PPh}_3)_3]$	229
7.2.6 $^{31}\text{P}\{^1\text{H}\}$ NMR spectrum of the product mixture of the reaction between 4.10 and $[\text{RuCl}_2(\text{PPh}_3)_3]$	230
7.2.7 $^{31}\text{P}\{^1\text{H}\}$ NMR spectrum of the product mixture of the reaction between 4.9 and $[\text{RuCl}_2(\text{PPh}_3)_3]$	231
7.2.8 $^{31}\text{P}\{^1\text{H}\}$ NMR spectrum of the product mixture of the reaction between 4.8 and $[\text{RuCl}_2(\text{PPh}_3)_3]$	232

List of Schemes

Scheme 1 Synthesis of biodiesel from triglycerides using methanol	5
Scheme 2 Synthesis of butanol <i>via</i> crotonaldehyde hydrogenation (top) and the Reppe synthesis (bottom)	8
Scheme 3 Synthesis of butanol <i>via</i> the oxo process	9
Scheme 4 General scheme for the upgrading of alcohols <i>via</i> the Guerbet reaction.....	10
Scheme 5 Optimised Ru catalysed Guerbet synthesis of n-butanol published in Mitsubishi Chemical Corporation patent.....	17
Scheme 6 Initial reaction conditions for ethanol upgrading employed by the Wass group.	18
Scheme 7 [RuCl ₂ (dppm) ₂] Catalysed Guerbet synthesis of n-butanol developed by Wass and co-workers.....	18
Scheme 8 Mixed PN ligands tested with [RuCl ₂ (η ⁶ -p-cymene)] ₂ for ethanol upgrading	19
Scheme 9 Upgrading of ethanol to n-butanol performed by Szymczak and co-workers	20
Scheme 10 Upgrading of ethanol to n-butanol performed by Milstein and co-workers	20
Scheme 11 System with highest n-butanol yield reported by Milstein and co-workers	21
Scheme 12 Formation of sodium acetate <i>via</i> the Cannizzaro reaction	22
Scheme 13 Formation of sodium acetate <i>via</i> the Tishchenko reaction	22
Scheme 14 Claisen-Schmidt reaction catalysed by Fe(BTC) by Garcia and co-workers	28
Scheme 15 Aldol coupling of acetone to mesityl oxide performed by He and co-workers	28
Scheme 16 UiO-66(Zr) catalysed formation of jasminaldehyde by De Vos and co-workers	29
Scheme 17 Synthesis of Pd/NH ₂ -UiO-66 by Ahn and co-workers for the transfer hydrogenation of aniline	33

Scheme 18 Synthesis of Pd pincer complex by Wade and co-workers and subsequent incorporation into a MOF	34
Scheme 19 Mechanism for the Guerbet synthesis of n-butanol proposed by Li and co-workers.....	36
Scheme 20 Proposed homogeneous/heterogeneous catalysed Guerbet upgrading of ethanol to n-butanol	40
Scheme 21 Synthesis of UiO-66(Zr) (2.1)	52
Scheme 22 Reaction pathway for the Guerbet synthesis of n-butanol from ethanol: a) dehydrogenation of ethanol to acetaldehyde, b) conversion of acetaldehyde to ethyl acetate, c) aldol coupling of acetaldehyde to crotonaldehyde, d) hydrogenation of crotonaldehyde to n-butanol, e) further Guerbet reactions using n-butanol as a substrate	61
Scheme 23 Synthetic strategies employed for the synthesis of different analogues of UiO-66(Zr) with varying loadings of acetic acid modulator.....	68
Scheme 24 Proposed reactions catalysed by UiO-66(Zr) in the Guerbet reaction of ethanol: a) dehydration of ethanol to diethyl ether, b) aldol condensation of ethanol to acetaldehyde, c) further aldol coupling of longer chained aldehydes	73
Scheme 25 Modulated synthesis pathways employed towards the UiO-analogues UiO-66(Hf) (2.5) and UiO-66(Zr)-NH ₂ (2.6).....	74
Scheme 26 Schematic pathway to recycle UiO-66(Zr) from a Guerbet reaction of ethanol, to use as an aldol catalyst in a subsequent Guerbet reaction	83
Scheme 27 Schematic pathway employed to recycle UiO-66(Zr) and {RuCl ₂ (dppm) ₂ } as catalysts in the Guerbet synthesis of n-butanol for use in multiple reactions	86
Scheme 28 Post-synthetic exchange of biphenyl-4,4'-dicarboxylic acid linkers in UiO-67(Zr) with [RuCl(cymene)(bipy-COOH)]Cl	98
Scheme 29 Synthesis of [RuCl(cymene)(bipy)]Cl (a) and [RuCl(cymene)(phen)]Cl (b)	99

Scheme 30 Synthesis of 1,10-phenanthroline-3,8-dicarboxylic acid <i>via</i> di-n-butyl-1,10-phenanthroline-3,8-dicarboxylate as reported by Bessmertnykh-Lemeune <i>et al.</i>	102
Scheme 31 Synthesis of [RuCl(cymene)(bipy-COOH)]Cl.....	103
Scheme 32 Preparation of UiO-66(Zr) (3.5), UiO-66(Zr)-NH ₂ (3.6) and UiO-67(Zr) (3.7) according to a modified literature procedure from Katz <i>et al.</i>	107
Scheme 33 post-synthetic exchange reactions to incorporate [RuCl(cymene)(bipy-COOH)]Cl into the linkers of UiO-67(Zr) (3.7), with varying ratios of UiO-67(Zr):[RuCl(cymene)(bipy-COOH)]Cl (i - 20:1. ii - 6.7:1, iii - 5 :1) Modified from Su and co-workers. ²	110
Scheme 34 Attempted synthesis of UiO-67(Zr)-Bipy	118
Scheme 35 Methodology to immobilise [RuCl ₂ (cymene)] ₂ on the bipyridine linkers of UiO-67(Zr)-Bipy (nature of the 'UiO-67(Zr)-Bipy) unconfirmed from prior SEM analysis)	120
Scheme 36 Synthesis of ruthenium pincer complexes and their immobilisation within zirconium derived MOFs demonstrated by Wade and co-workers	127
Scheme 37 Attempted synthesis of tert-butyl ester functionalised pincer ligand according to modified literature procedure.....	128
Scheme 38 Michael addition of amines across [RuCl ₂ (dppEth) ₂] by Sama	139
Scheme 39 Proposed Michael addition of amino acids across [RuCl ₂ (dppEth) ₂]	139
Scheme 40 Synthesis of [RuCl ₂ (dppEth) ₂]. (Adapted from Barkley <i>et al.</i> ⁵).....	140
Scheme 41 Attempted Michael additions of glycine across [RuCl ₂ (dppEth) ₂] in toluene	140
Scheme 42 Attempted Michael addition of amino acids across [RuCl ₂ (dppEth) ₂] in toluene at 80 °C over 4 days.....	143
Scheme 43 Amino acid zwitterion formation equilibrium	145
Scheme 44 Attempted Michael addition of amino acids across [RuCl ₂ (dppEth) ₂] <i>via</i> pre-activation of the amino Acids to their corresponding sodium salts	146

Scheme 45 Attempted Michael addition of sodium glycinate across [RuCl ₂ (dppEth) ₂] in DCM at room temperature.....	147
Scheme 46 Synthesis of phosphino azomethinylate ligands conducted by Cole	149
Scheme 47 Attempted formation of monochelate sodium phosphino azomethinylate complexes with [RuCl ₂ (η ⁶ -p-cymene)] ₂ as a precursor, and predicted possible binding modes of the ligand to the metal	151
Scheme 48 Attempted formation of bischelate sodium phosphino azomethinylate complexes with [RuCl ₂ (PPh ₃) ₃] as a precursor, and predicted possible binding modes of the ligands to the metal.	154
Scheme 49 Predicted formation of bischelate phosphino azomethinylate ruthenium complexes in-situ in the Guerbet upgrading of ethanol - a) bischelate complex with bidentate ligands, b) bischelate complex with a bidentate and tridentate ligand, c) bischelate complex with tridentate ligands	162
Scheme 50 Potential difference in catalytic activity for the Guerbet reactions detailed in Table 24 and Table 25	170
Scheme 51 Potential route to immobilising phosphino azomethinylate ligands on etched UiO-66(Zr)	178
Scheme 52 : Formation of PCNCP ligands as Demonstrated by Shaw <i>et al.</i>	180

List of Figures

Figure 1 Change in global surface temperature over time.....	1
Figure 2 Breakdown of global anthropogenic greenhouse gas emissions from 1990 to 2019	2
Figure 3 Typical PEM fuel cell.....	3
Figure 4 Production of bioethanol from different feedstocks	6
Figure 5 Formation of n-butanol from ethanol using Sr-HAP catalysts - a) dehydrogenation, b) keto-enol tautomerisation, c) hydrogenation.....	14
Figure 6 Structure of MOF-5	24
Figure 7 Structures of different MOFs with Zn ₄ O SBUs	25
Figure 8 Different SBUs combined with BDC to form different MOFs	26
Figure 9 Lu and co-workers' method to immobilising a homogeneous Cu catalyst on UiO-66-NH ₂	30
Figure 10 PSE method employed by Su and co-workers to immobilise Ru and Rh complexes in UiO-67	31
Figure 11 Aperture-opening encapsulation of [RuH(CO)(Cl)(^t BuPNP)] developed by Tsung and co-workers.....	32
Figure 12 Pd@UiO-66 catalyst prepared by Li and co-workers for the Guerbet synthesis of n-butanol	35
Figure 13 RuNi@MOF catalysts prepared by Neumann <i>et al.</i> for the Guerbet upgrading of ethanol to n-butanol.....	37
Figure 14 Methods of synthesising ML _n @UiO-67 <i>via</i> : a – using homogeneous complexes directly in the synthesis of the MOF, b – using a MOF with linkers that can act as homogeneous ligands to co-ordinate ML _n , c – using a pristine MOF in a post synthetic exchange reaction with a compatible homogeneous complex	41

Figure 15 Zr ₆ node structure of UiO-66(Zr)	51
Figure 16 Comparing PXRD patterns of pristine UiO-66(Zr), and UiO-66(Zr) recovered after being used in a Guerbet synthesis of n-butanol	57
Figure 17 Comparing post-reaction ³¹ P{ ¹ H} NMR spectra from Guerbet reactions of ethanol utilising NaOEt at 150 °C (i), NaOEt at 210 °C (ii) or UiO-66(Zr) at 210 °C (iii) with [RuCl ₂ (dppm) ₂] as a transfer hydrogenation catalyst	58
Figure 18 Comparing the PXRD patterns of the analogues of 2.1 , 2.2 , 2.3 and 2.4	69
Figure 19 Comparing EtOH conversion and n-BuOH selectivity of the Guerbet reactions using MOFs prepared with different degrees of modulation (2.1 , 2.2 , 2.3 and 2.4).....	72
Figure 20 Comparing the PXRD patterns of 2.1 , 2.5 and 2.6	75
Figure 21 Different homogeneous ruthenium transfer hydrogenation catalysts to be tested as transfer hydrogenation catalysts with UiO-66(Zr) in the Guerbet upgrading of ethanol: 2.7 -[RuCl ₂ (dppm) ₂] (pre-synthesised), 2.8 -[RuCl ₂ (dppe) ₂] (pre-synthesised), 2.9 -[RuCl ₂ (dppp) ₂] (pre-synthesised), 2.10 -[RuCl(cymene)(dppm)] (made in situ), 2.11 -[RuCl(cymene)(dppe)] (made in situ), 2.12 -[RuCl(cymene)(dppp)] (pre-formed), 2.13 -Ru-MACHO (pre-formed), 2.14 -[RuCl(cymene)(2-(Diphenylphosphino)-3-methyl-1H-indole)] (made in situ).	77
Figure 22 Comparing EtOH conversion, n-BuOH selectivity and EtOAc selectivity percentages of the Guerbet reactions conducted with different ruthenium transfer hydrogenation catalysts.....	80
Figure 23 Comparing EtOH conversion, n-BuOH selectivity, EtOAc selectivity and higher alcohol selectivity of the catalyst recyclability study.	87
Figure 24 Comparing the PXRD patterns of pristine UiO-66(Zr) and UiO-66(Zr) recovered the reaction detailed in Table 15, Entry 6	89
Figure 25 Structure of [RuCl(cymene)(bipy-COOH)]Cl.....	97
Figure 26 Structure of 1,10-phenanthroline-3,8-dicarboxylic acid	99

Figure 27 Comparison of terephthalic acid (a) and [RuCl(cymene)(bipy-COOH)]Cl (b)	105
Figure 28 Comparison of biphenyl-4,4'-dicarboxylic acid (a) and [RuCl(cymene)(bipy-COOH)]Cl (b)	106
Figure 29 SEM image of 3.8 (a), SEM image of 3.9 (b), SEM image of 3.10 (c)	112
Figure 30 a) SEM image and C, O and Zr elemental maps of 3.8, b) SEM image and C, O and Zr elemental maps of the product of 3.9, c) SEM image and C, O and Zr elemental maps of 3.10	113
Figure 31 Cl elemental map (top) and full EDX spectrum (bottom) of 3.8	114
Figure 32 Ti elemental map (top) and full EDX spectrum (bottom) of 3.9	115
Figure 33 Na elemental map (top) and full EDX spectrum (bottom) obtained of 3.10	115
Figure 34 SEM images of the product of the UiO-67(Zr)-Bipy synthesis (3.11)	119
Figure 35 SEM image of 3.12 (a), SEM image of 3.13 (b), SEM image of 3.14 (c)	122
Figure 36 SEM image and elemental maps of 3.12 (a), SEM image and elemental map of 3.13 (b), SEM image and elemental map of 3.14 (c)	123
Figure 37 a) SEM image used for EDX analysis of 3.11 (left), map of Zr atoms in 3.11, map of O atoms in 3.11, b) EDX spectrum of 3.11.	125
Figure 38 Structures of [RuHCl(CO)(PCNCP- ^t Bu)] (3.21) and [RuHCl(CO)(PCNCP-Ph)] (3.22)	129
Figure 39 Method of immobilising carboxylate functionalised ruthenium complex onto etched UiO-66-NH ₂ by Xiao <i>et al.</i>	137
Figure 40 ³¹ P{ ¹ H} NMR spectra of [RuCl ₂ (dppEth) ₂] (A) and the products of the reaction of [RuCl ₂ (dppEth) ₂] with glycine under various conditions in toluene as detailed in Scheme 41. Condition i (B) Condition ii (C) Condition iii (D) Condition iv (E) Condition v (F)	142

Figure 41 $^{31}\text{P}\{^1\text{H}\}$ NMR spectra of $[\text{RuCl}_2(\text{dppEth})_2]$ (A) and 4.3 (B), 4.4(C) and 4.5 (D).	144
Figure 42 Ruthenium bischelate PNO Complexes Previously Synthesised by Adshead	148
Figure 43 Targeted phosphino azomethinylate ligand set, and predicted binding modes of these ligands to ruthenium centres.	148
Figure 44 $^{31}\text{P}\{^1\text{H}\}$ NMR spectra of the products of the reactions of $[\text{RuCl}_2(\eta^6\text{-p-cymene})]_2$ with 4.8 (A), 4.9 (B) and 4.10 (C) to target monochelate complex formation	152
Figure 45 $^{31}\text{P}\{^1\text{H}\}$ NMR spectra of the products of the reactions of $[\text{RuCl}_2(\text{PPh}_3)_3]$ with 4.8 (A), 4.9 (B), 4.10 (C), 4.11 (D) and 4.12 (E) targeting bischelate complex formation.	156
Figure 46 Proposed formation of tridentate bound phosphino azomethinylate complexes in the Guerbet reactions detailed in Table 22, Entries 1 (a), 2 (b) and 3 (c).....	160
Figure 47 Proposed formation of bidentate bound phosphino azomethinylate complexes in the Guerbet reactions detailed in Table 22, Entries 4 (a) and 5 (b).	161
Figure 48 Predicted structures of ruthenium complexes formed in the reactions detailed in Table 23 Entries 1 (a) and 2 (b).	164
Figure 49 Predicted structures of ruthenium complexes formed in the reactions detailed in Table 23 Entries 4 (a) and 5 (b).	165
Figure 50 n-BuOH calibration curve	190

List of Tables

Table 1 Comparison of fuel properties of gasoline, ethanol and butanol.....	7
Table 2 Phosphine ligand screen for the upgrading of EtOH to n-BuOH conducted by Ishii and co-workers	16
Table 3 Guerbet upgrading of ethanol using Lewis Acids as aldol catalysts	50
Table 4 Guerbet upgrading of ethanol using UiO-66(Zr) and [RuCl ₂ (dppm) ₂] as co-catalysts at various reaction temperatures	53
Table 5 Comparing the performance of NaOEt mediated Guerbet systems with UiO-66(Zr) co-catalysed systems, with [RuCl ₂ (dppm) ₂] as a transfer hydrogenation catalyst	55
Table 6 Reaction duration screen for the Guerbet upgrading of ethanol employing UiO-66(Zr) and [RuCl ₂ (dppm) ₂] as co-catalysts.....	60
Table 7 UiO-66(Zr) Loading screen for the Guerbet upgrading of ethanol with [RuCl ₂ (dppm) ₂] as a transfer hydrogenation catalyst.....	63
Table 8 Stirring rate for the Guerbet upgrading of ethanol with UiO-66(Zr) and [RuCl ₂ (dppm) ₂] as co-catalysts.....	64
Table 9 Water loading screen for the Guerbet upgrading of ethanol with UiO-66(Zr) and [RuCl ₂ (dppm) ₂] as co-catalysts.....	66
Table 10 Comparing the effect of modulation in the synthesis of UiO-66(Zr) on catalytic activity in the Guerbet reaction	70
Table 11 Comparing the Guerbet upgrading of ethanol utilising UiO-66(Zr), UiO-66(Hf) or UiO-66(Zr)-NH ₂ as aldol catalysts	76
Table 12 Screen of different [Ru] transfer hydrogenation catalysts in the Guerbet upgrading of ethanol.....	79
Table 13 Screening 5% Ru/Charcoal as a heterogeneous transfer hydrogenation catalyst in the Guerbet upgrading of ethanol	82

Table 14 Comparing catalytic activity in the Guerbet upgrading of ethanol using pristine and recycled UiO-66(Zr).....	84
Table 15 Recyclability study on the evolution of UiO-66(Zr) and [RuCl ₂ (dppm) ₂] co-catalysts in the Guerbet upgrading of ethanol.....	86
Table 16 Guerbet syntheses of n-butanol using [RuCl ₂ (cymene)] ₂ and nitrogen containing ligands as transfer hydrogenation catalyst precursors	97
Table 17 Guerbet upgrading of ethanol using [RuCl(cymene)(bipy)]Cl and [[RuCl(cymene)(phen)]Cl as transfer hydrogenation catalysts with NaOEt	100
Table 18 Guerbet upgrading of ethanol using [RuCl(cymene)(bipy)]Cl and [[RuCl(cymene)(phen)]Cl as transfer hydrogenation catalysts with UiO-66(Zr).....	101
Table 19 Guerbet upgrading of ethanol using [RuCl(cymene)(bipy)]Cl with NaOEt (at 150 °C) and UiO-66(Zr) (at 210 °C).....	103
Table 20 Guerbet upgrading of ethanol with [RuCl ₂ (dppm) ₂] and 3.5 , 3.6 or 3.7	108
Table 21 Guerbet upgrading of ethanol using [RuHCl(CO)(PCNCP- ^t Bu)] and [RuHCl(CO)(PCNCP-Ph)] as transfer hydrogenation catalysts with UiO-66(Zr).....	130
Table 22 Guerbet upgrading of ethanol using sodium phosphino azomethinylate ligands with [RuCl ₂ (η ⁶ -p-cymene)] ₂ (2:1) ratio) as transfer hydrogen catalyst precursors	159
Table 23 Guerbet upgrading of ethanol using sodium phosphino azomethinylate ligands with [RuCl ₂ (η ⁶ -p-cymene)] ₂ (4:1) ratio) as transfer hydrogen catalyst precursors	163
Table 24 Guerbet upgrading of ethanol using sodium phosphino azomethinylate ligands with [RuCl ₂ (η ⁶ -p-cymene)] ₂ (2:1) ratio) as transfer hydrogen catalyst precursors	167
Table 25 Guerbet upgrading of ethanol using sodium phosphino azomethinylate ligands with [RuCl ₂ (η ⁶ -p-cymene)] ₂ (4:1) ratio) as transfer hydrogen catalyst precursors	168
Table 26 Guerbet upgrading of ethanol using sodium phosphino azomethinylate ligands with [RuCl ₂ (η ⁶ -p-cymene)] ₂ (4:1) ratio) as transfer hydrogen catalyst precursors	171

List of Abbreviations

ABE – Acetone Butanol Ethanol

BDC – 1,4-benzenedicarboxylate or terephthalic acid

BET – Brunauer-Emmett-Teller

bipy - 2,2'-Bipyridine

bipy-COOH – 2,2'-Bipyridine-5,5'-dicarboxylic acid

BTB – 4,4',4''-Benzene-1,3,5-triyl-tris(benzoic acid)

BTC – 1,3,5-Benzenetricarboxylic acid

cod – 1,5-cyclooctadiene

CVD – Chemical Vapour Deposition

DCM – Dichloromethane

DMF – Dimethylformamide

DMSO – Dimethyl sulfoxide

dppb – 1,4-bis(diphenylphosphino)butane

dppe – 1,2-bis(diphenylphosphino)ethane

dppEth – 1,1-bis(diphenylphosphino)ethylene

dppm – bis(diphenylphosphino)methane

dppp – 1,4-bis(diphenylphosphino)propane

EtOH – Ethanol

EtOAc – Ethyl acetate

EDS / EDX – Energy-dispersive X-ray spectroscopy

FCEVs – Fuel cell electric vehicles

GC – Gas Chromatography

ICP-MS – Inductively Coupled Plasma-Mass Spectrometry

IPA – Isopropanol

MeCN – Acetonitrile

MeOH – Methanol

MOF – Metal-Organic Framework

n-BuOH – *n*-Butanol

NaOEt – Sodium ethoxide

NDC – Naphthalene dicarboxylic acid

nbd – Norbornadiene

NMR – Nuclear Magnetic Resonance

NP – Nanoparticle

Phen – 1,10-Phenanthroline

Phen-COOH – 1,10-Phenanthroline-3,8-dicarboxylic acid

PTFE – Polytetrafluoroethylene

PXRD – Powder X-Ray Diffraction

PNP – 2,6-Bis((di-*tert*-butyl- phosphino)methyl)pyridine

PSE – Post Synthetic Exchange

PEM – Polymer Electrolyte Membrane

SEM – Scanning Electron Microscopy

SBU – Secondary Building Units

TGA – Thermogravimetric analysis

TEM – Transmission Electron Microscopy

THF – Tetrahydrofuran

XPS – X-ray Photoelectron Spectroscopy

Chapter 1 – Introduction

1.1 Climate change and global warming

Climate change and global warming remain an ever-present threat to the survival of the planet, with human activities likely attributing to between 0.8 °C and 1.3 °C of global warming since 1850, with a best estimate of 1.07 °C.¹ It is likely that greenhouse gas emissions have resulted in a global surface temperature increase of 1.0 to 2.0 °C, while other human contributions such as aerosol emissions have contributed to a global cooling effect of 0.0 to 0.8 °C.¹ The extent of modern global warming is highlighted in Figure 1.

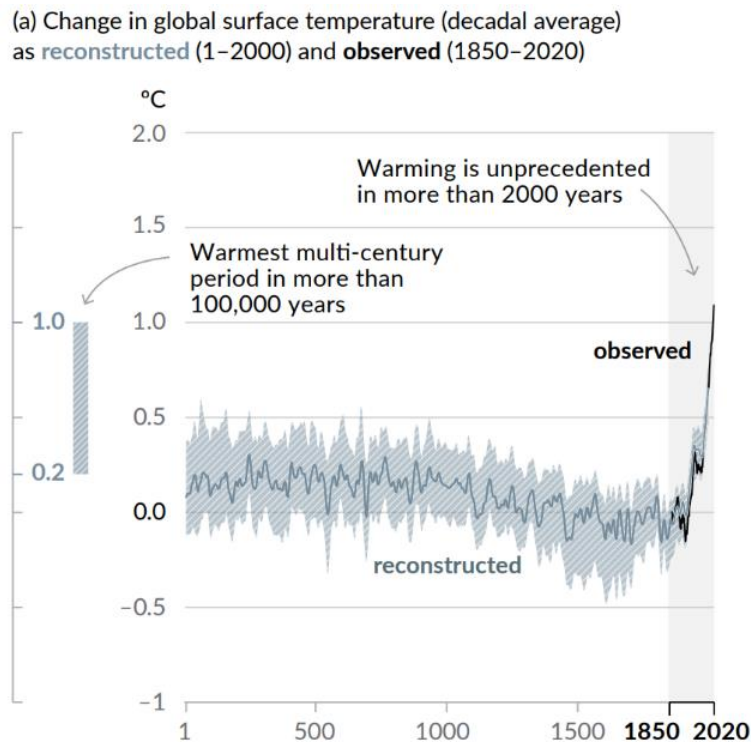


Figure 1: Change in global surface temperature over time.¹

In 2019, it was predicted that global warming would likely reach the 1.5 °C threshold set out by the Paris accord between 2030 and 2052, if it were to increase at current rates.² While a 1.5 °C increase in global temperature would pose risks to natural and human systems, it is imperative global warming is kept below 2 °C.² While global warming has already almost certainly had a detrimental impact on the planet, a 2 °C temperature increase on pre-industrial levels would start to show catastrophic effects on the planet.

Global warming of 2 °C would result in some regions being more likely to experience drought, with other areas at a higher risk of heavy precipitation events like tropical cyclones. This level of global warming would result in increased levels of species loss and extinction on land, and reduced ocean oxygen levels would impact the survival and abundance of a wide range of aquatic species. At 2 °C of global warming, humans would be affected in a multitude of ways, including increased levels of poverty and lower food security in the developing world, as well as increased heart-related morbidity and mortality.²

It is therefore evident that reducing greenhouse gas emissions is vital in limiting global warming to protect the planet. In 2019, CO₂ was shown to account for 75% of all greenhouse gas emissions, with 64% of total greenhouse gas emissions attributed to CO₂ from fossil fuel and industry (Figure 2),³ highlighting the need for a global reduction in CO₂ emissions to combat climate change.

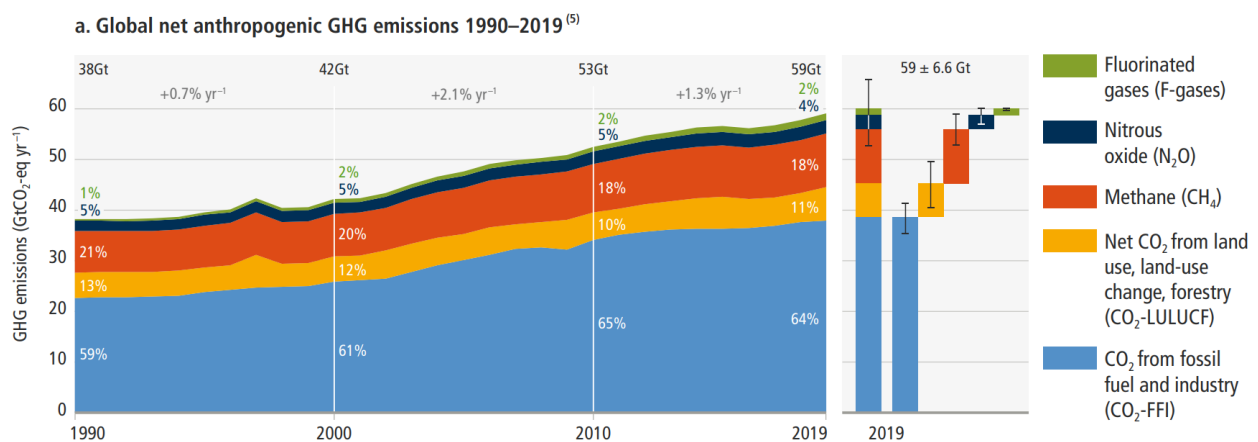


Figure 2: Breakdown of global anthropogenic greenhouse gas emissions from 1990 to 2019.³

1.2 Renewable transportation fuels

The transport industry accounted for 15% of net anthropogenic greenhouse gas emissions in 2019,³ and it has previously been predicted that 95% of the World's transportation energy comes from petroleum derived fuels.⁴ Replacing petroleum fuels with renewable, net-zero CO₂ emission alternatives could have a significant impact in

reducing global greenhouse gas emissions and global warming. Three common renewable alternatives to petroleum are hydrogen fuel, biodiesel, and bioethanol.⁵

1.2.1 Hydrogen

Fuel cell electric vehicles (FCEVs) that are powered by hydrogen fuel cells are an emerging alternative to traditional, combustion engine powered vehicles. Compressed hydrogen gas is fed into a FCEV in a similar way to which petrol or diesel is fed into a traditional car and is stored in a tank inside the vehicle.^{6,7} The most common fuel cell used in vehicles is the polymer electrolyte membrane (PEM) fuel cell, where an electrolyte membrane lies between an anode and cathode (Figure 3).

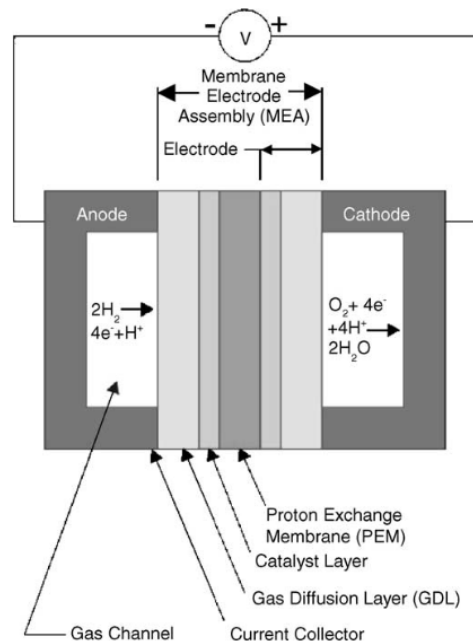


Figure 3: Typical PEM fuel cell.⁸

Hydrogen is added to the anode and oxygen from the air is added to the cathode, and the hydrogen is split at the anode to form protons and electrons. The electrons travel through an external circuit to power the vehicle, recombining with the previously formed protons, and oxygen at the cathode to produce water vapour which is emitted from the vehicle.⁷ Hydrogen fuel cells have advantages over traditional combustion engines. The only by-products of hydrogen powered fuel cells are water and heat, with no greenhouse gas or pollutant emissions,⁹ hence the use of hydrogen fuel cells does not contribute to the greenhouse effect. Also, hydrogen fuel cells operate with a much higher energy

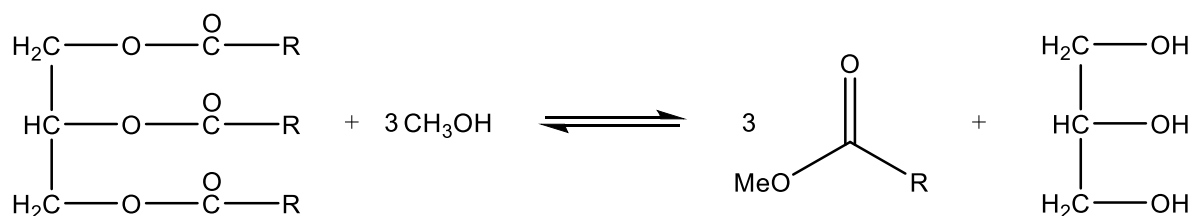
efficiency than internal combustion engines.⁹ However, using hydrogen as an alternative to petroleum in the transport sector has several limitations. As of mid-2021, there were only 48 open hydrogen stations in the USA,¹⁰ highlighting the lack of current infrastructure for hydrogen fuel to be employed by most of the population of the USA. Due to its low density, the storage density of hydrogen must be increased for economic viability.¹¹ The most common methods of hydrogen storage are traditionally mechanical storage methods, like cryogenic cooling or compression;¹² however, these storage techniques are problematic. To power a vehicle efficiently, compressed hydrogen needs to be stored at pressures of 35-70 MPa, while liquid hydrogen needs to be cooled to -253 °C, hence both of these storage methods would require complex engineering solutions that would be difficult to implement to the consumer market on a large scale.¹³ Potentially the biggest limitation with hydrogen fuel however is the fact that approximately 95% of hydrogen is produced by the steam methane reforming of natural gas.¹⁴ This process results in significant emissions of CO₂,¹⁴ so while the direct use of a hydrogen fuel cell does not lead to the production of greenhouse gases, the current sourcing of the hydrogen fuel does contribute to the greenhouse effect.

1.2.2 Biofuels

Biofuels are renewable liquid fuels that are produced using plant-based biomass feedstocks.¹⁵ Biofuels are viewed as advantageous to traditional petrochemical fuels as the net-emissions of CO₂ produced through their use are close to zero.¹⁶ Although burning biofuels produces CO₂, the plants grown to produce biofuels capture CO₂ from the atmosphere through photosynthesis, hence they are defined as carbon-neutral.¹⁶ Biofuels can be categorised into different generations, that are defined by the biomass source of the fuel. First generation biofuels are sourced from food crops like sugarcane and vegetable oil, second generation biofuels are derived from non-edible crops and third generation biofuels are sourced from microalgae biomass.¹⁷ Food crops are currently the most used biomass source for biofuels, which is controversial as a debate is raised over using land for biofuel production vs. food production to feed the growing world population.¹⁷ Hence, producing second and third generation biofuels are advantageous. The two most common biofuels currently used are biodiesel and ethanol.¹⁸

1.2.2.1 Biodiesel

Biodiesel is a diesel analogue that is produced from oils that are extracted from different organic feedstocks. Biodiesels are typically produced *via* transesterification reactions, where triglycerides are broken down into fatty acid methyl esters (biodiesel) and glycerol by an alcohol (which is typically methanol due to its low cost and high availability) with a catalyst (Scheme 1).^{19,20} The glycerol is separated by decanting and the fatty acid methyl esters are purified for use as a biofuel.²¹



Scheme 1: Synthesis of biodiesel from triglycerides using methanol.

CO₂ is emitted through burning the fatty acid methyl esters as a diesel alternative, however, as the source of the fuel is plant derived, the CO₂ released from biodiesel combustion can be offset against the CO₂ recycled from the atmosphere during the next biodiesel crop production.²² However, diesel engines typically can't run on 100% biodiesel (B100), and require blends of biodiesel and conventional diesel.²³ In general, most diesel engines can run on B20 (or lower) biodiesel, which consists of 20% biodiesel, and 80% petrochemical diesel.²³ While burning B20 biodiesel is advantageous to using traditional diesel in combustion engines, there are still considerable greenhouse gas emissions associated with burning the petrochemical diesel in the fuel blend.²³ There are also concerns as to whether using crops to produce biofuels like biodiesel will lead to increased food prices and lower food security, as the main feedstocks are agricultural products.²⁴

1.2.2.2 Ethanol

Bioethanol is another example of a biofuel, and it is produced on a larger scale worldwide compared to biodiesel. Lignocellulosic biomass has been identified as a source to produce bioethanol as a sustainable second-generation biofuel, while corn and sugarcane can also be used as biomass sources for the sugars required for ethanol production by fermentation (Figure 4).²¹ The cellulose present in lignocellulosic biomass

is hydrolysed to produce fermentable sugars, in a process typically catalysed by cellulase enzymes. These sugars are subsequently converted to ethanol by fermentation with bacteria or yeasts.²⁵

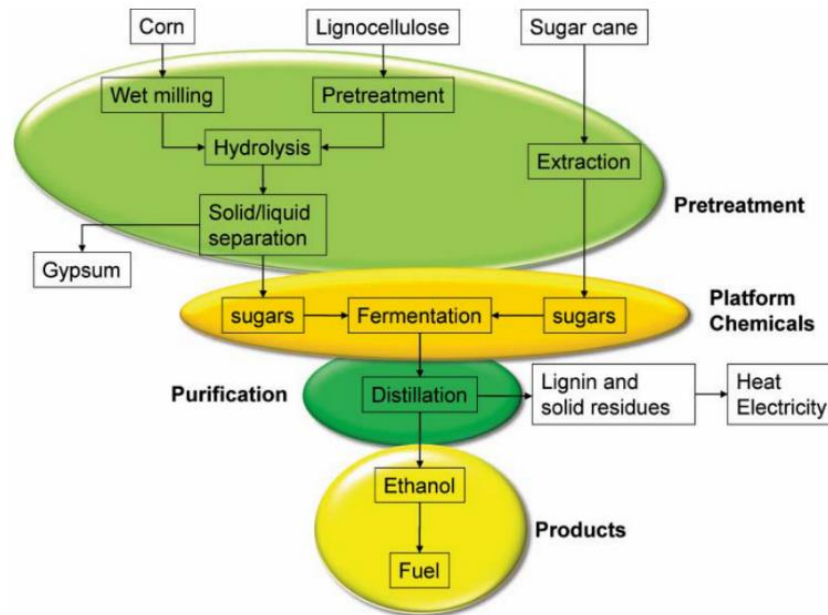


Figure 4: Production of bioethanol from different feedstocks.²¹

Ethanol is typically blended with gasoline for use in current vehicles, similarly how biodiesel is blended with petrochemical diesel in commercial fuels. In the USA, more than 98% of available gasoline contains ethanol, typically in a blend of 10% ethanol and 90% gasoline (E10).²⁶ While this blend is lower in biofuel content than B20 biodiesel, higher ethanol content fuel is widely useable. E85 fuel is an ethanol-gasoline blend that contains between 51% and 83% ethanol,²⁷ and this higher ethanol content fuel can be used in flexible fuel vehicles, of which there were more than 21 million in the USA in 2018.²⁸ While utilising ethanol as a biofuel in blends carries the advantages of reduced net greenhouse emissions that are inherent of a biofuel, there are disadvantages to its use. Ethanol is corrosive to existing pipelines, and it has also been known to cause engine burns and corrosion.^{29,30} And ethanol is fully miscible with water,³¹ which leads to problems considering storage and separation, as biofuel blends employed with ethanol run a greater risk of introducing water to an engine.³⁰

1.3 Butanol as an alternative to ethanol

Butanol has been described as an advanced biofuel,³² with several properties that render it a more advantageous biofuel compared to ethanol.³³ Butanol can be used as a pure 100% blend, or blended with any amount of gasoline, while ethanol can only be used in an 85% blend with petrochemical gasoline in certain vehicles, hence butanol could be used as a fuel by itself in current car engines, without the requirement of any modifications.³³ While ethanol was described as miscible with water in 1.2.2.2, butanol on the other hand is not hygroscopic, allowing easier storage and distribution of butanol when compared to ethanol. And when fuel spills are considered, butanol will not contaminate groundwater while ethanol will.³³ Butanol is less corrosive than ethanol, and unlike ethanol, butanol is compatible with current infrastructure.³³ Ethanol has a low relative energy content compared to gasoline (65%), while the energy density of butanol is much higher (90% of that of gasoline), which renders butanol as a more efficient fuel compared to ethanol.³³ Butanol is also safer to handle than both gasoline and ethanol due to the fact that it has a lower flash point and vapour pressure than both.³⁴ A comparison of properties of ethanol, butanol and gasoline that are relevant to their use as fuels is shown in Table 1.

Table 1: Comparison of fuel properties of gasoline, ethanol and butanol^{33,35}

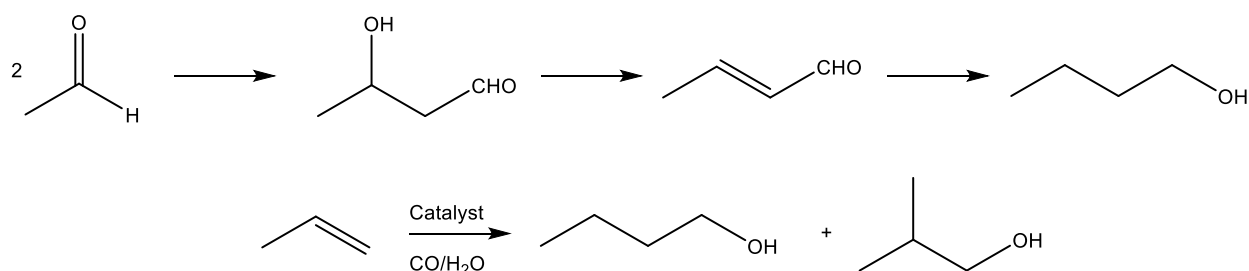
Fuel	Caloric value (MJ/L)	Air-fuel ratio	Research Octane Number	Solubility of compound in water at 20 °C (wt%)	Reid Vapour Pressure (kPa)	Flash Point Closed Cup (°C)
Gasoline	32.5	14.6	91-99	Negligible	54-103	-43
Ethanol	21.2	3.0	129	Miscible	16.0	13
Butanol	29.2	11.2	96	7.7	2.2	29

Two established methods of producing butanol on a large scale are the oxo process and the ABE (acetone butanol ethanol) fermentation process.

1.3.1 Petrochemical synthesis of butanol

1.3.1.1 Reppe synthesis and crotonaldehyde hydrogenation

Until the 1950s, the predominant petrochemical synthesis of *n*-butanol was based on crotonaldehyde hydrogenation. Initially, acetaldehyde would react in an aldol condensation at ambient temperature and pressure with an alkaline catalyst to form 3-hydroxybutanal. This was then dehydrated using acetic or phosphoric acids to form crotonaldehyde, which was subsequently hydrogenated using a copper catalyst (Scheme 2).³⁶

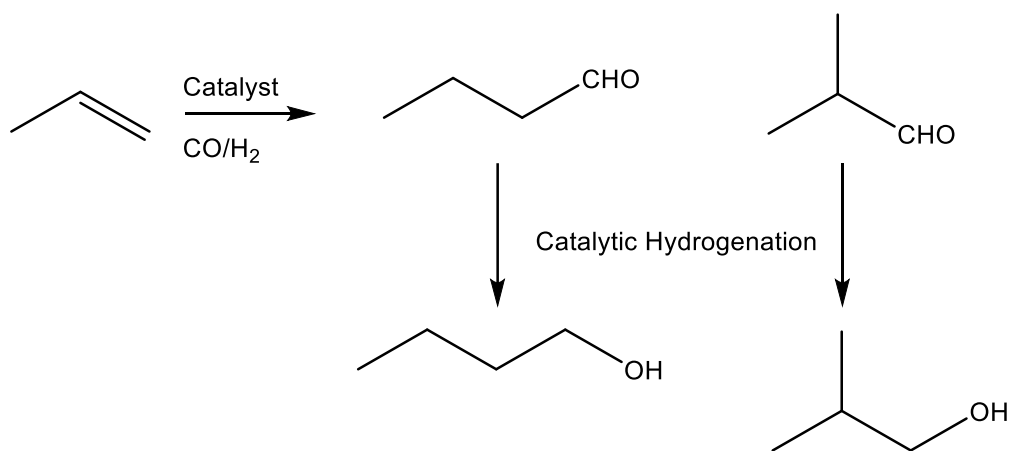


*Scheme 2: Synthesis of butanol via crotonaldehyde hydrogenation (top) and the Reppe synthesis (bottom).*³⁶

The Reppe synthesis is another petrochemical method to synthesise butanol. A mixture of propene, carbon monoxide and water react in the presence of a catalyst at $0.5\text{-}2 \times 10^6$ Pa at $100\text{ }^\circ\text{C}$ to form a mixture of *n*-butanol and isobutanol in a ratio of 86:14 (Scheme 2).³⁶ Both of these petrochemical processes to produce butanol were replaced with the oxo process, which is the most common route to synthesise butanol from petrochemically derived starting materials.^{36,37}

1.3.1.2 The oxo process

The oxo synthesis of butanol is based on the hydroformylation of propene, where initially, a catalyst converts a feed stream of propylene and syngas ($\text{CO} + \text{H}_2$) to butyraldehyde and isobutyraldehyde. A subsequent catalytic hydrogenation of the butyraldehyde isomers yields butanol in the form of *n*-butanol and isobutanol (Scheme 3).



Scheme 3: Synthesis of butanol via the oxo process.^{36,38}

Until the 1970s, the process relied on high pressures of 20-30 MPa CO/H₂ at 100-180 °C to achieve yields of around 75% *n*-butanol and 25% isobutanol with a cobalt catalyst, while more modern processes utilise lower pressures of 1-5 MPa with ruthenium catalysts to achieve yields of 95% *n*-butanol and 5% isobutanol.³⁶ While the oxo process is an efficient method of producing butanol on an industrial scale, the reaction relies on a petroleum derived feedstock (propene), hence the synthesis of butanol by the oxo process can not be described as renewable. Nor can the final butanol product be described as a biofuel, as the synthesis of the propene feedstock contributes to the greenhouse effect.

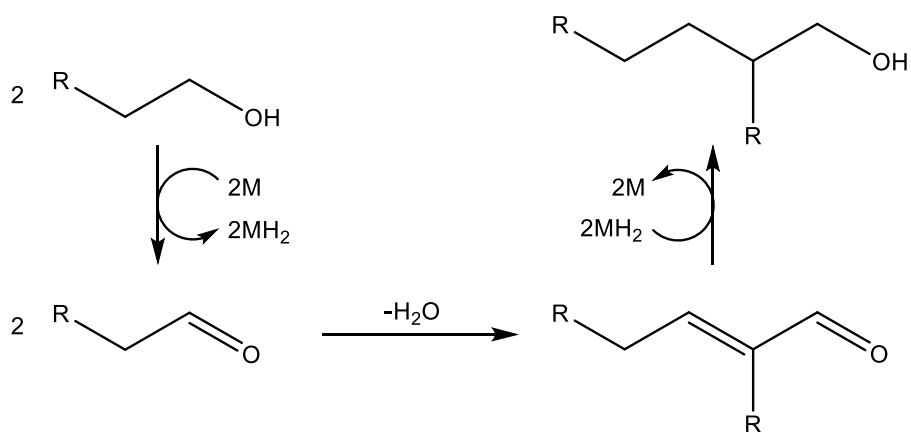
1.3.2 Butanol synthesis by the ABE fermentation process

The ABE fermentation process is a renewable alternative to the Oxo process for the production of butanol on an industrial scale. The process utilises bacteria to convert starches and sugars into solvents, with the most studied bacteria for the process being *Clostridium Acetobutylicum*.³⁹ The process has two stages, the first being a growth stage where acetic and butyric acids are made, and the second comprised of acid re-assimilation into acetone, butanol and ethanol solvents.³⁹ While the ABE fermentation process presents a renewable alternative to the oxo process for butanol production, there are limitations with ABE fermentation. The primary problem with the ABE fermentation process is that *n*-butanol is toxic to the culture that is used to produce the solvent mixture.⁴⁰ The toxic nature of *n*-butanol in the reaction causes premature termination of the fermentation over long reaction durations.⁴⁰ The ABE fermentation process to produce

butanol is also limited by low butanol yields, as well as high feedstock costs.⁴⁰ The limitations of the current industrial methods to produce butanol have driven research into alternative methodologies to efficiently produce it in a sustainable manner.

1.4 The Guerbet reaction

The Guerbet reaction was first reported in 1899 by Marcel Guerbet, who described the use of sodium alkoxide catalysts in coupling two alcohols together to form a longer chained alcohol product at 200 °C.⁴¹ Veibel and Neilsen proposed the widely accepted mechanism of the Guerbet reaction in 1967 (Scheme 4).⁴² In the Guerbet reaction, two starting alcohol molecules are dehydrogenated to form their corresponding aldehydes, which then undergo an aldol coupling reaction. The aldol coupled product is hydrogenated to form the longer chained alcohol product. Several different systems can be utilised to drive the transfer hydrogenation and aldol steps in the Guerbet reaction. The transfer hydrogenation reaction can be catalysed by homogeneous or heterogeneous transition metal catalysts for example, usually in combination with a homogeneous alkaline base to facilitate the aldol condensation,⁴³ while heterogeneous catalysts can also be utilised on their own in the Guerbet reaction.⁴³



Scheme 4: General scheme for the upgrading of alcohols via the Guerbet reaction.

1.5 Guerbet synthesis of butanol

Scheme 4 shows a general Guerbet reaction pathway, but if the starting alcohol in the reaction is ethanol, then the product of the reaction is *n*-butanol. In the Guerbet synthesis of *n*-butanol, two ethanol molecules are dehydrogenated to form acetaldehyde molecules, which undergo an aldol condensation reaction to form crotonaldehyde. The crotonaldehyde is then hydrogenated to form *n*-butanol. The Guerbet synthesis of *n*-butanol from ethanol has attracted a lot of attention in recent years, as the reaction has been identified as a potential sustainable method of synthesising butanol for use as a biofuel on an industrial scale. In 1.2.2.2, the process of fermenting sugars that have been isolated from lignocellulosic biomass was described as a sustainable source of ethanol for use as a biofuel, however, problems with water miscibility, corrosion and low blend ratios with petrochemical gasoline were highlighted as limitations of the fuel. Butanol was identified as an advantageous biofuel alternative to ethanol in 1.3, but the problems with the current industrial synthetic processes to make butanol on a large scale were detailed in 1.3.1. The Guerbet reaction presents a viable method of converting sustainably sourced lower quality ethanol into a higher quality butanol biofuel in a catalytic process. While the Guerbet coupling of ethanol presents a route to synthesise *n*-butanol from renewable sources, the reaction is difficult to control.⁴⁴ This is because *n*-butanol itself can act as a substrate in the Guerbet reaction, and undergo coupling with ethanol, or more *n*-butanol to form longer chained (higher) alcohols.⁴⁴ When considering the Guerbet coupling of ethanol to form *n*-butanol as a sustainable alternative fuel, the formation of higher alcohols (C₆+) is undesired. Nevertheless, heterogeneous and homogeneous catalysis for the upgrading of ethanol to *n*-butanol has become a well-established field of research.

1.5.1 Heterogeneous catalysis for Guerbet synthesis of *n*-butanol from ethanol

Heterogeneous catalysts have been well studied in recent years for the upgrading of ethanol to *n*-butanol, with two intrinsic characteristics required to allow them to catalyse the Guerbet reaction.⁴⁵ Heterogeneous Guerbet catalysts must have a solid basic component, while also being able to facilitate alcohol dehydrogenation at the desired

reaction temperature.⁴⁵ Basic metal oxides, hydroxyapatites and supported transition metals have all been areas of study in the heterogenous catalytic upgrading of ethanol to butanol *via* the Guerbet reaction.⁴⁵

1.5.1.1 Basic metal oxides

Basic metal oxides have been studied for their catalytic activity in the Guerbet reaction, with MgO being identified as the standard to which other catalysts are compared.⁴⁵ Studies on MgO catalysis in the Guerbet synthesis of *n*-butanol have included isotopic transient analysis of ethanol coupling over a commercial MgO catalyst at 673 K,⁴⁶ with a focus on quantifying the turnover frequency of the reaction and probing the nature of surface adsorption of ethanol and intermediate products. High surface adsorption of ethanol, and unfavourable dehydrogenation to acetaldehyde led to a turnover frequency of 0.040 s⁻¹.⁴⁶ Recently, a study was conducted into the Guerbet coupling of ethanol to *n*-butanol at 623 K over MgO catalysts prepared *via* different methods, where a number of factors including basicity, MgO surface area and the crystallite size had an impact on catalyst activity in the production of butanol.⁴⁷

To increase the activity of MgO catalysts in the Guerbet upgrading of ethanol to butanol, aluminium can be incorporated into the MgO. Aluminium is a stronger Lewis acid than magnesium, which can increase the activity of the catalyst by creating a higher number of acid-base pairs of desired strength.⁴⁵ These catalysts are commonly made by synthesising hydrotalcite layered materials where Mg(OH)₂ is partially substituted with aluminum.⁴⁵ Apesteguia and co-workers probed hydrotalcite-derived Mg-Al catalysts with different Mg:Al ratios for the conversion of ethanol to *n*-butanol.⁴⁸ They found that increasing the proportion of Al in the mixed oxide samples improved *n*-butanol formation rate, up to a nominal molar composition of 0.50.⁴⁸ Increasing Al loading further improved ethanol conversion rate, however formation of dehydration by-products like diethyl ether and ethylene was predominant, where pure Al₂O₃ was highly active for ethylene formation and inactive for *n*-butanol formation.⁴⁸ This activity was also shown by Appel and co-workers who showed Mg-Al mixed oxides prepared from the thermal decomposition of hydrotalcite materials were more active for *n*-butanol formation than MgO, Al₂O₃ and a mix of MgO and Al₂O₃.⁴⁹ Another acid-base bifunctional material family that have been

tested as catalysts for ethanol conversion to butanol are mixed oxides of MgO and ZrO₂, however, it was found that the introduction of ZrO₂ at the surface of samples of the mixed oxide were detrimental to *n*-butanol formation from ethanol.⁵⁰

1.5.1.2 Hydroxyapatite

Hydroxyapatite (Ca₅(PO₄)₃OH) catalysts are another class of acid-base heterogeneous catalysts that have been studied for the Guerbet coupling of ethanol to butanol.⁴⁵ Stoichiometric hydroxyapatite has a Ca/P molar ratio of 1.67, however hydroxyapatite can exist in non-stoichiometric forms with Ca/P molar ratios between 1.5 and 1.7.⁵¹ The relationship between the Ca/P ratio in hydroxyapatite catalysts and catalytic activity for the Guerbet upgrading of ethanol to butanol was tested by Tsuchida *et al.*, who found that a non-stoichiometric hydroxyapatite catalyst with a Ca/P ratio of 1.64 was the most effective that they tested at 673 K, facilitating an ethanol conversion of 22.7 % with a selectivity towards *n*-butanol of 62.4 %.⁵¹ Ogo *et al.* managed to improve the *n*-butanol selectivity of the reaction to 81.2% at a lower reaction temperature of 573 K by using a hydroxyapatite analogue where Ca had been substituted by Sr (Sr₁₀(PO₄)₆(OH)₂).⁵² While this maximum selectivity was achieved at a modest ethanol conversion of 7.6 %, *n*-butanol selectivity was greater than 70% at an ethanol conversion of 24%.⁵² Ogo *et al.* tested non-stoichiometric analogues of the Sr₁₀(PO₄)₆(OH)₂ (Sr-HAP) catalyst in the Guerbet upgrading of ethanol to butanol, where they found that a Sr-HAP with a Sr/P molar ratio of 1.70 improved the selectivity of the reaction compared to the stoichiometric analogue previously tested.⁵³ This catalyst managed to achieve a *n*-butanol selectivity of 86.4 % at an ethanol conversion of 11.3 %.⁵³ The Mechanism for the synthesis of *n*-butanol from ethanol using Sr-HAP catalysts is shown in Figure 5.⁵³

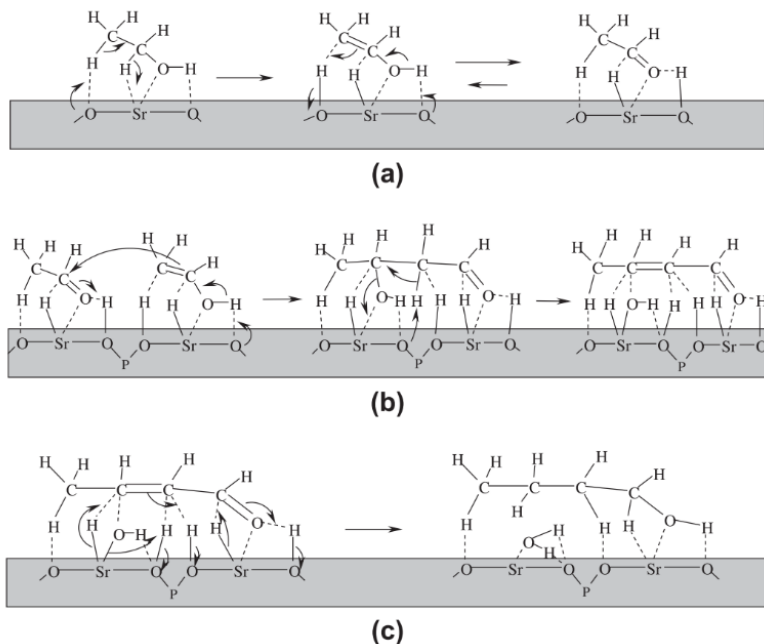


Figure 5: Formation of *n*-butanol from ethanol using Sr-HAP catalysts - a) dehydrogenation, b) keto-enol tautomerisation, c) hydrogenation.

1.5.1.3 Transition metal catalysis

Transition metals incorporated on a basic support have attracted attention as heterogeneous catalysts in the Guerbet upgrading of ethanol to butanol, as the supported metal can enable enhanced activity at lower reaction temperatures compared to metal oxides employed on their own.⁴⁵ Marcu *et al.* studied Cu-Mg-Al mixed oxide catalysts for the conversion of ethanol to butanol, synthesising a variety of Cu_xMgAl_yO catalysts, with different metal loadings.⁵⁴ Catalysts with different ratios of Mg/Al were tested as catalysts in the Guerbet upgrading of ethanol, and it was found that the Mg/Al ratio present in the catalyst had a minimal effect on activity.⁵⁴ The loading of copper present in the catalyst had a significant effect on activity, where loadings of 5-10 % of copper with respect to the cations were optimal for ethanol conversion to *n*-butanol.⁵⁴ A Cu₇MgAl₍₃₎O catalyst facilitated a 4.5 % conversion of ethanol with a selectivity towards butanol of 35.6 % over 5 hours at 473 K, and demonstrated good stability over three catalytic cycles.⁵⁴ Marcu *et al.* investigated the conversion of ethanol to *n*-butanol over a variety of mixed metal oxides consisting of transition metals and Mg/Al.⁵⁵ Pd, Ag, Mn, Fe, Cu, Sm and Yb were supported on Mg/Al oxide supports, where each sample was prepared with 5% loading of transition metal.⁵⁵ Over 5 hours at a reaction temperature of 473 K, the supported Pd

catalyst performed best, facilitating a butanol selectivity of 72.7%, albeit at a low ethanol conversion of 3.8 %.⁵⁵ Although ethanol conversion was slightly lower than the previous Cu catalyst reported by Marcu *et al.*, the selectivity towards butanol was much higher, and the catalyst was highly stable over 3 successive runs.⁵⁵

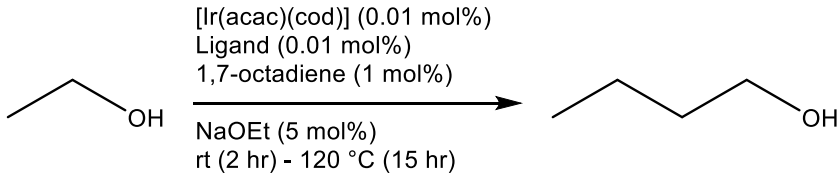
1.5.2 Homogeneous catalysis for Guerbet synthesis of butanol from ethanol

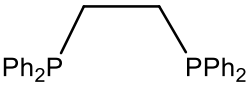
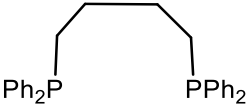
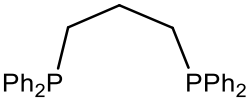
While heterogeneous catalysis is advantageous over homogeneous catalysis when considering aspects like catalyst recovery and recycling, the heterogeneous catalysed systems reported for the Guerbet upgrading of ethanol to butanol are all limited by low ethanol conversions, and as a result, low yields of *n*-butanol (less than 20% in the literature reported in 1.5.1). Homogeneous catalysis for Guerbet upgrading of ethanol to butanol has also been extensively studied in recent times.⁴⁴ Homogeneous systems for the Guerbet upgrading of ethanol to butanol typically utilise a transition metal transfer hydrogenation catalyst (to dehydrogenate ethanol, and subsequently hydrogenate crotonaldehyde), with an alkali metal base present to drive the aldol condensation of acetaldehyde.⁴⁴

1.5.2.1 Iridium catalysis

Ishii and co-workers were the first group to report a homogeneous system for the catalytic upgrading of ethanol to *n*-butanol *via* the Guerbet reaction.⁵⁶ Based on previous work conducted by the group on the coupling of primary to beta-alkylated alcohols,⁵⁷ they screened homogeneous systems with iridium transfer hydrogenation catalysts for the upgrading of ethanol to *n*-butanol.⁵⁶ The group screened a number of diphosphine ligands with different bite angles, as well as the monochelating triphenylphosphine (PPh₃) ligand with [Ir(acac)(cod)] (1,5-cyclooctadiene) as a catalyst precursor, with sodium ethoxide base and 1,7-octadiene for the catalytic Guerbet synthesis of *n*-butanol from ethanol (Table 2).⁵⁶

Table 2: Phosphine ligand screen for the upgrading of EtOH to *n*-BuOH conducted by Ishii and co-workers⁵⁶



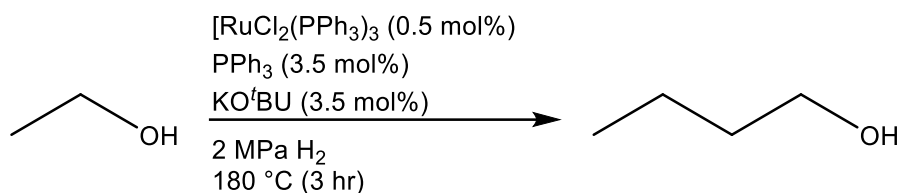
Ligand	EtOH conversion (%)	<i>n</i> -BuOH selectivity (%)	<i>n</i> -BuOH yield (%)	Turnover Number (TON)
PPh ₃	7	43	3	152
 (dppe)	8	38	3	159
 (dppb)	18	67	12	594
 (dppp)	41	51	21	1220

The monodentate PPh₃ and the small bite angle 1,2-bis(diphenylphosphino)ethane (dppe) ligands facilitated low ethanol conversions and *n*-butanol yields, and although the large bite angle 1,4-bis(diphenylphosphino)butane (dppb) ligand promoted the highest selectivity of the reaction towards *n*-butanol, the dppp ligand promoted the highest yield of *n*-butanol with [Ir(acac)(cod)].⁵⁶ The group also screened different iridium precursor catalysts with the optimised dppp ligand, and although substituting [Ir(acac)(cod)] for [IrCl(cod)]₂ promoted a marginal increase in *n*-BuOH yield (22%) over the system detailed in Table 2 (21%), the turnover number for the [Ir(acac)(cod)]/dppp catalysed reaction (1220) was much greater than that of the [IrCl(cod)]₂/dppp catalysed reaction (513).⁵⁶ The addition of 1,7-octadiene was required for an active catalytic system, and in an analogous reaction to that shown in Table 2 (dppp) conducted in the absence of 1,7-octadiene, no *n*-butanol was formed.⁵⁶ The authors proposed that 1,7-octadiene played a vital role in

the reaction as a hydrogen acceptor, or a weakly coordinating ligand to stabilise intermediate iridium species in the reaction.⁵⁶ The requirement of 1,7-octadiene in the system adds experimental complexity, and as a result, negatively affects this process when considering industrial scale-up.⁴⁴

1.5.2.2 Ruthenium catalysis

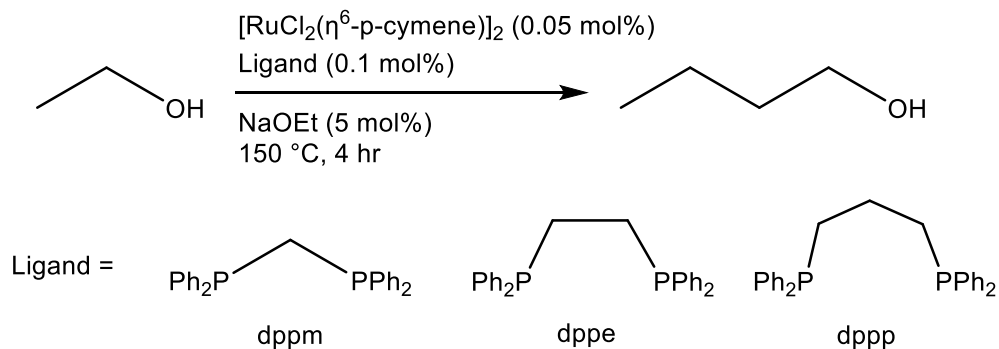
Ruthenium catalysis has also been employed in the catalytic upgrading of ethanol to butanol. A patent from the Mitsubishi Chemical Corporation in 2010 detailed the use of a variety of group VIII-X metal catalysts with phosphine ligands for the Guerbet synthesis of butanol.⁵⁸ In the patent, the use of $[\text{RuCl}_2(\text{PPh}_3)_3]$ and $[\text{Ru}(\text{acac})_3]$ precursors with excess triphenylphosphine and potassium *tert*-butoxide were detailed as catalytic systems for ethanol upgrading under hydrogen pressure.⁵⁸



Scheme 5: Optimised Ru catalysed Guerbet synthesis of n-butanol published in Mitsubishi Chemical Corporation patent.⁵⁸

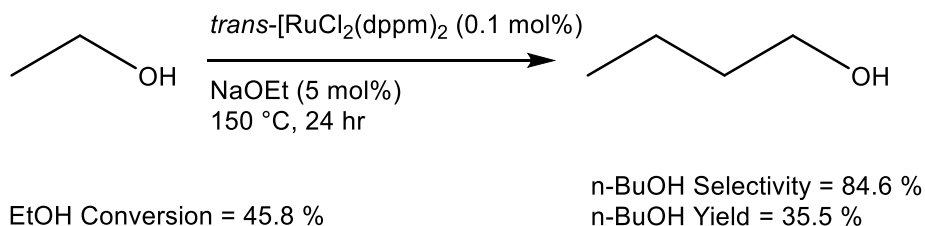
Under the conditions detailed in Scheme 5, *n*-butanol yields of up to 21 % were reported with high selectivities towards *n*-butanol of up to 93 %. In the absence of an H_2 atmosphere, the catalytic system was less active and selective, facilitating an *n*-butanol yield of 18 % with a selectivity of 59 % to the target product.⁵⁸

In 2013, the Wass group reported on the ruthenium catalysed Guerbet upgrading of ethanol to *n*-butanol employing bidentate diphosphine ligands.⁵⁹ Initial studies were conducted according to Scheme 6, where two equivalents of diphosphine ligand were added to the reaction relative to $[\text{RuCl}_2(\eta^6\text{-p-cymene})]_2$, to form $[\text{RuCl}_2(\eta^6\text{-p-cymene})(\text{Ligand})]_2$ catalysts *in situ* for the transfer hydrogenation steps in the Guerbet synthesis of *n*-butanol.⁵⁹



Scheme 6: Initial reaction conditions for ethanol upgrading employed by the Wass group.⁵⁹

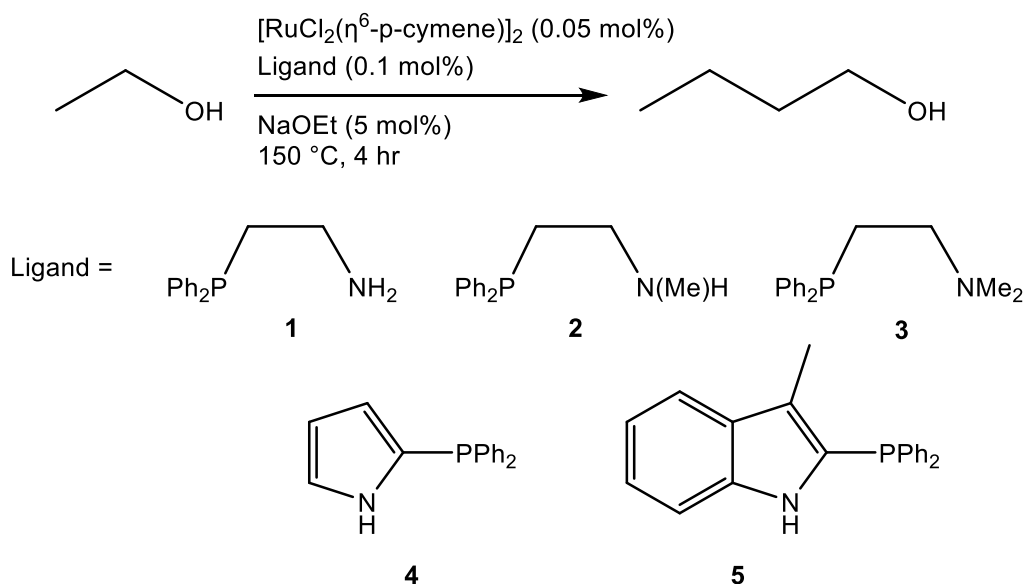
When dppe and dppp were used as the ligands in the reaction, low ethanol conversions were observed (10.2 % and 11.8 % respectively). However, when the small bite-angle bis(diphenylphosphino)methane (dppm) was employed in the reaction, the catalytic system facilitated a relatively high ethanol conversion of 20.4 %, with high selectivity towards *n*-butanol (90.0 %).⁵⁹ Unlike previously reported homogeneous catalytic systems for the upgrading of ethanol to butanol, there was no requirement for a hydrogen acceptor, or a hydrogen atmosphere. A limitation of the process shown in Scheme 6 was that under the reaction conditions employed, the ruthenium catalyst tended to be unstable, forming nanoparticles that showed low activity (and poor selectivity towards *n*-butanol) in the reaction.⁵⁹ By using the bischelate dppm complex [RuCl₂(dppm)₂] in the reaction in place of [RuCl₂(η⁶-p-cymene)(dppm)], the catalyst remained homogeneous in the system and did not decompose, allowing for longer reaction times and at the time of publication, unprecedented yields of *n*-butanol (Scheme 7).⁵⁹



Scheme 7: [RuCl₂(dppm)₂] Catalysed Guerbet synthesis of *n*-butanol developed by Wass and co-workers.⁵⁹

[RuCl₂(dppm)₂] proved to be a stable catalyst under the reaction conditions over 24 hours, and gave a high ethanol conversion of 45.8 %, while still acting as a highly selective catalyst for *n*-butanol formation (84.6 %).⁵⁹

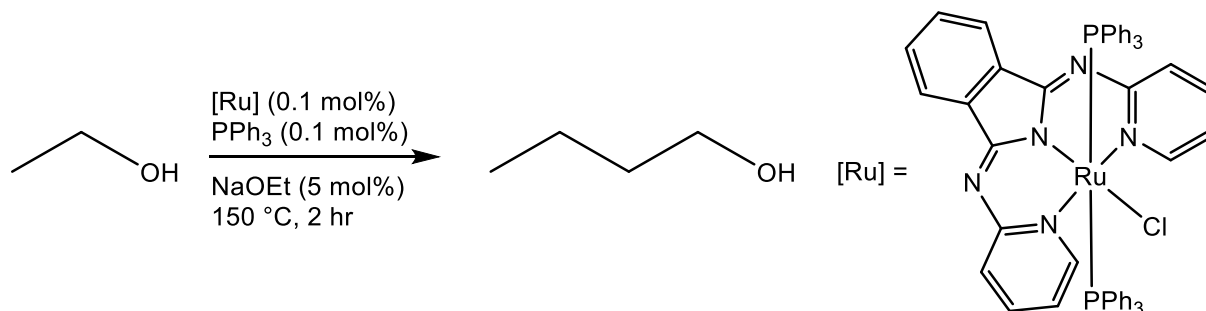
The Wass group reported again on the Guerbet upgrading of ethanol to *n*-butanol in 2015, investigating bidentate mixed donor phosphine-amine ligands.⁶⁰ In a catalytic system analogous to that shown in Scheme 6, [RuCl₂(η⁶-p-cymene)(Ligand)] catalysts were generated *in situ* using one equivalent of [RuCl₂(η⁶-p-cymene)]₂ and two equivalents of a variety of P-N ligands (Scheme 8).⁶⁰



Scheme 8: Mixed PN ligands tested with [RuCl₂(η⁶-p-cymene)]₂ for ethanol upgrading.⁶⁰

The P-N ligand **5** (Scheme 8) facilitated a good ethanol conversion of 31.4 % with a high selectivity of 92.7 % towards *n*-butanol.⁶⁰ This system was more active and selective than any of the monochelate diphosphine analogues tested by the Wass group in their previous work (Scheme 6).^{59,60} While less active than ligand **5**, the reaction using ligand **1** (Scheme 8) with [RuCl₂(η⁶-p-cymene)]₂ was more active and selective than the analogous system previously tested with dppm (Scheme 6), giving an *n*-butanol yield of 21.9 % compared to a 17.5 % yield where dppm was used. The system employed with ligand **1** also proved advantageous over that using dppm with regards to water tolerance.⁶⁰ When 10 % water was added to the reaction system, when using ligand **1** in the upgrading of ethanol according to Scheme 8, an *n*-butanol yield of 9.8 % was

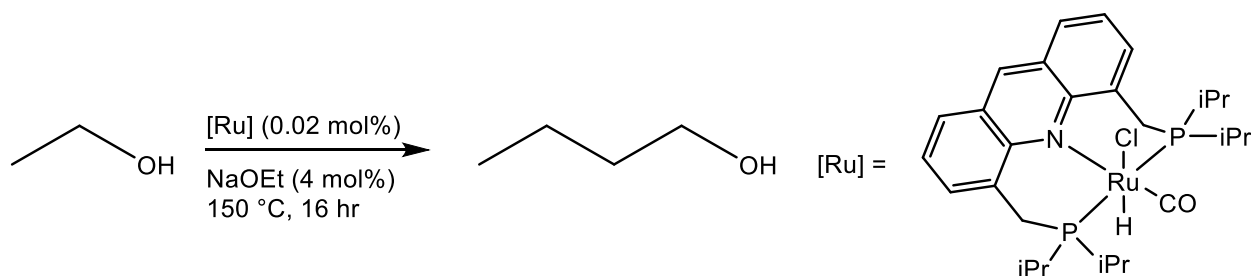
demonstrated compared to a yield of 5.3 % in an analogous system using dppm, showing the increased water tolerance of ligand **1** in the reaction.



Scheme 9: Upgrading of ethanol to *n*-butanol performed by Szymczak and co-workers.⁶¹

Szymczak and co-workers reported on air-stable ruthenium catalysts utilising amide derived N,N,N complexes (Scheme 9).⁶¹ Through the reaction shown in Scheme 9, the group were able to achieve a high ethanol conversion of 49% in a catalytic system that maintained good selectivity towards *n*-butanol (84 %), giving a yield of *n*-butanol of 41 %.⁶¹ At the time of publication, the ruthenium catalyst shown in Scheme 9 was the first active Ru-Guerbet catalyst that could be prepared in air.⁶¹

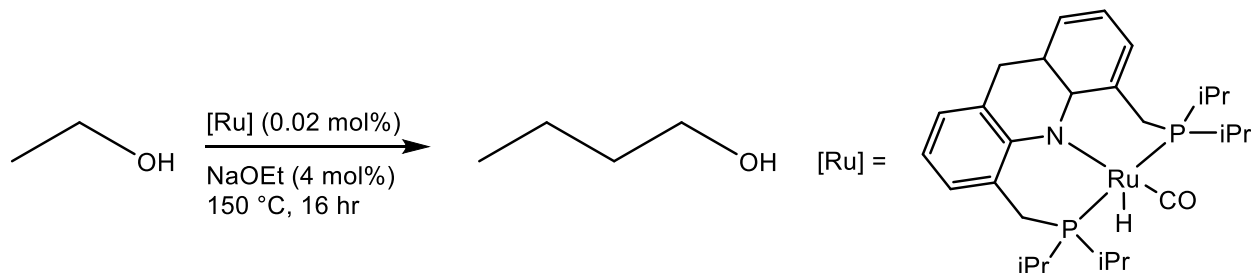
Milstein and co-workers also reported on the ruthenium catalysed Guerbet upgrading of ethanol to butanol, utilising pincer ligands to achieve very high ethanol conversions with modest *n*-butanol selectivities.⁶²



Scheme 10: Upgrading of ethanol to *n*-butanol performed by Milstein and co-workers.⁶²

The complex shown in Scheme 10 proved a highly active catalyst for the Guerbet upgrading of ethanol to *n*-butanol. Under the detailed reaction conditions (Scheme 10), the system achieved an ethanol conversion of 62.4 % with a selectivity towards *n*-butanol of 68.1 % (*n*-butanol yield of 42.5 %). The remarkable activity of the catalytic system

comes at the expense of *n*-butanol selectivity; however, the system is high yielding.⁶² Milstein and co-workers ran a similar reaction to that shown in Scheme 10, instead with 0.004 mol% of [Ru] (Scheme 10) over 168 hours, which gave a reaction TON of 18209.⁶²



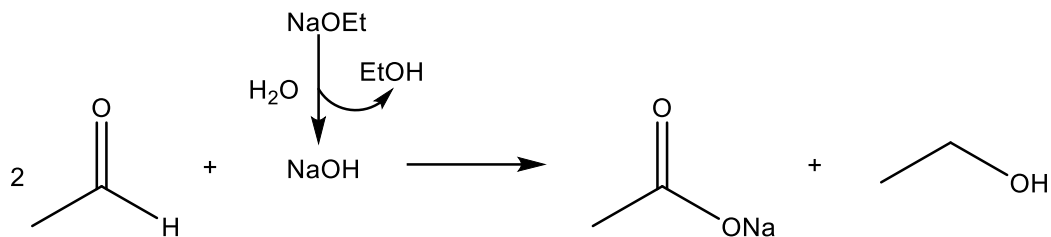
*Scheme 11: System with highest *n*-butanol yield reported by Milstein and co-workers.⁶²*

Through utilising the pincer complex shown in Scheme 11 to catalyse the transfer hydrogenation in the Guerbet upgrading of ethanol to *n*-butanol, the Milstein group achieved a very high *n*-butanol yield of 38.4 %.⁶²

1.5.2.3 Limitations of current homogeneous systems

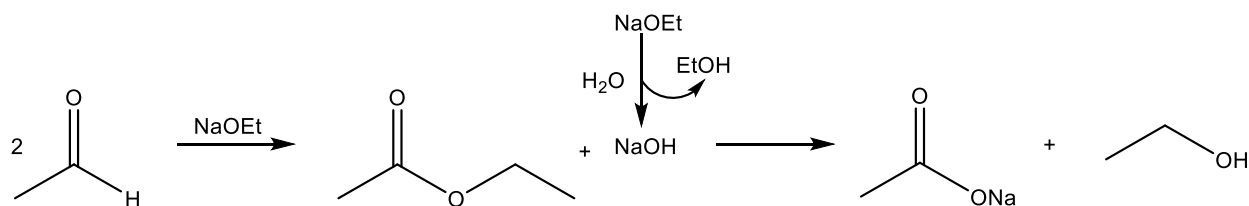
The catalytic systems described in 1.5.2 for the homogeneous catalysed Guerbet coupling of ethanol to *n*-butanol offer advantages over the heterogeneous systems outlined in 1.5.1 in terms of higher activity for ethanol conversion and in many cases, higher selectivity towards the desired *n*-butanol product. While the heterogeneous catalysts described in 1.5.1 are intrinsically basic to allow the aldol condensation of acetaldehyde to proceed, the homogeneous transfer hydrogenation catalysts described in 1.5.2 require the addition of a base to drive the same aldol condensation. Most of the systems described rely on the addition of sodium ethoxide to facilitate this aldol condensation, which is problematic for several reasons.

As shown in Scheme 4, the aldol condensation step in the Guerbet reaction produces water, which can react with the sodium ethoxide present in the homogeneous catalysed Guerbet systems to form sodium hydroxide. The presence of sodium hydroxide in the system can lead to the formation of sodium acetate *via* the Cannizzaro reaction (Scheme 12).



Scheme 12: Formation of sodium acetate via the Cannizzaro reaction.

In this reaction, sodium hydroxide can react with acetaldehyde present in the reaction to form sodium acetate as a solid by-product. The presence of sodium hydroxide in the reaction can also lead to the formation of sodium acetate by the Tishchenko reaction (Scheme 13).



Scheme 13: Formation of sodium acetate via the Tishchenko reaction.

In the Tishchenko reaction, sodium ethoxide that is added to the reaction as a homogeneous base can react with acetaldehyde to form ethyl acetate. The ethyl acetate that is formed can react with the sodium hydroxide that is produced *in situ* to form sodium acetate. The hydrolysis of sodium ethoxide to sodium hydroxide in the homogeneous catalysed Guerbet reaction is undesired from a technical standpoint. As the reagent added to the reaction to drive the aldol condensation of acetaldehyde is degrading, the whole Guerbet reaction cannot be described as catalytic, as sodium ethoxide would need to be replenished in the reaction for continuous production of *n*-butanol. And, as shown in Schemes 12 and 13, the presence of sodium hydroxide in the reaction leads to the formation of solid sodium acetate *via* the Cannizzaro and the Tishchenko reactions. There is a tendency in the literature surrounding the homogeneous upgrading of ethanol to *n*-butanol to report reaction selectivities relative to products in the liquid fraction of the product mixture that are analysed by gas chromatography (GC), while solid by-products are omitted from reported reaction selectivities. As a result, the high reaction selectivities to *n*-butanol reported by homogeneous catalytic systems for the Guerbet upgrading of

ethanol to *n*-butanol are almost certainly an over-estimation, and as a result, so are the *n*-butanol yields.

1.6 Alternative catalytic systems

Heterogeneous catalysis is advantageous to homogeneous catalysis for the upgrading of ethanol to butanol when considering the lack of alkoxide base required to drive the aldol condensation of acetaldehyde. As discussed in 1.5.2.3, the requirement for sodium ethoxide base with homogeneous transfer hydrogenation catalysts presents challenges, concerning sodium ethoxide degradation and the formation of sodium acetate by-product through Cannizzaro and Tishchenko reactions. However, homogeneous transfer hydrogenation catalysis has the major benefit over the heterogeneous systems of higher activity. There is precedent to further investigate the heterogeneous upgrading of ethanol to *n*-butanol to improve the reaction yields, as heterogeneous catalysts present advantages over homogeneous catalysts with respect to catalyst recyclability and re-use. There is also an opportunity to improve the transition metal homogeneous catalysed Guerbet reaction through the introduction of an alternative species to sodium ethoxide to drive the aldol condensation of acetaldehyde, to make truly catalytic systems that avoid the formation of side products through competing reactions. A class of materials that could be used to improve both these reactions are metal-organic frameworks (MOFs).

1.7 Metal-organic frameworks (MOFs)

Metal-organic frameworks (MOFs) are a class of materials that are characterised by nodes/metal-containing secondary building units (SBUs) that are connected by organic linkers.⁶³ Secondary building units are metal ions or clusters, while the organic linkers are species that can co-ordinate to the SBUs.⁶⁴ SBUs of different geometries have the capability of forming bonds with different numbers of linkers, while linkers can have different valency, thus MOFs can form in a variety of 1D, 2D and 3D structures.⁶⁴ MOFs are commonly synthesised *via* solvothermal reactions, where metal salts and organic linkers are combined in high boiling point solvents and heated at relatively low

temperatures.⁶⁵ However, different techniques can be employed to synthesise MOFs, like microwave irradiation,⁶⁶ mechanochemistry,⁶⁷ and sonochemistry.⁶⁸

One of the first reported MOFs was MOF-5, which consisted of Zn cluster SBUs that were connected by 1,4-benzenedicarboxylate linkers.⁶⁹ $Zn_4(O)$ tetrahedra form the basis of the SBUs in MOF-5, which are connected by 1,4-benzenedicarboxylate (BDC) linkers. The cubic unit cell of MOF-5 is shown in Figure 6, where these unit cells join to form a three-dimensional metal-organic framework.

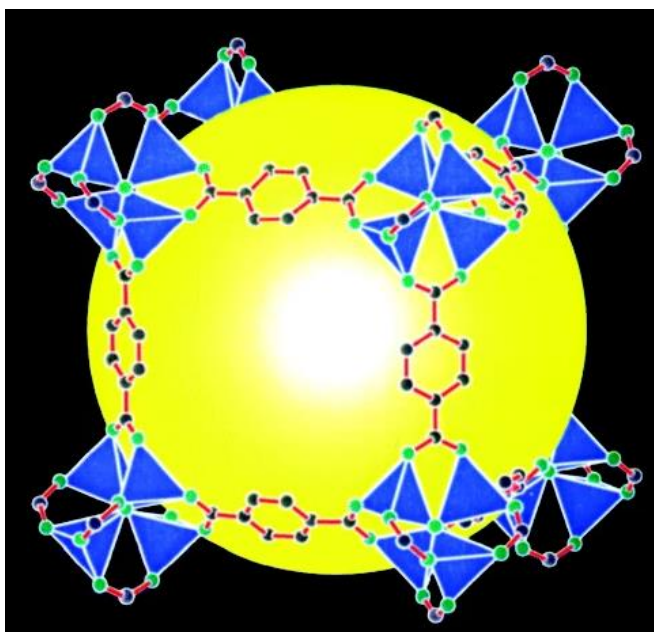


*Figure 6: Structure of MOF-5.*⁶⁹

The combination of $Zn_4(O)$ SBUs and BDC linkers leads to the formation of MOF-5, however, different linkers can be used instead of BDC with the same SBU metal cluster to form MOFs with different geometries and pore sizes (Figure 7).⁷⁰ As shown in Figure 7, the combination of the $Zn_4(O)$ cluster and BDC forms MOF-5, however, BDC can be used in combination with another linker of a different size to make a new structure with similar cubic geometry. If BDC is combined with naphthalene dicarboxylic acid (NDC) then the UMCM-8 MOF is formed, a framework with different pore sizes. Using the trivalent linker 4,4',4''-Benzene-1,3,5-triyl-tris(benzoic acid) (BTB) with $Zn_4(O)$ as a SBU leads to the formation of MOF-177, while a linker mixture of BTB and NDC with $Zn_4(O)$ SBUs forms the MOF DUT-6.⁷⁰ These different structures highlight how changing the

linker in a MOF can have a profound effect on the structure and pore size of the resulting framework, when using the same exact metal cluster as an SBU in the MOF.⁷⁰

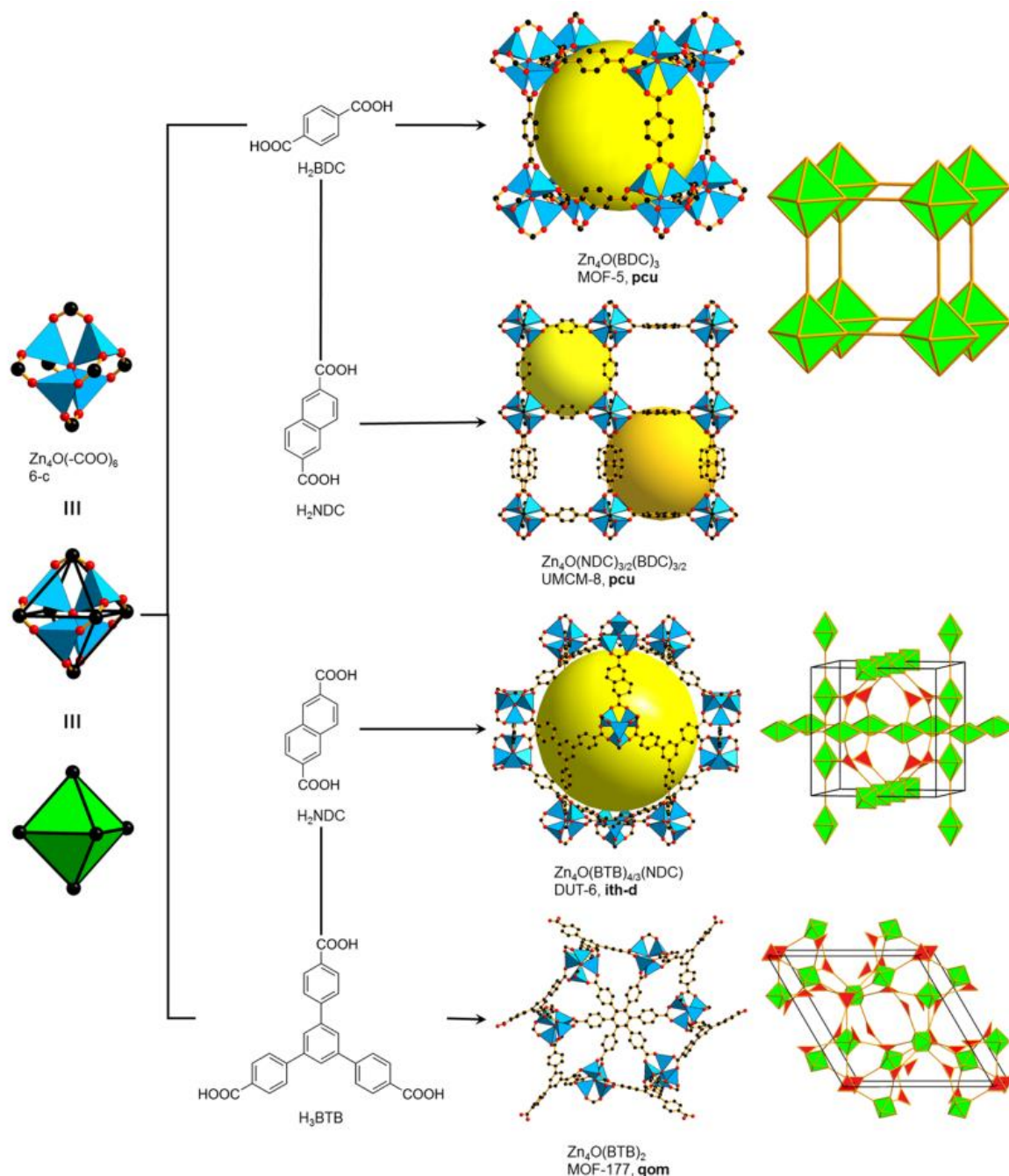


Figure 7: Structures of different MOFs with Zn_4O SBUs.⁷⁰

Another method that can be employed to vary the structure of a MOF is to change the connection geometry of the metal cluster SBU. Through changing the geometry of the SBU, and the number of metal linkers that can connect to it, different SBUs with identical

linkers can be used to make MOF structures with different geometries and pore sizes (Figure 8).⁷¹

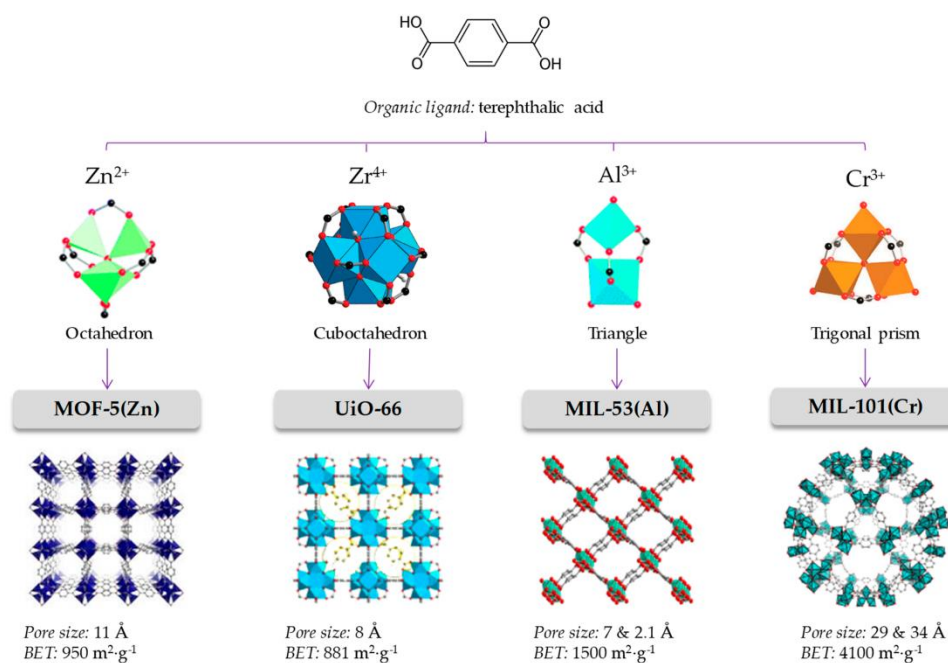


Figure 8: Different SBUs combined with BDC to form different MOFs.⁷¹

As previously detailed, the combination of BDC (terephthalic acid) with Zn^{2+} octahedra leads to the formation of MOF-5, while Zr^{4+} SBUs in combination with BDC forms UiO-66 as a structure. Triangular Al^{3+} and trigonal prismatic Cr^{3+} nodes in combination with BDC form MIL-53 and MIL-101 structures respectively.⁷¹ All these structures have very different pore sizes and surface areas, which further highlights how the choice of metal cluster SBU and organic linker have a dramatic effect on the structure of the resulting MOF made through their connectivity.

MOFs are a diverse class of materials that have been studied for a variety of applications. One of which is hydrogen gas storage, where the porous nature of MOFs and their high surface area can be utilised as physisorbent materials for the storage of hydrogen, while on some frameworks, reaction sites can be exploited for post-synthetic modification to introduce sites for stronger binding.⁷² The versatility in MOF structure, in terms of their tunable size, morphology and chemical properties, as well as their high surface area render MOFs ideal drug carriers, and they have been researched in drug

delivery for cancer therapy for example.⁷³ Luminescent MOFs have been screened as sensor devices for environmental pollutants,⁷⁴ while MOFs also have characteristics which make them ideal heterogeneous catalysts.

1.8 MOF Catalysis

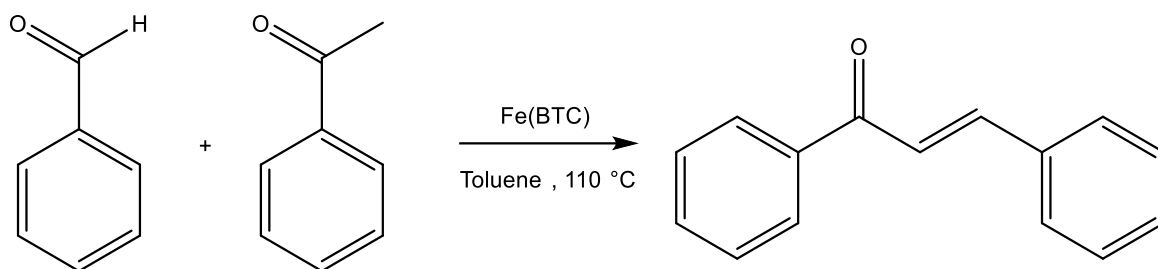
MOFs have a general set of characteristics that make them ideal heterogeneous catalysts like well-defined porosity, structural diversity and the presence of accessible organic linkers and open metal sites.⁷⁵ The catalytic activity of a MOF can come from a variety of different functionalities, where the framework can have intrinsic catalytic activity, but can also act as a support for a catalytically active moiety.⁷⁵

1.8.1 Catalysis by open metal sites

The intrinsic catalytic activity of a MOF can stem from the metal nodes. MOFs can be synthesised that intrinsically possess open metal sites on SBUs that are catalytically active, and there are many literature examples of reactions that are catalysed by the open metal sites on MOFs. Some examples of catalysis by open metal sites on MOFs include the aerobic oxidation of cyclooctane to cyclooctenone and cyclooctanol in the absence of peroxides or radical initiators by Fe(BTC) (1,3,5-benzenetricarboxylic acid),⁷⁶ while Lewis acidic Cu sites on $\text{Cu}_3(\text{BTC})_2$ (HKUST-1) catalyse the cyanosilation of benzaldehyde.⁷⁷ There has been literature interest in this branch of MOF catalysis, with many open metal site catalysed reactions covered in recent reviews of the field as a whole.^{75,78,79} However, when considering the applicability utilising MOFs in the Guerbet reaction, their ability to catalyse aldol condensation reactions is of particular interest.⁷⁹

1.8.1.1 Aldol catalysis by MOFs

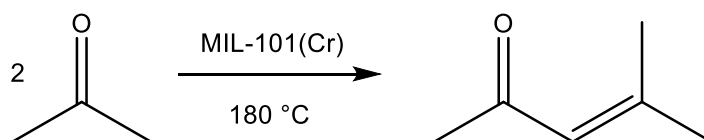
Garcia and co-workers investigated the Claisen-Schmidt condensation reaction between benzaldehyde and acetophenone using a variety of different MOFs as catalysts in the reaction (Scheme 14).⁸⁰



Scheme 14: Claisen-Schmidt reaction catalysed by Fe(BTC) by Garcia and co-workers.⁸⁰

The reaction shown in Scheme 14 details the optimised reaction system developed by the group for the crossed aldol condensation reaction, where the iron-based Fe(BTC) MOF was the most active catalyst that they tested in the reaction, facilitating a 98 % yield of the chalcone product.⁸⁰ Fe(BTC) is composed of trimers of Fe octahedra that are joined together by 1,3,5-benzenetricarboxylic acid linkers, where the Lewis acidic iron SBUs are the active catalyst for the Claisen Schmidt reaction of acetophenone and benzaldehyde (Scheme 14).⁸⁰

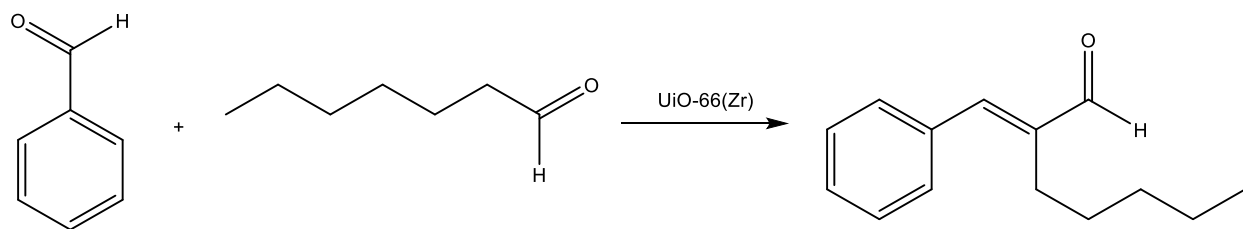
He and co-workers investigated the aldol coupling of acetone to mesityl oxide using MIL-101(Cr) as a catalyst (Scheme 15).⁸¹ MIL-101 is a MOF that is formed by SBU trimers of chromium octahedra that are connected by BDC linkers to form an augmented MTN zeotype structure.⁸²



Scheme 15: Aldol coupling of acetone to mesityl oxide performed by He and co-workers.⁸¹

Under the conditions specified in Scheme 15, the MIL-101(Cr) facilitated a 60.1 % conversion of acetone with a selectivity towards mesityl oxide of 74.9 %.⁸¹ The Lewis acidic chromium centres present at the SBUs of the MIL-101(Cr) framework act as active catalytic sites for this aldol coupling of acetone, and subsequent dehydration reaction to form mesityl oxide.⁸¹

The use of UiO-66(Zr) as a catalyst in the aldol condensation of benzaldehyde and heptanal to form jasminaldehyde was investigated by De Vos and co-workers (Scheme 16).⁸³



Scheme 16: UiO-66(Zr) catalysed formation of jasminaldehyde by De Vos and co-workers.⁸³

UiO-66(Zr) is comprised of $Zr_6O_4(OH)_4$ SBUs that are joined together by terephthalate linkers, and has a high thermal stability.⁸³ In a solvent free system, the UiO-66(Zr) catalyst that the group tested facilitated a yield of jasminaldehyde of 85% over 24 hours, while an analogue prepared using amino-terephthalic acid ligands was more active, giving a yield of 92%.⁸³ The Lewis acid sites from the zirconium SBU activate benzaldehyde, while $-NH_2$ groups in close proximity activate heptanal to enhance the crossed-aldol cross coupling.⁸³

The aldol condensation reactions detailed here by MOFs all utilise frameworks based on different metals SBUs, however they all share the same property in Lewis acidity. Lewis acidic MOFs have shown activity in a variety of aldol condensation reactions and propose an alternative aldol catalyst in the Guerbet upgrading of ethanol to *n*-butanol.

1.8.2 Catalysis by immobilised metals

Not only can a MOF demonstrate intrinsic catalytic properties, but they can also act as support materials for catalytically active species in a variety of different ways. Metal nanoparticles (NP) can be introduced into the pores of MOFs to form NP@MOF composite materials through processes like chemical vapour deposition (CVD) and solid grinding, and NP@MOF composites made *via* these methods have been shown to be catalytically active in several reactions.⁸⁴ For example, Fischer and co-workers demonstrated that Cu@MOF-5 prepared *via* CVD was catalytically active for the production of methanol from syngas.⁸⁵

MOFs can act as a support for catalytically active nanoparticles; however, MOFs have also been applied as supports for immobilised homogeneous catalysts. One example of how this can be achieved is by functionalising the linkers of a MOF to contain an

immobilised ligand and using this ligand to co-ordinate a metal complex. An example of this method has been demonstrated by Lu and co-workers (Figure 9).⁸⁶



Figure 9: Lu and co-workers' method to immobilising a homogeneous Cu catalyst on UiO-66-NH₂.⁸⁶

The group immobilised Cu²⁺ ions onto a MOF by first synthesising UiO-66-NH₂, a framework with amine functionalised linkers. By reacting this MOF with salicylaldehyde, the linker was functionalised with an N-O ligand that was used to co-ordinate CuCl₂, Cu(NO₃)₂ and Cu(OAc)₂, forming frameworks that supported an immobilised homogeneous complex.⁸⁶ The UiO-66-Sal-CuCl₂ catalyst shown in Figure 9 was the most active catalyst of the three variants for the aerobic oxidation of benzyl alcohol, with no leaching of the copper catalyst observed.⁸⁶

Another method that has been employed to incorporate molecular catalysts into MOFs is *via* a post-synthetic exchange reaction, an example of this method being from Su and co-workers.⁸⁷ Through synthesising the MOF UiO-67, with Zr₆-derived SBUs and biphenyl-4,4'-dicarboxylate linkers, a post synthetic exchange (PSE) reaction could be carried out to replace some of the linkers with homogeneous ruthenium and rhodium complexes (Figure 10).⁸⁷

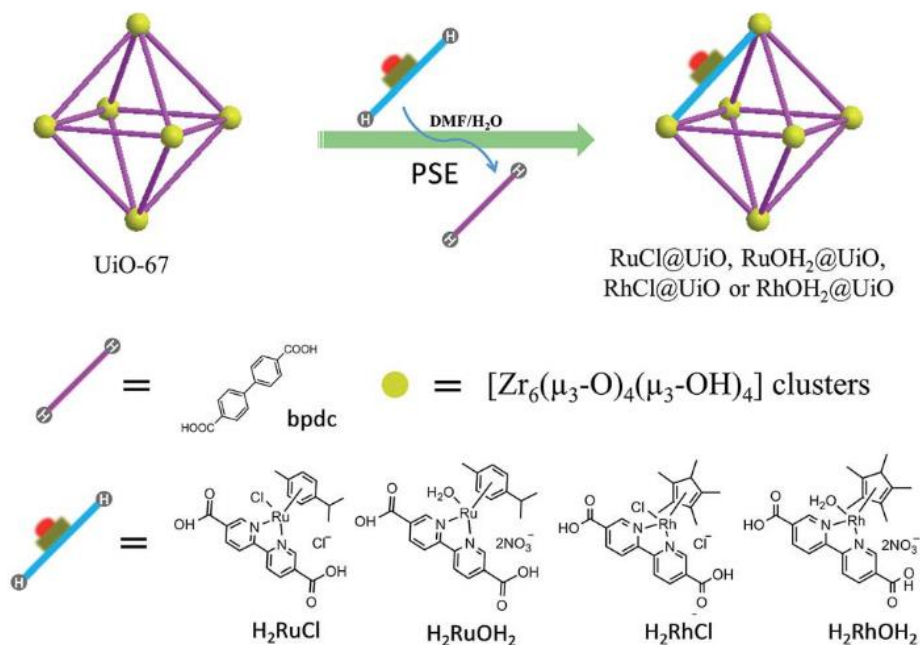


Figure 10: PSE method employed by Su and co-workers to immobilise Ru and Rh complexes in UiO-67.⁸⁷

Through taking the pristine MOF and reacting it with homogeneous complexes with 2,2-bipyridyl-5,5-dicarboxylic acid in a mixture of H₂O and DMF, the group managed to exchange linkers on the pristine UiO-67 MOF with a variety of Ru and Rh complexes, thus immobilising them within the framework.⁸⁷ The resulting catalysts were active for hydrogen evolution and CO₂ reductions.⁸⁷

Another technique that has been utilised to incorporate homogeneous complexes within a MOF is through aperture-opening encapsulation. This method (Figure 11) has been used by Tsung and co-workers, who encapsulated a well-known homogeneous CO₂ hydrogenation catalyst, [RuH(CO)(Cl)(^tBuPNP)] (PNP = 2,6-bis((di-tert-butylphosphino)methyl)pyridine) within the pores of UiO-66(Zr), developing a MOF-immobilised catalyst that had advantages over the homogeneous analogue, such as the ability to be recycled five times with and a lack of catalyst decomposition.⁸⁸

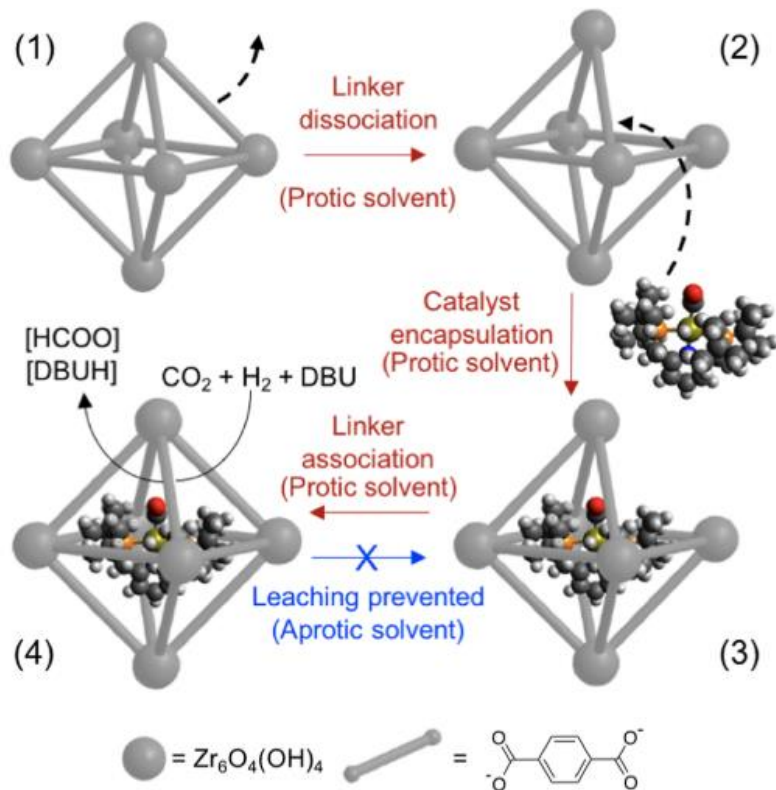


Figure 11: Aperture-opening encapsulation of $[\text{RuH}(\text{CO})(\text{Cl})(\text{tBuPNP})]$ developed by Tsung and co-workers.⁸⁸

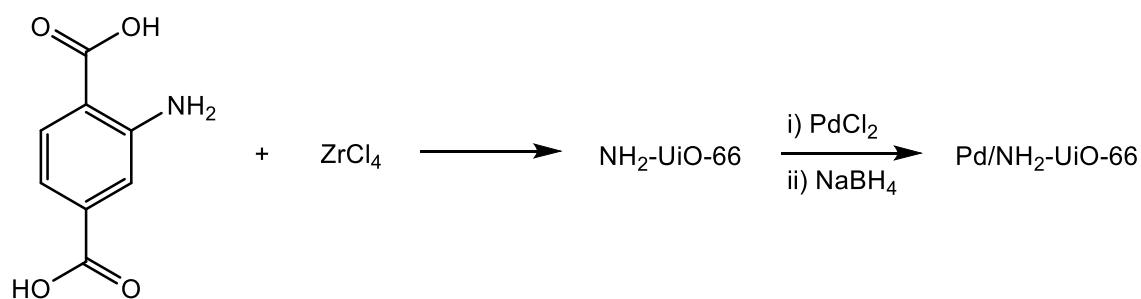
By reacting the pristine UiO-66 with MeOH, an aperture opens in the framework by removal of a BDC linker (Figure 11, (2)), which is large enough in size to allow the homogeneous $[\text{RuH}(\text{CO})(\text{Cl})(\text{tBuPNP})]$ complex to enter the pores of the framework.⁸⁸ Through association of the BDC linker back onto the framework, the complex is trapped inside the UiO-66, as the pore size of the framework is too small to allow it to leach.⁸⁸ This resulting MOF encapsulated Ru catalyst is active for the hydrogenation of CO_2 to formate, and through carrying out catalysis in DMF as a solvent, leaching of the catalyst is prevented.⁸⁸ The encapsulation of $[\text{RuH}(\text{CO})(\text{Cl})(\text{tBuPNP})]$ inside UiO-66 forms a catalyst with benefits over the homogeneous analogue, as the catalyst could be recycled with no bimolecular decomposition, and was less prone to poisoning.⁸⁸ The poisoning of the ruthenium catalyst by thiols is known, and *via* exposure of the encapsulated catalyst to thiols of different size, it was shown that sterically hindered thiols reduced the activity of $[\text{RuH}(\text{CO})(\text{Cl})(\text{tBuPNP})]$ to a much greater extent than the analogous encapsulated

catalyst. This comes as a result of slow diffusion of the thiol through the MOF structure to access the active homogeneous catalyst.

When considering the Guerbet upgrading of ethanol to *n*-butanol, transfer hydrogenation catalytic activity would be a property that would be desired from a metal-organic framework, and some of the principles described in 1.8.2 have been applied to synthesise MOF transfer hydrogenation catalysts.

1.8.2.1 MOF Transfer hydrogenation catalysis

Nanoparticles supported on MOFs have been demonstrated as transfer hydrogenation catalysts. For example, Ahn and co-workers synthesised Pd nanoparticles encapsulated in an amine functionalised derivative of UiO-66 (Pd/NH₂-UiO-66) for the catalytic transfer hydrogenation of nitrobenzene to aniline with formic acid as a hydrogen source.⁸⁹ The group synthesised pristine NH₂-UiO-66 from ZrCl₄ and 2-aminoterephthalic acid, and then prepared immobilised Pd nanoparticles within the structure through an anionic exchange with a subsequent chemical reduction (Scheme 17).⁸⁹

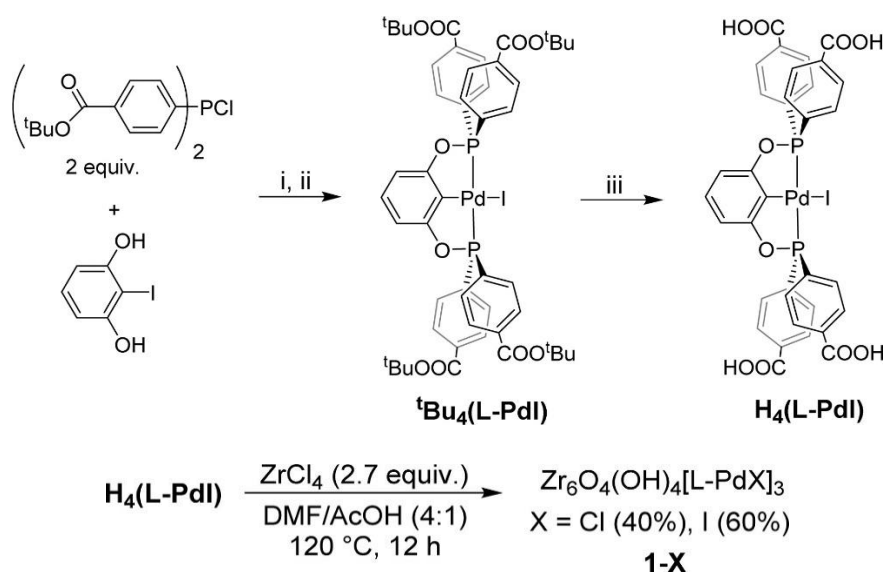


Scheme 17: Synthesis of Pd/NH₂-UiO-66 by Ahn and co-workers for the transfer hydrogenation of aniline.⁸⁹

The Pd/NH₂-UiO-66 catalyst was tested for the transfer hydrogenation of nitrobenzene to aniline and was highly active and selective (98 % conversion, 99 % selectivity),⁸⁹ while a NH₂-UiO-66 analogue without the presence of immobilised Pd nanoparticles was inactive for the same conversion,⁸⁹ indicating that the immobilised nanoparticles were catalysing the transfer hydrogenation reaction. Another example of transfer hydrogenation catalysis from nanoparticles immobilised within a MOF is the hydrogenation of cinnamaldehyde to cinnamyl alcohol by Pt nanoparticles in a UiO-66 framework by Hou and co-workers.⁹⁰ By adding H₂PtCl₆·6H₂O into the reaction mixture of a UiO-66 synthesis reaction, the group

synthesised Pt nanoparticles embedded in a UiO-66 framework (Pt/UiO-66), which was an active catalyst for the transfer hydrogenation of cinnamaldehyde with isopropanol (IPA) as a hydrogen source.⁹⁰

Transition metal immobilisation chemistry within the linkers of a MOF has also been demonstrated as a way to incorporate a transfer hydrogenation catalyst onto a MOF. Wade and co-workers have investigated the transfer hydrogenation of benzaldehydes using a MOF catalyst with Pd complexes immobilised within the linkers of the framework.⁹¹ They synthesised a homogeneous Pd pincer complex, with tetra carboxylate functionality, allowing the complex to act as a linker in the synthesis of a zirconium derived MOF (Scheme 18).⁹¹



Scheme 18: Synthesis of Pd pincer complex by Wade and co-workers and subsequent incorporation into a MOF.⁹¹

Subsequent ligand exchange of I⁻ for TFA⁻ on the Pd centres of the MOF generated a highly active catalyst for the transfer hydrogenation of benzaldehyde with formic acid as a source of hydrogen. The homogeneous Pd analogue of the catalytically active MOF was inactive for the same transfer hydrogenation reaction, due to catalyst decomposition, while the immobilisation of the Pd catalyst within the MOF prevented decomposition.⁹¹

1.8.3 MOFs in Guerbet catalysis

While the area of MOF catalysis has become well established in recent years, examples of MOF catalysed Guerbet chemistry are limited in literature. This is surprising considering that MOF catalysed aldol condensations and transfer hydrogens have been well reported in literature.

Li and co-workers reported on Pd@UiO-66 catalysts for the catalytic upgrading of ethanol to *n*-butanol *via* the Guerbet reaction.⁹² Through an impregnation method, the group prepared Pd@UiO-66 catalysts with different loadings of Pd within the pores of the MOF and tested these materials as catalysts for the continuous upgrading to *n*-butanol (Figure 12).⁹²

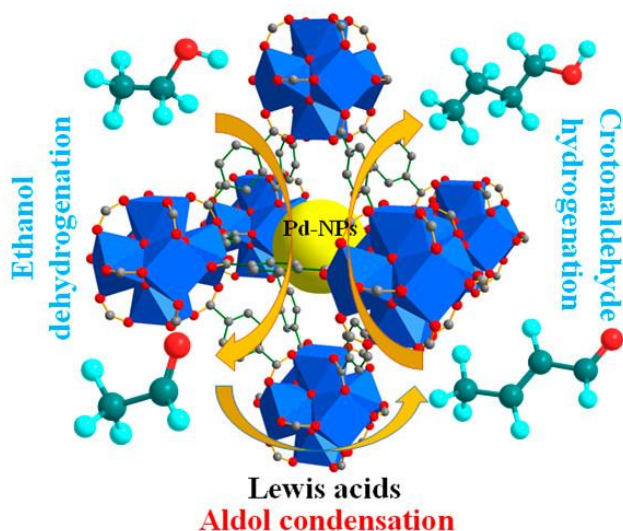
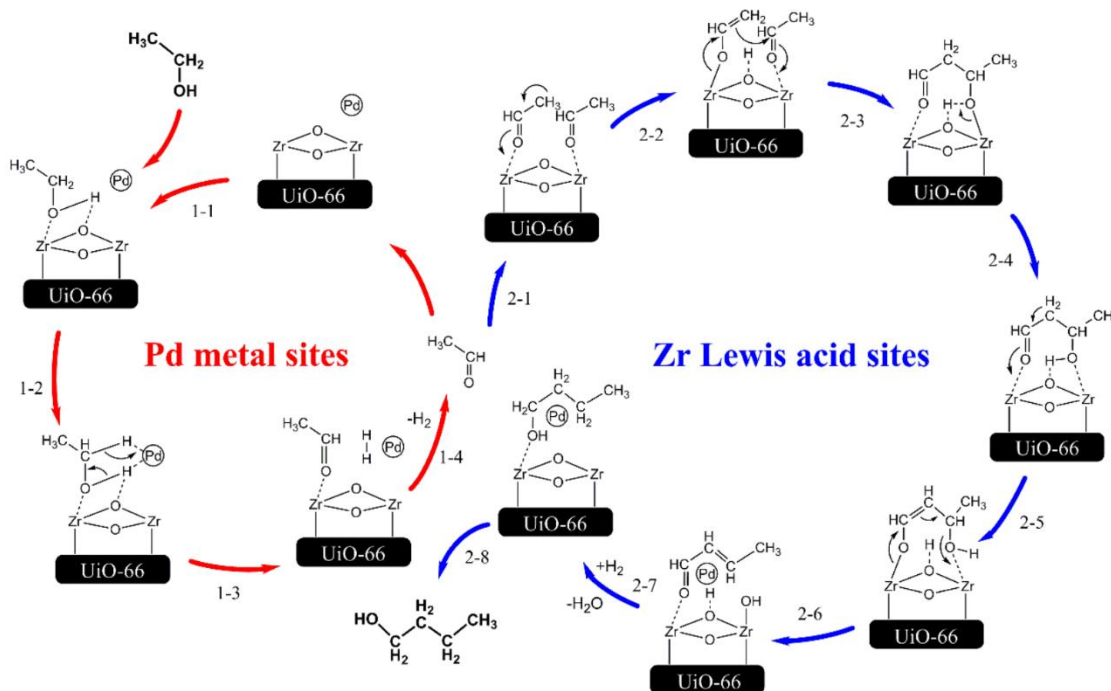


Figure 12: Pd@UiO-66 catalyst prepared by Li and co-workers for the Guerbet synthesis of *n*-butanol.⁹²

UiO-66(Zr) was chosen as the MOF to support the Pd nanoparticles due to the Lewis acidic nature of the SBUs, which catalyse the aldol condensation of acetaldehyde.⁹² While the Pd nanoparticles supported within the MOF catalyse the dehydrogenation of ethanol to acetaldehyde, and the hydrogenation of the crotonaldehyde that is formed from the node catalysed aldol condensation of acetaldehyde (Scheme 19).⁹²



Scheme 19: Mechanism for the Guerbet synthesis of *n*-butanol proposed by Li and co-workers.⁹²

A variety of analogues of Pd@UiO-66 were tested for the Guerbet synthesis of *n*-butanol, with different wt % loadings of Pd-H present in the pores of the framework. 2wt %Pd@UiO-66(Zr) was the most active, and over 200 hours at 250 °C, facilitated an ethanol conversion of 49.8 % with a selectivity towards *n*-butanol of 48.6% (24.2 % yield) in a continuous system.⁹² Over the long reaction duration of 200 hours, the catalyst showed good stability which the authors attributed to the electrostatic attraction between the Pd nanoparticles inside the pores of the MOF with the Zr₆ nodes, as well as a confinement effect provided by the pores.⁹² The authors claimed this to be the first MOF-supported metal catalyst for the upgrading of ethanol to *n*-butanol in a continuous system.⁹²

MOF supported nanoparticle transfer hydrogenation chemistry for the Guerbet upgrading of ethanol to *n*-butanol was also investigated by Neumann *et al.*, who synthesised bimetallic RuNi nanoparticles supported on a nickel derived MOF (RuNi@MOF).⁹³ The group synthesised Nickel MOFs (Figure 13 - Ni₈(OH)₄(OH₂)₂(L1)₆ and Ni₃(OH)₄(OH₂)₂(L2)₆), and used these frameworks to enclose [Ru(nbd)Cl₂]_n (norbornadiene) (Figure 13).⁹³

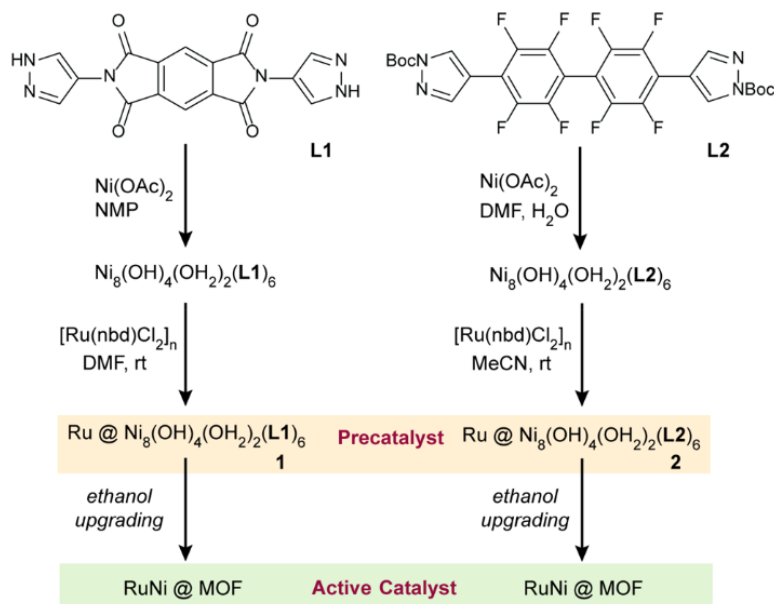


Figure 13: RuNi@MOF catalysts prepared by Neumann et al. for the Guerbet upgrading of ethanol to *n*-butanol.⁹³

These MOFs were then tested as transfer hydrogenation catalysts for the Guerbet upgrading of ethanol to *n*-butanol with the addition of sodium ethoxide base as an aldol catalyst. The catalytic reactions were conducted at 170 °C, which led to the reduction of the Ru complex inside the MOFs to form Ru nanoparticles, while also inducing the partial reduction of the nickel nodes of the MOF, leading to the formation of catalytic bimetallic RuNi nanoparticles supported on the MOF.⁹³ The two active catalysts highlighted in Figure 13 were tested as transfer hydrogenation catalysts in the Guerbet upgrading of ethanol with various loadings of sodium ethoxide base.⁹³ With a 5.7 wt% loading of NaOEt in the reaction over 14.5 hours, the RuNi@MOF catalyst derived from L2 could achieve a selectivity towards *n*-butanol of 99.9 % when considering products in the liquid phase, and 99 % when all products of the reaction are considered. This is a remarkable selectivity towards Guerbet coupled products, as this catalyst can effectively negate higher alcohol coupling of the butanol product, while also limiting undesired sodium acetate formation. However, these metrics are achieved with a small ethanol conversion of 3.9 %.⁹³ Maximum TON (729,526) could be achieved with a 21 % loading of NaOEt using the catalyst derived from L1 (Figure 13), maintaining a very high selectivity towards *n*-butanol in the product liquid fraction of the reaction (99.9 %), however, this was

achieved with more solid by-product formation (overall selectivity = 69 %) over a long reaction duration of 89 hours with moderate ethanol conversion (21.2 %).⁹³

1.8.3.1 Limitations of current MOF Guerbet catalysts

The work of Li and co-workers and of Neumann *et al.* present interesting methods to how MOF-catalysis can be applied to the Guerbet reaction,^{92,93} and are important pioneering works in this newly developing field. However, the catalytic systems detailed in 1.8.3 do have some drawbacks compared to some of the prior traditional heterogeneous and homogeneous catalytic systems described in 1.5. The work of Neumann *et al.* presents a heterogeneous transfer hydrogenation catalyst that can be used in place of the homogeneous catalysts detailed in 1.5.2, which has the inherent advantageous properties of catalyst recovery and recycling that arise from being heterogeneous. However, to form *n*-butanol from ethanol, the RuNi@MOF catalysts require the presence of alkali metal base, which as a result, leads to sodium acetate production.⁹³ Although solid by-product formation can be limited by the addition of low loadings of sodium ethoxide, this comes with the sacrifice of low ethanol conversions. And even when sodium ethoxide loading is increased to maximise TON at the expense of higher solid by-product formation, ethanol conversion is still modest when compared to some of the pure homogeneous systems outlined in 1.5.2.

The Pd@UiO-66(Zr) catalyst developed for the Guerbet upgrading of ethanol to *n*-butanol by Li and co-workers presents a true heterogeneous catalyst for the reaction, utilising Lewis acidic Zr nodes and supported Pd nanoparticles to catalyse the aldol and transfer hydrogenation steps in the Guerbet reaction respectively.⁹² Thus providing a recoverable and re-usable catalyst for the Guerbet reaction that is more active for ethanol conversion than the heterogeneous Guerbet catalysts described in 1.5.1, without the requirement for sodium ethoxide base.⁹² However, the high activity comes with lower product selectivity towards *n*-butanol, where under reaction conditions optimised for butanol yield, selectivity towards the target product is just over 50 %, which is relatively low compared to other heterogeneous systems.⁹² The Pd@UiO-66 catalyst from Li and co-workers also requires a high temperature of 250 °C to achieve this activity, which is considerably higher than temperatures required to achieve more selective reactions (to

products in the liquid fraction) by homogeneous catalysed systems for the Guerbet upgrading of ethanol.⁹²

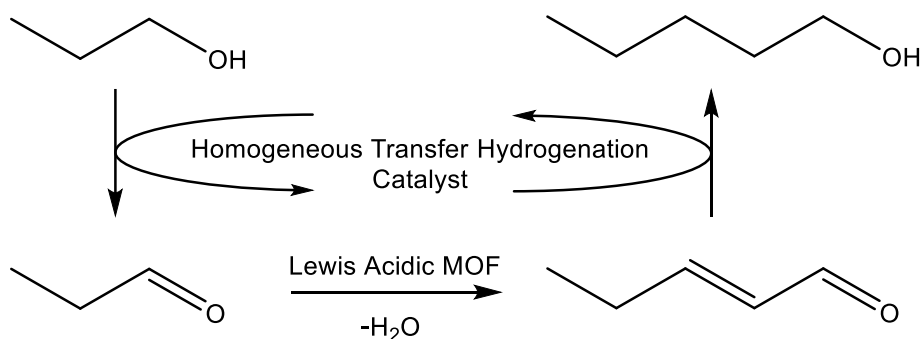
Neither of the MOF catalysts developed for the Guerbet upgrading of ethanol to butanol have resolved all of the issues associated with previously reported homogeneous and heterogeneous catalytic systems. However, both systems rely on supported metal nanoparticles within the frameworks to catalyse the dehydrogenation of ethanol and hydrogenation of crotonaldehyde. An area of MOF catalysis that has yet to be explored for the transfer hydrogenation steps in the Guerbet reaction is the immobilisation of homogeneous transition metal catalysts within a framework. The concept of using MOF linkers to immobilise transition metal catalysts was introduced in 1.8.2, and an example from Wade and co-workers showed how immobilised Pd complexes on the linkers of a MOF were utilised for the transfer hydrogenation of benzaldehyde with formic acid.⁹¹ Although Neumann *et al.* encased $[\text{Ru}(\text{nbd})\text{Cl}_2]_n$ within a MOF, under catalytic conditions for the Guerbet reaction, the complex reduced to nanoparticles.⁹³ The immobilisation of homogeneous transition metal transfer hydrogenation catalysts within the framework of a MOF presents an ideal route to forming an active and selective transfer hydrogenation catalyst for the Guerbet reaction, considering the high ethanol conversions and *n*-butanol selectivities that homogeneous complexes have been shown to facilitate. Combining immobilised transfer hydrogenation catalysts within the framework of a MOF with Lewis acidic SBUs has the potential to form a highly active and selective single heterogeneous catalyst for the Guerbet synthesis of *n*-butanol.

1.9 Thesis scope

The area of MOF catalysed Guerbet chemistry is further explored in this thesis, in both looking at how heterogeneous MOFs can be implemented into traditional homogeneous catalysed Guerbet reactions, while also exploring the potential of immobilising homogeneous transfer hydrogenation catalysts into MOFs.

The Lewis acidic nature of certain MOFs have been utilised in aldol condensation reactions, while in the Pd@UiO-66 catalyst developed by Li and co-workers,⁹² the Lewis

acidic zirconium nodes of the framework catalyse the aldol condensation of acetaldehyde in the Guerbet synthesis of *n*-butanol. The role of examining MOFs as heterogeneous Lewis acid aldol catalysts in catalytic Guerbet systems with homogeneous transfer hydrogenation catalysts is yet to be explored and presents an interesting alternative to sodium ethoxide base traditionally used in these reactions (Scheme 20).



*Scheme 20: Proposed homogeneous/heterogeneous catalysed Guerbet upgrading of ethanol to *n*-butanol.*

Lewis acidic MOFs present an attractive alternative to conventional sodium ethoxide base to catalyse the aldol condensation in the Guerbet upgrading of ethanol. Firstly, unlike the sodium ethoxide base, which is hydrolysed in the reaction by water generated from the aldol condensation of acetaldehyde, the presence of a heterogeneous catalyst offers the prospect of a truly catalytic reaction using a homogeneous transfer hydrogenation catalyst. While the lack of sodium ethoxide base in the reaction would prevent the formation of sodium acetate *via* the Tishchenko and Cannizaro reactions, which would be beneficial towards the reaction in terms of product isolation, waste management and overall reaction selectivity towards the desired *n*-butanol product. By using a heterogeneous MOF aldol catalyst alongside a homogeneous transfer hydrogenation catalyst, the benefits of traditional homogeneous catalysed ethanol upgrading reactions like high ethanol conversion and high selectivity towards butanol (of liquid products) could be achieved with a recyclable catalyst without the formation of undesired byproducts. The combined homogeneous/heterogeneous catalysed Guerbet upgrading of ethanol has been explored, screening different MOFs and homogeneous transfer hydrogenation catalysts to optimise the process, while the recyclability of this type of system has also been tested.

The idea of immobilising a homogeneous transfer hydrogenation on a Lewis acidic MOF has also been studied, with the aim of synthesising a heterogeneous Guerbet catalyst with high activity and selectivity towards *n*-butanol for the upgrading of ethanol. Different methods have been explored to incorporate homogeneous complexes into MOFs, including pre-forming homogeneous complexes and using them as linkers in the synthesis of MOFs (Figure 14 – **a**), using pre-formed MOFs with linker ligands to complex transition metals (Figure 14 – **b**), and attempting post-synthetic exchange reactions with homogeneous complexes and pristine MOFs (Figure 14 – **c**).

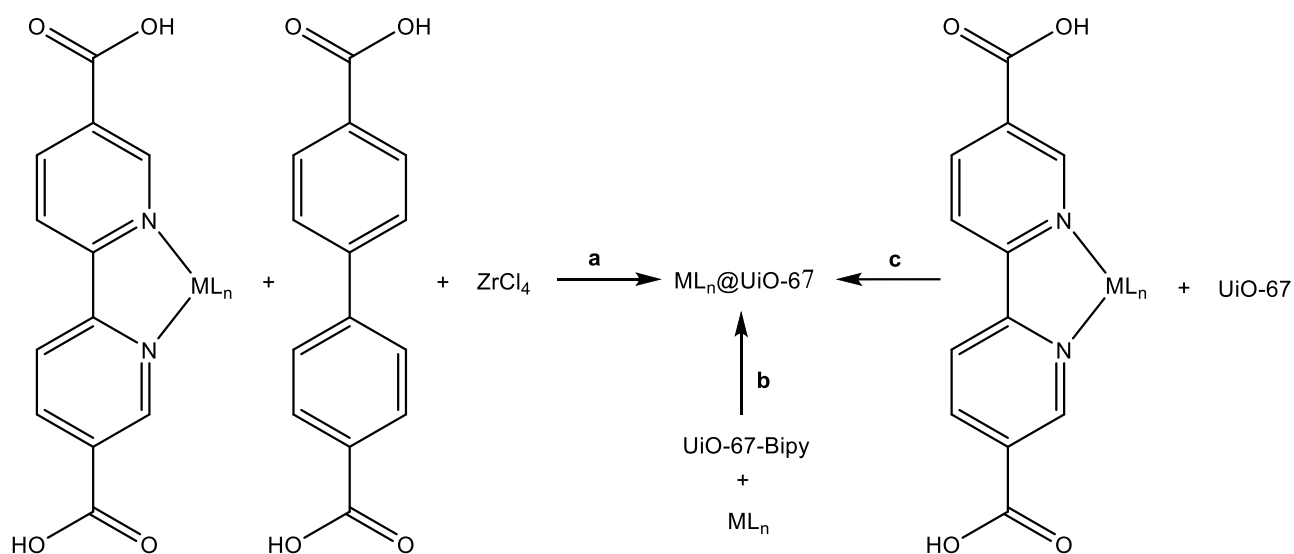


Figure 14: Methods of synthesising $ML_n@UiO-67$ via: **a** – using homogeneous complexes directly in the synthesis of the MOF, **b** – using a MOF with linkers that can act as homogeneous ligands to co-ordinate ML_n , **c** – using a pristine MOF in a post synthetic exchange reaction with a compatible homogeneous complex.

Immobilised homogeneous catalysts on MOFs were tested as catalysts for the Guerbet upgrading of ethanol to *n*-butanol in the absence of sodium ethoxide base, and the results of these reactions have been compared to homogeneous analogues. The concept of immobilising homogeneous complexes on MOF nodes was also explored, with novel homogeneous ruthenium complexes synthesised for this purpose.

1.10 References

- 1 Intergovernmental Panel on Climate Change, *Climate Change 2021 The Physical Science Basis WGI*, 2021, vol. 34.
- 2 Intergovernmental Panel on Climate Change, *Global warming of 1.5°C*, 2019.
- 3 Intergovernmental Panel on Climate Change, *Climate Change 2022 - Mitigation of Climate Change - Full Report*, 2022.
- 4 United States Environmental Protection Agency, <https://www.epa.gov/ghgemissions/global-greenhouse-gas-emissions-data#Reference> 1, (accessed 4 January 2023).
- 5 S. J. Davis, N. S. Lewis, M. Shaner, S. Aggarwal, D. Arent, I. L. Azevedo, S. M. Benson, T. Bradley, J. Brouwer, Y. M. Chiang, C. T. M. Clack, A. Cohen, S. Doig, J. Edmonds, P. Fennell, C. B. Field, B. Hannegan, B. M. Hodge, M. I. Hoffert, E. Ingersoll, P. Jaramillo, K. S. Lackner, K. J. Mach, M. Mastrandrea, J. Ogden, P. F. Peterson, D. L. Sanchez, D. Sperling, J. Stagner, J. E. Trancik, C. J. Yang and K. Caldeira, *Science*, 2018, **360**, DOI: 10.1126/science.aas9793
- 6 California Air Resources Board, [https://driveclean.ca.gov/hydrogen-fuel-cell#:~:text=How They Work,powers the car's electric motors](https://driveclean.ca.gov/hydrogen-fuel-cell#:~:text=How%20They%20Work,powers%20the%20car's%20electric%20motors). (accessed 5 January 2023).
- 7 U.S. Department of Energy, https://afdc.energy.gov/vehicles/fuel_cell.html, (accessed 5 January 2023).
- 8 S. Litster and G. McLean, *Journal of Power Sources*, 2004, **130**, 61–76.
- 9 Connecticut Hydrogen-Fuel Cell Coalition, <https://chfcc.org/resources/hydrogen-fuel-cell-benefits/>, (accessed 5 January 2023).
- 10 U.S. Department of Energy, https://afdc.energy.gov/fuels/hydrogen_infrastructure.html, (accessed 5 January 2023).
- 11 J. Andersson and S. Grönkvist, *International Journal of Hydrogen Energy*, 2019, **44**, 11901–11919.

- 12 D. J. Durbin and C. Malardier-Jugroot, *International Journal of Hydrogen Energy*, 2013, **38**, 14595–14617.
- 13 U. Eberle, M. Felderhoff and F. Schüth, *Angew. Chem. Int. Ed.*, 2009, **48**, 6608–6630.
- 14 IDTechEx, <https://www.idtechex.com/en/research-article/fuel-cells-are-not-the-problem-the-hydrogen-fuel-is/25913>, (accessed 5 January 2023).
- 15 U.S. Energy Information Administration, <https://www.eia.gov/energyexplained/biofuels/>, (accessed 6 January 2023).
- 16 F. L. P. Resende, in *Reactor and Process Design in Sustainable Energy Technology*, ed. F. Shi, Elsevier, 1st edn, Amsterdam, 2014, ch. 1, pp 1–25.
- 17 N. S. Mat Aron, K. S. Khoo, K. W. Chew, P. L. Show, W. H. Chen and T. H. P. Nguyen, *Int J Energy Res*, 2020, **44**, 9266–9282.
- 18 National Renewable Energy Laboratory, <https://www.nrel.gov/research/re-biofuels.html>, (accessed 6 January 2023).
- 19 D. Singh, D. Sharma, S. L. Soni, S. Sharma, P. Kumar Sharma and A. Jhalani, *Fuel*, 2020, **262**, 116553.
- 20 H. Fukuda, A. Kondo and H. Noda, *J. Biosci. Bioeng.*, 2001, **92**, 405–416.
- 21 D. M. Alonso, J. Q. Bond and J. A. Dumesic, *Green Chem.*, 2010, **12**, 1493–1513.
- 22 N. L. Panwar, S. C. Kaushik and S. Kothari, *Renewable and Sustainable Energy Reviews*, 2011, **15**, 1513–1524.
- 23 U.S. Department of Energy, https://afdc.energy.gov/fuels/biodiesel_blends.html, (accessed 5 January 2023).
- 24 T. Koizumi, *Renewable and Sustainable Energy Reviews*, 2015, **52**, 829–841.
- 25 Y. Sun and J. Cheng, *Bioresource Technology*, 2002, **83**, 1–11.
- 26 U.S. Department of Energy, https://afdc.energy.gov/fuels/ethanol_fuel_basics.html, (accessed 6 January 2023).

- 27 U.S. Department of Energy, https://afdc.energy.gov/fuels/ethanol_e85.html, (accessed 6 January 2023).
- 28 U.S. Department of Energy, https://afdc.energy.gov/vehicles/flexible_fuel.html, (accessed 6 January 2023).
- 29 C. Jin, M. Yao, H. Liu, C. F. F. Lee and J. Ji, *Renewable and Sustainable Energy Reviews*, 2011, **15**, 4080–4106.
- 30 N. Ayas, in *Comprehensive Energy Systems*, ed. I Dincer, Elsevier Ltd., Amsterdam, 2018, vol. 2.13, pp 368-395.
- 31 B. G. Harvey and H. A. Meylemans, *J Chem Technol Biotechnol*, 2011, **86**, 2–9.
- 32 C. Xue, X. Q. Zhao, C. G. Liu, L. J. Chen and F. W. Bai, *Biotechnology Advances*, 2013, **31**, 1575–1584.
- 33 P. Dürre, *Biotechnol. J.*, 2007, **2**, 1525–1534.
- 34 M. Mascal, *Biofuels, Bioprod. Bioref.*, 2012, **6**, 483–493.
- 35 J. Yanowitz, E. Christensen and R. McCormick, *Utilization of Renewable Oxygenates as Gasoline Blending Components*, NREL Technical Report, August 2011, <https://www.nrel.gov/docs/fy11osti/50791.pdf>
- 36 M. Uyttebroek, W. van Hecke and K. Vanbroekhoven, *Catalysis Today*, 2015, **239**, 7–10.
- 37 M. Brito and F. Martins, *Fuel*, 2017, **208**, 476–482.
- 38 Mitsubishi Chemical Group, https://www.m-chemical.co.jp/en/petrochem-license/technologies/pdf/Introduction_MCC_Oxo_Process.pdf, (accessed 9 January 2023).
- 39 E. M. Green, *Current Opinion in Biotechnology*, 2011, **22**, 337–343.
- 40 A. Kujawska, J. Kujawski, M. Bryjak and W. Kujawski, *Renewable and Sustainable Energy Reviews*, 2015, **48**, 648–661.
- 41 M. Guerbet, *C. R. Acad. Sci. Paris*, 1899, **128**, 1002–1004.

- 42 S. Veibel and J. I. Nielsen, *Tetrahedron*, 1967, **23**, 1723–1733.
- 43 D. Gabriëls, W. Y. Hernández, B. F. Sels, P. van der Voort and A. Verberckmoes, *Catal. Sci. Technol.*, 2015, **5**, 3876–3902.
- 44 H. Aitchison, R. L. Wingad and D. F. Wass, *ACS Catal.*, 2016, **6**, 7125–7132.
- 45 J. T. Kozlowski and R. J. Davis, *ACS Catal.*, 2013, **3**, 1588–1600.
- 46 T. W. Birky, J. T. Kozlowski and R. J. Davis, *Journal of Catalysis*, 2013, **298**, 130–137.
- 47 S. A. Susanto, R. T. Yunarti, R. R. Widjaya, Y. Maryati, A. A. Dwiatmoko, F. Aulia and N. Rinaldi, *IOP Conf. Ser.: Mater. Sci. Eng*, 2021 DOI:10.1088/1757-899X/1011/1/012028.
- 48 J. I. di Cosimo, V. K. Díez, M. Xu, E. Iglesia and C. R. Apesteguía, *Journal of Catalysis*, 1998, **178**, 499–510.
- 49 D. L. Carvalho, R. R. de Avillez, M. T. Rodrigues, L. E. P. Borges and L. G. Appel, *Applied Catalysis A: General*, 2012, **415–416**, 96–100.
- 50 J. T. Kozlowski, M. Behrens., R. Schlögl and R. J. Davis, *ChemCatChem*, 2013, **5**, 1989–1997.
- 51 T. Tsuchida, S. Sakuma, T. Takeguchi and W. Ueda, *Ind. Eng. Chem. Res.*, 2006, **45**, 8634–8642.
- 52 S. Ogo, A. Onda and K. Yanagisawa, *Applied Catalysis A: General*, 2011, **402**, 188–195.
- 53 S. Ogo, A. Onda, Y. Iwasa, K. Hara, A. Fukuoka and K. Yanagisawa, *Journal of Catalysis*, 2012, **296**, 24–30.
- 54 I. C. Marcu, D. Tichit, F. Fajula and N. Tanchoux, *Catalysis Today*, 2009, **147**, 231–238.
- 55 I. C. Marcu, N. Tanchoux, F. Fajula and D. Tichit, *Catal Lett*, 2013, **143**, 23–30.
- 56 K. Koda, T. Matsu-ura, Y. Obora and Y. Ishii, *Chemistry Letters*, 2009, **38**, 838–839.

- 57 T. Matsu-Ura, S. Sakaguchi, Y. Obora and Y. Ishii, *J. Org. Chem.*, 2006, **71**, 8306–8308.
- 58 Mitsubishi Chemical Corp. US. Pat., US20100298613A1, 2010.
- 59 G. R. M. Dowson, M. F. Haddow, J. Lee, R. L. Wingad and D. F. Wass, *Angew. Chem. Int. Ed.*, 2013, **52**, 9005–9008.
- 60 R. L. Wingad, P. J. Gates, S. T. G. Street and D. F. Wass, *ACS Catal.*, 2015, **5**, 5822–5826.
- 61 K. N. T. Tseng, S. Lin, J. W. Kampf and N. K. Szymczak, *Chem. Commun.*, 2016, **52**, 2901–2904.
- 62 Y. Xie, Y. Ben-David, L. J. W. Shimon and D. Milstein, *J. Am. Chem. Soc.*, 2016, **138**, 9077–9080.
- 63 H. Furukawa, K. E. Cordova, M. O’Keeffe and O. M. Yaghi, *Science*, 2013, **341**, DOI:10.1126/science.1230444.
- 64 P. Puthiaraj and W. S. Ahn, in *Catalyst Immobilization: Methods and Applications*, ed. M. Benaglia and A. Puglisi, Wiley-VCH, Weinheim, Germany, 2019, ch. 5, pp. 159-185
- 65 R. J. Kuppler, D. J. Timmons, Q. R. Fang, J. R. Li, T. A. Makal, M. D. Young, D. Yuan, D. Zhao, W. Zhuang and H. C. Zhou, *Coordination Chemistry Reviews*, 2009, **253**, 3042–3066.
- 66 J. Klinowski, F. A. Almeida Paz, P. Silva and J. Rocha, *Dalton Trans.*, 2011, **40**, 321–330.
- 67 T. Friić, *J. Mater. Chem.*, 2010, **20**, 7599–7605.
- 68 N. Stock and S. Biswas, *Chem. Rev.*, 2012, **122**, 933–969.
- 69 H. Li, M. Eddaoudi, M. O’Keeffe and O. M. Yaghi, *Nature*, 1999, **402**, 276-279
- 70 A. Schoedel and S. Rajeh, in *Metal-Organic Framework. From Design to Applications*, ed. X. H. Bu, M. J. Zaworotoko and Z. Zhang, Springer Chem, 1st edn, 2020, ch. 1, pp 1-55.

- 71 P. Rocío-Bautista, I. Taima-Mancera, J. Pasán and V. Pino, *Separations*, 2019, **6**, 1–21.
- 72 D. Zhao, D. Yuan and H. C. Zhou, *Energy Environ. Sci.*, 2008, **1**, 222–235.
- 73 M-X. Wu and Y-W. Yang, *Adv. Mater.*, 2017, **29**, DOI: 10.1002/adma.201606134
- 74 G. L. Yang, X. L. Jiang, H. Xu and B. Zhao, *Small*, 2021, **17**, DOI:10.1002/smll.202005327.
- 75 A. Bavykina, N. Kolobov, I. S. Khan, J. A. Bau, A. Ramirez and J. Gascon, *Chem. Rev.*, 2020, **120**, 8468–8535.
- 76 N. Nagarjun and A. Dhakshinamoorthy, *Molecular Catalysis*, 2019, **463**, 54–60.
- 77 K. Schlichte, T. Kratzke and S. Kaskel, *Microporous and Mesoporous Materials*, 2004, **73**, 81–88.
- 78 J. Lee, O. K. Farha, J. Roberts, K. A. Scheidt, S. T. Nguyen and J. T. Hupp, *Chem. Soc. Rev.*, 2009, **38**, 1450–1459.
- 79 A. Dhakshinamoorthy, M. Opanasenko, J. Čejka and H. Garcia, *Adv. Synth. Catal.*, 2013, **355**, 247–268.
- 80 Amarajothi. Dhakshinamoorthy, M. Alvaro and H. Garcia, *Adv. Synth. Catal.*, 2010, **352**, 711 – 717.
- 81 Y. Pan, B. Yuan, Y. Li and D. He, *Chem. Commun.*, 2010, **46**, 2280–2282.
- 82 S. Bhattacharjee, C. Chen and W. S. Ahn, *RSC Adv.*, 2014, **4**, 52500–52525.
- 83 F. Vermoortele, A. Vimont, C. Serre and D. de Vos, *Chem. Commun.*, 2011, **47**, 1521–1523.
- 84 J. Yu, C. Mu, B. Yan, X. Qin, C. Shen, H. Xue and H. Pang, *Mater. Horiz.*, 2017, **4**, 557–569.
- 85 S. Hermes, M. K. Schröter, R. Schmid, L. Khodeir, M. Muhler, A. Tissler, R. W. Fischer and R. A. Fischer, *Angew. Chem. Int. Ed.*, 2005, **44**, 6237–6241.

- 86 J. Hou, Y. Luan, J. Tang, A. M. Wensley, M. Yang and Y. Lu, *Journal of Molecular Catalysis A: Chemical*, 2015, **407**, 53–59.
- 87 W. M. Liao, J. H. Zhang, Z. Wang, S. Y. Yin, M. Pan, H. P. Wang and C. Y. Su, *J. Mater. Chem. A*, 2018, **6**, 11337–11345.
- 88 Z. Li, T. M. Rayder, L. Luo, J. A. Byers, C.-K. Tsung, *J. Am. Chem. Soc.*, 2018, **140**, 2021.
- 89 C. K. P. Neeli, P. Puthiaraj, Y. R. Lee, Y. M. Chung, S. H. Baeck and W. S. Ahn, *Catalysis Today*, 2018, **303**, 227–234.
- 90 H. Ye, H. Zhao, Y. Jiang, H. Liu and Z. Hou, *ACS Appl. Nano Mater.*, 2020, **3**, 12260–12268.
- 91 S. A. Burgess, A. Kassie, S. A. Baranowski, K. J. Fritzsching, K. Schmidt-Rohr, C. M. Brown and C. R. Wade, *J. Am. Chem. Soc.*, 2016, **138**, 1780–1783.
- 92 D. Jiang, G. Fang, Y. Tong, X. Wu, Y. Wang, D. Hong, W. Leng, Z. Liang, P. Tu, L. Liu, K. Xu, J. Ni and X. Li, *ACS Catal.*, 2018, **8**, 11973–11978.
- 93 C. N. Neumann, S. J. Rozeveld, M. Yu, A. J. Rieth and M. Dincă, *J. Am. Chem. Soc.*, 2019, **141**, 17477–17481.

Chapter 2 – Homogeneous/heterogeneous catalysed Guerbet upgrading of *n*-butanol

In this chapter, a range of MOFs were synthesised and tested as heterogeneous aldol catalysts in the Guerbet upgrading of ethanol with homogeneous transfer hydrogenation catalysts. The recyclability of UiO-66(Zr) as a catalyst in the reaction was also investigated, as well as examining whether the combination of a homogeneous and heterogeneous catalyst produced a recyclable system for Guerbet chemistry.

2.1 Homogeneous Lewis acid screen

In aid of determining suitable MOFs to act as heterogeneous aldol catalysts in the Guerbet upgrading of ethanol, homogeneous Lewis acids were initially tested under standard reaction conditions. A variety of Lewis acid catalysts were screened alongside [RuCl₂(dppm)₂] (a known transfer hydrogenation catalyst in the Guerbet upgrading of ethanol) in the Guerbet synthesis of *n*-butanol at 210 °C over a reaction duration of 20 hours. Instead of a 5 mol% loading of sodium ethoxide (NaOEt) in the reaction to drive the aldol condensation of acetaldehyde, 1 mol% of a variety of homogeneous Lewis acids were added to the reaction mixture (Table 3).

Table 3: Guerbet upgrading of ethanol using Lewis Acids as aldol catalysts

		[RuCl ₂ (dppm) ₂] (0.1 mol%) Lewis Acid (1.0 mol%)					
2		→		+ H ₂ O			
		20 hr, 210 °C					
		Selectivity (%) ^b					
Entry	Lewis Acid	EtOH Conversion (%) ^a	<i>n</i> -BuOH	Higher			
				EtOAc	2-BuOH	Alcohols ^c	Other ^d
1	Cu(OTf) ₂	88	-	2	-	-	98
2	Zn(OTf) ₂	66	-	3	-	-	97
3	Al(OTf) ₂	86	-	2	-	-	98
4	B(C ₆ F ₅) ₃	21	-	76	-	-	24
5	Zr(OEt) ₄	18	77	16	-	-	7

^a Conversion of ethanol calculated based on total liquid products obtained determined *via* GC analysis. ^b Selectivity to Guerbet products in liquid fraction determined *via* GC analysis. ^c C₆ and C₈ alcohol products calibrated *via* GC analysis. ^d Liquid products not characterised from GC calibration.

A variety of different triflate compounds were tested as Lewis acid catalysts in the reaction (Table 3, Entries 1-3); however, they proved to be inactive catalysts for the aldol condensation of acetaldehyde in the Guerbet synthesis of *n*-butanol. Interestingly, the use of these three catalysts promoted very high ethanol conversions, which has been attributed to the high activity of these triflate species for the dehydration of ethanol to diethyl ether. ¹H NMR evidence from the post reaction mixtures of these Guerbet reactions shows a high quantity of diethyl ether formation, hence the activity of the triflate species for the dehydration of ethanol is shown here. B(C₆F₅)₃ (BCF) also proved to be an inactive catalyst for the aldol condensation of acetaldehyde (Table 3, Entry 4), but it was very selective for the formation of ethyl acetate (EtOAc) with [RuCl₂(dppm)₂] in the Guerbet reaction of ethanol. This suggested that BCF was inactive for aldol condensation catalysis, while being a highly active Tishchenko catalyst, as EtOAc is the product of the Tishchenko reaction of acetaldehyde, in the absence of NaOH. Interestingly, while facilitating a modest conversion of ethanol of 18 %, in the reaction using Zr(OEt)₄ and

[RuCl₂(dppm)₂] catalysts, a high selectivity towards the formation of *n*-butanol (*n*-BuOH) with the mitigation of higher alcohol production was demonstrated (Table 3 Entry 5). This result indicated that UiO-66(Zr) might be an ideal MOF to trial as a heterogeneous Lewis acid catalyst alongside [RuCl₂(dppm)₂] as a transfer hydrogenation catalyst, owing to the structure of the nodes of the MOF. The nodes of UiO-66(Zr) are [Zr₆O₄(OH)₄], with zirconium atoms bound *via* oxygen atoms in a cuboctahedral structure (Figure 15).¹

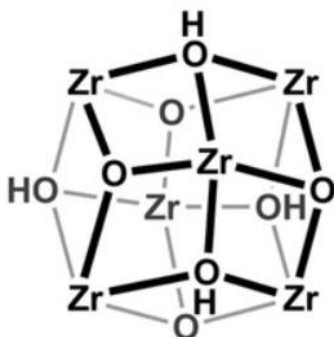


Figure 15: Zr₆ node structure of UiO-66(Zr).¹

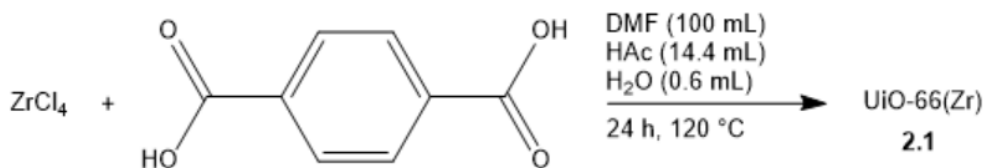
As the homogeneous Zr(OEt)₄ proved to be an active aldol catalyst in the Guerbet upgrading of ethanol with [RuCl₂(dppm)₂], it was postulated that the [Zr₆O₄(OH)₄] nodes of UiO-66(Zr) would also show activity with the homogeneous ruthenium catalyst. While the Lewis acidic nodes of UiO-66(Zr) have previously been demonstrated as catalytic aldol sites on Pd@UiO-66 for the Guerbet upgrading of ethanol,² the compatibility of the parent MOF as an aldol catalyst with homogeneous transfer hydrogenation catalysts has yet to be determined.

2.2 UiO-66(Zr) and [RuCl₂(dppm)₂] as heterogeneous and homogeneous catalysts in the Guerbet upgrading of ethanol

2.2.1 Reaction Temperature Screen

Initially, a sample of UiO-66(Zr) was prepared according to a modified literature procedure (Scheme 21),² and tested as an aldol condensation catalyst in place of sodium

ethoxide in the homogeneous catalytic upgrading of ethanol to *n*-butanol with $[\text{RuCl}_2(\text{dppm})_2]$ as a homogeneous transfer hydrogenation catalyst.



Scheme 21: Synthesis of UiO-66(Zr) (2.1).

The initial experimental conditions were chosen based off previous work conducted on this homogeneous transfer hydrogenation catalyst from the Wass group.³ 0.1 mol% of the transfer hydrogenation catalyst was added to the reaction mixture, and instead of a 5 mol% loading of NaOEt, 0.1 mol% of **2.1** was added to the system. The Guerbet upgrading of ethanol to butanol was tested in a 100 mL autoclave under inert conditions over a duration of 20 hours at a temperature of 150 °C (Table 4, Entry 1). Under these conditions, the catalytic system employed for *n*-butanol synthesis was poor. A small ethanol conversion of 13.7 % was observed, to a distribution of products that consisted of lundesired side-products, not *n*-butanol. However, the Guerbet upgrading of ethanol was trialled at 150 °C with UiO-66(Zr) (0.1 mol%) in the absence of $[\text{RuCl}_2(\text{dppm})_2]$, where the system was inactive for ethanol conversion (Table 4, Entry 7), which showed the requirement for both catalysts in the reaction to facilitate any ethanol conversion to *n*-BuOH. The poor activity of the reaction system was attributed to the temperature being too low for the heterogeneous UiO-66(Zr) aldol catalyst to efficiently operate, hence the reaction temperature was increased to 180 °C (Table 4, Entry 2).

Table 4: Guerbet upgrading of ethanol using UiO-66(Zr) and $[\text{RuCl}_2(\text{dppm})_2]$ as co-catalysts at various reaction temperatures

Entry	Temp (°C)	Selectivity (%) ^b					
		EtOH Conversion (%) ^a	<i>n</i> -BuOH	Higher Alcohols ^c			Other ^d
				EtOAc	2-BuOH		
1	150	13.7	5.1	15.3	2.2	-	77.4
2	180	30.8	29.2	9.4	1.3	4.9	55.2
3	190	27.6	29.3	8.0	0.7	5.1	56.9
4	200	30.9	40.5	7.4	-	12.9	39.2
5	210	44.6	37.2	7.2	0.7	15.0	39.9
6	220	75.1	23.0	7.7	0.7	14.2	54.4
7 ^e	150	-	-	-	-	-	-

^a Conversion of ethanol calculated based on total liquid products obtained determined *via* GC analysis. ^b Selectivity to Guerbet products in liquid fraction determined *via* GC analysis. ^c C₆ and C₈ alcohol products calibrated *via* GC analysis. ^d Products not characterised from GC calibration.

^e Reaction in the absence of $[\text{RuCl}_2(\text{dppm})_2]$.

This minor change to the reaction conditions had a substantial effect on the activity of the catalytic system. By increasing the reaction temperature by 30 °C, ethanol conversion by the same combination of catalysts was more than doubled, while selectivity to the *n*-butanol facilitated by the combination of catalysts was increased by a factor of over 5, resulting in an over 10 times yield of butanol being produced at 180 °C (9.0 % *n*-BuOH yield) compared to that synthesised at 150 °C (0.7 % *n*-BuOH yield). While the increase of reaction temperature to 180 °C was advantageous for *n*-BuOH production, the system was less than 50 % selective to known products (C₈> alcohols and EtOAc). As the selectivity of the system towards *n*-BuOH was high compared to that of calibrated higher alcohols (C₆ and C₈), this is an indication that even longer chain alcohols (longer than C₈) do not make up the remainder of this product distribution, and that UiO-66(Zr) was catalysing side reactions like the dehydration of ethanol to diethyl ether.

As this preliminary temperature increase proved advantageous for *n*-BuOH synthesis by a combination of [RuCl₂(dppm)₂] and UiO-66(Zr) catalysts, the reaction was repeated at higher temperatures increasing at increments of 10 °C (Table 4, Entries 3-6). A general trend of increased ethanol conversion with increasing temperature is observed when examining the results in Table 4, with minor increases in ethanol conversion demonstrated between 190 and 210 °C (Table 4, Entries 3-5). Interestingly, increasing the reaction temperature from 210 °C (Table 4, Entry 5) to 220 °C (Table 4, Entry 6) has a dramatic effect on the activity of the reaction, with EtOH conversion increasing from 44.6 % at 210 °C, to 75.1 % at 220 °C. While the catalytic system is highly active for ethanol conversion at 220 °C, this high conversion comes with a sacrifice towards selectivity of the desired *n*-butanol product. At 210 °C, the catalytic system generates *n*-BuOH more selectively than at any of the temperatures that were tested (37.2 %), while increasing the reaction temperature to 220 °C results in selectivity towards *n*-BuOH falling to 23.0 %. Interestingly, selectivity towards C₆ and C₈ alcohols slightly decreases when increasing the reaction temperature from 210 °C to 220 °C, which is a strong indication that at 220 °C, the catalytic system is more active for the generation of C₈+ alcohols that have not been calibrated in the GC analysis used to calculate the product distribution of C₈+ alcohols. The catalytic upgrading of ethanol conducted at 210 °C was not only the most selective reaction towards *n*-BuOH tested here, but also the least selective to unknown side-products. The ethanol upgrading reaction conducted at 220 °C was slightly higher yielding (*n*-BuOH yield of 17.2 %) than that at 210 °C (*n*-BuOH yield of 16.6 %), however, the benefits of increased reaction selectivity rendered 210 °C an optimum reaction temperature for the catalytic upgrading of EtOH to *n*-BuOH by [RuCl₂(dppm)₂] and UiO-66(Zr).

The temperature optimised system for the [RuCl₂(dppm)₂]/UiO-66(Zr) catalysed upgrading of ethanol to *n*-butanol was compared against homogeneous systems using NaOEt as a homogeneous aldol mediator. As previously reported,³ the Guerbet upgrading of ethanol was trialed with [RuCl₂(dppm)₂] (0.1 mol%) and NaOEt (5 mol%) at 150 °C, while this combination of homogeneous species was also trialed for ethanol upgrading at 210 °C. As with the [RuCl₂(dppm)₂]/UiO-66(Zr) temperature optimised reaction detailed in Table 4 Entry 5, both NaOEt mediated reactions were run over a

reaction time of 20 hours. The product distributions of these reactions are detailed in Table 5 and compared against the $[\text{RuCl}_2(\text{dppm})_2]/\text{UiO-66}(\text{Zr})$ temperature optimised reaction.

Table 5: Comparing the performance of NaOEt mediated Guerbet systems with UiO-66(Zr) co-catalysed systems, with $[\text{RuCl}_2(\text{dppm})_2]$ as a transfer hydrogenation catalyst

Entry ^a	Aldol catalyst (mol%)	EtOH Conversion (%) ^b	Selectivity (%) ^c				
			<i>n</i> -BuOH (EtOAc	2-BuOH	Higher	Other
						Alcohols ^d	^e
1 ^f	NaOEt (5)	42.2	56.6	4.7	-	23.7	15.0
2	NaOEt (5)	40.9	36.2	4.2	-	19.6	40.0
3	2.1 (0.1)	44.6	37.2	7.2	0.7	15.0	39.9

^a Reaction temperature of 210 °C unless specified otherwise. ^b Conversion of ethanol calculated based on total liquid products obtained determined *via* GC analysis. ^c Selectivity to Guerbet products in liquid fraction determined *via* GC analysis. ^d C₆ and C₈ alcohol products calibrated *via* GC analysis. ^e Products not characterised from GC calibration. ^f Reaction temperature of 150 °C.

The $[\text{RuCl}_2(\text{dppm})_2]/\text{UiO-66}(\text{Zr})$ catalysed reaction at 210 °C (Table 5, Entry 3) is advantageous to the $[\text{RuCl}_2(\text{dppm})_2]/\text{NaOEt}$ system at the same temperature (Table 5, Entry 2). The selectivity towards *n*-BuOH in the product fraction of the Guerbet reaction of ethanol is higher when UiO-66(Zr) is used as the aldol catalyst while selectivity towards higher alcohols is lower. Ethanol conversion is higher when UiO-66(Zr) (0.1 mol%) is used compared to NaOEt (5 mol%) at 210 °C, which indicates that the UiO-66(Zr) is partially catalysing the direct conversion of ethanol through side reactions, like the dehydration of ethanol to diethyl ether, while product selectivity towards ethyl acetate is higher using UiO-66(Zr) at 210 °C. However, the lack of NaOEt in the reaction means that NaOH can't be generated through base hydrolysis, and as a result, neither can sodium acetate. The low selectivity of the NaOEt base catalysed reactions towards ethyl acetate can be

explained by the conversion of ethyl acetate to sodium acetate by sodium hydroxide generated in these reactions. The reaction using NaOEt carried out under previously reported conditions at the lower temperature of 150 °C (Table 5, Entry 1) is higher yielding than the temperature optimised UiO-66(Zr) catalysed reaction (Table 5, Entry 3) for *n*-BuOH. However, results presented in Table 5 Entry 3 represent an early stage of reaction development, using a much lower loading of aldol catalyst than that of NaOEt, with the potential advantages previously described of using a Lewis acidic MOF over NaOEt described in 1.9. Further reaction optimisation was warranted of the [RuCl₂(dppm)₂]/UiO-66(Zr) catalysed upgrading of ethanol to *n*-butanol, to further improve *n*-butanol yield.

2.2.1.1 Effect of temperature optimised reaction conditions on the catalysts

A lack of degradation of the aldol catalyst is a proposed advantage of using a MOF in place of NaOEt in the Guerbet upgrading of EtOH with [RuCl₂(dppm)₂] as a transfer hydrogenation catalyst. A method to determine the structural integrity of UiO-66(Zr) in the reaction is through post-reaction powder XRD (PXRD), where the structure of the MOF can be compared to that of the pristine UiO-66(Zr), to determine whether the structure UiO-66(Zr) is maintained in the reaction. Hence, to test whether the structure of UiO-66(Zr) was being maintained in the EtOH upgrading reaction conducted at 210 °C, the reaction detailed in Table 4 Entry 5 was repeated, with a higher loading of UiO-66(Zr) in the reaction. The previously optimised system used a 0.1 mol% loading of UiO-66(Zr) to match the loading of [RuCl₂(dppm)₂] in the reaction, a quantity too low to acquire a PXRD pattern. Hence the loading of UiO-66(Zr) was increased from 0.1 mol% to 0.68 mol%, so that the quantity of post-reaction UiO-66(Zr) was great enough to acquire a PXRD pattern. This reaction would allow for a rationalisation as to whether the optimised EtOH upgrading reaction (Table 4 Entry 5) was conducted under conditions that prevented the decomposition of the aldol catalyst. The UiO-66(Zr) aldol catalyst was isolated post-reaction and an PXRD pattern of the post reaction solid was collected and compared to that of a pristine sample of pre-reaction UiO-66(Zr) (Figure 16).

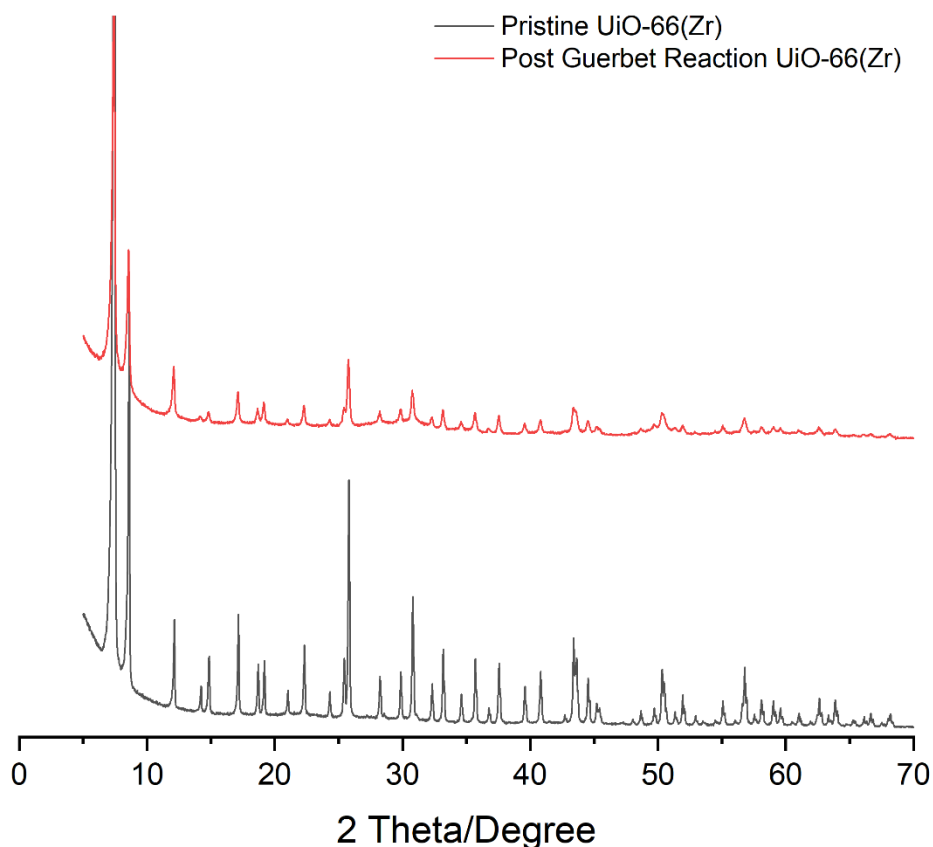


Figure 16: Comparing PXRD patterns of pristine UiO-66(Zr), and UiO-66(Zr) recovered after being used in a Guertbet synthesis of *n*-butanol.

Although the PXRD pattern of the UiO-66(Zr) that was obtained from the post Guertbet reaction sample is poorly resolved, likely owing to sample preparation or a greater quantity of amorphous material in the sample, it can be seen in Figure 16 that this sample of UiO-66(Zr) shares identical PXRD peaks to the pristine sample of UiO-66(Zr). Hence the structural integrity of the MOF at the optimised Guertbet reaction temperature of 210 °C can be confirmed.

The structure of the UiO-66(Zr) in the catalytic upgrading of ethanol was shown to remain intact when subject to the optimised temperature of 210 °C, but the effect of its presence in the reaction mixture on the homogeneous $[\text{RuCl}_2(\text{dppm})_2]$ catalyst had not been determined. This can be determined *via* analysing the liquid fraction of the Guertbet reaction by $^{31}\text{P}\{^1\text{H}\}$ NMR spectroscopy, to probe the phosphorous ligands present on the ruthenium catalyst. To determine how the $[\text{RuCl}_2(\text{dppm})_2]$ evolved in the Guertbet reaction described in Table 4 Entry 5, the post reaction liquid product fraction was analysed *via*

$^{31}\text{P}\{^1\text{H}\}$ NMR spectroscopy and compared to post reaction $^{31}\text{P}\{^1\text{H}\}$ NMR spectra from Guerbet reactions conducted using $[\text{RuCl}_2(\text{dppm})_2]$ (0.1 mol%) and NaOEt (5 mol%) at 150 °C and 210 °C (Figure 17).

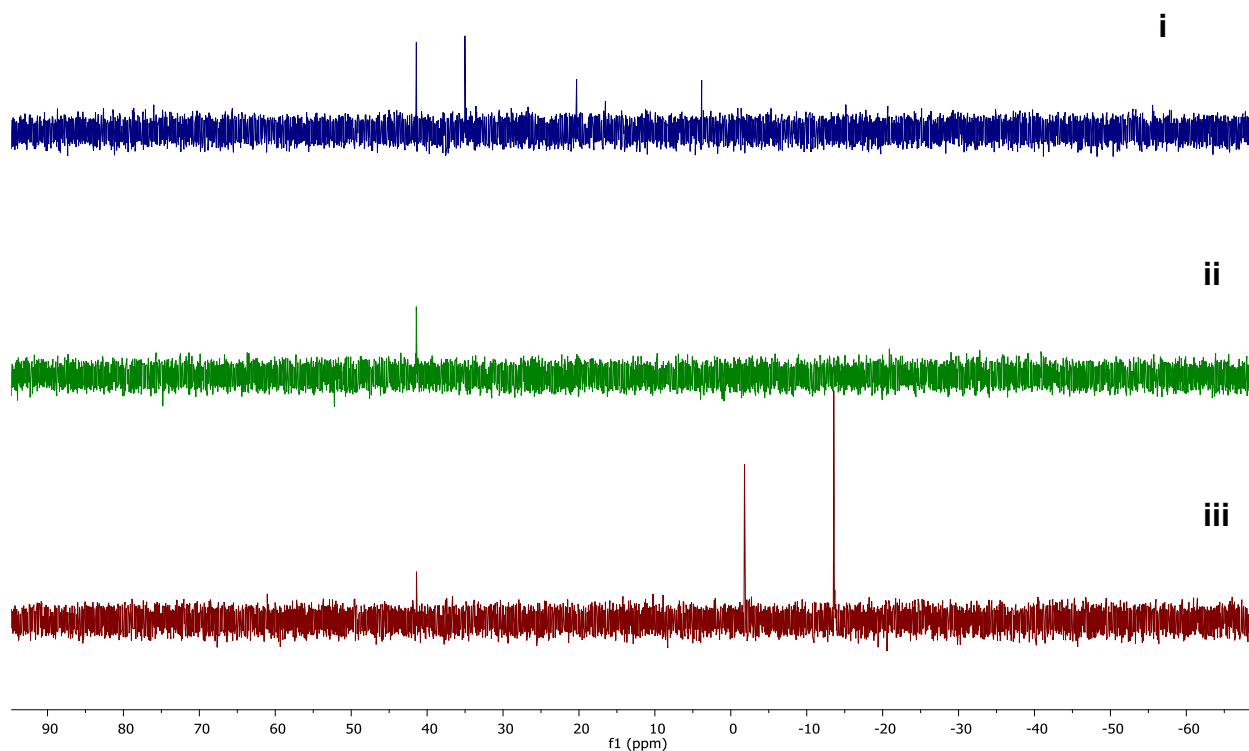


Figure 17: Comparing post-reaction $^{31}\text{P}\{^1\text{H}\}$ NMR spectra from Guerbet reactions of ethanol utilising NaOEt at 150 °C (i), NaOEt at 210 °C (ii) or UiO-66(Zr) at 210 °C (iii) with $[\text{RuCl}_2(\text{dppm})_2]$ as a transfer hydrogenation catalyst.

When comparing the three $^{31}\text{P}\{^1\text{H}\}$ NMR spectra in Figure 17, it becomes apparent that the $[\text{RuCl}_2(\text{dppm})_2]$ (characteristic peak at -7.82 ppm) transfer hydrogenation catalyst evolves in different ways when different aldol catalysts are employed in the Guerbet upgrading of ethanol. All three spectra share the same peak at approximately 42 ppm and this is the only peak in the post reaction ^{31}P spectrum of the NaOEt aldol catalysed reaction at 210 °C (Figure 17, ii), while there are two much stronger resonances upfield in the spectrum of the post reaction mixture of the UiO-66(Zr) aldol catalysed reaction at the same temperature (Figure 15, iii). Interestingly, neither of these signals are indicative of the initial $[\text{RuCl}_2(\text{dppm})_2]$ catalyst (-7.82 ppm). The $^{31}\text{P}\{^1\text{H}\}$ NMR spectra of the post

reaction liquid from the Guerbet upgrading of ethanol using NaOEt as an aldol catalyst at 150 °C (Figure 17, i) shows more signals than the same system conducted at 210 °C (Figure 17, ii). When using NaOEt as an aldol catalyst, the increase in temperature prevents the formation of the majority of the Ru species that are made at 150 °C, however, at the higher temperature of 210 °C, using UiO-66(Zr) in place of NaOEt facilitates the formation of more post reaction Ru species with upfield $^{31}\text{P}\{^1\text{H}\}$ NMR signals. The species that these resonances correspond to has not yet been determined, however the upfield nature of the signals suggests that these Ru species possess dppm ligands, which have not been oxidised.

2.2.2 Further reaction optimisation

Previous testing on optimising the UiO-66(Zr)/[RuCl₂(dppm)₂] catalysed system for the upgrading of ethanol focused on changing the reaction temperature with other reaction variables like catalyst loading, reaction duration and stirring rate remaining fixed. Previous work on the homogeneous NaOEt/[RuCl₂(dppm)₂] catalysed upgrading of ethanol was used as to determine these parameters, however, as the temperature screen showed, the previously reported temperature of 150 °C was not optimised for the new UiO-66(Zr)/[RuCl₂(dppm)₂] system. Hence further work was conducted on investigating changing the catalytic reaction parameters to improve *n*-BuOH yield.

Initially, the effect of changing the duration of the reaction was investigated for the upgrading of ethanol by UiO-66(Zr) (0.1 mol%) and [RuCl₂(dppm)₂] (0.1 mol%) at the optimised reaction temperature of 210 °C. *n*-Butanol Guerbet synthesis reactions using this combination of catalysts were conducted over 2 hours, 4 hours and 65 hours, and compared against the previous reaction conducted over 20 hours (Table 6). Over the shortest reaction time of 2 hours (Table 6, Entry 1), the activity of the catalytic system for ethanol conversion is low (11.3 % EtOH conversion). This is an indication that the [RuCl₂(dppm)₂] transfer hydrogenation catalyst requires a longer reaction duration to activate, as the dehydrogenation of ethanol catalysed by this homogeneous complex is the first step in the Guerbet reaction, and low EtOH conversion signals that this initial dehydrogenation is not efficiently proceeding. Increasing the reaction duration to 4 hours (Table 6, Entry 2) dramatically improves ethanol conversion facilitated by the system

(40.5 %), however, the selectivity of the product distribution to *n*-BuOH is low (18.3 %). As the UiO-66(Zr)/[RuCl₂(dppm)₂] catalyst system is inactive for higher alcohol production at this reaction duration, the low selectivity of the reaction towards *n*-BuOH can be attributed to the activity of the UiO-66(Zr) aldol catalyst. As EtOH conversion is high, and *n*-BuOH selectivity is low with no higher alcohol production, the predominant product of the 4-hour EtOH upgrading reaction is highly likely to be acetaldehyde, forming from the dehydrogenation of ethanol. Over 4 hours, the UiO-66(Zr) aldol catalyst shows low activity for the aldol condensation of the acetaldehyde produced from this initial reaction, hence acetaldehyde is likely to be the main product.

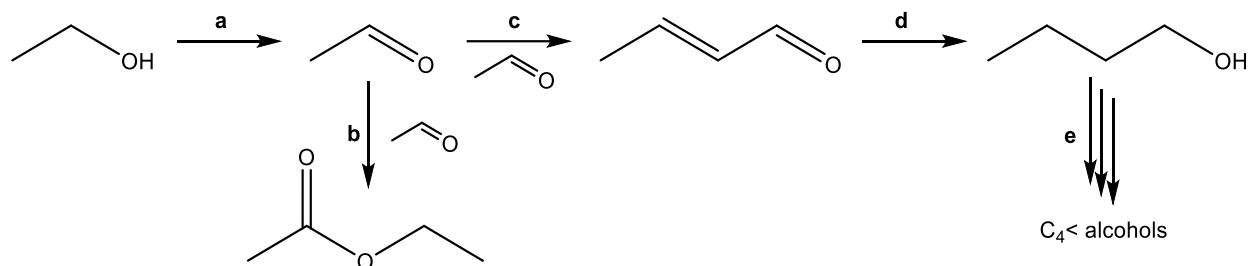
Table 6: Reaction duration screen for the Guerbet upgrading of ethanol employing UiO-66(Zr) and [RuCl₂(dppm)₂] as co-catalysts

Entry	Reaction Time (hr)	EtOH Conversion (%) ^a	Selectivity (%) ^b				
			<i>n</i> -BuOH	EtOAc	2-BuOH	Higher	Other
						Alcohols ^c	^d
1	2	11.3	4.4	23.9	-	-	71.7
2	4	40.5	18.3	6.4	-	-	75.3
3	20	44.6	37.2	7.2	0.7	15.0	39.9
4	65	55.7	34.8	12.2	0.7	15.6	36.7

^a Conversion of ethanol calculated based on total liquid products obtained determined *via* GC analysis. ^b Selectivity to Guerbet products in liquid fraction determined *via* GC analysis. ^c C₆ and C₈ alcohol products calibrated *via* GC analysis. ^d Products not characterised from GC calibration.

The considerable increase in reaction duration from 4 hours to 20 hours (Table 6, Entry 3) doesn't result in a significant increase in system activity. Ethanol conversion is only increased by 4.1 % over the reaction terminated after 4 hours, however, there is a large increase in product selectivity towards *n*-BuOH. The 4-hour Guerbet reaction under the conditions detailed in Table 6 (Entry 2) yields 7.4 % *n*-BuOH, while the 20-hour reaction facilitates a yield of 16.6 % of *n*-BuOH. The 4-hour reaction is inactive for the formation of higher alcohols, however, the reaction over the extended 20-hour duration shows a 15

% selectivity towards the formation of C₆ and C₈ alcohols. Increasing the reaction duration further to 65 hours (Table 6, Entry 4) shows a minor increase in catalytic system activity over the 20-hour reaction, and a small increase in *n*-BuOH yield (19.4 %), the highest reported by this combination of catalysts thus far. However, the system is less selective towards synthesis of the desired *n*-BuOH product. The results of these EtOH upgrading reactions by the UiO-66(Zr)/[RuCl₂(dppm)₂] catalytic system give indications as to the role of each catalyst in the mechanism, and their induction period at 210 °C.



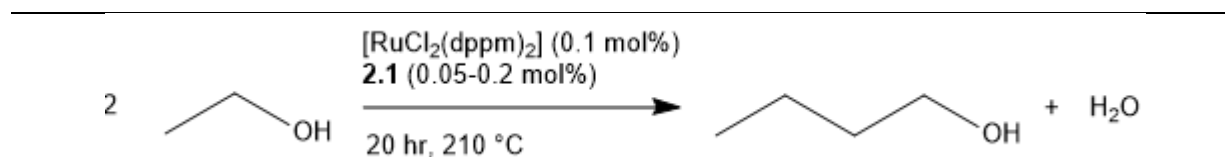
*Scheme 22: Reaction pathway for the Guerbet synthesis of *n*-butanol from ethanol: a) dehydrogenation of ethanol to acetaldehyde, b) conversion of acetaldehyde to ethyl acetate, c) aldol coupling of acetaldehyde to crotonaldehyde, d) hydrogenation of crotonaldehyde to *n*-butanol, e) further Guerbet reactions using *n*-butanol as a substrate.*

Ethanol conversion after 2 hours is low, and increases dramatically after 4 hours, showing a limited increase by increasing the reaction duration up to 65 hours. This indicates that the [RuCl₂(dppm)₂] catalyst evolves and becomes highly active for the dehydrogenation of ethanol to acetaldehyde (Scheme 22, a) between 2 and 4 hours into this Guerbet reaction. Previous studies on the nature of the Ru catalyst in 2.2.1.1 showed that after a 20-hour reaction, there was no [RuCl₂(dppm)₂] present in the system, which suggests that the evolution of the starting [RuCl₂(dppm)₂] complex takes place between 2 and 4 hours in the reaction, to a species that is more active for ethanol dehydrogenation. Of the reaction durations tested for ethanol upgrading by the UiO-66(Zr)/[RuCl₂(dppm)₂] catalytic system, the largest increase in *n*-BuOH yield came between 4 hours (7.4 % yield) and 20 hours (16.6%). Over the extended duration of 20 hours, the system also becomes active for the formation of C₆ and C₈ alcohols, meaning that other uncharacterised products may be even longer chained alcohols. As ethanol conversion only increased by 4.1 % between 4 and 20 hours, this large increase in alcohol product yield indicates that a longer reaction duration is required for the UiO-66(Zr) to catalyse the aldol condensation of acetaldehyde

(Scheme 22, **c**) and the aldol condensation steps in the formation of higher alcohols (Scheme 22, **e**). The data presented in Table 6 suggests that there is an optimum reaction duration between 4 and 20 hours for ethanol upgrading by the UiO-66(Zr)/[RuCl₂(dppm)₂] catalyst mixture for a more selective formation of *n*-BuOH, without the formation of higher alcohol products. The Guerbet reaction run over 65 hours (Table 6, Entry 4) shows higher activity for ethyl acetate formation, an indication that the Lewis acidic aldol catalyst becomes more active for the Tishchenko reaction over extended reaction periods.

Although the ethanol upgrading reaction catalysed by UiO-66(Zr) (0.1 mol%) and [RuCl₂(dppm)₂] (0.1 mol%) at 210 °C yielded the most *n*-butanol over a duration of 65 hours (Table 6, Entry 4), a 20 hour reaction was more selective for the formation of the target product. While a substantially large increase in reaction time was required for a modest improvement in yield (2.8 % increase). Hence of the reaction durations tested, 20 hours was determined to be optimal. Attention turned to examining the effect of changing the loading of the UiO-66(Zr) aldol catalyst in the reaction, hence the synthesis of *n*-butanol was tested with loadings of 0.05 mol% and 0.2 mol%, at 210 °C over 20 hours with a loading of 0.1 mol% of [RuCl₂(dppm)₂] (Table 7).

Table 7: UiO-66(Zr) Loading screen for the Guerbet upgrading of ethanol with $[RuCl_2(dppm)_2]$ as a transfer hydrogenation catalyst



Entry	UiO-66(Zr) load (mol%)	EtOH Conversion (%) ^a	Selectivity (%) ^b				
			<i>n</i> -BuOH	EtOAc	2-BuOH	Higher Alcohols ^c	Other ^d
1	0.05	51.2	34.8	4.3	0.8	12.5	47.6
2	0.10	44.6	37.2	7.2	0.7	15.0	39.9
3	0.20	59.2	33.4	7.4	0.5	20.8	37.9

^a Conversion of ethanol calculated based on total liquid products obtained determined *via* GC analysis. ^b Selectivity to Guerbet products in liquid fraction determined *via* GC analysis. ^c C₆ and C₈ alcohol products calibrated *via* GC analysis. ^d Products not characterised from GC calibration.

When considering the results of the ethanol upgrading reactions conducted with different loadings of UiO-66(Zr) in the reaction, there does not seem to be a correlation between ethanol conversion activity and catalyst loading. A system utilising 0.05 mol% of the Lewis acidic MOF (Table 7, Entry 1) promoted more ethanol conversion than that with 0.1 mol% (Table 7, Entry 2), while a 0.2 mol% loading of UiO-66(Zr) resulted in the highest observed ethanol conversion of these three reactions (Table 7, Entry 3). All three reactions detailed in Table 7 showed similar selectivity in their respective product distributions towards *n*-butanol, and similar *n*-BuOH yields. The reaction utilising 0.05 mol% of UiO-66(Zr) yielded 17.8 % *n*-BuOH, a 0.1 mol% loading of UiO-66(Zr) in the system resulted in a 16.6% yield of *n*-BuOH while 0.2 mol% yielded 19.8 % *n*-BuOH, the highest *n*-BuOH yield achieved so far by a UiO-66(Zr)/ $[RuCl_2(dppm)_2]$ catalytic system. These results show that a loading of 0.05 mol% of the UiO-66(Zr) aldol catalyst provides an excess of catalytically active Lewis acid sites to allow facile aldol condensation chemistry in the Guerbet synthesis on *n*-butanol. Lower loadings of the aldol catalyst may still facilitate high ethanol conversions with good yields of *n*-butanol. A general trend of higher selectivity towards higher C₆ and C₈ alcohol products in the Guerbet upgrading of ethanol can be seen with increased

loadings of UiO-66(Zr) from Table 7. As the reaction conducted with 0.1 mol% of UiO-66(Zr) was the most selective reaction towards *n*-BuOH formation of those tested with different Lewis acid catalyst loadings, further Guerbet optimisation experiments were conducted using this loading of Lewis acid catalyst in the reaction.

Previous catalytic reactions had been conducted at a stirring rate of 500 rpm, and it was theorised that increasing the stirring rate would increase the activity of the catalytic system. Hence the Guerbet synthesis of *n*-butanol was trialled at stirring rates of 750 rpm and 1000 rpm, with loadings of 0.1 mol% of UiO-66(Zr) and [RuCl₂(dppm)₂], at 210 °C over 20 hours (Table 8).

Table 8: Stirring rate for the Guerbet upgrading of ethanol with UiO-66(Zr) and [RuCl₂(dppm)₂] as co-catalysts

Entry	Stirring Rate (rpm)	EtOH Conversion (%) ^a	Selectivity (%) ^b				
			<i>n</i> -BuOH	EtOAc	2-BuOH	Higher Alcohols ^c	Other ^d
1	500	44.6	37.2	7.2	0.7	15.0	39.9
2	750	39.9	39.3	9.3	0.5	15.8	35.1
3	1000	43.0	40.9	7.7	0.7	17.9	32.8

^a Conversion of ethanol calculated based on total liquid products obtained determined *via* GC analysis. ^b Selectivity to Guerbet products in liquid fraction determined *via* GC analysis. ^c C₆ and C₈ alcohol products calibrated *via* GC analysis. ^d Products not characterised from GC calibration.

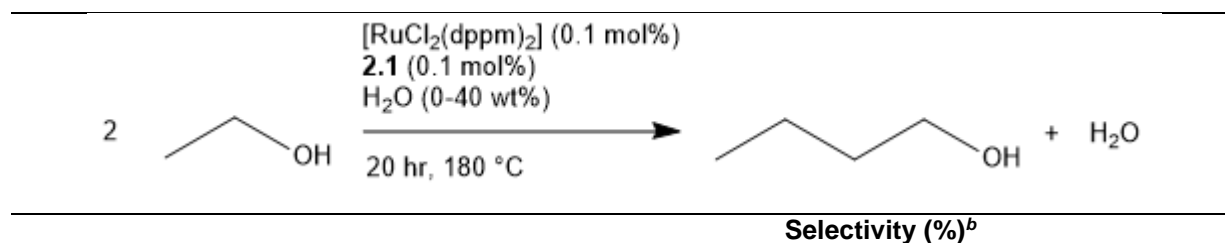
The catalytic results in Table 8 show that as the stirring rate of the reaction increases, there is a trend of increased product selectivity towards *n*-butanol and higher alcohols. While the reaction is less selective towards the synthesis of unknown side products. There doesn't appear to be a correlation between ethanol conversion facilitated by the catalyst mixture and the stirring rate of the Guerbet reaction. As prior catalytic reactions

were conducted at a stirring rate of 500 rpm, to allow for easier determination of improved reaction optimisation, further Guerbet reactions were to be conducted at a stirring rate of 500 rpm.

2.2.3 Effect of water on the system

As described in 1.2.2.2, ethanol is miscible with water, hence when considering it as a feedstock in the Guerbet reaction, separating any water becomes more challenging. The production of water in the Guerbet reaction, and its effect on sodium ethoxide in the homogeneous catalytic upgrading of ethanol was described in 1.5.2.3, where water in the reaction leads to the formation of sodium acetate through Tishchenko and Cannizaro chemistry. A potential advantage of using a MOF in place of NaOEt as an aldol catalyst with a homogeneous transfer hydrogenation catalyst in the Guerbet reaction is increased system tolerance towards water if the MOF is water stable. Not only would this prevent the formation of sodium acetate, but also have practical system implications when considering water separation from the ethanol feedstock if the system was water tolerant. Hence the Guerbet upgrading of ethanol by $[\text{RuCl}_2(\text{dppm})_2]$ (0.1 mol%) and UiO-66(Zr) (0.1 mol%) catalysts (180 °C, 20 hours) was tested with increasing loadings of water added to the reaction (Table 9).

Table 9: Water loading screen for the Guerbet upgrading of ethanol with UiO-66(Zr) and [RuCl₂(dppm)₂] as co-catalysts



Entry	H ₂ O Loading (wt%)	EtOH Conversion (%) ^a	Selectivity (%) ^b				
			<i>n</i> -BuOH	EtOAc	2-BuOH	Higher Alcohols ^c	Other ^d
1	0	30.8	29.2	9.4	1.3	4.9	55.2
2	10	16.0	16.3	21.3	2.5	1.9	58.0
3	20	14.5	13.1	25.5	1.4	1.4	58.6
4	30	17.8	5.1	15.2	1.1	1.1	77.5

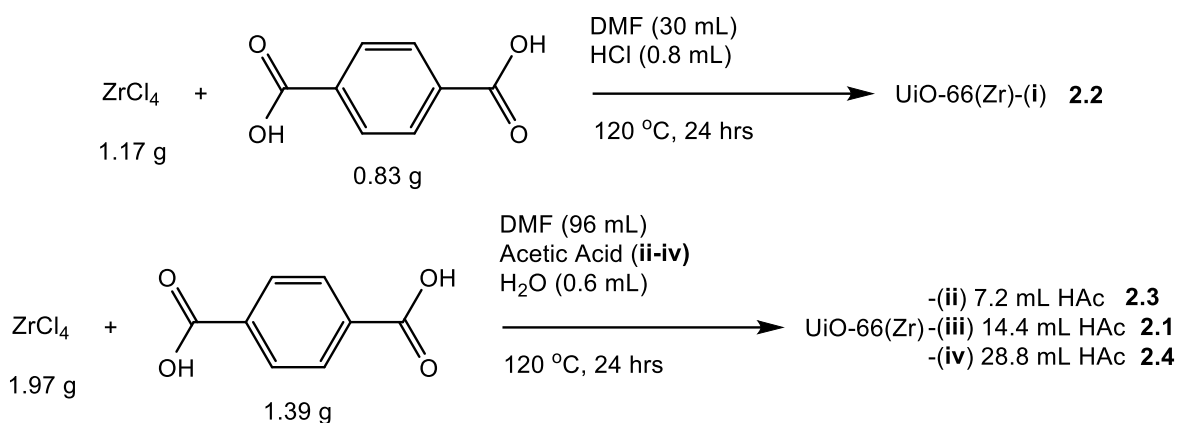
^a Conversion of ethanol calculated based on total liquid products obtained determined *via* GC analysis. ^b Selectivity to Guerbet products in liquid fraction determined *via* GC analysis. ^c C₆ and C₈ alcohol products calibrated *via* GC analysis. ^d Products not characterised from GC calibration.

When considering the results presented in Table 9, it becomes apparent that the introduction of water into the reaction mixture is detrimental for the Guerbet production of *n*-butanol from ethanol. When 10 wt% of water is added to the system (Table 9, Entry 2), the catalytic system becomes much less active for ethanol conversion compared to an analogous reaction with no water added to the system (Table 9, Entry 1). Interestingly, the addition of further aliquots of 10 wt% H₂O do not appear to impact the activity of the system for the conversion of ethanol (Table 9, Entries 2-4). However, the addition of water affects the catalytic system when considering the production of *n*-butanol. When considering Entries 1-4 in Table 9, the addition of increasing quantities of water to the ethanol upgrading reaction results in lower product selectivities to both *n*-BuOH and higher alcohols. While the water-free reaction at 180 °C facilitates a yield of *n*-BuOH of 9.0 %, when 30 wt% H₂O is added to the system, a yield of only 0.9 % is demonstrated (Table 9, Entry 4). Increasing the concentration of water in the system may lead to degradation of the transfer hydrogenation catalyst, which would be a valid theory to explain the decreasing yields of *n*-butanol and higher alcohols observed as higher

quantities of water are added to the system (Table 9), if the dehydrogenation of ethanol to acetaldehyde was hindered. The reasonably consistent ethanol conversions observed after water is added to the system (Table 9, Entries 2-4) may be explained by UiO-66(Zr) catalysed reactions of ethanol, like dehydration to diethyl ether that are not affected by the presence of water in the system.

2.3 Changing the MOF

The reactions detailed for the optimisation of the $[\text{RuCl}_2(\text{dppm})_2]/\text{UiO-66}(\text{Zr})$ catalysed Guerbet synthesis of *n*-butanol detailed in Section 2.2 used UiO-66(Zr) (**2.1**) that was synthesised according to Scheme 21. In the synthesis of this MOF, 14.4 mL of acetic acid was added to the reaction mixture to act as a modulating agent.² In the synthesis of MOFs, modulators tend to have the same functionality as the linker species that allows for the coordination of the framework, however, instead of being multifunctional, they are monofunctional.⁴ In the case of the synthesis of UiO-66(Zr), monocarboxylic acetic acid can be used as a modulator with the dicarboxylic terephthalic acid.⁴ The monocarboxylic acid competes to coordinate to the zirconium SBUs with the dicarboxylic acid during the synthesis of the MOF, and thermal activation of the MOF after synthesis can be utilised to remove the modulator groups from the nodes of the framework, thus leaving a framework with defect sites.⁴ The defect sites on modulated UiO-66(Zr) are open zirconium sites present on the nodes of the framework, and these open sites can be used for Lewis acidic catalysis.⁴ The UiO-66(Zr) that had been tested as an aldol catalyst in the Guerbet upgrading of ethanol described in 2.2 was made according to a modified literature procedure where 14.4 mL of acetic acid was added to the reaction mixture to create catalytically active defect sites, hence, different analogues of UiO-66(Zr) were synthesised with different loadings of acetic acid to determine whether the yield of *n*-BuOH could be increased through the creation of more catalytically active Lewis acid sites (Scheme 23).



Scheme 23: Synthetic strategies employed for the synthesis of different analogues of UiO-66(Zr) with varying loadings of acetic acid modulator.

An analogue of UiO-66(Zr) was synthesised in the absence of acetic acid in the reaction mixture. This MOF (**2.2**) was synthesised with the addition of HCl to the reaction mixture, which was added as a crystallising agent in the synthesis, according to a modified literature procedure from Zhang and co-workers.⁵ Two more samples of UiO-66(Zr) were prepared, with 7.2 mL (**2.3**) and 28.8 mL (**2.4**) of acetic acid added to the synthesis reaction mixture. These loadings of acetic acid were added to their respective syntheses as they represented half and double the loading to that in the synthesis of the UiO-66(Zr) (14.4 mL acetic acid) that had previously been tested as an aldol catalyst in the Guerbet upgrading of ethanol with $[\text{RuCl}_2(\text{dppm})_2]$ (Previous studies on the use of UiO-66(Zr) in the Guerbet upgrading of ethanol in Chapter two were conducted using **2.1**). Each of these frameworks was analysed *via* PXRD analysis to determine whether the increased or decreased loadings of acetic acid in the synthesis mixture affected the formation of the UiO-66(Zr) framework (Figure 18).

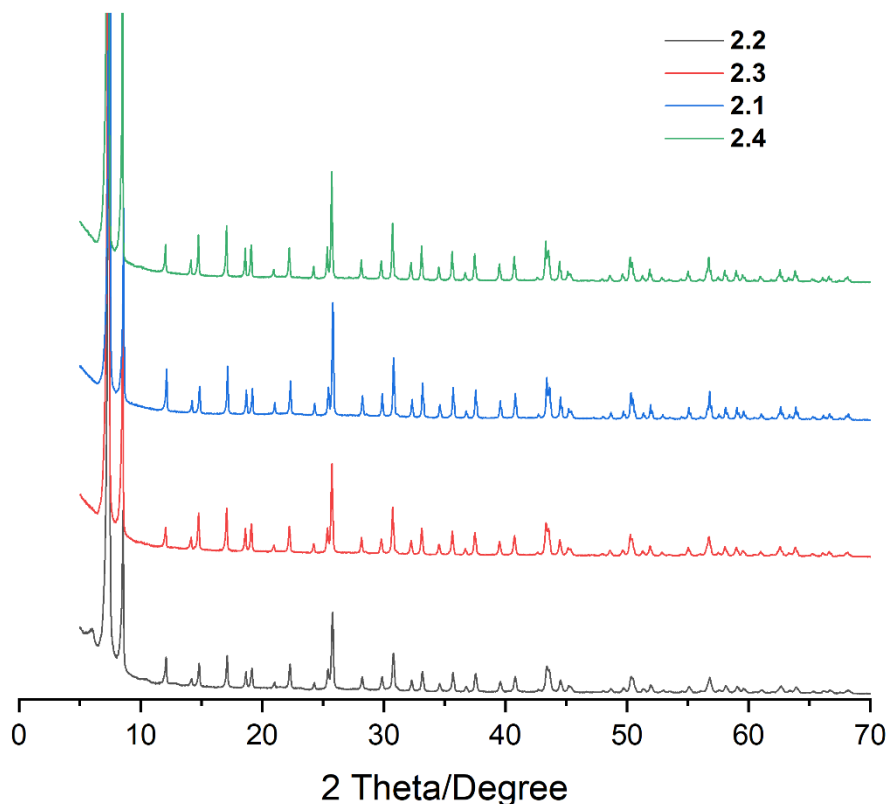


Figure 18: Comparing the PXRD patterns of the analogues of **2.1**, **2.2**, **2.3** and **2.4**

As shown in Figure 18, the UiO-66(Zr) analogues prepared with varying degrees of modulation (according to Scheme 23) all share the same characteristic diffraction pattern of UiO-66, hence differences in catalytic activity could be attributed to the degree of modulation in the synthesis of the MOF, as opposed to frameworks of different topology forming in the synthesis. Comparing the activity of the $[\text{RuCl}_2(\text{dppm})_2]/\text{UiO-66}(\text{Zr})$ catalysed Guerbet synthesis of *n*-butanol with these four different UiO-66(Zr) derivatives would show how the effect of modulation on UiO-66(Zr) catalysts in their synthesis affects their performance as an aldol catalyst. The four samples of UiO-66(Zr) (0.1 mol%) prepared with varying degrees of modulation (Scheme 23) were tested as aldol catalysts in the Guerbet upgrading of ethanol with $[\text{RuCl}_2(\text{dppm})_2]$ (0.1 mol%) as a transfer hydrogenation catalyst over a 20-hour reaction duration at 210 °C (Table 10).

Table 10: Comparing the effect of modulation in the synthesis of UiO-66(Zr) on catalytic activity in the Guerbet reaction

Entry	UiO-66(Zr)	EtOH Conversion (%) ^a	Selectivity (%) ^b				
			<i>n</i> -BuOH	EtOAc	2-BuOH	Higher Alcohols ^c	Other ^d
1	2.2	37.1	44.7	10.8	0.8	21.8	21.9
2	2.3	44.3	38.6	8.1	0.9	20.5	31.9
3	2.1	44.6	37.2	7.2	0.7	15.0	39.9
4	2.4	50.0	33.2	8.4	0.6	20.4	37.4

^a Conversion of ethanol calculated based on total liquid products obtained determined *via* GC analysis. ^b Selectivity to Guerbet products in liquid fraction determined *via* GC analysis. ^c C₆ and C₈ alcohol products calibrated *via* GC analysis. ^d Products not characterised from GC calibration.

When considering the results presented in Table 10, some interesting effects of the degree of modulation of the UiO-66(Zr) aldol catalyst on the Guerbet reaction can be evaluated. A general trend of increased ethanol conversion is observed with increased levels of modulation in the synthesis of the UiO-66(Zr), which initially appears to be advantageous. But when the reaction mechanism of the Guerbet reaction is considered, then this increased system catalytic activity is detrimental. Ethanol is initially converted to acetaldehyde by the homogeneous Ru catalyst in the system, and the aldol catalyst shouldn't affect this reaction. The increased ethanol conversion observed when increasing modulated UiO-66(Zr) catalysts are utilised in the reaction suggests that a greater number of defect catalytic sites results in the MOF catalysing undesired reactions such as the dehydration of ethanol to diethyl ether. This theory is further justified when considering the product distribution selectivity of the reactions detailed in Table 10 (Entries 1-3). Using the UiO-66(Zr) catalyst synthesised with no acetic acid (**2.2**) resulted in the most selective conversion of ethanol to both *n*-BuOH and higher alcohols of the different UiO-66(Zr) analogues tested. The product selectivity of the Guerbet reactions of

ethanol towards *n*-BuOH and higher alcohols sequentially fell when UiO-66(Zr) samples of increasing modulation were used, while selectivity towards uncharacterised side products increased, when **2.2**, **2.3** and **2.1** are considered. The *n*-BuOH yields of the reactions using these three UiO-66(Zr) samples are remarkably similar, while the yields of higher alcohols showed no trend. This suggests that as the loading of acetic acid (from 0 to 14.4 mL), and hence modulation of the aldol catalyst increases, the MOF retains similar activity as an aldol catalyst, while becoming more active for undesired side reactions. When the loading of acetic acid in the synthesis of the aldol catalyst is further increased to 28.8 mL (**2.4**), Table 10 Entry 4), the ethanol conversion percentage is the highest of the four analogues tested, while product selectivity towards *n*-BuOH is the lowest. The ethanol conversion percentage and selectivity towards *n*-BuOH of the four Guerbet reactions of ethanol conducted with [RuCl₂(dppm)₂] and the UiO-66(Zr) samples of different modulation are shown in Figure 19, highlighting a clear trend of increasing ethanol conversion and lower reaction selectivity towards *n*-BuOH with increased modulation of the aldol catalyst.

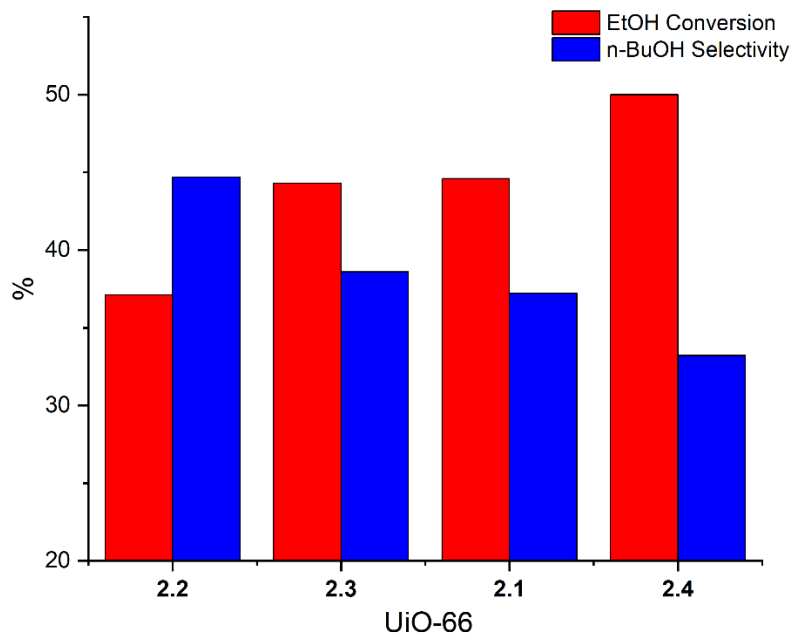
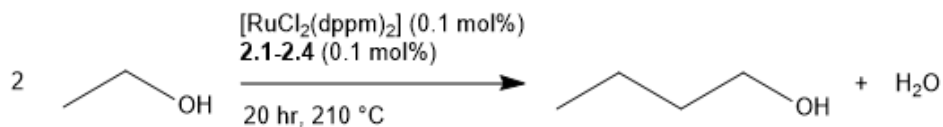
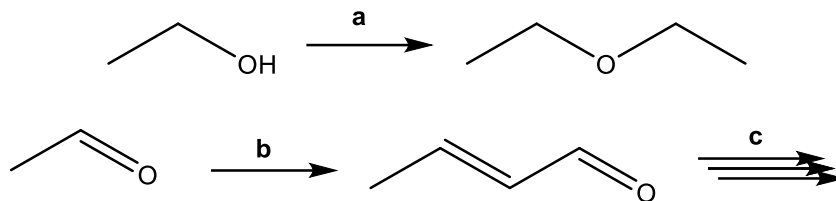


Figure 19: Comparing EtOH conversion and *n*-BuOH selectivity of the Guerbet reactions using MOFs prepared with different degrees of modulation (**2.1**, **2.2**, **2.3** and **2.4**)

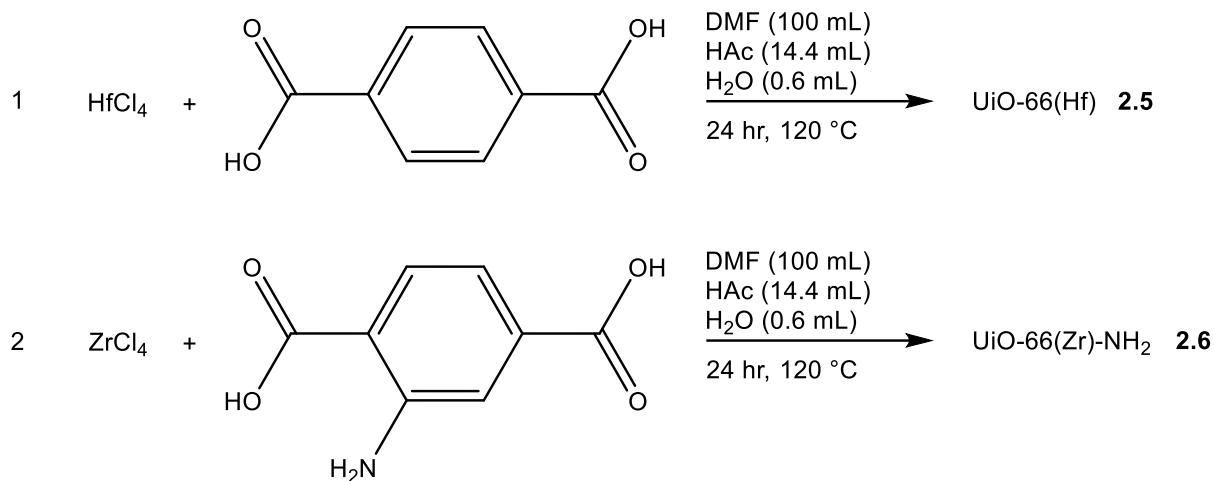
When considering the result of the Guerbet coupling of ethanol conducted with **2.4** (Table 10, Entry 4), the reaction selectivity towards higher alcohols increases over the reaction with **2.1**, while the yield of *n*-BuOH remains similar to the other reactions presented in Table 10. The selectivity of the reaction towards other uncharacterised products also decreases compared to the reaction using **2.1**, indicating that the higher levels of modulation forms a UiO-66(Zr) catalyst that is more active for the formation of higher alcohols (that have not been calibrated for *via* GC analysis) through aldol coupling, hence less selective for the unconfirmed side reaction (assumed to be ethanol dehydration) observed to a greater extent when using **2.1** as the aldol catalyst.



Scheme 24: Proposed reactions catalysed by UiO-66(Zr) in the Guerbet reaction of ethanol: a) dehydration of ethanol to diethyl ether, b) aldol condensation of ethanol to acetaldehyde, c) further aldol coupling of longer chained aldehydes.

The proposed reactions that the aldol catalyst influences in the Guerbet synthesis of *n*-butanol are shown in Scheme 24, where reaction **a** is promoted by increasing the modulation in the synthesis of UiO-66(Zr) with up to 14.4 mL of acetic acid (**2.1**). Increasing the modulation of the framework by adding 28.8 mL of acetic acid in the synthesis doesn't have a further effect on this reaction, however, increases the formation of higher alcohols through reactions using crotonaldehyde as a substrate to react with acetaldehyde or subsequently formed long chain aldehydes (Scheme 24, **c**). The aldol condensation of acetaldehyde (Scheme 24, **b**) was largely unaffected by the degree of modulation of the UiO-66(Zr) catalysts tested in the Guerbet reaction of ethanol with [RuCl₂(dppm)₂].

As UiO-66(Zr) proved to be an active aldol catalyst in the Guerbet upgrading of ethanol with [RuCl₂(dppm)₂] as a transfer hydrogenation catalyst, the idea of using alternative MOFs in the reaction was explored. Two different analogues of UiO-66 were synthesised (with an analogous structure to UiO-66(Zr)), with the same loading of acetic acid modulator as the UiO-66(Zr) tested in 2.2 (Scheme 21). One of these UiO-66 samples made was a hafnium derivative (UiO-66(Hf), **2.5**), where the nodes of the SBU would be Hf₆ based instead of Zr₆, as UiO-66(Hf) is known to be more Brønsted acidic than UiO-66(Zr) (Scheme 25, **2.5**).⁶ The other MOF synthesised was based on zirconium nodes, with 2-aminoterephthalic acid linkers instead of the terephthalic acid linkers usually found on UiO-66(Zr) (UiO-66(Zr)-NH₂ (Scheme 25, **2.6**).



Scheme 25: Modulated synthesis pathways employed towards the UiO-analogues UiO-66(Hf) (2.5) and UiO-66(Zr)-NH₂ (2.6).

PXRD patterns of the MOFs synthesised according to the procedures detailed in Scheme 25 were obtained and compared to the PXRD pattern of **2.1**, as these MOFs were all prepared with the same loading of acetic acid in the synthesis as a modulating agent. These PXRD patterns are compared in Figure 20.

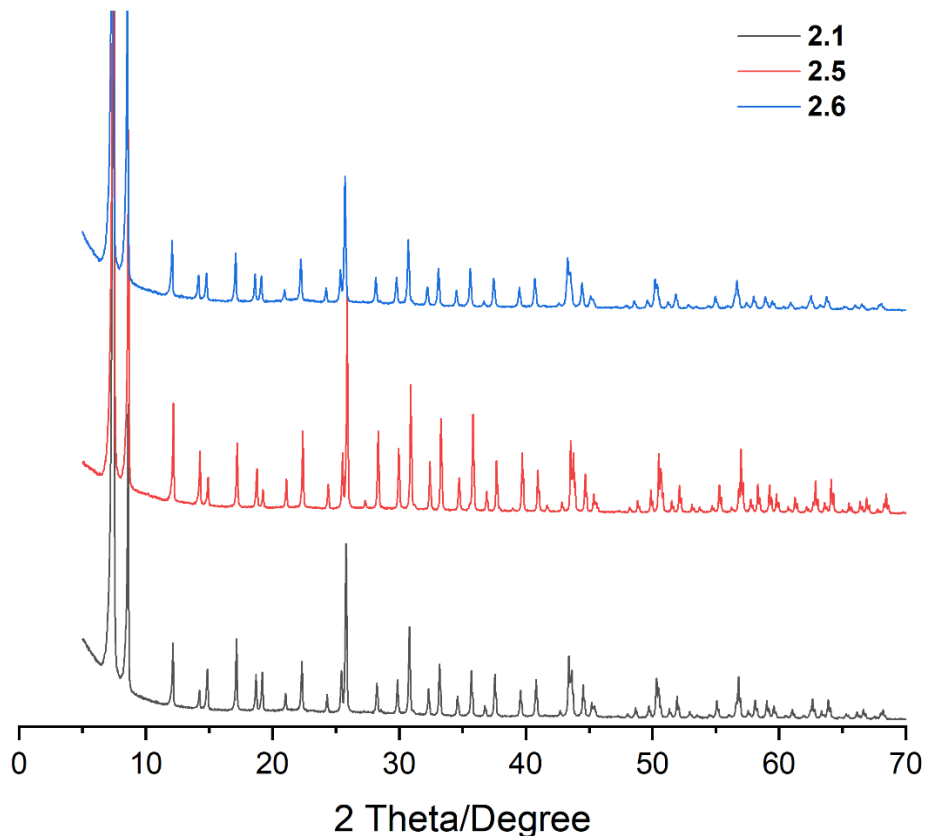


Figure 20: Comparing the PXRD patterns of **2.1**, **2.5** and **2.6**.

When comparing the PXRD patterns shown in Figure 20, it is clear that the three different MOFs share the same diffraction pattern. Although the structures of **2.5** and **2.6** differ from **2.1** with regards to SBU metal and linker respectively, the fact that the PXRD patterns in Figure 20 show identical peaks highlights that the MOFs synthesised according to Scheme 25 have the same UiO-66 topology as **2.1**. The structures of **2.1**,⁷ **2.5**⁸ and **2.6**⁷ were confirmed by comparing the diffraction patterns presented in Figure 20 against patterns reported in literature for the same materials.

Hence these MOFs could be compared as heterogeneous catalysts in the Guerbet synthesis of *n*-butanol, where differences in the components of each framework could be attributed to any observed change in catalytic activity. **2.5** and **2.6** were trialled as aldol catalysts in the Guerbet upgrading of ethanol with $[\text{RuCl}_2(\text{dppm})_2]$ as a transfer hydrogenation catalyst at 210 °C over 20 hours (Table 11).

Table 11: Comparing the Guerbet upgrading of ethanol utilising UiO-66(Zr), UiO-66(Hf) or UiO-66(Zr)-NH₂ as aldol catalysts

		[RuCl ₂ (dppm) ₂] (0.1 mol%) MOF (0.1 mol%) 20 hr, 210 °C					
2							
		Selectivity (%) ^b					
Entry	MOF	EtOH Conversion (%) ^a	Higher				Other ^d
			<i>n</i> -BuOH	EtOAc	2-BuOH	Alcohols ^c	
1	2.1	44.6	37.2	7.2	0.7	15.0	39.9
2	2.5	39.4	44.4	6.1	0.8	20.6	28.1
3	2.6	53.8	35.7	7.1	0.6	18.4	38.2

^a Conversion of ethanol calculated based on total liquid products obtained determined *via* GC analysis. ^b Selectivity to Guerbet products in liquid fraction determined *via* GC analysis. ^c C₆ and C₈ alcohol products calibrated *via* GC analysis. ^d Products not characterised from GC calibration.

When **2.5** was tested in the Guerbet reaction (Table 11, Entry 2), the catalytic system was less active for ethanol conversion than when **2.1** was used. However, the product distribution was more selective towards *n*-BuOH and higher alcohols than that when the zirconium analogue was implemented. The selectivity of the reaction towards uncharacterised products was lower when **2.5** was used compared to **2.1**, which is an indication that the hafnium analogue may be a more active aldol catalyst than the zirconium analogue in the reaction with [RuCl₂(dppm)₂] as a transfer hydrogenation catalyst, while being less active for side reactions like the dehydration of ethanol to diethyl ether. This difference in catalytic activity can be deduced by the lower ethanol conversion facilitated by **2.5** compared to **2.1**, in conjunction with the high selectivity of the hafnium analogue towards aldol coupled products. **2.6** Was the most active UiO-66 structure trialled in the Guerbet upgrading of ethanol with [RuCl₂(dppm)₂], but the least selective towards *n*-BuOH formation (Table 11 Entry 3). This system using **2.6** was more selective towards higher alcohol formation than that which used **2.1**, suggesting that the amine functionalised MOF was more active for the aldol coupling of longer chained aldehyde species than **2.1**.

2.4 Changing the transfer hydrogenation catalyst

The work presented thus far on the use of UiO-66(Zr) as an aldol catalyst in the upgrading of ethanol had been conducted using $[\text{RuCl}_2(\text{dppm})_2]$ as a transfer hydrogenation catalyst. Previous studies by the Wass group had shown this catalyst to be optimal in the Guerbet reaction with NaOEt at 150 °C,³ however, under the optimal conditions tested with UiO-66(Zr) as an aldol catalyst, the reaction temperature was increased to 210 °C. This increase in reaction temperature warranted an investigation into the nature of the homogenous transfer hydrogenation being used in the Guerbet reaction alongside UiO-66(Zr), to determine whether there was a different transfer hydrogenation catalyst that was more active under the increased temperature.

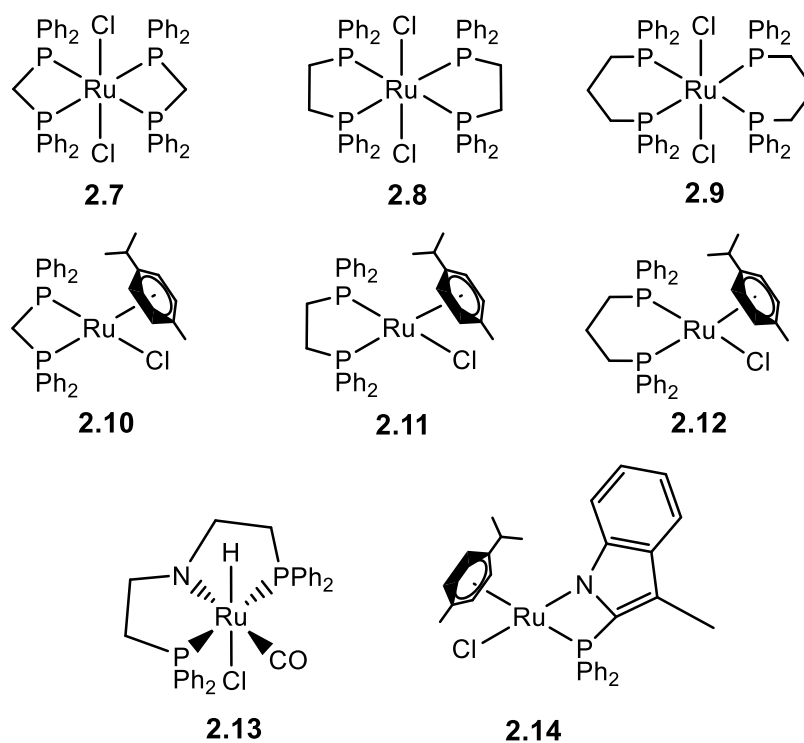
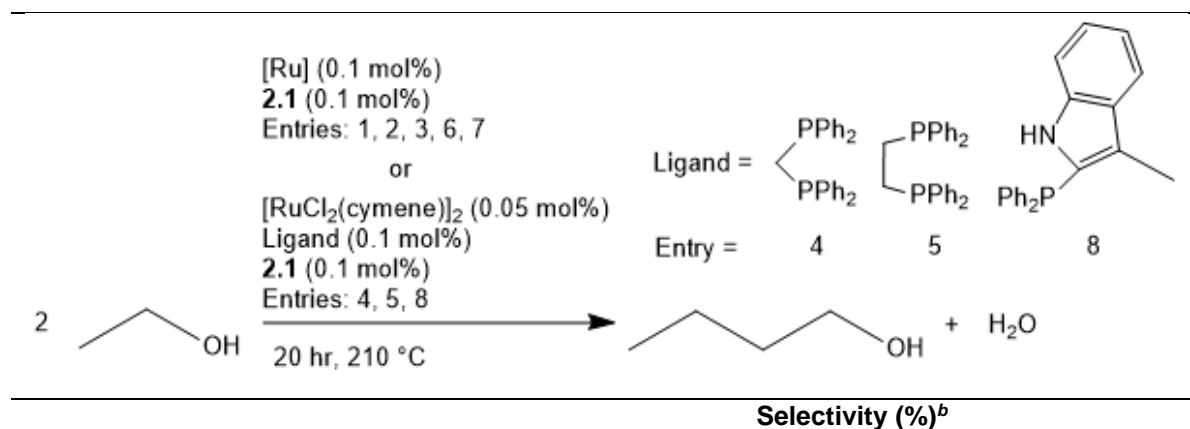


Figure 21: Different homogeneous ruthenium transfer hydrogenation catalysts to be tested as transfer hydrogenation catalysts with UiO-66(Zr) in the Guerbet upgrading of ethanol: **2.7**- $[\text{RuCl}_2(\text{dppm})_2]$ (pre-synthesised), **2.8**- $[\text{RuCl}_2(\text{dppe})_2]$ (pre-synthesised), **2.9**- $[\text{RuCl}_2(\text{dppp})_2]$ (pre-synthesised), **2.10**- $[\text{RuCl}(\text{cymene})(\text{dppm})]$ (made in situ), **2.11**- $[\text{RuCl}(\text{cymene})(\text{dppe})]$ (made in situ), **2.12**- $[\text{RuCl}(\text{cymene})(\text{dppp})]$ (pre-formed), **2.13**-Ru-MACHO (pre-formed), **2.14**- $[\text{RuCl}(\text{cymene})(2\text{-}(\text{Diphenylphosphino})\text{-3-methyl-1H-indole})]$ (made in situ).

The homogeneous ruthenium catalysts that were tested alongside UiO-66(Zr) in the Guerbet upgrading of ethanol are shown in Figure 21. The different transfer hydrogenation catalysts would be compared against [RuCl₂(dppm)₂] (Figure 21, **2.7**), the benchmark transfer hydrogenation catalyst that had been used to optimise the homogeneous/MOF catalyst Guerbet reaction. Analogous diphosphine bischelate complexes to [RuCl₂(dppm)₂] were tested in the reaction, with the larger bite angle dppe (Figure 21, **2.8**) and dppp ligands (Figure 21, **2.9**). Monochelate complexes using these three diphosphine ligands of increasing bite angle were also tested as transfer hydrogenation catalysts with UiO-66(Zr) in the newly optimised Guerbet reaction. Homogeneous complexes based on the structure of [Ru(Cl)(cymene)(L)], using dppm (Figure 21, **2.10**), dppe (Figure 21, **2.11**) and dppp (Figure 21, **2.12**) as monochelate diphosphine ligands were the catalysts tested with UiO-66(Zr) for the Guerbet upgrading of ethanol. In addition to these 6 complexes using diphosphine ligands, Ru-MACHO (Figure 21, **2.13**) was also tested, as well complex **2.14** (Figure 21), a cymene chloride complex using with a monochelate 2-(Diphenylphosphino)-3-methyl-1H-indole ligand. All the complexes shown in Figure 21 (0.1 mol%) were trialed as homogeneous transfer hydrogenation catalysts with UiO-66(Zr) (prepared according to Scheme 21) at 210 °C over a reaction duration of 20 hours (Table 12).

Table 12: Screen of different [Ru] transfer hydrogenation catalysts in the Guerbet upgrading of ethanol



Entry	[Ru] (from Figure 21)	EtOH Conversion (%) ^a	Selectivity (%) ^b				
			<i>n</i> -BuOH	EtOAc	2-BuOH	Higher Alcohols ^c	Other ^d
1	2.7	44.6	37.2	7.2	0.7	15.0	39.9
2	2.8	25.0	32.8	7.2	-	4.0	56.0
3	2.9	38.1	33.3	55.4	5.5	6.0	-
4	2.10	26.8	36.9	40.3	1.9	6.4	14.5
5	2.11	40.2	42.3	22.1	1.5	16.7	17.4
6	2.12	40.3	18.4	54.3	6.2	3.2	17.9
7	2.13	9.2	33.7	-	-	5.4	60.9
8	2.14	15.5	34.8	43.2	-	14.2	7.8

^a Conversion of ethanol calculated based on total liquid products obtained determined *via* GC analysis. ^b Selectivity to Guerbet products in liquid fraction determined *via* GC analysis. ^c C₆ and C₈ alcohol products calibrated *via* GC analysis. ^d Products not characterised from GC calibration.

The catalytic system employed for the upgrading of ethanol using the [RuCl₂(dppm)₂] transfer hydrogenation catalyst showed the highest activity for ethanol conversion of all those trialed with different Ru catalysts (Table 12, Entry 1). When considering the diphosphine bischelate catalysts (Table 12, Entries 1-3) increasing the bite angle of the ligands does not have a great effect on the selectivity of the respective catalytic systems towards *n*-BuOH. The smaller bite angle dppe and dppe analogues show low product selectivity towards *n*-BuOH, while using the [RuCl₂(dppp)₂] catalyst facilitates a highly selective reaction towards the synthesis of ethyl acetate (Table 12, Entry 3). The most

selective reaction towards ethyl acetate formation of those using the $[\text{Ru}(\text{Cl})(\text{cymene})(\text{L})]$ complexes ($\text{L} = \text{dppm}, \text{dppe}$ or dppp) (Table 12, Entries 4-6) was $[\text{Ru}(\text{Cl})(\text{cymene})(\text{dppp})]$. Hence of the bischelate and monochelate dppm, dppe and dppp complexes trialed as transfer hydrogenation catalysts with $\text{UiO-66}(\text{Zr})$ for ethanol upgrading to *n*-butanol, using dppp as a ligand in both of these catalyst motifs produced the most active analogue for ethyl acetate formation (Figure 22).

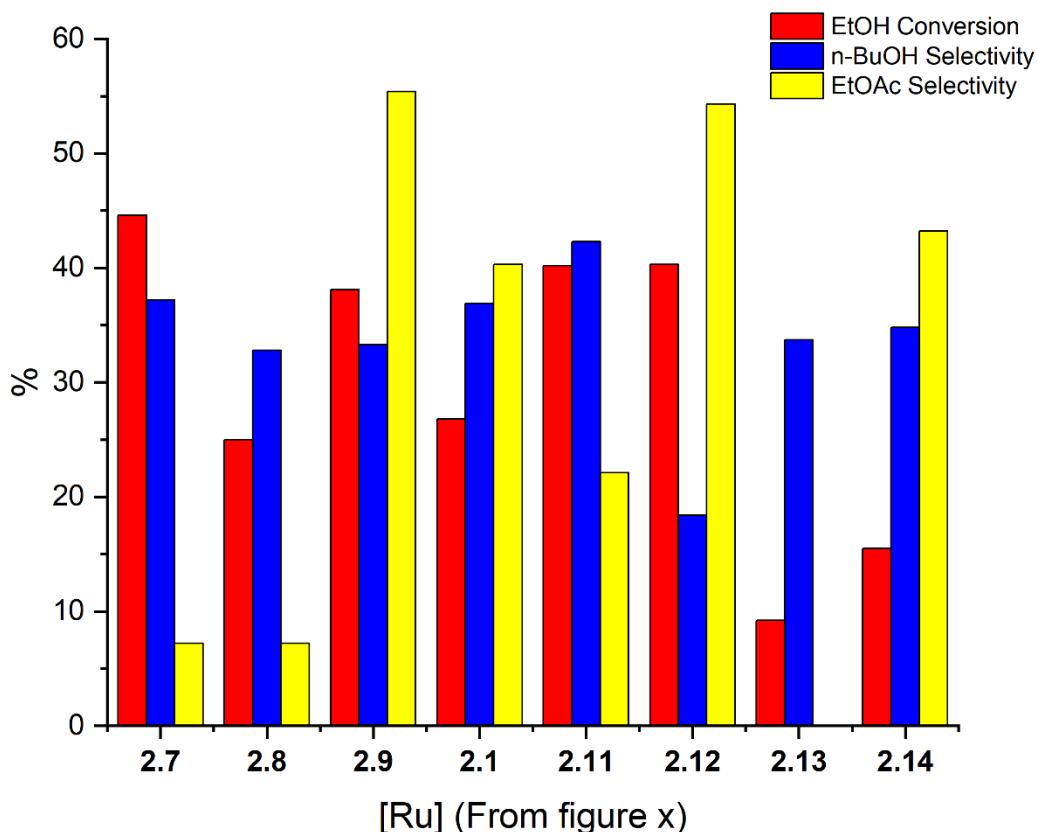


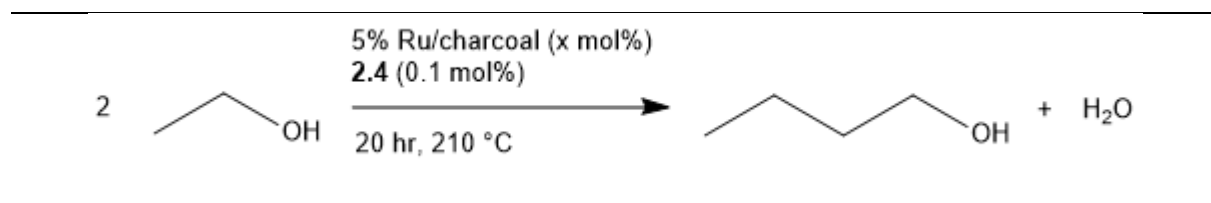
Figure 22: Comparing EtOH conversion, *n*-BuOH selectivity and EtOAc selectivity percentages of the Guerbet reactions conducted with different ruthenium transfer hydrogenation catalysts

When considering the dppm, dppe and dppp bischelate transfer hydrogenation catalysts (Figure 21, **2.7-2.9**) there is no apparent relation between EtOH conversion activity of the catalytic system and ligand bite angle, while for the monochelating complexes (Figure 21, **2.10-2.12**) there is a slight increase in EtOH conversion with increasing bite angle of the ligand. Both Ru-MACHO (**2.13**) and **2.14** (Figure 21) showed low activity for ethanol conversion and moderate selectivity towards *n*-BuOH in the product distribution (Table 12, Entries 7 and 8), with complex h showing higher selectivity towards the formation of

ethyl acetate. When considering the results in Table 12, there appears to be a transfer hydrogenation catalyst that is more active for the formation of *n*-BuOH with UiO-66(Zr). The catalyst mixture using [Ru(Cl)(cymene)(dppe)] (Figure 21, **2.11**) facilitated a *n*-BuOH yield of 17.0 % compared to the 16.6 % yield recorded when [RuCl₂(dppm)₂] was used. However, this catalyst appears to suffer from a lack of stability at the elevated reaction temperature of 210 °C, as the post reaction mixture appeared as a dark brown/black colour opposed to a light orange colour of the starting catalyst, which is indicative of the breakdown of the homogeneous catalyst to nanoparticles. Hence, [RuCl₂(dppm)₂] was still considered to be the optimal homogeneous transfer hydrogenation catalyst out of those trialed with UiO-66(Zr) for the Guerbet reaction of ethanol.

The concept of introducing a heterogenous transfer hydrogenation catalyst in place of a homogeneous complex was briefly explored. This area was probed to develop a fully heterogenous catalytic Guerbet system using a Lewis acidic aldol catalyst and heterogeneous transfer hydrogenation catalyst, which would be advantageous when considering process chemistry and catalyst recovery. As previous studies on the homogeneous transfer hydrogenation catalyst using UiO-66(Zr) as an aldol catalyst for ethanol upgrading had focused on ruthenium transfer hydrogenation catalysis, 5% Ru/charcoal was studied as a heterogeneous alternative (Table 13).

Table 13: Screening 5% Ru/Charcoal as a heterogeneous transfer hydrogenation catalyst in the Guerbet upgrading of ethanol



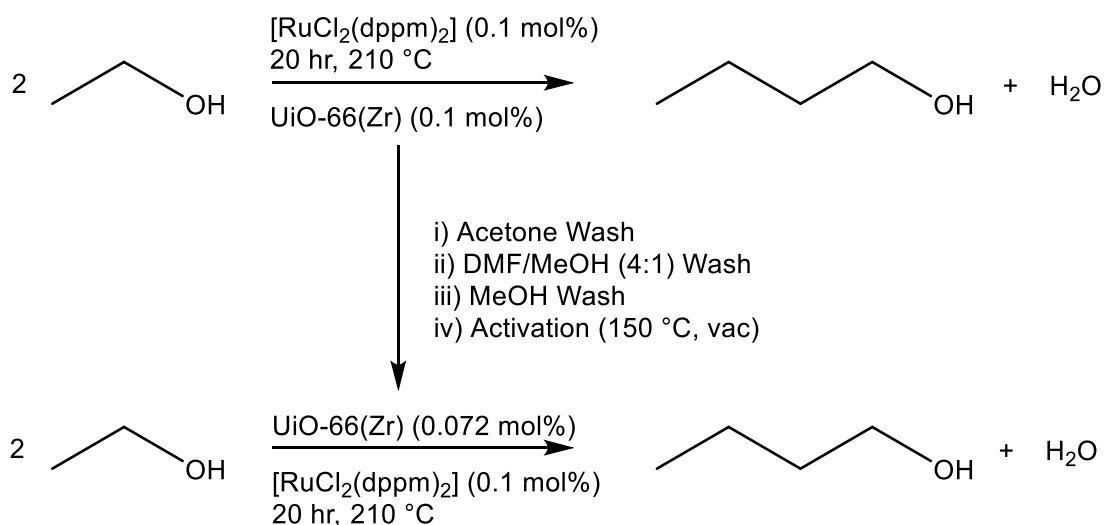
Entry	5% Ru/charcoal loading (mol%)	EtOH Conversion (%) ^a	Selectivity (%) ^b				
			<i>n</i> -BuOH	EtOAc	2-BuOH	Higher Alcohols ^c	Other ^d
1	0.05	14.8	41.9	12.2	-	8.1	37.8
2	0.1	16.7	51.5	11.4	-	16.8	20.3

^a Conversion of ethanol calculated based on total liquid products obtained determined *via* GC analysis. ^b Selectivity to Guerbet products in liquid fraction determined *via* GC analysis. ^c C₆ and C₈ alcohol products calibrated *via* GC analysis. ^d Products not characterised from GC calibration.

5% Ru/charcoal was trialed as a heterogeneous transfer hydrogenation catalyst with **2.4** for the Guerbet synthesis of *n*-butanol. While the catalytic systems using 5% Ru/charcoal showed good selectivity towards the synthesis of *n*-butanol, with a selectivity of over 50 % demonstrated with a loading of 0.1 mol% of the transfer hydrogenation catalyst (Table 13, Entry 2), the systems proved to be relatively inactive for ethanol conversion. A maximum ethanol conversion of 16.7 % was observed with a 0.1 mol% loading of 5% Ru/charcoal under previously optimised reaction conditions using UiO-66(Zr) as a Lewis acidic aldol catalyst, which is significantly lower than that demonstrated in systems using the homogenous [RuCl₂(dppm)₂] catalyst. While further reaction optimisation for the heterogeneous system detailed in Table 13 may have improved the activity of the heterogeneous transfer hydrogenation catalyst, the [RuCl₂(dppm)₂]/UiO-66(Zr) catalytic system was still superior to others trialed when considering the nature of the transfer hydrogenation catalyst.

2.5 UiO-66(Zr) Recycling

One of the key advantages of using a heterogeneous MOF alongside a homogeneous transfer hydrogenation catalyst for the Guerbet upgrading of ethanol is the potential for the aldol catalyst to be recycled. Sodium ethoxide base traditionally used as an aldol catalyst in this reaction hydrolyses in the presence of water that is generated *via* the aldol condensation of acetaldehyde and in the synthesis of higher alcohols; and the product of this hydrolysis leads to the formation of unwanted sodium acetate. Hence, the ability of UiO-66(Zr) to be recycled from a Guerbet reaction and reused as an aldol catalyst in a further reaction was tested. **2.1** was used as an aldol catalyst in the Guerbet synthesis of *n*-butanol, under the same reaction conditions detailed in Table 4, Entry 5 (210 °C, 20 hours, 0.1 mol% of UiO-66(Zr) and [RuCl₂(dppm)₂]). The post reaction solid was isolated and washed with acetone to remove any residual [RuCl₂(dppm)₂], then washed twice with DMF:MeOH (4:1) and twice with MeOH (literature MOF work up procedure ²) to remove any products of the previous Guerbet reaction from the pores of the MOF. Finally, the recycled UiO-66(Zr) was activated by heating under vacuum at 150 °C overnight to remove MeOH. This recycled UiO-66(Zr) was then used as an aldol catalyst in the Guerbet upgrading of ethanol with a new loading of [RuCl₂(dppm)₂] (0.1 mol%) under the same conditions as the previous Guerbet reaction (Scheme 26).



Scheme 26: Schematic pathway to recycle UiO-66(Zr) from a Guerbet reaction of ethanol, to use as an aldol catalyst in a subsequent Guerbet reaction.

Due to losses in the extensive work up procedure of the UiO-66(Zr) from the initial Guerbet reaction, a UiO-66(Zr) loading of 0.072 mol% was recovered for use as an aldol catalyst in the second Guerbet run of this recyclability trial. However, as a lower UiO-66(Zr) loading of 0.05 mol% was shown to actively catalyse the aldol condensation in this Guerbet reaction (Table 7 Entry 1), no significant decrease in catalytic activity was to be expected from the catalytic system using the recycled MOF. The results of the Guerbet reactions detailed in Scheme 26 are shown in Table 14.

Table 14: Comparing catalytic activity in the Guerbet upgrading of ethanol using pristine and recycled UiO-66(Zr)

		[RuCl ₂ (dppm) ₂] (0.1 mol%) 2.1 (x mol%) 20 hr, 210 °C						
2								
		Selectivity (%) ^b						
Entry	MOF (mol%)	EtOH Conversion (%) ^a	Selectivity (%) ^b				Higher Alcohols ^c	Other ^d
			<i>n</i> -BuOH	EtOAc	2-BuOH			
1	2.1 (0.1)	39.9	44.9	4.5	0.8	18.0	31.8	
2 ^e	2.1 (0.072)	38.1	44.4	10.0	1.0	18.4	26.2	

^a Conversion of ethanol calculated based on total liquid products obtained determined *via* GC analysis. ^b Selectivity to Guerbet products in liquid fraction determined *via* GC analysis. ^c C₆ and C₈ alcohol products calibrated *via* GC analysis. ^d Products not characterised from GC calibration.

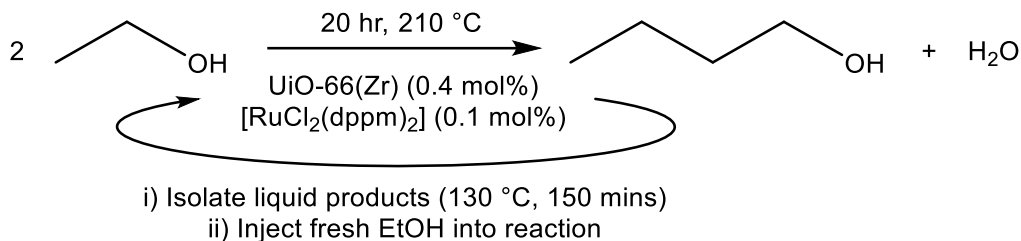
^e UiO-66(Zr) recovered from the reaction detailed in Entry 1.

The UiO-66(Zr) that was recovered from the initial Guerbet reaction of ethanol proves to be an active aldol catalyst in a further catalytic run. When considering the product distribution of the Guerbet reaction of the recycled MOF (Table 14, Entry 2), EtOH conversion is similar to the reaction using the pristine MOF (Table 14, Entry 1), while the reaction selectivity towards to the desired *n*-BuOH product is almost identical. The recycled UiO-66(Zr) is more active for the formation of ethyl acetate than the pristine MOF, indicating that this MOF is more active for Tishchenko catalysis, however, selectivity towards higher alcohols is almost identical to the reaction catalysed by the initial loading of UiO-66(Zr). When considering the selectivities of the reactions using the

pristine and recycled MOF towards known alcohols, the system using pristine UiO-66 converts EtOH with a selectivity towards alcohols of 63.7 % (Table 14, Entry 1), while the UiO-66(Zr) recycled from this reaction facilitates a selectivity towards alcohols of 63.8% (Table 14, Entry 2), when used as an aldol catalyst with a new loading of $[\text{RuCl}_2(\text{dppm})_2]$. These almost identical alcohol product selectivities, combined with the near identical ethanol conversions of the reactions shown in Table 14 show that the catalytic aldol activity of UiO-66(Zr) is maintained after one Guerbet reaction, and presents UiO-66(Zr) as re-usable heterogeneous aldol catalyst with $[\text{RuCl}_2(\text{dppm})_2]$ as a transfer hydrogenation catalyst. Whether or not the UiO-66(Zr) that was recycled from the reaction detailed in Table 14 Entry 2 was still intact as a MOF, or whether it had broken down in the reaction to a species that was still catalytically active could not be determined, as the quantity of catalyst from the reaction in Table 14 Entry 2 was too low to conduct post reaction XRD. Hence a new catalyst recycling methodology was developed, to allow for complete recovery of the MOF catalyst, while also testing the recyclability of the catalytic system as a whole, and not just the heterogeneous aldol catalyst.

2.6 Recyclability of entire catalytic system

A system was devised to conduct multiple catalytic cycles using recycled UiO-66(Zr) and $[\text{RuCl}_2(\text{dppm})_2]$, to determine whether the heterogeneous/homogeneous catalysed upgrading of ethanol was recyclable. A Guerbet reaction of ethanol would be run in an autoclave with a catalytic loading of UiO-66(Zr) and $[\text{RuCl}_2(\text{dppm})_2]$ and allowed to cool to room temperature post reaction. Once cooled, the liquid products of the reaction would be isolated, by evacuating the autoclave directly into an external liquid nitrogen cooled cold trap, at 130 °C under vacuum for 150 minutes. A fresh loading of ethanol would be injected into the autoclave containing the post reaction catalyst mixture from the previous Guerbet reaction, and a further ethanol upgrading reaction would be conducted using the recycled catalyst mixture. This process could then be repeated to continuously recycle both the UiO-66(Zr) and $[\text{RuCl}_2(\text{dppm})_2]$ and evaluate their catalytic performance for the Guerbet upgrading of ethanol over multiple reactions (Scheme 27).



*Scheme 27: Schematic pathway employed to recycle UiO-66(Zr) and $[\text{RuCl}_2(\text{dppm})_2]$ as catalysts in the Guerbet synthesis of *n*-butanol for use in multiple reactions.*

In the initial Guerbet upgrading of ethanol, instead of the standard 0.1 mol% loading of UiO-66(Zr), a loading of 0.4 mol% was added to the reaction as an aldol catalyst. This increased loading was not added in an attempt to improve yields, instead to give a quantity of post-reaction MOF that could be analysed by PXRD to determine whether the MOF was intact after multiple Guerbet reactions.

Table 15: Recyclability study on the evolution of UiO-66(Zr) and $[\text{RuCl}_2(\text{dppm})_2]$ co-catalysts in the Guerbet upgrading of ethanol

		Entry 1 - $[\text{RuCl}_2(\text{dppm})_2]$ (0.1 mol%), 2.1 (0.4 mol%) Entries 2-6 - Recycled catalysts from previous entry				
		20 hr, 210 °C				
		Selectivity (%) ^b				
Entry (run)	EtOH Conversion (%) ^a	<i>n</i> -BuOH	EtOAc	2-BuOH	Higher Alcohols ^c	Other ^d
1	29.1	36.8	9.6	-	12.4	41.2
2	12.2	51.6	17.2	-	10.7	20.5
3	15.7	38.9	13.4	-	7.0	40.7
4	26.8	62.6	16.4	0.7	25.0	-
5	40.9	54.0	16.9	1.2	20.5	7.4
6	40.8	51.7	21.6	1.7	17.2	7.8

^a Conversion of ethanol calculated based on total liquid products obtained determined *via* GC analysis. ^b Selectivity to Guerbet products in liquid fraction determined *via* GC analysis. ^c C₆ and C₈ alcohol products calibrated *via* GC analysis. ^d Products not characterised from GC calibration.

Analysis of the results of the system recycling experiment detailed in Table 15 highlights some interesting results. Initial recycling of the catalyst mixture from Table 15 Entry 1 results in a decrease in activity for the conversion of ethanol, to a product distribution that

is more selective towards alcohol formation. Ethanol conversion falls from 29.1 % to 12.2 % in the first reaction using recycled catalyst (Table 15, Entry 2) and remains low (15.7%) after a further cycle (Table 15, Entry 3). However, subsequent catalytic cycles see larger increases in ethanol conversion, where on the 5th recycling reaction (Table 15, Entry 5), ethanol conversion (40.9 %) is higher than the reaction catalysed by the starting catalytic mixture of UiO-66(Zr) and [RuCl₂(dppm)₂] (29.1 %) (Table 15, Entry 1). This high catalytic activity is maintained after a further cycle. This trend is represented in Figure 23, along with the development of *n*-BuOH selectivity and EtOAc selectivity of the reactions in the system recycling experiment.

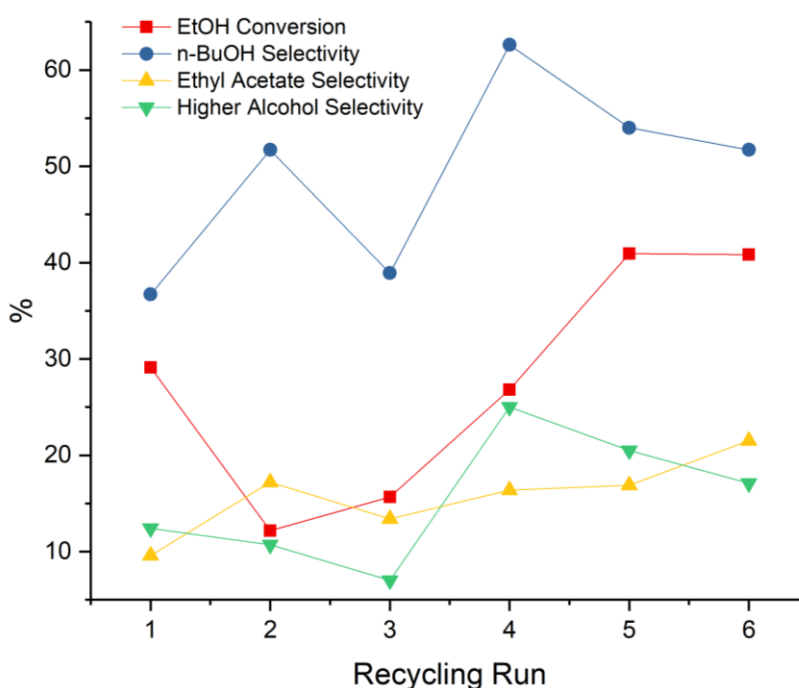


Figure 23: Comparing EtOH conversion, *n*-BuOH selectivity, EtOAc selectivity and higher alcohol selectivity of the catalyst recyclability study.

While there is a clear drop in ethanol conversion after one catalytic cycle, the selectivity of the Guerbet reaction towards *n*-BuOH appears independent of the EtOH conversion. The lowest reaction selectivity is observed from the initial Guerbet reaction using the pristine catalysts (Table 15, Entry 1), hence the decrease in reaction activity in runs 2 and 3 does not affect the ability of the UiO-66(Zr) to catalyse the aldol reaction in the Guerbet upgrading of EtOH. After 5 catalytic cycles, the catalytic mixture is more active for ethanol conversion, and more selective for *n*-BuOH formation than the initial system loaded with

2.1 (0.4 mol%) and $[\text{RuCl}_2(\text{dppm})_2]$ (0.1 mol %), giving an *n*-BuOH yield of 22.1 %, the highest recorded yield of *n*-BuOH recorded by a UiO-66(Zr)/ $[\text{RuCl}_2(\text{dppm})_2]$ catalytic system thus far. As observed in Figure 23, a further cycle using the recycled catalysts from the prior reaction for ethanol upgrading yields a remarkably similar result, with *n*-BuOH yield only falling to 21.1 % (Table 15, Entry 6). Throughout the course of the whole-system recycling experiment, the selectivity towards ethyl acetate shows a general trend of increasing selectivity (with some fluctuations), while selectivity towards higher alcohols follows the same trend as that towards *n*-BuOH from run 4 onwards. Interestingly, when considering Table 15 Entries 5 and 6, the selectivity towards uncharacterised products of the Guerbet reactions using the recycled catalyst are very low, hence undesired side reactions like the formation of C_8+ alcohols and uncharacterised side reactions are largely mitigated. Recycling run 4 (Table 15, Entry 4) presents a selectivity towards characterised products of over 100 %, hence warrants repeating to determine if there was a fault in the GC characterisation of the product liquid fraction. The maintained high selectivity of the Guerbet reactions in the whole-system recycling experiment towards *n*-BuOH suggested that the UiO-66(Zr) was retaining its activity as a catalyst for the aldol condensation of acetaldehyde throughout the continued recycling of the catalyst. Whether or not that was due to MOF breaking down to a homogeneous Lewis acid catalyst, or through the structural integrity of the UiO-66(Zr) was yet to be determined. The post reaction catalyst mixture from the Guerbet reaction described in Table 15 Entry 6 was analysed *via* PXRD and compared to a diffraction pattern to a sample of pristine UiO-66(Zr) (Figure 24).

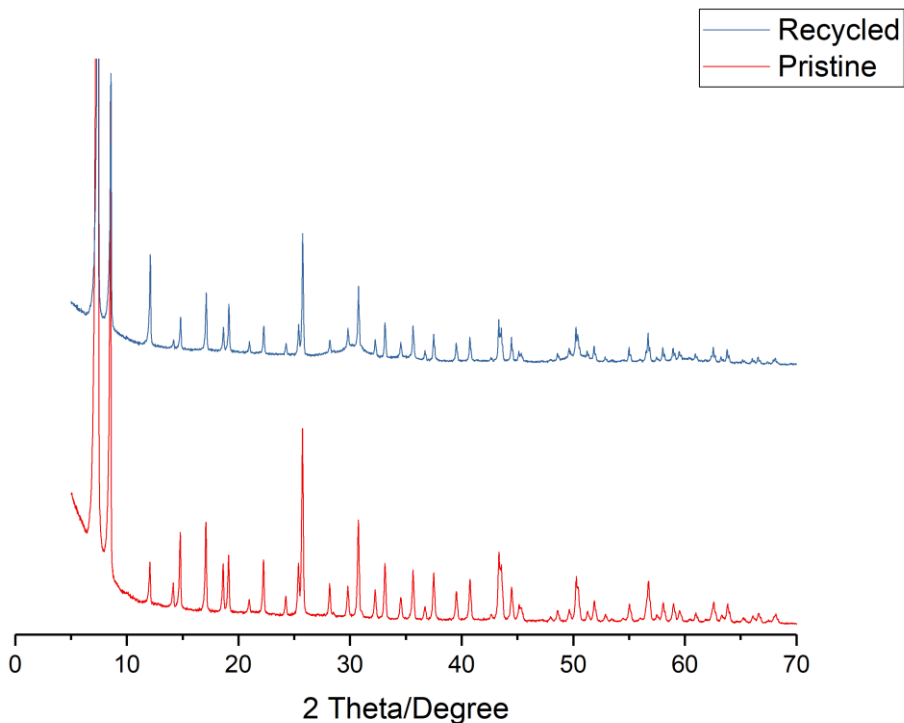


Figure 24: Comparing the PXRD patterns of pristine UiO-66(Zr) and UiO-66(Zr) recovered the reaction detailed in Table 15, Entry 6.

By comparing the diffraction patterns of pristine UiO-66(Zr) and the UiO-66(Zr) that was isolated from the post reaction mixture of Table 15 Entry 6 (Figure 24), it is clear that the structure of UiO-66(Zr) is maintained after six Guerbet reactions, and that it remains a heterogeneous Lewis acid aldol catalyst in the Guerbet upgrading of ethanol. This rationalises an important hypothesis as to why a Lewis acidic MOF would be alternative catalyst to NaOEt in the Guerbet upgrading of ethanol to *n*-butanol, as it does not degrade and is a recyclable aldol catalyst in the reaction.

While the structural integrity of the MOF has been demonstrated in the whole-system recycling reaction, an important question remains in how the homogeneous transfer hydrogenation catalyst is developing in the reaction. Ethanol conversion in the Guerbet mechanism primarily depends on the transfer hydrogenation catalyst dehydrogenating ethanol to acetaldehyde, and when the ethanol conversion over successive catalytic cycles in Figure 23 is considered, there is clearly a development in the nature of the [RuCl₂(dppm)₂] catalyst over the recycling experiment described in Scheme 27 and Table

15. The recycled catalytic mixture from the reaction using the pristine catalysts (Table 15, run 2) is much less active for ethanol conversion than the starting materials. However, ethanol conversion from sequentially recycled material increases from runs 2 to 5, where the system activity for ethanol conversion is higher than that of the starting catalysts after 5 runs and remains practically identical in run 6 (Figure 23). The increased conversion is not due to reactions of ethanol being converted to undesired side-products by UiO-66(Zr), because the yield of *n*-BuOH peaks after 5 cycles, indicating that the dehydrogenation of ethanol to acetaldehyde must be proceeding for the aldol condensation forming crotonaldehyde, which is hydrogenated to form *n*-butanol. This gives an indication that over the sequential catalytic cycles, the ruthenium transfer hydrogenation initially evolves to a species that is less active for ethanol dehydrogenation, but over further cycles evolves to more active dehydrogenation catalyst. The nature of this evolution is not yet known but requires further exploration as the interaction between the MOF and ruthenium over the sequential cycles may be forming a catalyst that could be synthesised, and show this desired high activity without having to develop it *in situ* over successive Guerbet runs. One theory is that the $[\text{RuCl}_2(\text{dppm})_2]$ catalyst is breaking down to form catalytic Ru-nanoparticles over time, which are being supported on, or inside the pores of the UiO-66(Zr) aldol catalyst. The encapsulation of Ru-nanoparticles inside the pores of the MOF presents an interesting explanation as to why the selectivity of the Guerbet reaction towards higher alcohols decreases after 4 cycles. If a greater proportion of nanoparticles were forming inside the MOF after successive Guerbet reactions, then shape selectivity that is provided by the MOF having a set pore size would slow the diffusion of longer chained alcohols into the framework, to access the transfer hydrogenation catalyst. This shape selectivity phenomena would slow the formation of longer chained alcohols and may explain the near linear decrease in reaction selectivity towards higher alcohols presented in Figure 23 after Run 4. The decrease in reaction selectivity towards *n*-BuOH after Run 4 appears to be approaching a plateau after run 6 (Figure 23), hence further runs would determine whether there was a continued decrease in higher alcohol selectivity with a constant reaction selectivity towards *n*-BuOH.

2.7 Conclusions

Through identifying $\text{Zr}(\text{OEt})_4$ as an active homogeneous Lewis acid aldol catalyst in the Guerbet synthesis of *n*-butanol, UiO-66(Zr) was extensively studied as a heterogeneous analogue. The combination of $[\text{RuCl}_2(\text{dppm})_2]$ and UiO-66(Zr) as transfer hydrogenation and aldol catalysts respectively proved active for ethanol conversion to *n*-butanol with catalytic loadings of 0.1 mol% of each of the species. At a reaction temperature of 150 °C, small yields of *n*-butanol were observed, however, increasing the reaction temperature rendered the catalyst mixture far more active for ethanol conversion and *n*-butanol yield. A variety of Guerbet reaction parameters were altered, like reaction duration and UiO-66(Zr) loading to try to improve catalytic activity, where optimal practical reaction conditions of 210 °C over 20 hours with 0.1 mol% loadings of the catalyst were deemed optimal. Changing the catalysts was also investigated. The effect of changing the modulation in the synthesis of the UiO-66(Zr) catalyst was studied for the effect of the activity of the resultant MOF for the aldol condensation of acetaldehyde in the Guerbet reaction, while the hafnium analogue of UiO-66, and UiO-66(Zr)-NH₂ were also screened as aldol catalysts in the reaction. Different homogeneous ruthenium complexes were evaluated as transfer hydrogenation catalysts alongside UiO-66(Zr) in the Guerbet upgrading of ethanol, as well as heterogeneous 5% Ru/charcoal. $[\text{RuCl}_2(\text{dppm})_2]$ was the optimal transfer hydrogenation catalyst tested and used with UiO-66(Zr) to determine the re-usability and recyclability of the homogeneous/heterogeneous catalysed system for the Guerbet upgrading of ethanol to *n*-butanol. UiO-66(Zr) was shown to be an active aldol catalyst after being recycled and used with a fresh loading of $[\text{RuCl}_2(\text{dppm})_2]$ in the Guerbet reaction, while interesting results were obtained when both the MOF and Ru catalyst were recycled in whole-system recycling studies. After an initial induction period, the catalytic mixture was shown to evolve to be more active than the initial loading of catalysts for the conversion of ethanol to *n*-butanol, and more selective towards the formation of the desired product. The structure of the UiO-66(Zr) was shown to remain intact over 6 catalytic cycles.

The demonstration of a recyclable catalytic system for the Guerbet upgrading of ethanol to *n*-butanol was a major success, when considering the thesis scope outlined in Section

1.9. A combination of homogeneous ruthenium complex and metal-organic framework catalysts have been shown to evolve together over successive catalytic cycles, where the sixth successive reaction is a more active system for ethanol conversion and selective reaction for the production of *n*-butanol than the initial reaction. A major reason for the investigation into MOFs as aldol catalysts in the Guerbet reaction was recyclability, compared to non-recyclable sodium ethoxide traditionally used in this class of reaction. The fact that UiO-66(Zr) was shown here to act as an aldol catalyst over numerous cycles proved this theory, and showed that the UiO-class of MOF was a viable support for the immobilisation of transfer hydrogenation catalysts in search of a single high yielding catalyst for the synthesis of *n*-butanol from ethanol.

2.8 Further work

When considering the optimisation of the $[\text{RuCl}_2(\text{dppm})_2]/\text{UiO-66}(\text{Zr})$ catalyst system for the Guerbet upgrading of ethanol to *n*-butanol, further studies on reaction duration are warranted. The results presented in Table 6 indicate that there is an optimum reaction duration between 4 and 20 hours, for the selective formation of *n*-butanol in the Guerbet reaction of ethanol at 210 °C. After 4 hours, no higher alcohols have formed in the reaction, while after 20 hours, the product distribution shows a 15 % selectivity towards the formation of C_6 and C_8 alcohols, with unknown alcohols of longer carbon chain lengths likely making up a proportion of other, uncharacterised products. These results indicate that there is an optimum reaction duration for the reaction in Table 6, for maximum selectivity towards *n*-butanol formation without the formation of higher alcohol products, hence a further reaction duration screen on different reaction durations between 4 and 20 hours to prove this hypothesis. Further studies on the quantity of UiO-66(Zr) loaded in the reaction are also warranted. When the 0.1 mol% loading of the Lewis acidic catalyst was halved and doubled, then trialed with $[\text{RuCl}_2(\text{dppm})_2]$ for the upgrading of ethanol (Table 7), the reaction with a smaller loading of 0.05 mol% gave a higher yield of *n*-butanol than that with 0.1 mol%. The increase was small, and may arise from experimental error, however, the sustained activity of the system with lower loadings of MOF suggests that even lower loadings of the catalyst may give reactions of equal activity, which gives

obvious benefits when considering reaction turnover numbers. Further Guerbet reactions according to the scheme in Table 7 with UiO-66(Zr) loadings lower than 0.05 mol% should be conducted, to maximise TOF while maintaining reaction selectivity towards *n*-butanol.

Analogues of UiO-66(Zr) were extensively studied here as Lewis acid catalysts in the Guerbet upgrading of ethanol, however, there are other Lewis acidic MOFs that are known as aldol catalysts. Some of these, like Fe(BTC) and MIL-101(Cr) were highlighted in Section 1.8.1.1, and present potential alternative aldol catalyst in the Guerbet reaction that require study. In Section 2.3, the effect of introducing varying levels on acetic acid in the synthesis of UiO-66(Zr) analogues was investigated, to determine whether varying the degrees of modulation in these MOF syntheses would affect their catalytic activity in the Guerbet upgrading of ethanol to *n*-butanol. While trends of increasing ethanol conversion activity and decreased product selectivity towards *n*-butanol were observed when the degree of modulation in the synthesis of the UiO-66(Zr) aldol catalyst was observed (Table 10), characterisation of the MOFs to confirm whether these trends were a result of MOF modulation was not completed. The increased modulation in the synthesis of the MOFs is a reasonable hypothesis to explain the change in activity observed in Table 10, however, characterisation on the different MOF samples is required to confirm this hypothesis. Thermogravimetric analysis (TGA) could be performed on the modulated MOFs before activation, to determine the extent of acetic acid removed from the UiO-66(Zr) samples before structural collapse. While Brunauer-Emmett-Teller (BET) analysis could be performed on the UiO-66(Zr) samples after activation, to determine whether the increasing levels of modulation in the synthesis led to increased surface area and volume. If the increasing modulation in the synthesis of the UiO-66(Zr) samples was shown to introduce more Lewis acidic sites in the UiO-66(Zr) samples detailed in Scheme 23, then the reactivity trend in Table 10 could be attributed to the increased modulation of the Lewis acidic catalysts with full confidence. The only modulating agent that was tested in the synthesis of UiO-66(Zr) analogues was acetic acid, while the use of other modulating agents like trifluoroacetic acid have been shown to produce MOFs with a higher activity than those modulated by acetic acid.⁴ Hence an interesting further study would be to investigate whether UiO-66(Zr) derivatives synthesised in the presence of trifluoroacetic acid showed a higher activity for ethanol conversion in the Guerbet

synthesis of *n*-butanol than analogues synthesised with acetic acid as a modulating agent.

The homogeneous ruthenium complexes tested with UiO-66(Zr) in the Guerbet synthesis of *n*-butanol were largely chosen as they had been previously studied within the Wass group, however, Ru-complexes like those shown in Section 1.5.2.2 (Schemes, 9, 10 and 11) from Szymczak and Milstein should also be screened alongside UiO-66(Zr) for the upgrading of ethanol. As shown in Figure 21 and Table 12, some of the homogeneous catalysts tested in the [Ru]/UiO-66(Zr) catalysed upgrading of ethanol in 2.4 were assumed to have formed from the addition of catalyst precursors (ligand and $[\text{RuCl}_2(\text{cymene})]_2$) to the reaction mixture. The reactions detailed in Table 12 (Entries 4, 5 and 8) that were conducted using transfer hydrogenation catalyst precursors should be repeated with the corresponding preformed catalyst detailed in Figure 21, to confirm that the same activity is observed.

The main unanswered question presented in this work comes from the whole-system recyclability experiment presented in Section 2.6, where, through recycling both $[\text{RuCl}_2(\text{dppm})_2]$ and UiO-66(Zr), catalyst system evolves to become more active and selective for the formation of *n*-butanol from ethanol. While the structure of the MOF was shown to remain intact after 6 catalytic cycles, the nature of the evolution of the homogeneous ruthenium catalyst has yet to be determined. After one catalytic cycle, the activity of the system falls dramatically, then after subsequent cycles, increases to show a higher ethanol conversion than the original system. This trend has been determined to be a result of an evolution of the transfer hydrogenation catalyst, as the MOF maintains its structure and activity as an aldol catalyst over the six cycles that were tested. What is happening to the $[\text{RuCl}_2(\text{dppm})_2]$ catalyst over the course of the whole-system recycling experiment remains unclear. One theory is that over time, the homogeneous complex is degrading and forming nanoparticles that are being supported by the UiO-66(Zr), where analysis of the post reaction MOF by SEM/EDS or TEM analysis could be used to determine whether catalytic Ru-nanoparticles were forming on or inside the MOF.

2.9 References

- 1 M. R. DeStefano, T. Islamoglu, S. J. Garibay, J. T. Hupp and O. K. Farha, *Chem. Mater.*, 2017, **29**, 1357–1361.
- 2 D. Jiang, G. Fang, Y. Tong, X. Wu, Y. Wang, D. Hong, W. Leng, Z. Liang, P. Tu, L. Liu, K. Xu, J. Ni and X. Li, *ACS Catal.*, 2018, **8**, 11973–11978.
- 3 G. R. M. Dowson, M. F. Haddow, J. Lee, R. L. Wingad and D. F. Wass, *Angew. Chem. Int. Ed.*, 2013, **52**, 9005–9008.
- 4 F. Vermoortele, B. Bueken, G. Le Bars, B. Van De Voorde, M. Vandichel, K. Houthoofd, A. Vimont, M. Daturi, M. Waroquier, V. Van Speybroeck, C. Kirschhock and D. E. De Vos, *J. Am. Chem. Soc.*, 2013, **135**, 11465–11468.
- 5 W. Xu, M. Dong, L. Di and X. Zhang, *Nanomaterials*, 2019, **9**, 10–13.
- 6 V. R. Bakuru, S. R. Churipard, S. P. Maradur and S. B. Kalidindi, *Dalton Trans*, 2019, **48**, 843–847.
- 7 M. Aghajanzadeh, M. Zamani, H. Molavi, H.K. Manjili, H. Danafar, A. Shojaei, *J Inorg Organomet Polym*, 2017, **28**, 177-186.
- 8 R.G Faria, D. Julião, S.S Balula, L. Cunha-Silva. *Compounds*, 2021, **1**, 3-14.

Chapter 3 – Linker Immobilisation of Homogeneous Complexes

In this chapter, background investigation into the synthesis of transfer hydrogenation catalysts bearing ligands with dicarboxylate functionality is reported. Various attempts at immobilising $[\text{RuCl}(\text{cymene})(\text{bipy-COOH})]\text{Cl}$ within the linkers of UiO-67(Zr) were attempted with SEM/EDX analysis being the technique used to evaluate whether complex immobilisation had been successful.

Where specified, reported experimental work in Section 3.1 was conducted by Elliot Rogers, a Masters' student who was conducting their 4th year research project in the Wass group. Experimental work conducted by Elliot Rogers reported here was done so under the supervision of Harry Jepson.

3.1 Background and preliminary study

The concept of homogeneous transition metal catalysts being immobilised in MOFs as structural linker groups was introduced in Chapter 1 (Section 1.8.2), and the idea of utilising this chemistry to synthesise a single heterogeneous catalyst for the upgrading of ethanol to *n*-butanol was introduced in Section 1.9. In Chapter 2, UiO-66(Zr) was shown to be an active aldol catalyst in the Guerbet upgrading of ethanol alongside homogeneous transfer hydrogenation catalysts, hence the concept of the immobilisation of a transfer hydrogenation catalyst within the linkers of a UiO-derived framework appeared plausible to synthesise a single heterogeneous catalyst for the upgrading of ethanol to *n*-butanol.

Previous unpublished work in the Wass group by Jason Lee showed that the combination of $[\text{RuCl}_2(\text{cymene})]_2$ and nitrogen containing ligands, as transfer hydrogenation catalyst precursors, were active in the Guerbet upgrading of ethanol with NaOEt at 150 °C (Table 16).¹

Table 16: Guerbet syntheses of *n*-butanol using $[\text{RuCl}_2(\text{cymene})]_2$ and nitrogen containing ligands as transfer hydrogenation catalyst precursors¹

2

1 =

2 =

Entry	Ligand	EtOH Conversion (%)	<i>n</i> -BuOH Selectivity (%)	<i>n</i> -BuOH Yield (%)
1	1	21.6	85	17.1
2	2	18.6	91	16.3

The results obtained by Jason Lee shown in Table 16 highlighted that bipyridine and phenanthroline reacted with $[\text{RuCl}_2(\text{cymene})]_2$ *in situ* in the Guerbet upgrading of ethanol, forming active transfer hydrogenation catalysts for the dehydrogenation of ethanol and the hydrogenation of crotonaldehyde.¹ In 1.8.2, the work of Su and co-workers was detailed, who successfully incorporated complexes bearing 2,2'-bipyridyl-5,5'-dicarboxylic acid ligands into the linkers of UiO-67 (according to the PSE reaction detailed in Figure 10), forming heterogenous catalysts for hydrogen evolution and CO_2 reduction reactions.² One of the homogeneous complexes successfully immobilised as linkers in a UiO-67(Zr) derived framework by Su and co-workers was $[\text{RuCl}(\text{cymene})(\text{bipy-COOH})]\text{Cl}$ (Figure 25).²

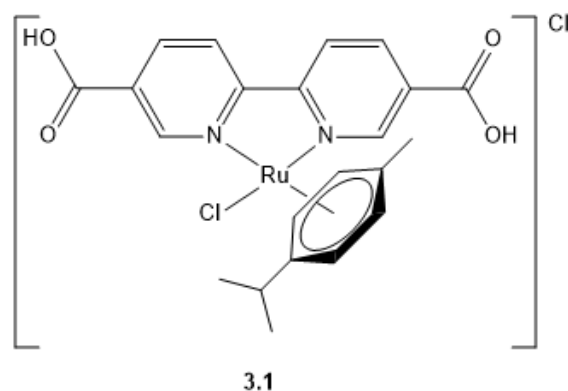
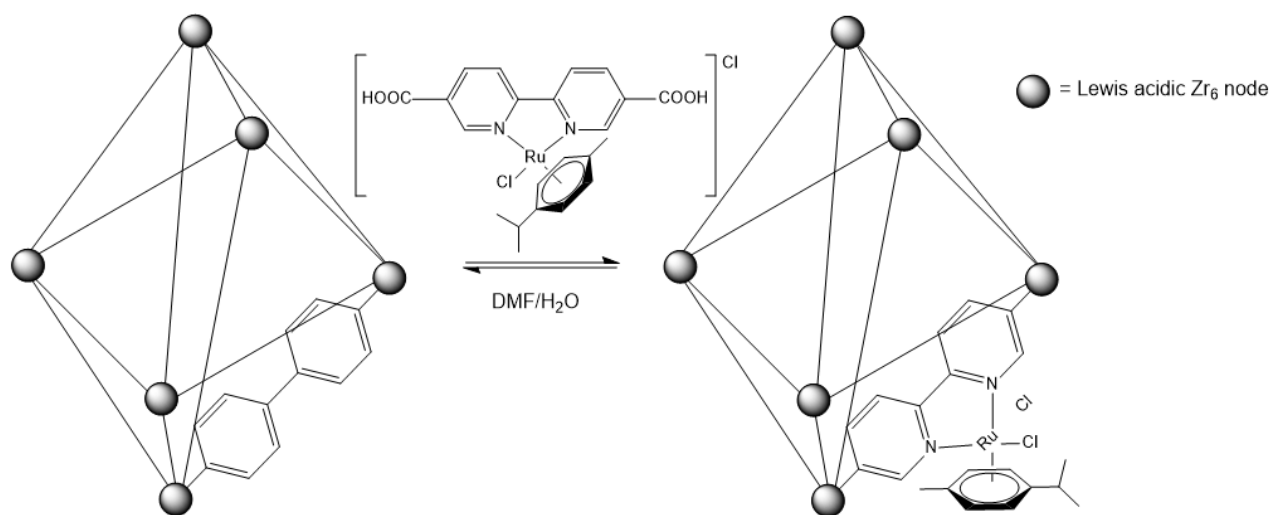


Figure 25: Structure of $[\text{RuCl}(\text{cymene})(\text{bipy-COOH})]\text{Cl}$.

When immobilised within the framework of UiO-67, the carboxylate groups of the 2,2'-bipyridyl-5,5'-dicarboxylic acid ligand of $[\text{RuCl}(\text{cymene})(\text{bipy-COOH})]\text{Cl}$ coordinate to Zr_6

nodes, leaving a $[\text{RuCl}(\text{cymene})(\text{bipy})]$ complex immobilised within the framework (Scheme 28).



Scheme 28: Post-synthetic exchange of biphenyl-4,4'-dicarboxylic acid linkers in UiO-67(Zr) with $[\text{RuCl}(\text{cymene})(\text{bipy-COOH})]\text{Cl}$.

As prior work had shown that $[\text{RuCl}_2(\text{cymene})]_2$ and bipyridine interacted to form an active transfer hydrogenation catalyst in the Guerbet synthesis of *n*-butanol with NaOEt (Table 16, Entry 1),¹ it was theorised that immobilisation of $[\text{RuCl}(\text{cymene})(\text{bipy-COOH})]\text{Cl}$ into the linkers of UiO-67(Zr) would produce a heterogeneous catalyst for the upgrading of ethanol to *n*-butanol. The resultant MOF would possess both the Lewis acidic functionality required for the aldol condensation of acetaldehyde (from the Zr_6 nodes of UiO-67), and the transfer hydrogenation activity required for the dehydrogenation of ethanol, and the hydrogenation of crotonaldehyde (from the immobilised ruthenium complex in the linkers of the MOF). It was also theorised that a dicarboxylate-functionalised phenanthroline ligand (Figure 26) could also be utilised to form complexes that could be immobilised within a UiO-67(Zr) framework, as $[\text{RuCl}_2(\text{cymene})]_2$ and phenanthroline were shown to interact to form an active transfer hydrogenation catalyst in the Guerbet upgrading of ethanol (Table 16, Entry 2).¹

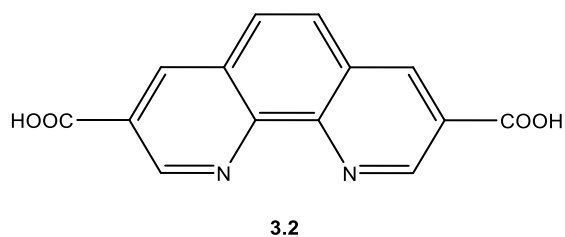
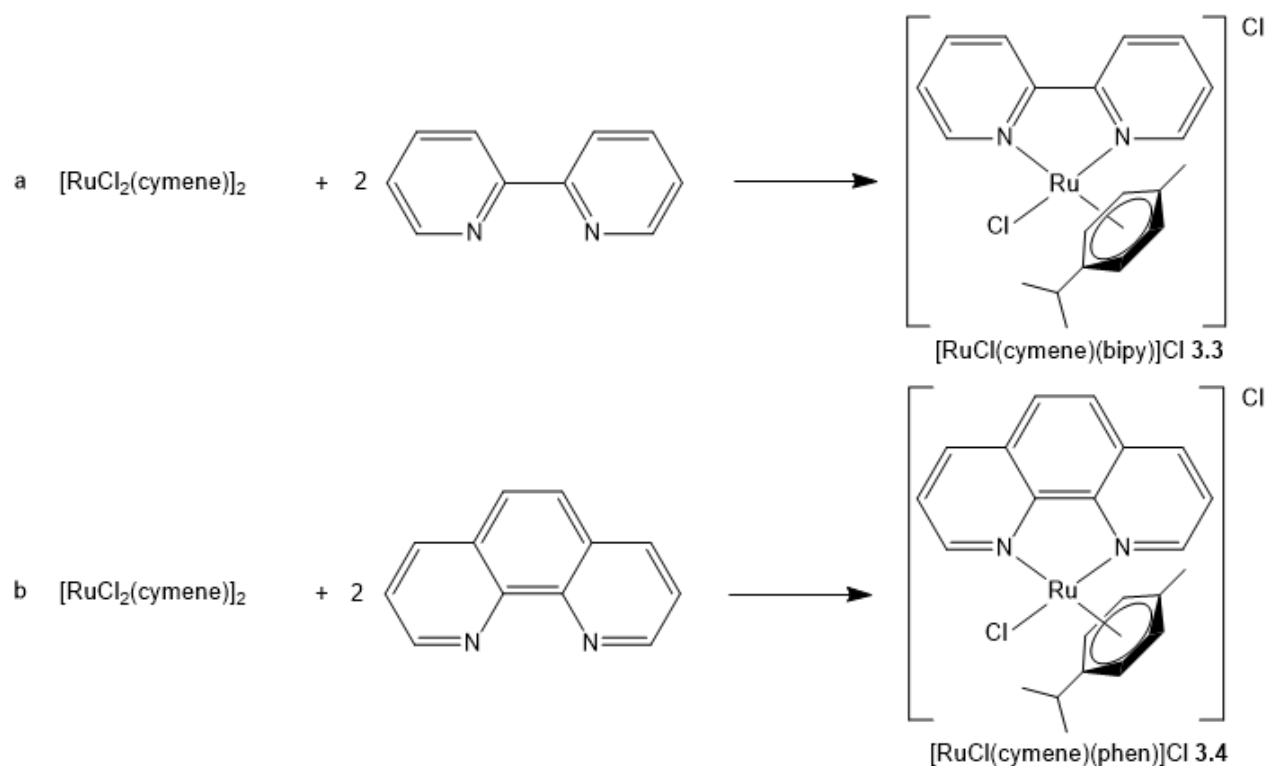


Figure 26: Structure of 1,10-phenanthroline-3,8-dicarboxylic acid.

A preliminary study on the immobilisation of ruthenium complexes bearing dicarboxylate functionalised N-N ligands as linkers in UiO-67(Zr) structures, to form catalysts for the Guerbet upgrading of ethanol was conducted by Elliot Rogers (Master's student in Wass group).³ Initially, the complexes, $[\text{RuCl}(\text{cymene})(\text{bipy})]\text{Cl}$ (**3.3**) and $[\text{RuCl}(\text{cymene})(\text{phen})]\text{Cl}$ (**3.4**) (Scheme 29) were synthesised, to determine the catalytic transfer hydrogenation activity of complexes bearing non-carboxylated N-N ligands in the Guerbet upgrading of ethanol at 210 °C with UiO-66(Zr) as an aldol catalyst.³



Scheme 29: Synthesis of $[\text{RuCl}(\text{cymene})(\text{bipy})]\text{Cl}$ (a) and $[\text{RuCl}(\text{cymene})(\text{phen})]\text{Cl}$ (b).

As these complexes were pre-formed, as opposed to adding the $[\text{RuCl}_2(\text{cymene})]_2$ and appropriate ligand in the Guerbet reaction as catalyst precursors (Table 16),¹ the

Guerbet upgrading of ethanol using NaOEt to facilitate the aldol condensation of ethanol was tested first, at 150 °C over a reaction duration of 20 hours (Table 17).

Table 17: Guerbet upgrading of ethanol using [RuCl(cymene)(bipy)]Cl and [[RuCl(cymene)(phen)]Cl as transfer hydrogenation catalysts with NaOEt

		Selectivity (%) ^b					
		EtOH	<i>n</i> -BuOH	EtOAc	2-BuOH	Higher Alcohols ^c	Other ^d
Entry	[Ru]	Conversion (%) ^a					
1	3.3	28.7	56.4	4.9	0.3	26.8	11.6
2	3.4	21.5	46.5	6.5	-	21.4	25.6

^a Conversion of ethanol calculated based on total liquid products obtained determined *via* GC analysis. ^b Selectivity to Guerbet products in liquid fraction determined *via* GC analysis. ^c C₆ and C₈ alcohol products calibrated *via* GC analysis. ^d Products not characterised by GC calibration.

The results of the Guerbet reactions detailed in Table 17 showed that the preformed [RuCl(cymene)(bipy)]Cl and [RuCl(cymene)(phen)]Cl complexes were active transfer hydrogenation catalysts in the upgrading of ethanol to *n*-butanol.³ The reaction utilising the [RuCl(cymene)(bipy)]Cl catalyst was the most active for ethanol conversion, while also being the most selective for the formation of *n*-butanol, resulting in a relatively high *n*-BuOH yield of 16.2 % (Table 17, Entry 1). The same transfer hydrogenation catalysts shown in Scheme 29 were then tested in the Guerbet upgrading of ethanol with UiO-66(Zr) as an aldol catalyst, at a higher reaction temperature of 210 °C over a reaction duration of 20 hours (Table 18).³

Table 18: Guerbet upgrading of ethanol using $[\text{RuCl}(\text{cymene})(\text{bipy})]\text{Cl}$ and $[\text{RuCl}(\text{cymene})(\text{phen})]\text{Cl}$ as transfer hydrogenation catalysts with UiO-66(Zr)

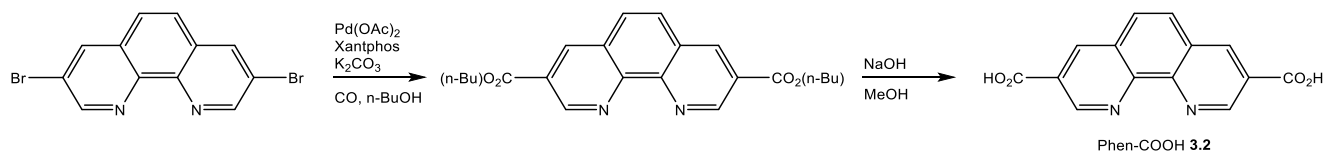
		Selectivity (%) ^b					
		EtOH	<i>n</i> -BuOH	EtOAc	2-BuOH	Higher Alcohols ^c	Other ^d
Entry	[Ru]	Conversion (%) ^a					
1	3.3	8.9	37.1	2.2	-	5.6	55.1
2	3.4	18.1	27.6	2.8	-	7.2	62.4

^a Conversion of ethanol calculated based on total liquid products obtained determined *via* GC analysis. ^b Selectivity to Guerbet products in liquid fraction determined *via* GC analysis. ^c C₆ and C₈ alcohol products calibrated *via* GC analysis. ^d Products not characterised by GC calibration.

When comparing the performance of $[\text{RuCl}(\text{cymene})(\text{bipy})]\text{Cl}$ and $[\text{RuCl}(\text{cymene})(\text{phen})]\text{Cl}$ as transfer hydrogenation catalysts in the Guerbet upgrading of ethanol with NaOEt at 150 °C (Table 17), and UiO-66(Zr) at 210 °C (Table 18), both display lower activity when used with the MOF at the elevated temperature. A slight reduction in *n*-butanol yield was predicted from the reactions detailed in Table 18 compared to those in Table 17, as in 2.2.1, when NaOEt mediated and UiO-66(Zr) catalysed Guerbet upgrading of ethanol with $[\text{RuCl}_2(\text{dppm})_2]$ were compared (Table 5), the system with NaOEt added (at 150 °C) to facilitate the aldol condensation of acetaldehyde was more active for the production of *n*-butanol. However, the extent to which the $[\text{RuCl}(\text{cymene})(\text{bipy})]\text{Cl}$ and $[\text{RuCl}(\text{cymene})(\text{phen})]\text{Cl}$ catalysed reactions are hindered by the temperature increase and replacement of NaOEt with UiO-66(Zr) is dramatic. When comparing the results in Table 17 and Table 18, the *n*-butanol yield of the $[\text{RuCl}(\text{cymene})(\text{bipy})]\text{Cl}$ catalysed reaction decreases from 16.2 % to just 3.3 % when NaOEt is replaced with UiO-66(Zr), and reaction temperature increased from 150 °C to 210 °C. While the same change in reaction conditions reduced the yield of the $[\text{RuCl}(\text{cymene})(\text{phen})]\text{Cl}$ catalysed reaction from 10.0 % to 5.0 %, suggesting that the $[\text{RuCl}(\text{cymene})(\text{phen})]\text{Cl}$ complex is more stable than the $[\text{RuCl}(\text{cymene})(\text{bipy})]\text{Cl}$

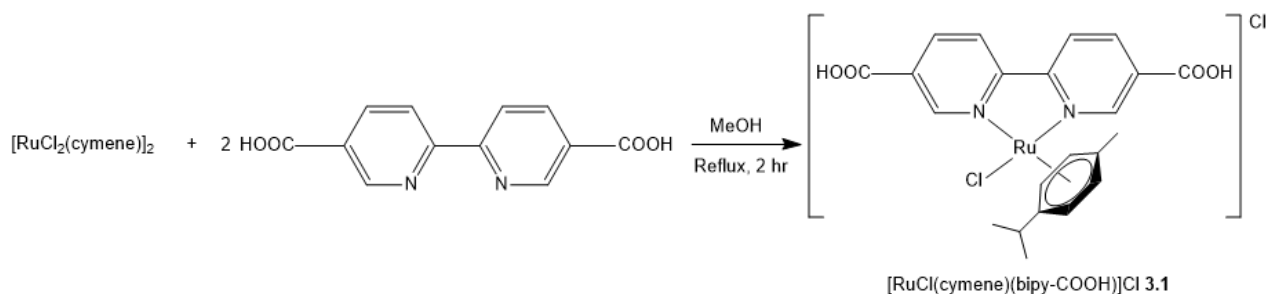
complex at the elevated reaction temperature of 210 °C, as a smaller reduction in *n*-BuOH yield is reported by the system employing this transfer hydrogenation catalyst. Although *n*-BuOH yields were hindered by increasing reaction temperature and introducing UiO-66(Zr) as an aldol catalyst, the systems reported in Table 18 were still active for the production of *n*-BuOH, hence further investigation on analogous complexes bearing dicarboxylate functionalised N-N ligands was warranted.

In order to possess the desired characteristic for linker immobilisation within a MOF, the N-N ligands present in the complexes shown in Scheme 29 would require dicarboxylate functionality. Further work focused on the synthesis of these complexes and testing them as homogeneous transfer hydrogenation catalysts in the Guerbet upgrading of ethanol.³ Initially, the synthesis of 1,10-phenanthroline-3,8-dicarboxylic acid was attempted *via* a literature procedure reported from Bessmertnykh-Lemeune *et al.* (Scheme 30).⁴



*Scheme 30: Synthesis of 1,10-phenanthroline-3,8-dicarboxylic acid via di-n-butyl-1,10-phenanthroline-3,8-dicarboxylate as reported by Bessmertnykh-Lemeune et al.*⁴

The synthesis of 1,10-phenanthroline-3,8-dicarboxylic acid was targeted, to be used as a ligand in the formation of a dicarboxylate analogue to [RuCl(cymene)(phen)]Cl (RuCl(cymene)(phen-COOH)]Cl). However, the initial conversion of 3,8-dibromophenanthroline to di-*n*-butyl-1,10-phenanthroline-3,8-dicarboxylate could not be achieved, hence attention turned to the synthesis of a dicarboxylate analogue of [RuCl(cymene)(bipy)]Cl ([RuCl(cymene)(bipy-COOH)]Cl). The synthesis of [RuCl(cymene)(bipy-COOH)] was achieved following the procedure detailed in Scheme 31.³



Scheme 31: Synthesis of [RuCl(cymene)(bipy-COOH)]Cl.

The $[\text{RuCl}(\text{cymene})(\text{bipy-COOH})]\text{Cl}$ complex shown in Scheme 31 was successfully synthesised and characterised by mass spectrometry (Appendix 7.1.1). The predominant peak in the mass spectrum of **3.1** was 515.03, corresponding to the positively charged $[\text{RuCl}(\text{cymene})(\text{bipy-COOH})]^+$ species. As this fragment was the major signal in the mass spectrum in Appendix 7.1.1, it was known that the complex had successfully formed. On synthesis of **3.1** complex, it was trialed as a homogeneous transfer hydrogenation catalyst at a loading of 0.1 mol% in the Guerbet synthesis of *n*-butanol with NaOEt (5.0 mol%) at 150 °C, and with UiO-66(Zr) (**2.1**) (0.1 mol%) at 210 °C. The results of these Guerbet reactions are presented in Table 19.³

Table 19: Guerbet upgrading of ethanol using [RuCl(cymene)(bipy)]Cl with NaOEt (at 150 °C) and UiO-66(Zr) (at 210 °C)

Entry	Aldol Catalyst/Base (mol%)	EtOH Conversion (%) ^a	Selectivity (%) ^b				
			<i>n</i> -BuOH	Higher			
				EtOAc	2-BuOH	Alcohols ^c	Other ^d
1	NaOEt (5.0)	35.3	39.9	4.8	-	27.5	27.8
2	UiO-66(Zr) (0.1)	11.0	25.5	6.4	-	1.8	66.3

^a Conversion of ethanol calculated based on total liquid products obtained determined *via* GC analysis. ^b Selectivity to Guerbet products in liquid fraction determined *via* GC analysis. ^c C₆ and C₈ alcohol products calibrated *via* GC analysis. ^d Products not characterised by GC calibration.

As observed when [RuCl(cymene)(bipy)]Cl was trialed as a homogeneous transfer hydrogenation catalyst in the Guerbet upgrading of ethanol (Table 17 and Table 18), increasing the reaction temperature and introducing UiO-66(Zr) as an aldol catalyst was detrimental to the catalytic activity of the system. At a reaction temperature of 150 °C with NaOEt (5.0 mol%), [RuCl(cymene)(bipy-COOH)]Cl was an active transfer hydrogenation in the Guerbet synthesis of *n*-butanol, facilitating an *n*-butanol yield of 14.1 % (Table 19, Entry 1). Although this reaction was significantly less selective towards *n*-butanol formation than the analogous reaction using the non carboxylated [RuCl(cymene)(bipy)] complex (Table 17, Entry 1), an increased ethanol conversion led to an *n*-BuOH yield close to that shown by the system using the [RuCl(cymene)(bipy)]Cl catalyst (14.1 % vs 16.2 %, Table 19, Entry 1 and Table 17, Entry 1 respectively). When [RuCl(cymene)(bipy-COOH)]Cl was used as a transfer hydrogenation catalyst with UiO-66(Zr) (0.1 mol%) at 210 °C, ethanol conversion dropped to 11.0 % while *n*-butanol yield was reduced to 2.8 % (Table 19, Entry 2). While [RuCl(cymene)(bipy-COOH)]Cl was a poor performing transfer hydrogenation catalyst in the Guerbet upgrading of ethanol with UiO-66(Zr) at 210 °C (Table 19, Entry 2), there was still logic in investigating the immobilisation of the complex within a UiO-derived framework in search of a single heterogeneous Guerbet catalyst. The vast difference in activity between the two reactions detailed in Table 19 was attributed to the change in reaction temperature, as opposed to the change of aldol catalyst. As previously highlighted, the catalytic results in Section 2.2.1 suggest a predicted drop in *n*-butanol production activity by the UiO-66(Zr) catalysed system (210 °C) compared to the system using NaOEt (150 °C); however, not to the extent that is shown by the reactions detailed in Table 19. A lack of stability of [RuCl(cymene)(bipy-COOH)]Cl at 210 °C compared to 150 °C is predicted to be the reason for the vast difference in catalytic activity by the Guerbet reaction systems detailed in Table 19, but this change in stability would not necessarily be detrimental to a transfer hydrogenation catalyst supported within the linkers of a MOF. If the MOF linker-supported catalyst were to degrade under the harsher reaction conditions of 210 °C, the formation of ruthenium nanoparticles may be observed within the pores or on the surface of the MOF, which could act as catalytically active sites reactions targeted by the homogeneous catalyst. While the stability of the linker immobilised ruthenium complex may differ from the truly

homogeneous analogue and may show increased activity compared to the homogeneous $[\text{RuCl}(\text{cymene})(\text{bipy-COOH})]\text{Cl}$ transfer hydrogenation catalyst. Hence, it was of interest to study the immobilisation of $[\text{RuCl}(\text{cymene})(\text{bipy-COOH})]\text{Cl}$ within a Lewis acidic MOF, in search of a single, heterogeneous catalyst for the Guerbet upgrading of ethanol to *n*-butanol.

3.2 UiO-67 as a heterogeneous aldol catalyst

Previous studies on the use of a heterogeneous aldol catalyst in the Guerbet synthesis of *n*-butanol in Chapter 2 focused on UiO-66(Zr), however when the terephthalic acid linkers of UiO-66(Zr) are compared with $[\text{RuCl}(\text{cymene})(\text{bipy-COOH})]\text{Cl}$ (Figure 27), it is clear that UiO-66(Zr) cannot be used to immobilise the complex as linkers in its structure.

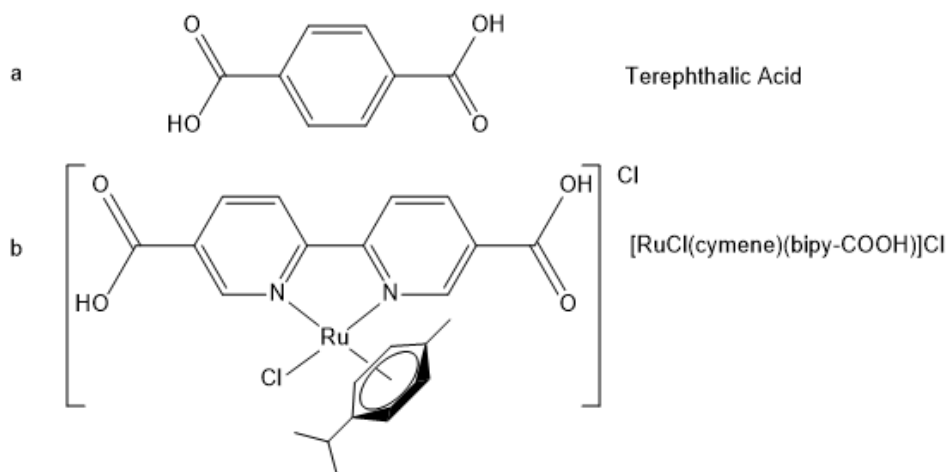


Figure 27: Comparison of terephthalic acid (a) and $[\text{RuCl}(\text{cymene})(\text{bipy-COOH})]\text{Cl}$ (b).

As the 2,2'-bipyridyl-5,5'-dicarboxylic acid ligand of $[\text{RuCl}(\text{cymene})(\text{bipy-COOH})]\text{Cl}$ is significantly longer than the terephthalic acid linkers present in UiO-66(Zr), UiO-66 does not present a framework that is suitable to immobilise the homogeneous complex within a MOF. However, when the biphenyl-4,4'-dicarboxylic acid linkers of UiO-67 are compared to $[\text{RuCl}(\text{cymene})(\text{bipy-COOH})]\text{Cl}$ (Figure 28), UiO-67(Zr) presents a suitable framework to immobilise the complex.

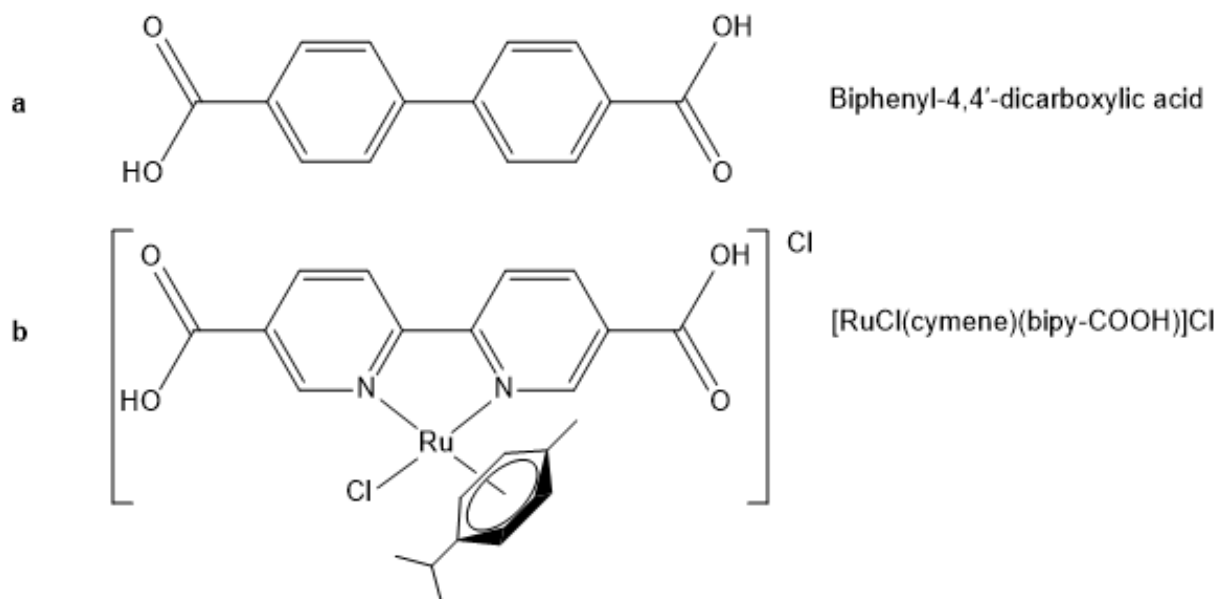
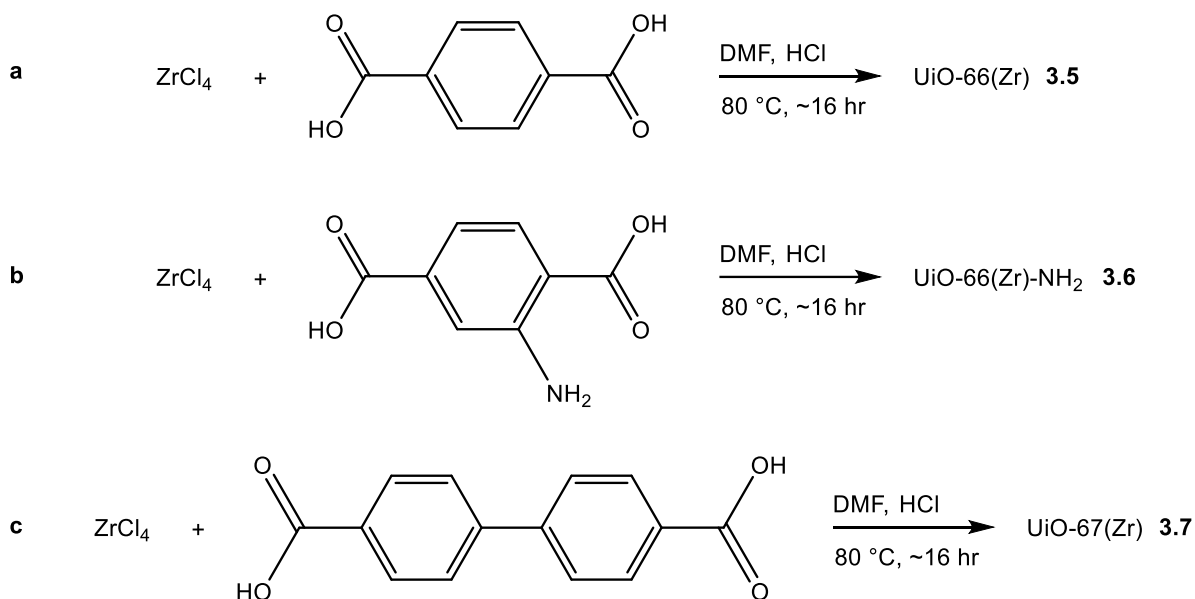


Figure 28: Comparison of biphenyl-4,4'-dicarboxylic acid (a) and [RuCl(cymene)(bipy-COOH)]Cl (b).

The comparable length of biphenyl-4,4'-dicarboxylic acid and the 2,2'-bipyridyl-5,5'-dicarboxylic acid ligand of [RuCl(cymene)(bipy-COOH)]Cl renders UiO-67(Zr) a suitable MOF for linker immobilisation of the complex, and it was used previously by Su and co-workers to immobilise the same complex.² While differing in the length of the linkers, UiO-66(Zr) and UiO-67(Zr) share the same Zr_6 node structure (Figure 15), hence were predicted to display comparable activity as Lewis acidic catalysts for the aldol condensation of acetaldehyde in the Guerbet synthesis of *n*-butanol. Hence, prior to attempting immobilisation of [RuCl(cymene)(bipy-COOH)]Cl within the linkers of the framework, UiO-67(Zr) was benchmarked as an aldol catalyst in the Guerbet upgrading of ethanol with [RuCl₂(dppm)₂] as a transfer hydrogenation catalyst.

Initially, UiO-67(Zr) (**3.7**) was prepared according to a modified literature procedure reported by Katz *et al.* (Scheme 32, c),⁵ where instead of heating the reaction mixture in an autoclave (as previously conducted in Chapter 2), the combination of linker and metal node precursor were heated at a lower temperature in a Schott bottle, in the absence of acetic acid modulator. A sample of UiO-66(Zr) (**3.5**) was prepared according to the same process (Scheme 32, a), to allow for a direct comparison between UiO-66(Zr) and UiO-67(Zr) as aldol catalysts in the Guerbet reaction. A sample of UiO-66(Zr)-NH₂ (**3.6**) was

also prepared according to the literature procedure modified from Katz *et al.*,⁵ and is shown in Scheme 32 (b).



*Scheme 32: Preparation of UiO-66(Zr) (3.5), UiO-66(Zr)-NH₂ (3.6) and UiO-67(Zr) (3.7) according to a modified literature procedure from Katz *et al.*⁵*

The MOFs prepared according to procedures in Scheme 32 were characterised by recording their pXRD spectra (Appendices 7.1.2, 7.1.3 and 7.1.4), and comparing them against reference spectra from the same MOFs in a literature source.⁵ After characterisation, the UiO-derived frameworks prepared according to the syntheses shown in Scheme 32 were trialed as heterogeneous aldol catalysts in the Guerbet upgrading of ethanol, under reaction conditions previously optimised in Chapter 2 (210 °C, 20 hours, 0.1 mol% MOF loading) with [RuCl₂(dppm)₂] (0.1 mol%) as a transfer hydrogenation catalyst. The results of these reactions are shown in Table 20.

Table 20: Guerbet upgrading of ethanol with $[\text{RuCl}_2(\text{dppm})_2]$ and **3.5**, **3.6** or **3.7**

		[RuCl ₂ (dppm) ₂] (0.1 mol%) MOF (0.1 mol%)					
2		20 hr, 210 °C		+ H ₂ O			
		Selectivity (%) ^b					
Entry	MOF (from Scheme 32)	EtOH Conversion (%) ^a	<i>n</i> -BuOH	Higher			Other ^d
				EtOAc	2-BuOH	Alcohols ^c	
1	3.5	31.6	34.2	7.3	0.9	9.5	48.1
2	3.6	34.1	37.5	5.3	1.2	11.4	44.6
3	3.7	27.1	33.6	10.0	1.5	7.7	47.2

^a Conversion of ethanol calculated based on total liquid products obtained determined *via* GC analysis. ^b Selectivity to Guerbet products in liquid fraction determined *via* GC analysis. ^c C₆ and C₈ alcohol products calibrated *via* GC analysis. ^d Products not characterised by GC calibration.

When comparing the MOFs prepared in Scheme 32 as aldol catalysts in the Guerbet upgrading of ethanol with $[\text{RuCl}_2(\text{dppm})_2]$, the system employing UiO-66(Zr)-NH₂ was the most active for ethanol conversion and yielded the highest percentage of *n*-butanol (Table 20, Entry 3). As with UiO-66(Zr) derived samples prepared in Section 2.3, when UiO-66(Zr) (**2.1**) and UiO-66(Zr)-NH₂ (**2.6**) analogues were prepared with equal amounts of acetic acid modulator (Table 11), UiO-66(Zr)-NH₂ (**3.6**) prepared in the absence of modulating agent was a more active aldol catalyst in the Guerbet upgrading of ethanol than similarly prepared UiO-66(Zr) (**3.5**) (Table 20, Entries 1 and 3). UiO-67(Zr) was the least active aldol catalyst of those prepared according to Scheme 32, that were tested as catalysts in the reactions detailed in Table 20. The Guerbet reaction carried out with UiO-67(Zr) as an aldol catalyst (Table 20, Entry 2) was marginally less active for the conversion of ethanol than that which employed UiO-66(Zr) as a Lewis acid (Table 20, Entry 1), but showed very similar product selectivity towards the target *n*-BuOH product. As a result, only a partial decrease in *n*-BuOH yield (9.1 %) was observed by using UiO-67(Zr) as an aldol catalyst in the Guerbet reaction detailed in Table 20 (Entry 2), compared to that facilitated by an analogous reaction employing UiO-66(Zr) (10.8 %) (Table 20, Entry 1).

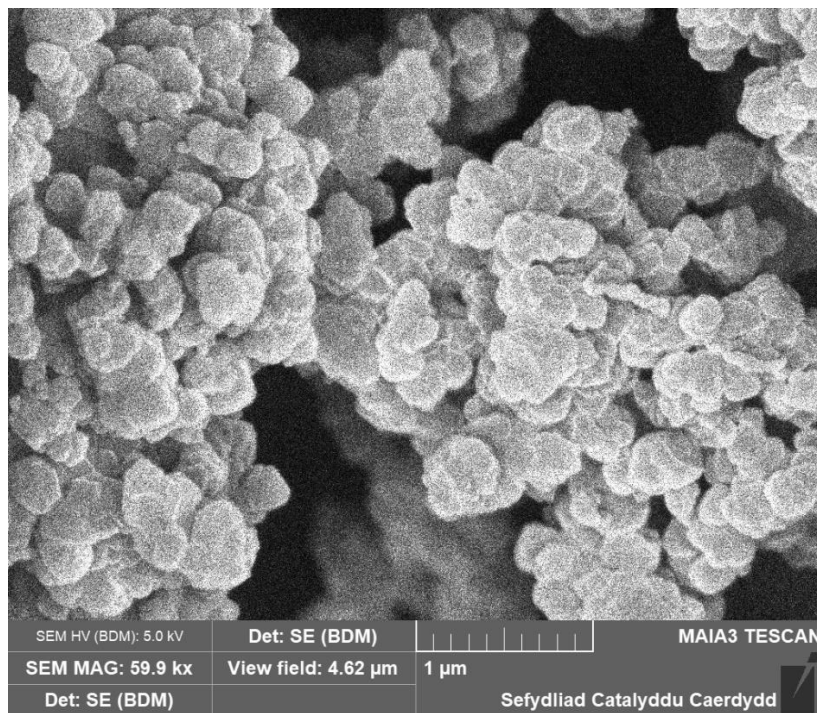
The results in Table 20 show that UiO-67(Zr) is a suitable MOF to form the support for linker supported transition metal transfer hydrogenation catalysts in a heterogeneous catalyst for the Guerbet synthesis of *n*-butanol, as UiO-67(Zr) was only a slightly worse performing Lewis acidic aldol catalyst in the reaction than UiO-66(Zr) (Table 20, Entries 1 and 2). When comparing the performance of the catalytic system utilising the UiO-66(Zr) catalyst prepared in Scheme 32 (Table 20, Entry 1), to those using UiO-66(Zr) samples that were prepared at a higher temperature (**2.1**, **2.2**, **2.3** and **2.4**, Scheme 23, Table 10), the lower temperature synthesis of the UiO-derived samples in Scheme 32 seems to reduce catalytic performance in the Guerbet reaction of ethanol. A sample of UiO-66(Zr) (**2.2**) prepared in the absence of acetic acid modulator at 120 °C generated an *n*-butanol yield of 16.6 % with [RuCl₂(dppm)₂] from ethanol (Table 10, Entry 1), while under the same reaction conditions with identical catalyst loadings, the Guerbet reaction using the UiO-66(Zr) sample prepared in Scheme 32 (**3.5**) at 80 °C generated a considerably reduced yield of 10.8 % of *n*-butanol (Table 20, Entry 1). These results indicate that the UiO-66(Zr) prepared at the lower temperature of 80 °C is intrinsically less active than prepared at the higher temperature of 120 °C, and that the catalytic activity of UiO-67(Zr) in the Guerbet reaction could be improved from that synthesised according to the procedure detailed in Scheme 32, potentially by increasing the reaction temperature used to prepare the aldol catalyst.

3.3 Linker immobilisation of [RuCl(cymene)(bipy-COOH)] in UiO-67(Zr)

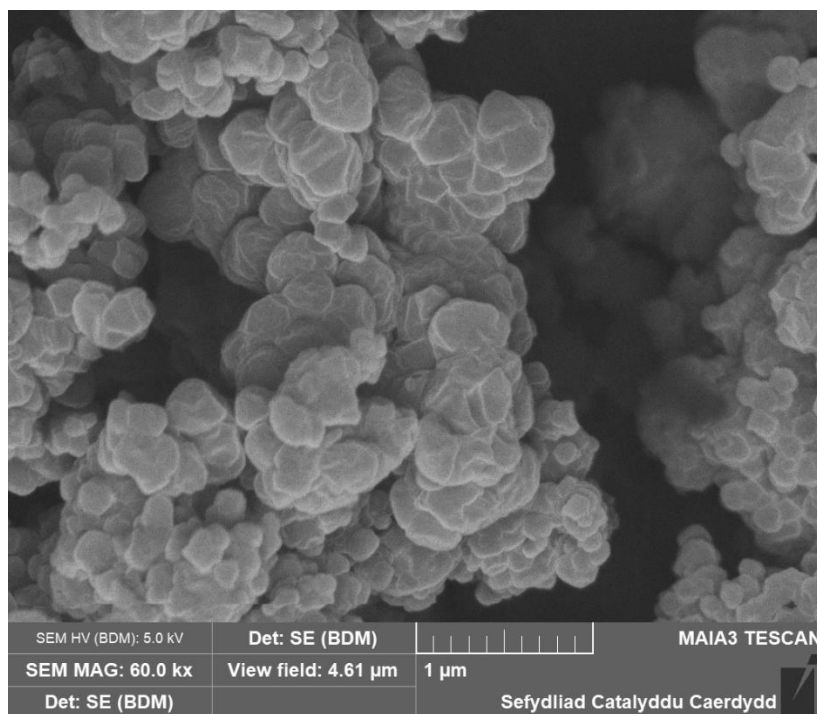
3.3.1 Post-synthetic modification of UiO-67(Zr) - exchanging [RuCl(cymene)(bipy-COOH)]Cl with UiO-67(Zr) linkers

As the activity of UiO-67(Zr) (**3.7**) prepared according to Scheme 32 had been demonstrated in catalysing the aldol condensation reaction in the Guerbet upgrading of ethanol, investigation began into the immobilisation of [RuCl(cymene)(bipy-COOH)]Cl within the linkers of the framework, in search of a single heterogeneous catalyst for the Guerbet synthesis of *n*-butanol.

a



b



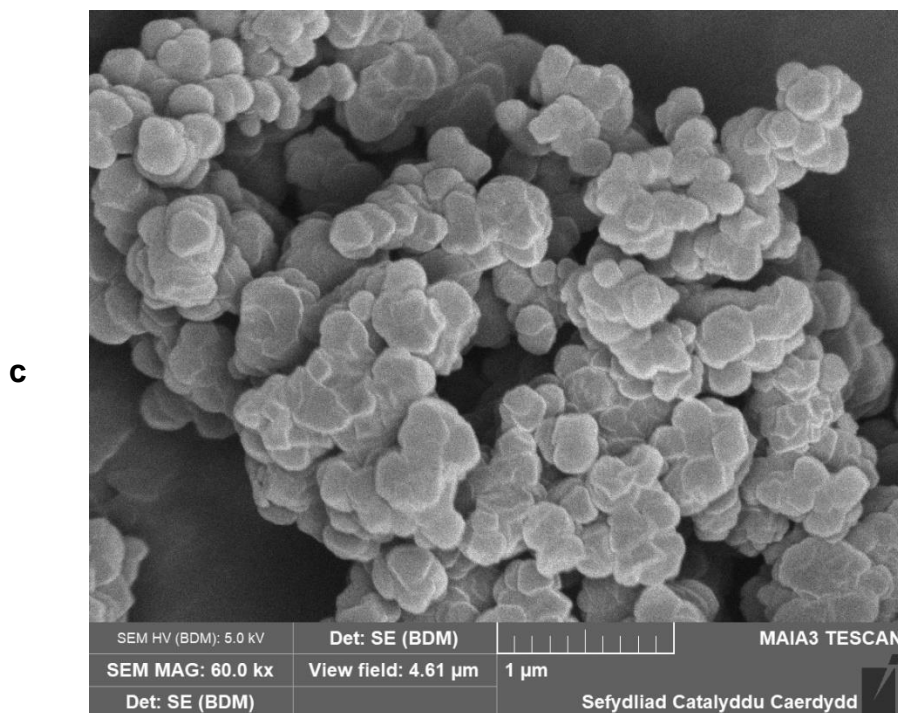


Figure 29: SEM image of **3.8** (a), SEM image of **3.9** (b), SEM image of **3.10** (c).

All of 3.8, 3.9 and 3.10 possess a similar, granular morphology. The SEM images displayed in Figure 29 show that when varying levels of $[\text{RuCl}(\text{cymene})(\text{bipy-COOH})]\text{Cl}$ were added to the PSE reaction relative to that of the starting UiO-67(Zr), the size and shape of the resultant MOF particles were similar. While the reactions conducted in Scheme 33 were not conducted on a large enough scale to obtain the quantity of product required to obtain clean pXRD patterns of **3.8**, **3.9** and **3.10**, when comparing the SEM images in Figure 29 to those published by Su and co-workers of products of similar reactions to those highlighted in Scheme 33,² the size and shape of the MOF particles are similar. This is a strong indication that the structure of UiO-67(Zr) has been maintained in the PSE reactions described in Scheme 33, especially as Su and co-workers were able to analyse products of PSE reactions by pXRD which were consistent with pristine UiO-67(Zr). As the structure of UiO-67(Zr) was determined to be maintained in the PSE syntheses of **3.8**, **3.9** and **3.10**, EDX was used to rationalise whether successful immobilisation of $[\text{RuCl}(\text{cymene})(\text{bipy-COOH})]\text{Cl}$ within the framework had been achieved. EDX analysis was conducted on **3.8**, **3.9** and **3.10** (Figure 30).

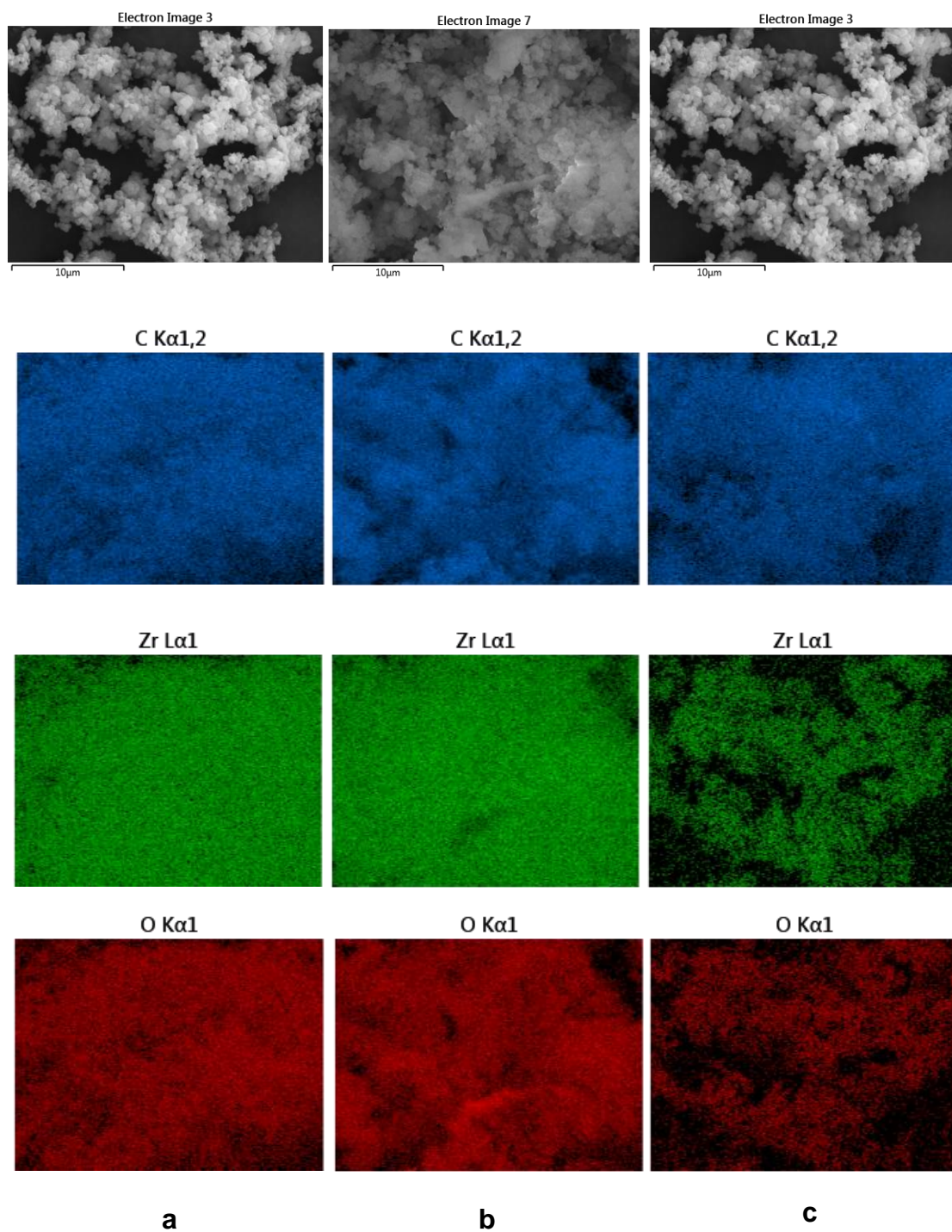


Figure 30: **a)** SEM image and C, O and Zr elemental maps of **3.8**, **b)** SEM image and C, O and Zr elemental maps of the product of **3.9**, **c)** SEM image and C, O and Zr elemental maps of **3.10**

As shown from in the EDX maps in Figure 30, the products of the PSE reactions to immobilise [RuCl(cymene)(bipy-COOH)] within the linkers of UiO-67(Zr), with differing ratios of the two reactants show the characteristic C, Zr and O emissions that would be

expected in pristine UiO-67(Zr), as, apart from hydrogen, these are the only elements that are present in the framework. The overall EDX maps of these samples also showed the presence of other elemental traces in the materials; however, none showed the presence of ruthenium. The EDX maps of elements other than C, Zr and O, and the corresponding EDX spectra for the products of **3.8**, **3.9** and **3.10** are shown in Figures 31, 32 and 33.

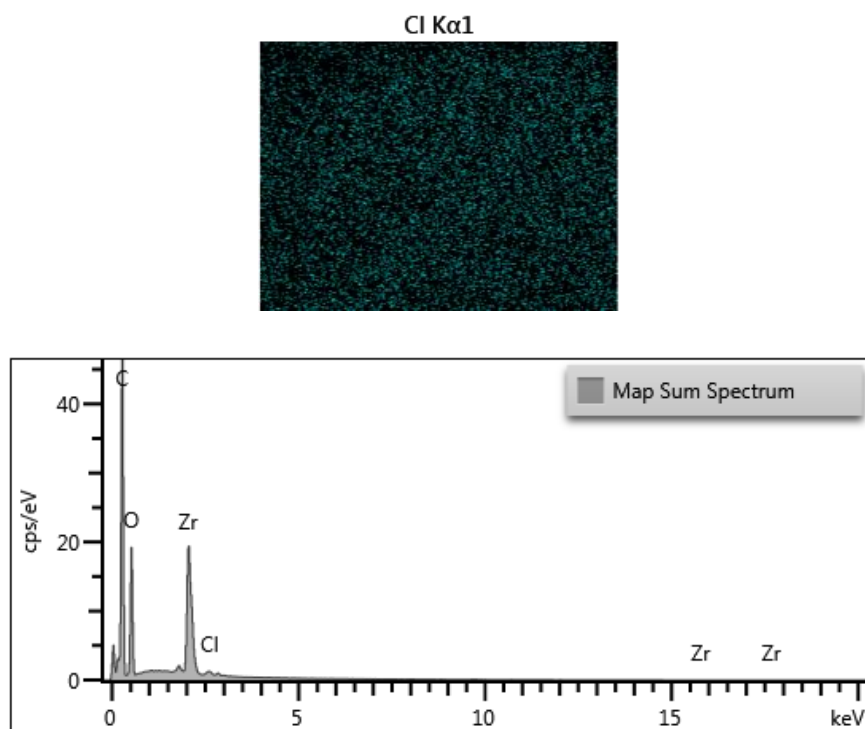


Figure 31: Cl elemental map (top) and full EDX spectrum (bottom) of **3.8**

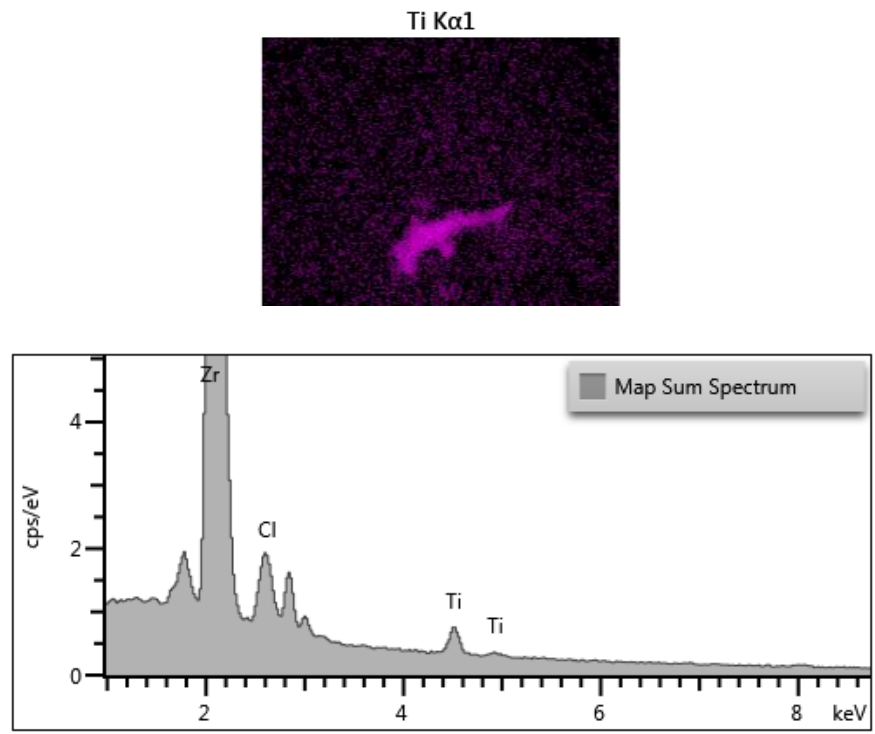


Figure 32: Ti elemental map (top) and full EDX spectrum (bottom) of **3.9**

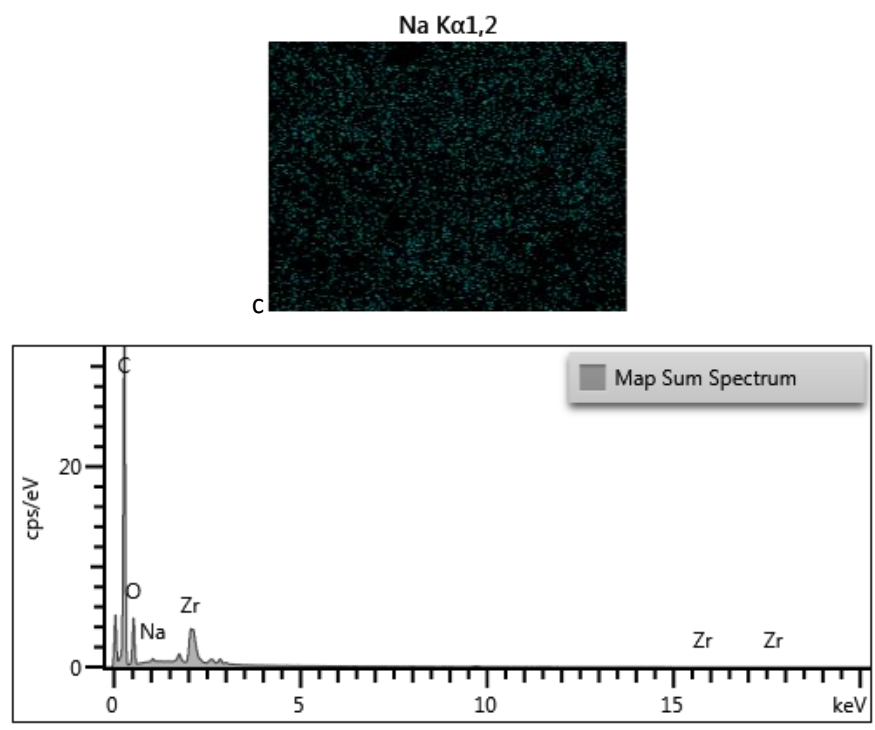


Figure 33: Na elemental map (top) and full EDX spectrum (bottom) obtained of **3.10**

Product **3.10**, formed in a reaction where a 5:1 ratio of UiO-67(Zr) and [RuCl(cymene)(bipy-COOH)]Cl were added to immobilise the ruthenium complex within the framework, shows X-ray emissions in its corresponding EDX spectra that suggest that Na is present in the sample (Figure 33). The presence of this Na peak appears to arise from a contamination in the sample, as the Na K_{α} peak of 1.041 eV does not overlap with the C (K_{α}), Zr (L_{α}) or O (K_{α}) peaks that are present in the spectrum shown in Figure 30 (c), and it doesn't overlap with the expected Ru L_{α} peak of 2.558 eV, which would be expected to be observed in the sample if successful immobilisation of the complex in the PSE reaction shown in Scheme 33 (iii) had taken place. The loading of Na in the sample corresponding to the spectra shown in Figure 33 was calculated to be 0.22 wt% (Appendix 7.1.5), which indicated that the presence of Na results from a form of impurity. The results presented Figure 33 show that the synthesis of **3.10** was unsuccessful.

The EDX spectrum of **3.9**, where a 6.7:1 ratio of UiO-67(Zr) and [RuCl(cymene)(bipy-COOH)]Cl were in the synthesis added is curious, as a dense cluster of Ti atoms is suggested by the data presented by the map that is detailed in Figure 32. The Ti K_{α} emission of 4.508 eV is clear on the EDX spectrum in Figure 32, while this peak does not overlap with the C (K_{α}), Zr (L_{α}) or O (K_{α}) peaks that correspond to elements that are known to be present in the sample (Figure 30, b). As the Ti K_{α} emission of 4.508 eV is much greater in energy than the expected Ru L_{α} peak of 2.558 eV, elemental overlap cannot be attributed to the presence of the apparent Ti cluster shown in Figure 32, and the origin of this cluster remains unknown. As the loading of Ti in the sample **3.9** was relatively high (1.93 wt%, Appendix 7.1.6), further investigation is warranted to determine whether this arose from a significant impurity in the sample, or from elsewhere.

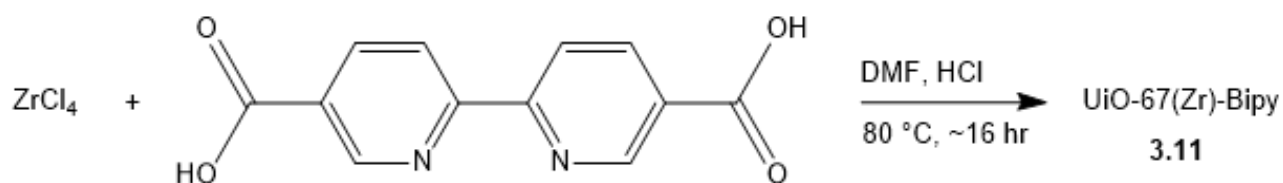
The EDX spectrum of the product **3.8**, where a 20:1 ratio of UiO-67(Zr) and [RuCl(cymene)(bipy-COOH)]Cl were added to the reaction highlights that the only element other than the C, Zr and O of the pristine UiO-67(Zr) MOF is Cl (Figure 31). Successful immobilisation of [RuCl(cymene)(bipy-COOH)] within the linkers of UiO-67(Zr) would lead to the Cl ligands of the immobilised complex being detectable *via* EDX analysis, however, in the EDX spectra and elemental map presented in Figure 31, no ruthenium is present hence it is apparent that the reaction detailed in Scheme 33 (i) was

also unsuccessful. The detected Cl K_{α} emission of 2.621 KeV is close in energy to the characteristic Ru L_{α} emission of 2.558 eV, giving rise to potential peak overlap which could mask the presence of characteristic Ru X-ray emissions being detected. However, the lack of [Ru] immobilisation in **3.9** and **3.10**, combined with the Cl K_{α} emission peak in the EDX spectrum presented in Figure 31 suggests that the assigned Cl K_{α} peak probably is a result of background continuum X-ray emission, and not of Cl ligands present on immobilised [RuCl(cymene)(bipy-COOH)]Cl within UiO-67(Zr).

The EDX spectra and elemental maps obtained from the products of the PSE reactions detailed in Scheme 33 showed that the attempted immobilisation of [RuCl(cymene)(bipy-COOH)]Cl within the linkers of UiO-67(Zr) were unsuccessful. This was a disappointing result, as previously, Su and co-workers showed this approach to be a viable method of immobilising the same homogeneous complex into the linkers of UiO-67(Zr).² The explanation for the failure of the reactions detailed in Scheme 33 may come from the nature of the preparation of the UiO-67(Zr) that was used as the MOF for immobilisation of the [RuCl(cymene)(bipy-COOH)]Cl complex. The UiO-67(Zr) framework used by Su and co-workers for successful immobilisation of [RuCl(cymene)(bipy-COOH)]Cl within the linkers of the framework was prepared with the addition of acetic acid modulator,² where the UiO-67(Zr) used in the unsuccessful PSE reactions described in Scheme 33 was prepared according to the procedure shown in Scheme 32 (c), where no modulator was added to the reaction mixture. As previously detailed Section 2.3, the addition of modulator into MOF synthesis reaction mixtures is designed to introduce inherent defect sites into the resultant framework, with 'missing linkers' leading to open co-ordination sites on the metal nodes of the MOF. While the immobilisation of [RuCl(cymene)(bipy-COOH)]Cl within the linkers of UiO-67(Zr) is described as a PSE reaction by Su and co-workers,² the modulation of the parent MOF used in the reactions they described may aid immobilisation of the complex, as it had been synthesised to possess missing linkers by design, which would be free for immobilisation of [RuCl(cymene)(bipy-COOH)]Cl. The UiO-67(Zr) (**3.7**) used in the reactions described in Scheme 33 was not synthesised to possess missing linkers through modulation, and the lack of these vacant sites may explain the unsuccessful PSE of the biphenyl-4,4'-dicarboxylic acid linkers of this analogue of UiO-67 with [RuCl(cymene)(bipy-COOH)]Cl.

3.3.2 Immobilisation of $[\text{RuCl}_2(\text{cymene})]_2$ on the linkers of UiO-67(Zr)-Bipy

As the PSE method outlined in 3.3.1 to immobilise $[\text{RuCl}(\text{cymene})(\text{bipy-COOH})]\text{Cl}$ within the linkers of UiO-67(Zr) was unsuccessful, a different approach was taken to synthesise the target framework. Instead of attempting to exchange biphenyl-4,4'-dicarboxylic acid linkers of UiO-67(Zr) with $[\text{RuCl}(\text{cymene})(\text{bipy-COOH})]\text{Cl}$ to immobilise the complex, a UiO-67(Zr) derivative with 2,2'-bipyridyl-5,5'-dicarboxylic acid linkers would be synthesised (UiO-67(Zr)-Bipy), and this framework would be used to directly coordinate $[\text{RuCl}_2(\text{cymene})]_2$ to the MOF. Using a similar methodology to that shown in Scheme 32 for the synthesis of UiO-derived MOFs, the synthesis of UiO-67(Zr)-Bipy was attempted from ZrCl_4 and 2,2'-bipyridyl-5,5'-dicarboxylic acid (Scheme 34).



Scheme 34: Attempted synthesis of UiO-67(Zr)-Bipy.

SEM images were taken of the resultant solid from the UiO-67(Zr)-Bipy synthesis reaction conducted in Scheme 34, and these are detailed in Figure 34.

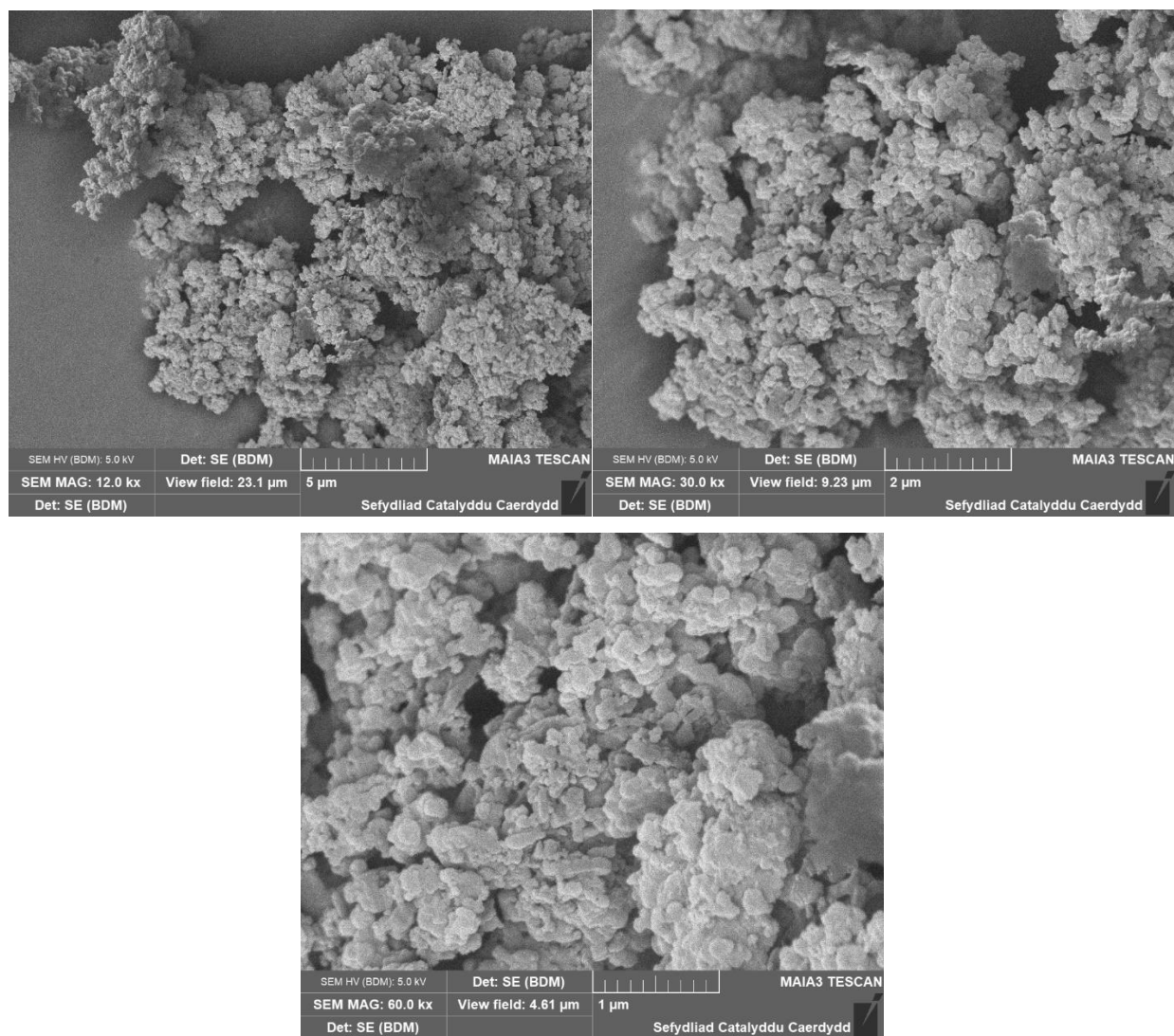
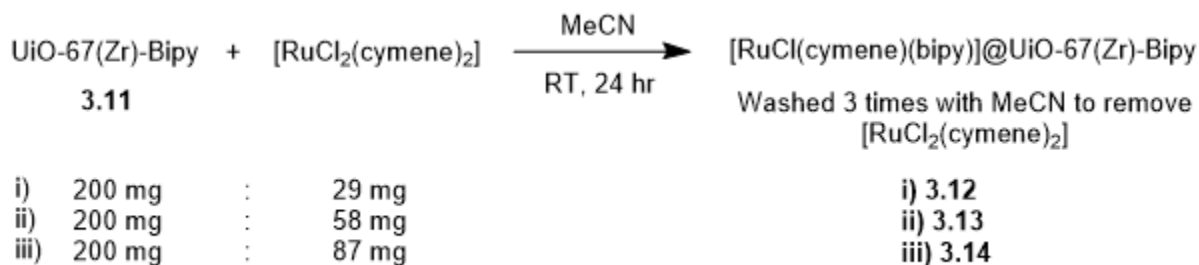


Figure 34: SEM images of the product of the UiO-67(Zr)-Bipy synthesis (**3.11**).

When analysing the morphology of the structure of the product of the UiO-67(Zr)-Bipy synthesis (**3.11**), the particles appear to be granular, and smaller than the particles of the products of the PSE reactions previously carried out in Scheme 33 (Figure 29). It was unclear from the SEM images presented in Figure 34 whether **3.11** was a MOF structure, as the size and shape of the particles are inconsistent. Confirmation of the formation of UiO-67(Zr)-Bipy needs to be determined *via* pXRD analysis, but **3.11** was used as a precursor for the formation of [RuCl(cymene)(bipy)]@UiO-67(Zr). [RuCl₂(cymene)]₂ would be used as a precursor complex to coordinate to the bipyridine linkers of **3.11** (if UiO-67(Zr)-Bipy had formed in the synthesis detailed in Scheme 34), to synthesise the target [RuCl(cymene)(bipy)]@UiO-67(Zr)-Bipy MOF. The synthetic methodology detailed

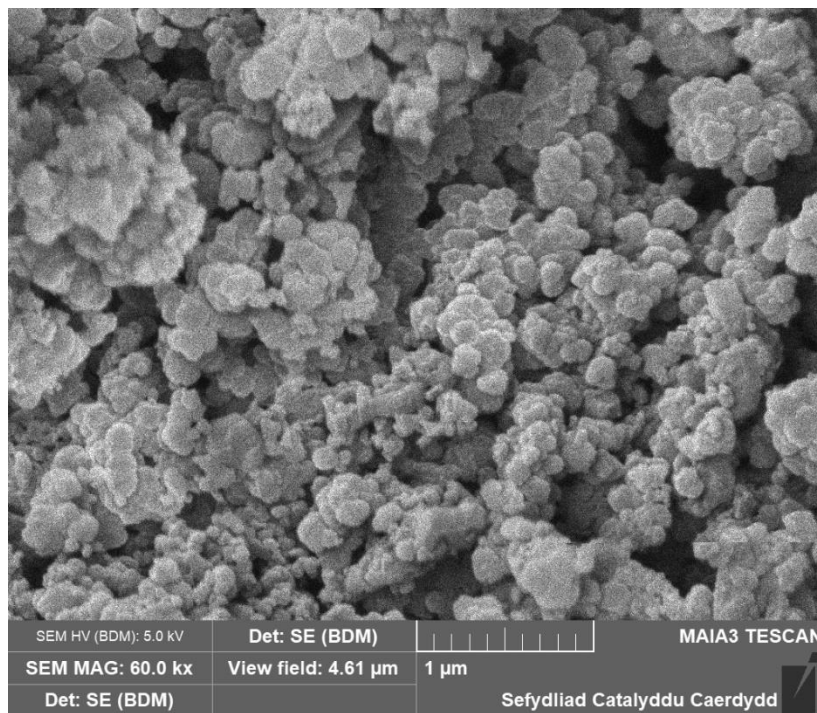
in Scheme 35 was employed to synthesise $[\text{RuCl}(\text{cymene})(\text{bipy})]@\text{UiO-67}(\text{Zr})\text{-Bipy}$ from $\text{UiO-67}(\text{Zr})\text{-Bipy}$.



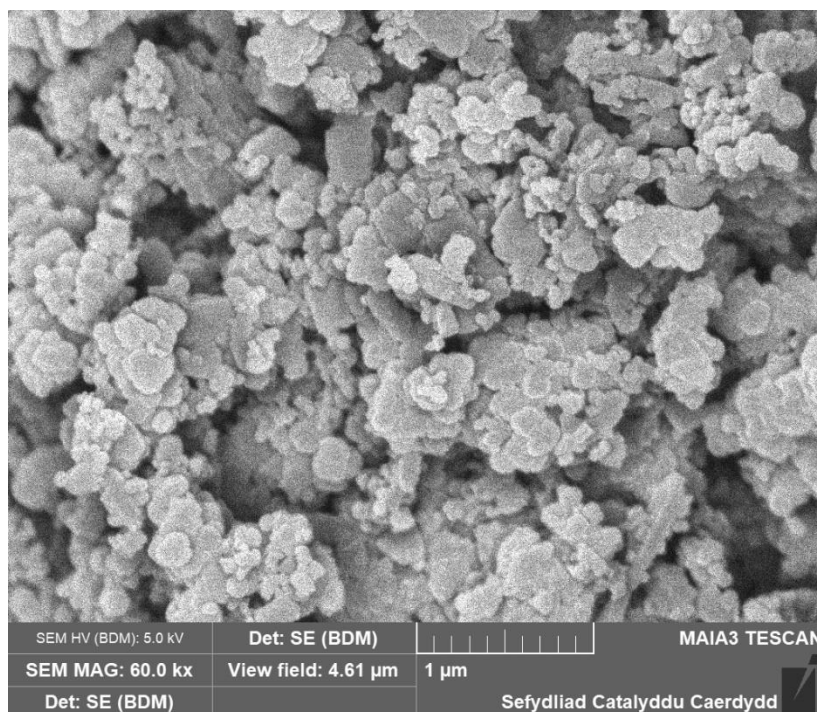
Scheme 35: Methodology to immobilise $[\text{RuCl}_2(\text{cymene})_2]$ on the bipyridine linkers of $\text{UiO-67}(\text{Zr})\text{-Bipy}$ (nature of the $\text{UiO-67}(\text{Zr})\text{-Bipy}$ unconfirmed from prior SEM analysis).

The precursor $[\text{RuCl}_2(\text{cymene})_2]$ complex was dissolved in MeCN, then **3.11** was added to the solution and stirred at room temperature for 24 hours. The resulting solid was isolated *via* centrifugation, and then washed three times with MeCN to remove any unreacted $[\text{RuCl}_2(\text{cymene})_2]$ from the product. As shown in Scheme 35, the reaction was conducted three times with increasing loadings of the precursor $[\text{RuCl}_2(\text{cymene})_2]$ complex relative to the isolated sample of $\text{UiO-67}(\text{Zr})\text{-Bipy}$ (from Scheme 34), to determine whether a proportional increase in complex immobilisation relative to $[\text{RuCl}_2(\text{cymene})_2]$ loading would be observed (if this proved a viable route to formation of $[\text{RuCl}(\text{cymene})(\text{bipy})]@\text{UiO-67}(\text{Zr})\text{-Bipy}$). As with the PSE experiments conducted in Section 3.3.1, SEM-EDX analysis was used to determine the morphology of **3.12**, **3.13** and **3.14**, and whether successful immobilisation of the $[\text{RuCl}_2(\text{cymene})_2]$ precursor complex on bipyridine nodes of $\text{UiO-67}(\text{Zr})\text{-Bipy}$ had taken place. EDX analysis could also indicate whether **3.11** was indeed a MOF structure. As elemental maps of C, Zr and O could be analysed to determine whether dense quantities of these elements existed together, which would be indicative of the presence of a MOF. SEM images of the products of the three reactions detailed in Scheme 35 are shown in Figure 35.

a



b



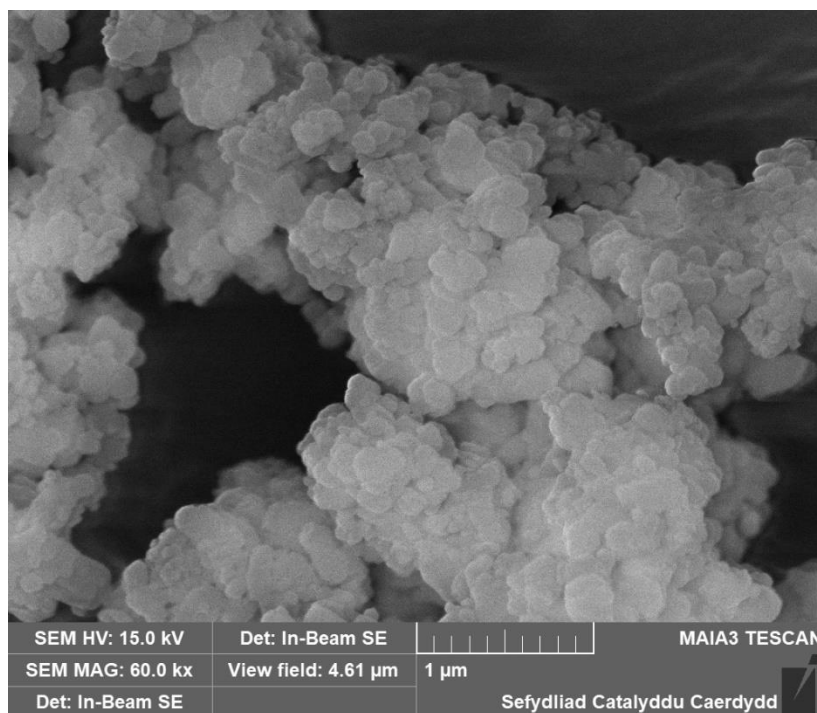
c

Figure 35: SEM image of **3.12** (a), SEM image of **3.13** (b), SEM image of **3.14** (c).

The particles from the products of the reactions shown in Scheme 35 appear to retain their granular morphology and have a similar wide range of shape and size when compared to the support added to these reactions. This can be determined by comparing the SEM images of **3.12**, **3.13** and **3.14** (Figure 35) to the images taken of **3.11** (Figure 34). While these reactions were conducted on a small scale and did not yield enough product to characterise the structure of the products by pXRD, the similarity in morphologies shown in the SEM images of the UiO-67(Zr)-Bipy precursor MOF and post-immobilisation products gave no further evidence as to whether they showed the presence of a MOF, or of a different species. EDX analysis was used to characterise the elemental composition of the products of the immobilisation reactions (Scheme 35), and to determine whether successful complexation of the $[\text{RuCl}_2(\text{cymene})]_2$ precursor complex to bipyridine nodes of UiO-67(Zr)-Bipy had taken place. The C, Zr and O element maps obtained from **3.12**, **3.13** and **3.14** are shown in Figure 36.

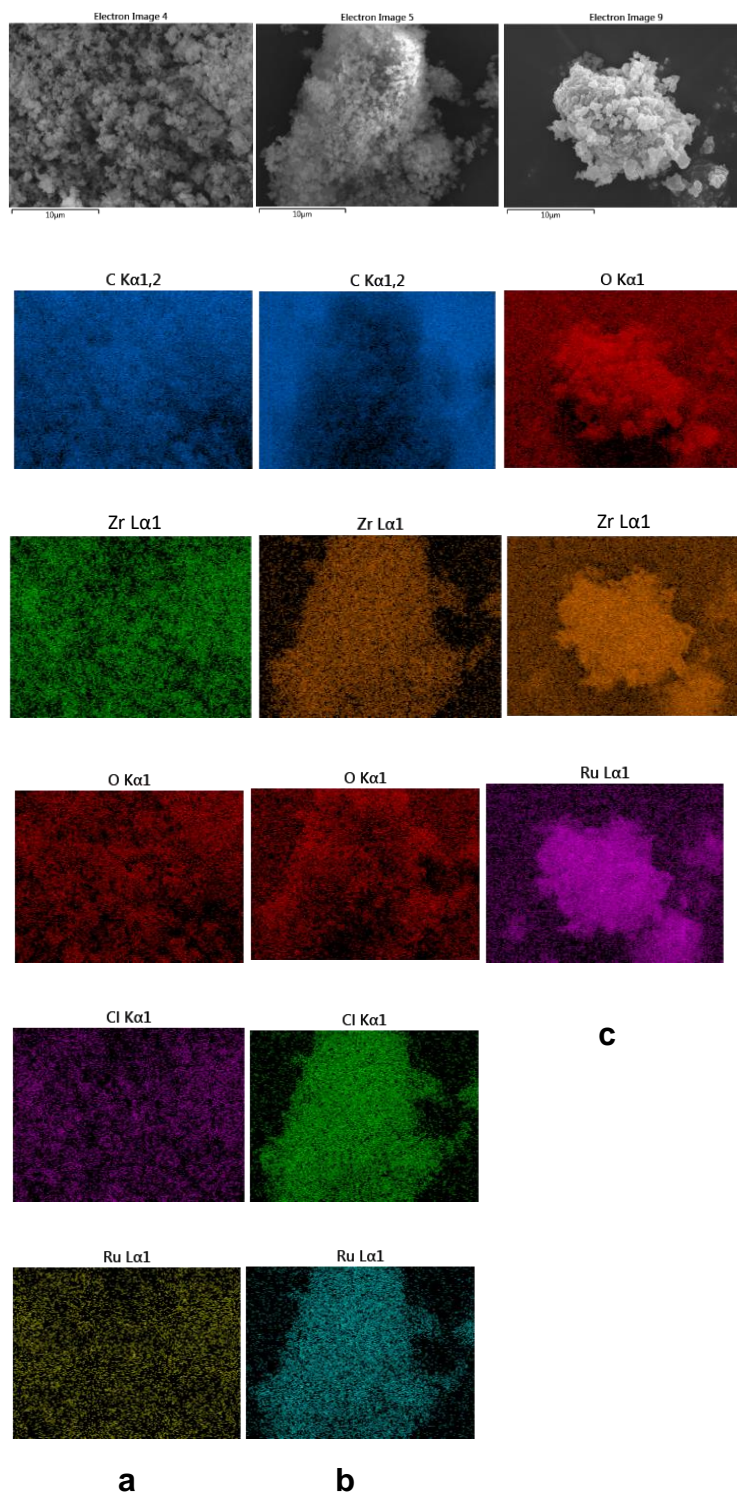


Figure 36: **a)** SEM image and elemental maps of **3.12** (**a**), SEM image and elemental map of **3.13** (**b**), SEM image and elemental map of **3.14** (**c**).

The elemental C, Zr and O maps obtained from EDX analysis of **3.12**, **3.13** and **3.14** indicate that the **3.11** was not a MOF structure, and most likely zirconium oxide (ZrO_2).

When initially processed, the labelled Zr L_{α} maps in **a** and **c** (Figure 36) were ascribed as Pt M_{α} maps. As the Pt M_{α} emission of 2.048 KeV closely overlaps with the Zr L_{α} emission of 2.042 KeV, the fact that neither of these structures were expected to exhibit Pt, combined with the fact that **3.13** was correctly refined to show a Zr L_{α} map meant that Pt M_{α} maps of **3.12** (Figure 36 - **a**) and **3.14** (Figure 36 - **c**) were re-labeled as Zr L_{α} maps. The elemental C, Zr and O maps obtained from EDX analysis of the product **3.12** (Scheme 35) are unclear and does not yield much information as to what the nature of the support is in the reaction. However, the elemental maps in **b** and **c** (Figure 36) give a strong indication that what was synthesised instead of UiO-67(Zr)-Bipy in the reaction described in Scheme 35 was in fact zirconium oxide. When considering the elemental maps of C, Zr and O shown in **b** (Figure 36), the zirconium and oxygen atoms appear in densely populated areas together, however, in the areas where zirconium and oxygen exist, carbon does not appear in great quantity. This indicates that instead of a MOF, where C, Zr and O would show densely packed regions together on EDX maps, zirconium dioxide was formed in the UiO-67(Zr)-Bipy synthesis reaction in Scheme 34 and used as a support in the reactions shown in Scheme 35. This is further rationalised by the EDX maps presented in **c** (Figure 36 where no carbon was detected at all. In the Zr and O maps presented in Figure 36 (**c**), it can again be seen that zirconium and oxygen rich environments exist in the same areas of the sample analysed by EDX, giving a further indication that ZrO_2 was being used as a support in the immobilisation reactions described in Scheme 35 as opposed to the UiO-67(Zr)-Bipy that was intended. The ZrO_2 nature of the heterogeneous support shown in the EDX maps in Figure 36 was confirmed from EDX analysis of the product of **3.11** (Figure 37).

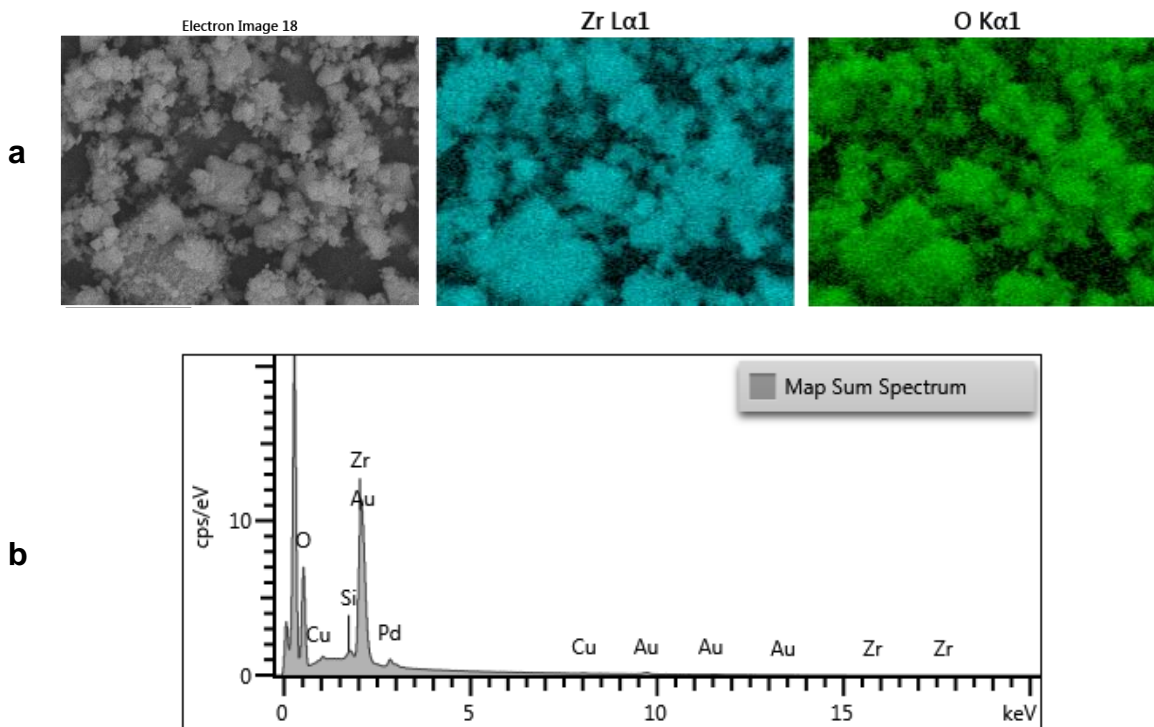


Figure 37: **a)** SEM image used for EDX analysis of **3.11** (left), map of Zr atoms in **3.11**, map of O atoms in **3.11**, **b)** EDX spectrum of **3.11**.

The elemental maps of **3.11** show densely populated areas of Zr and O atoms (Figure 37, **a**), while the EDX spectrum of the same material shows the absence of C atoms (Figure 37, **b**). These observations confirmed the theory extrapolated from the EDX spectra presented in Figure 36, that instead of UiO-67(Zr)-Bipy, the support that was being used in the immobilisation reactions described in Scheme 35 was instead ZrO₂.

As the nature of the support for immobilised ruthenium in the reactions described in Scheme 35 was determined to be ZrO₂ as opposed to the UiO-67(Zr)-Bipy that was initially targeted, the immobilisation reactions using this support were predicted to have failed, as it did not possess the desired bipyridyl functionality for immobilisation of the homogeneous [RuCl₂(cymene)]₂ complex. However, when the elemental Ru and Cl maps obtained from EDX analysis of **3.13** and **3.14** are examined (Figure 36), ruthenium is present on the ZrO₂ support.

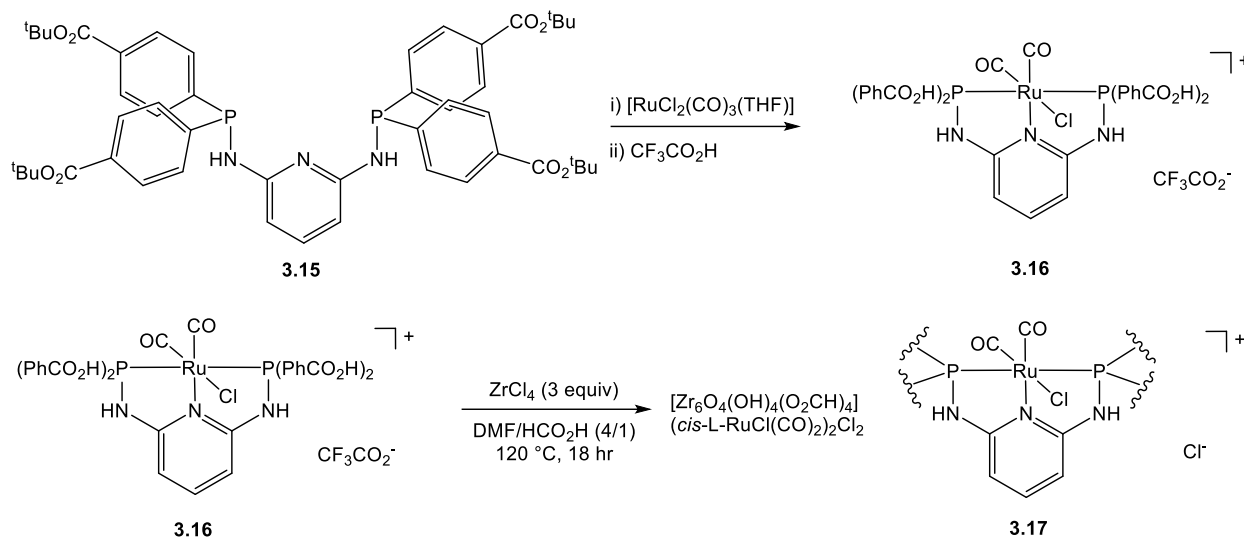
Like the C, Zr and O elemental maps of **3.12** (Figure 36, **a**), the Ru and Cl maps of the same sample do not yield a great deal of information as to whether ruthenium has been

deposited on the ZrO₂ support, as the random distribution of Ru and Cl suggests that background signals result in these elemental maps. However, the Ru and Cl maps (Figure 36 (b) and Figure 36 (c)) acquired from EDX analysis of **3.13** and **3.14**, reactions where more ruthenium was used, show that ruthenium is supported on the ZrO₂ (that was made when trying to synthesise UiO-67(Zr)-Bipy). When the EDX maps of Ru and Cl of **3.13** are considered (Figure 36, b), it appears that both Ru and Cl are being deposited on the ZrO₂ surface, as there are densely populated areas of both Ru and Cl in the same regions that Zr and O are on the same material (Figure 36, b). However, only Ru is detected in **3.14**, and the dense cluster of Ru atoms (Figure 36, c), appears in the same area as Zr and O atoms on the same sample (Figure 36, c). As the ZrO₂ support does not contain the bipyridyl functionality for coordination of the [RuCl₂(cymene)]₂ complex, it would be predicted that the detection of ruthenium on this support would arise from the formation of Ru nanoparticles, and as the characteristic Ru L_α X-ray emission of 2.558 KeV overlaps with the Cl K_α X-ray emission of 2.621 KeV, the detection of Cl in the EDS maps detailed in Figure 36 (a and b) have been falsely resolved, and that they represent the presence of Ru *via* a L_α X-ray emission. As the predicted method of homogeneous complex immobilisation on bipyridyl functionalised linkers could not proceed using a ZrO₂ support, the most likely reason for the observation of ruthenium in the EDX maps shown in Figure 36 is due to the partial breakdown of [RuCl₂(cymene)]₂ over the relatively long reaction time of 24 hours in air (Scheme 35), leading to the formation of Ru nanoparticles that were deposited on the surface of the ZrO₂ support.

3.4 Immobilisation of pincer complexes in MOFs – preliminary study

In 1.8.2.1, the work of Wade and co-workers was introduced, on the immobilisation of homogeneous Pd pincer complexes in a MOF with zirconium SBUs (Scheme 18) as a catalyst for the transfer hydrogenation of benzaldehyde with formic acid.⁶ Wade and a different set of co-workers also investigated the immobilisation of ruthenium pincer complexes as linkers in a zirconium MOF, to form heterogeneous hydrosylation catalysts.⁷ Similar methodology to that previously highlighted in Scheme 18 was employed by the group, where ruthenium complexes bearing pincer ligands chelating *via*

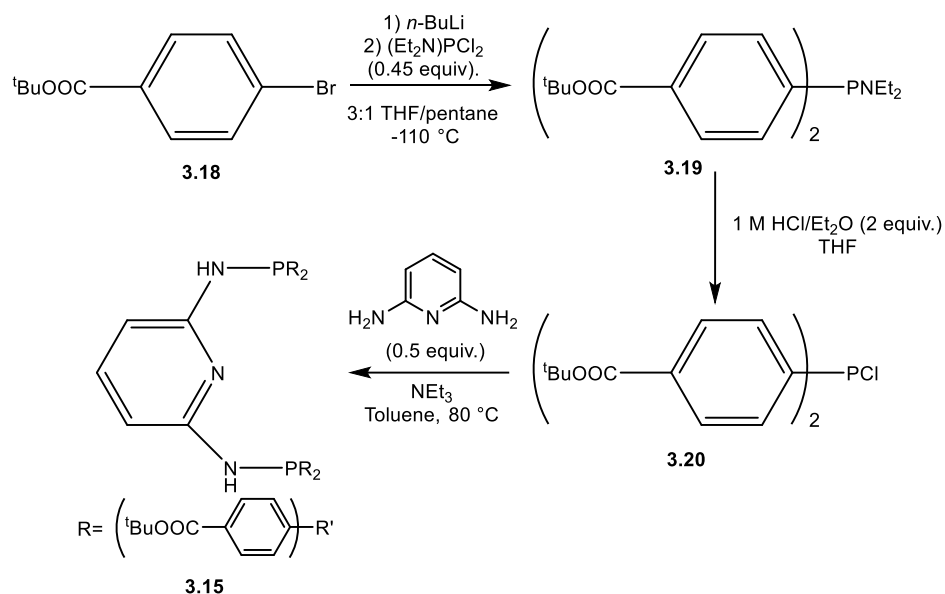
para-carboxylic acid functionalised aryl phosphines were incorporated into a MOF as linkers (Scheme 36).⁷



Scheme 36: Synthesis of ruthenium pincer complexes and their immobilisation within zirconium derived MOFs demonstrated by Wade and co-workers.⁷

It was postulated that a similar synthetic approach to that shown in Scheme 36 could be utilised to synthesise a heterogeneous catalyst for the Guerbet upgrading of ethanol to *n*-butanol, with transfer hydrogenation catalyst pincer complexes incorporated into the linkers of a framework consisting of Lewis acidic zirconium nodes.

To achieve this, successful synthesis of the *tert*-butyl ester functionalised pincer ligand (Scheme 36, **3.15**) was necessary, as a precursor for synthesis of the carboxylic acid functionalised complex (Scheme 36, **3.16**) that would be used for incorporation into a MOF (Scheme 36, **3.17**). Initially, the complexation of $[\text{RuCl}_2(\text{CO})_3(\text{THF})]$ to the pincer ligand (Scheme 36, **3.15**) was targeted to follow the literature procedure from Wade and co-workers,⁷ with the aim of the *tert*-butyl ester functionalised pincer ligand (Scheme 36, **3.15**) being the foundation for the synthesis of a variety of different ruthenium complexes as precursors for different of zirconium derived MOFs that would each be trialed as heterogeneous aldol catalysts in the Guerbet upgrading of ethanol to *n*-butanol. Synthesis of the *tert*-butyl ester functionalised pincer ligand (Scheme 36, **3.15**) was attempted according to a modified literature procedure from Wade and co-workers (Scheme 37).^{6,8}



Scheme 37: Attempted synthesis of *tert*-butyl ester functionalised pincer ligand according to modified literature procedure.^{6,8}

Initially, **3.19** (Scheme 37) was synthesised from 4-bromobenzoic acid *tert*-butyl ester (Scheme 37, **3.18**) and characterised *via* ³¹P NMR which showed a characteristic peak of 60.37 (Appendix 7.1.7). **3.19** was then used to synthesise **3.20** (Scheme 37), and although slightly contaminated with minor impurity peaks, the ³¹P NMR spectrum showed the product mixture predominantly consisted of the target chlorophosphine product (peak of 78.26, Appendix 7.1.8). Successful synthesis of the *tert*-butyl ester functionalised pincer ligand (Scheme 37, **3.15**) was not successfully achieved, due to synthetic issues and time constraints, however, the synthesis of this ligand, and subsequent synthesis of ruthenium complexes and MOFs based on it forms the foundation for further work on the synthesis of heterogeneous transfer hydrogenation catalysts for the Guerbet upgrading of ethanol to *n*-butanol.

Preliminary investigation into the use of homogeneous pincer complexes for the Guerbet upgrading ethanol with UiO-66(Zr) as a heterogeneous Lewis acidic catalyst was also conducted. While prior investigation in 3.5.2 was detailed in the synthesis of **3.15** (Scheme 36) as a ligand precursor for a homogeneous ruthenium complex (Scheme 36, **3.16**) to be immobilised in a zirconium MOF in search of a Guerbet catalyst, other pincer complexes, with pendant carboxylic acid functionality could also theoretically be made. Some of which may show improved activity as a transfer hydrogenation catalyst in the

Guerbet upgrading of ethanol to *n*-butanol. Hence, homogeneous pincer complexes, without carboxylate functionality (as when supported in a framework, carboxylate groups of the pincer ligands are coordinated to the nodes), were to be trialed as transfer hydrogenation catalysts in the Guerbet upgrading of ethanol with UiO-66(Zr). Although eventual frameworks using pincer ligands would not be of the UiO topology, trialing homogeneous pincer complexes with UiO-66(Zr) in the Guerbet reaction would give an idea into their activity under optimised Guerbet reaction conditions for systems including MOFs. Instead of ruthenium complexes bearing PNNNP ligands, those containing PCNCP ligands could be utilised for immobilisation in a MOF, hence two ruthenium complexes bearing non-carboxylate PCNCP ligands ($[\text{RuHCl}(\text{CO})(\text{PCNCP-}^t\text{Bu})]$ and $[\text{RuHCl}(\text{CO})(\text{PCNCP-Ph})]$) were initially tested as transfer hydrogenation catalysts in the Guerbet reaction (Figure 38).

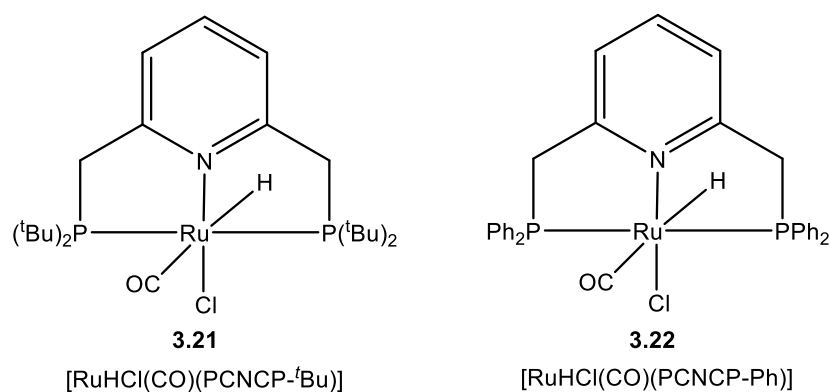


Figure 38: Structures of $[\text{RuHCl}(\text{CO})(\text{PCNCP-}^t\text{Bu})]$ (**3.21**) and $[\text{RuHCl}(\text{CO})(\text{PCNCP-Ph})]$ (**3.22**).

Guerbet upgrading reactions of ethanol were trialed with the two complexes shown in Figure 38 (0.1 mol%) with UiO-66(Zr) (0.1 mol%) as a Lewis acid aldol catalyst at a reaction temperature of 210 °C over 20 hours (Table 21).

Table 21: Guerbet upgrading of ethanol using $[RuHCl(CO)(PCNCP-^iBu)]$ and $[RuHCl(CO)(PCNCP-Ph)]$ as transfer hydrogenation catalysts with UiO-66(Zr)

		[Ru] (0.1 mol%) UiO-66(Zr) (0.1 mol%)		Selectivity (%) ^b			
		20 hr, 210 °C		<i>n</i> -BuOH		Higher	
Entry	[Ru] from Figure 38	EtOH Conversion (%) ^a		EtOAc	2-BuOH	Alcohols ^c	Other ^d
1	3.21	0.3	233.3	466.7	-	-	-
2	3.22	8.0	11.3	81.3			

^a Conversion of ethanol calculated based on total liquid products obtained determined *via* GC analysis. ^b Selectivity to Guerbet products in liquid fraction determined *via* GC analysis. ^c C₆ and C₈ alcohol products calibrated *via* GC analysis. ^d Products not characterised by GC calibration.

Both complexes shown in Figure 38 were poor transfer hydrogenation catalysts for the Guerbet upgrading of ethanol. The reaction detailed in Entry 1 (Table 21), warrants repeating, as the selectivity percentages to characterised products are well over 100 %, hence EtOH conversion cannot be true, however, the low yield of *n*-BuOH in this reaction showed **3.21** (Figure 38) to be barely active in dehydrogenation of ethanol to acetaldehyde. While the ethanol conversions and product selectivities recorded from the reaction detailed in Entry 2 (Table 21) are logical, they show **3.22** (Figure 38) to also be a poor transfer hydrogenation catalyst in the Guerbet synthesis of *n*-butanol with UiO-66(Zr). These complexes may be degrading under the high temperature reaction conditions, and immobilisation in a MOF may improve stability and transfer hydrogenation activity, or degradation within the linkers of a MOF may lead to the formation of catalytically active ruthenium nanoparticles within the framework. Or these complexes may be inherently poor catalysts for the dehydrogenation of ethanol to acetaldehyde.

3.5 Summary

Based on previous work conducted in the Wass group by Jason Lee,¹ the concept of synthesising ruthenium complexes bearing carboxylic acid functionalised derivatives of bipyridine and phenanthroline ligands was explored, for targeted immobilisation within the linkers of UiO-67(Zr) frameworks (with the aim of synthesising a single heterogeneous catalyst for the Guerbet reaction).

Preliminary work in this area was conducted by Elliot Rogers (Master's student), who investigated the synthesis and catalytic benchmarking of homogeneous complexes bearing dicarboxylate functionalised ligands as transfer hydrogenation catalysts in the Guerbet upgrading of ethanol to *n*-butanol.³ While the synthesis of 1,10-phenanthroline-3,8-dicarboxylic acid (**3.2**) according to the literature procedure of Bessmertnykh-Lemeune *et al.*⁴ was unsuccessful (Scheme 30), [RuCl(cymene)(bipy-COOH)]Cl was successfully synthesised according to the procedure shown in Scheme 31. This complex was tested as a homogeneous transfer hydrogenation catalyst in the Guerbet upgrading of ethanol to *n*-butanol with NaOEt at 150 °C and UiO-66(Zr) at 210 °C (Table 19), and while catalytic activity and *n*-BuOH yield were negatively affected by the increase in temperature, *n*-BuOH was still observed in the reaction conducted with UiO-66(Zr) as a heterogeneous aldol catalyst. Lack of catalyst stability was attributed to the reduction in activity at the elevated temperature of 210 °C, however, [RuCl(cymene)(bipy-COOH)]Cl remained a viable target complex for immobilisation within a MOF, as the immobilised complex may have proved more stable than the homogeneous analogue.

As UiO-67(Zr) was identified as a suitable framework for the linker immobilisation of [RuCl(cymene)(bipy-COOH)]Cl, an analogue of the MOF was synthesised according to a procedure previously reported by Katz *et al.* (Scheme 32, **c**).⁵ This analogue of UiO-67(Zr) (**3.7**) was shown to be an active heterogeneous transfer hydrogenation catalyst in the Guerbet upgrading of ethanol to *n*-butanol with [RuCl₂(dppm)₂] as a transfer hydrogenation catalyst (Table 20), hence investigation began into immobilising [RuCl(cymene)(bipy-COOH)]Cl into the linkers of UiO-67(Zr) derivatives.

Initially, an approach previously utilised by Su and co-workers to immobilise [RuCl(cymene)(bipy-COOH)]Cl into the linkers of UiO-67(Zr) was attempted.² Pristine UiO-67(Zr) and the ruthenium complex were reacted in a 1:1 mixture of DMF and H₂O, in a PSE reaction to remove biphenyl-4,4'-dicarboxylic acid linkers from the reactant MOF and replace them with [RuCl(cymene)(bipy-COOH)]Cl (Scheme 33). While this method had shown previous success in literature, attempts to immobilise with [RuCl(cymene)(bipy-COOH)]Cl complex in UiO-67(Zr) were unsuccessful, with varying ratios of complex to MOF in the reaction mixture (Scheme 33). SEM-EDX analysis on **3.8**, **3.9** and **3.10** showed that the structure of the MOF was maintained in the process (Figure 30), however, no ruthenium was observable on EDX maps of these materials. The lack of complex immobilisation in the reactions detailed in Scheme 33 has been attributed to the nature in which the UiO-67(Zr) starting material was prepared. The UiO-67(Zr) (**3.7**) utilised in Scheme 33 was prepared in the absence of a modulating agent where Su and co-workers achieved successful immobilisation of [RuCl(cymene)(bipy-COOH)]Cl into UiO-67(Zr) that was prepared with acetic acid modulation,² leaving defect linker sites accessible to coordination by [RuCl(cymene)(bipy-COOH)]Cl.

As the method outlined in Scheme 33 was unsuccessful in immobilising [RuCl(cymene)(bipy-COOH)]Cl within the linkers of UiO-67(Zr), a different approach was taken to synthesise this functionalised MOF. UiO-67(Zr)-Bipy was to be synthesised according to the procedure detailed in Scheme 34, and the bipyridine linkers of this framework would be used as ligands to co-ordinate [RuCl₂(cymene)]₂, thus synthesising the immobilised ruthenium complex on the linkers of the MOF. SEM images of **3.11** were inconclusive in determining whether the MOF had successfully formed (Figure 34), and the synthesis product was used 'as pure' in the [RuCl₂(cymene)]₂ immobilisation experiments detailed in Scheme 35. While SEM images of **3.12**, **3.13**, **3.14** (Figure 35) did not show whether MOF formation had occurred in preparation of **3.11**, EDX analysis suggested that the heterogeneous support was in fact ZrO₂, as opposed to UiO-67(Zr)-Bipy. EDX maps of Zr and O present in **3.13** and **3.14** showed densely populated areas of zirconium and oxygen atoms in the absence of carbon (Figure 36, **b** and **c**), while **3.14** showed no carbon present at all (Figure 36, **c**). These observations were indicative of the formation of ZrO₂ in the reaction described in Scheme 34, and not the targeted UiO-

67(Zr)-Bipy. Formation of ZrO₂ was confirmed from EDX analysis of a pristine sample of **3.11** (Figure 37). Interestingly, when considering the EDX maps of ruthenium present on **3.13** and **3.14** (Figure 36 (b) and Figure 36 (c)), the areas of Zr and O population were also shown to be populated by Ru. These observations suggested that the [RuCl₂(cymene)]₂ added to the reactions in Scheme 35 was partially breaking down under the employed reaction conditions to nanoparticles, which were being deposited on the surface of the ZrO₂ support. Preliminary investigation into the synthesis of pincer complexes with the desired carboxylate functionality for MOF immobilisation was also conducted. Based on the work of Wade and co-workers,⁶⁻⁸ carboxylate functionalised pincer ligands were targeted in search of active Guerbet transfer hydrogenation catalysts that could be immobilised within a Lewis acidic MOF. The synthesis of a variant of this ligand set was not achieved, and a limited investigation into the combination of homogeneous pincer complexes and UiO-66(Zr) as catalysts in the Guerbet synthesis of *n*-butanol was also unsuccessful.

3.6 Further work

The work presented in Chapter 3 focusses primarily on the immobilisation of [RuCl(cymene)(bipy-COOH)]Cl within the linkers of UiO-67 derivatives, owing to dicarboxylate functionality of the 2,2'-bipyridyl-5,5'-dicarboxylic acid ligand. In 3.1, the attempted synthesis of 1,10-phenanthroline-3,8-dicarboxylic acid (**3.2**) by Elliot Rogers according to the procedure detailed in Scheme 30 (Master's student) was outlined, however, it failed. This procedure was modified from Bessmertnykh-Lemeune *et al.*⁴ and hence warrants repetition, as this ligand is also a suitable linker replacement for biphenyl-4,4'-dicarboxylic acid in UiO-67(Zr). On successful synthesis of **3.2**, ruthenium complexes would be synthesised with it as a ligand, and these complexes would be trialed as homogeneous transfer hydrogenation catalysts in the Guerbet upgrading of ethanol to *n*-butanol. Any complex that showed catalytic transfer hydrogenation activity would be attempted to be immobilised into the linkers of UiO-67(Zr) derivatives, in search of a single

heterogeneous catalyst based on transition metal complex immobilisation for the Guerbet synthesis of *n*-butanol. 2,2'-Bipyridyl-5,5'-dicarboxylic could also be used as a ligand for transition metal complexes other than [RuCl(cymene)(bipy-COOH)]Cl, hence further investigation into the use of this ligand in the synthesis of transfer hydrogenation catalysts is also warranted.

Of the work presented in 3.3.1, the main area for further work would be to attempt the PSE reactions detailed in Scheme 33 again, with UiO-67(Zr) starting material that was prepared *via* a different route. The UiO-67(Zr) used in these reactions was prepared according to the reaction procedure in Scheme 32, without the presence of any modulating agent. As the methodology employed by Su and co-workers to immobilise the same [RuCl(cymene)(bipy-COOH)]Cl complex within the linkers of UiO-67(Zr) was successful (with UiO-67(Zr) prepared with acetic acid modulator),² the failure of the reactions detailed in Scheme 33 has been attributed to the nature of the UiO-67(Zr) that was used. UiO-67(Zr) would be prepared according to the same method employed by Su and co-workers,² and benchmarked as a heterogeneous aldol catalyst in the Guerbet upgrading of ethanol with [RuCl₂(dppm)₂] as a homogeneous transfer hydrogenation catalyst. This MOF would then be used as a support for [RuCl(cymene)(bipy-COOH)]Cl *via* linker immobilisation, and on successful immobilisation of the complex, tested as a single heterogeneous aldol catalyst for the Guerbet synthesis of *n*-butanol. UiO-67(Zr) derivatives prepared with other modulating species could also be synthesised and used as supports in the same PSE procedure for immobilisation of complexes bearing 2,2'-bipyridyl-5,5'-dicarboxylic ligands.

The methodology employed in 3.3.2 to synthesise immobilised [RuCl(cymene)(bipy-COOH)]Cl complex within the linkers of a MOF also warrants further investigation. As outlined in Scheme 34, the attempted synthesis of UiO-67(Zr)-Bipy was conducted, according to a modified procedure from the UiO-derived MOF syntheses outlined in Scheme 32. However, there was unsuccessful characterisation of **3.11** *via* SEM analysis. While pXRD analysis on this solid is still required, further EDX study showed that the **3.11** (Scheme 34) was in fact ZrO₂. As a result, this meant that the immobilisation reactions carried out according to Scheme 35 could not proceed, as the ZrO₂ support did not

contain the required bipyridyl functionality for complexation of the $[\text{RuCl}_2(\text{cymene})]_2$ precursor. Further investigation into the synthesis of UiO-67(Zr)-Bipy is warranted, and alternative synthetic methodologies could be employed to synthesise the target framework constituting Zr_6 nodes and 2,2'-bipyridyl-5,5'-dicarboxylic acid linkers. On successful synthesis and characterisation of this MOF, it would be tested as a heterogeneous aldol catalyst for the Guerbet upgrading of ethanol to *n*-butanol with $[\text{RuCl}_2(\text{dppm})_2]$, and then used as a heterogeneous ligand for complexation of $[\text{RuCl}_2(\text{cymene})]_2$ *via* the linkers of the MOF.

EDX analysis of **3.13** and **3.14** showed that there was ruthenium present on the ZrO_2 support, which was determined to be indicative of supported Ru nanoparticles. Further analysis (ICP-MS and XPS) of these materials is required to determine the nature and the quantity of ruthenium that was present on the structures represented in Figure 36 (**b**) and Figure 36 (**c**). It would also be of interest to determine whether these materials proved to be active heterogeneous catalysts for the Guerbet synthesis of *n*-butanol, with potential catalytic aldol activity arising from Lewis acidity of the ZrO_2 support, and transfer hydrogenation catalytic activity from the supported Ru nanoparticles.

Further investigation into the activity of other pincer complexes in the Guerbet reaction of ethanol, and subsequent linker immobilisation of carboxylated analogues is still required to determine whether this class of ligand and potential MOF forms an active heterogeneous Guerbet catalyst or acts as a precursor to an active Guerbet catalyst supporting nanoparticles.

3.7 References

- 1 J. Lee, PhD Thesis, University of Bristol, 2015.
- 2 W. M. Liao, J. H. Zhang, Z. Wang, S. Y. Yin, M. Pan, H. P. Wang and C. Y. Su, *J. Mater. Chem. A.*, 2018, **6**, 11337–11345.
- 3 Elliot Rogers, MChem Thesis, Cardiff University, 2021.
- 4 A. S. Abel, A. Yu Mitrofanov, A. A. Yakushev, I. S. Zenkov, G. V. Morozkov, A. D. Averin, I. P. Beletskaya, J. Michalak, S. Brandès and A. Bessmertnykh-Lemeune, *Asian J. Org. Chem.*, 2019, **8**, 2128–2142.
- 5 M. J. Katz, Z. J. Brown, Y. J. Colón, P. W. Siu, K. A. Scheidt, R. Q. Snurr, J. T. Hupp and O. K. Farha, *Chem. Commun.*, 2013, **49**, 9449–9451.
- 6 S. A. Burgess, A. Kassie, S. A. Baranowski, K. J. Fritzsching, K. Schmidt-Rohr, C. M. Brown and C. R. Wade, *J. Am. Chem. Soc.*, 2016, **138**, 1780–1783.
- 7 A. A. Kassie, P. Duan, M. B. Gray, K. Schmidt-Rohr, P. M. Woodward and C. R. Wade, *Organometallics*, 2019, **38**, 3419–3428.
- 8 B. R. Reiner, N. T. Mucha, A. Rothstein, J. S. Temme, P. Duan, K. Schmidt-Rohr, B. M. Foxman and C. R. Wade, *Inorg. Chem*, 2018., **57**, 2663–2672.

Chapter 4 – Development of Homogeneous Ruthenium Complexes for Node-Immobilisation on MOFs

The work presented here describes the investigation into the synthesis and utilisation of ruthenium complexes bearing carboxylate functionality in the Guerbet upgrading of ethanol. This class of complex was investigated as carboxylate functionality was targeted towards MOF-immobilisation.

Where specified, reported experimental work was conducted by Jess Cole, a BSc student who was conducting their 3rd year research project in the Wass group. Experimental work conducted by Jess Cole reported here was done so under the supervision of Dr Richard Wingad or Harry Jepson.

4.1 Background

The previous chapter detailed the investigation into immobilising homogeneous transfer hydrogenation catalysts into the linkers of UiO-66(Zr), to synthesise a heterogeneous catalyst for the Guerbet upgrading of ethanol. Recently, research published by Xiao *et al.* presented another pathway in the field of homogeneous complex immobilisation within UiO-66(Zr), using the metal nodes of the MOF to support a homogeneous catalyst (Figure 39).¹

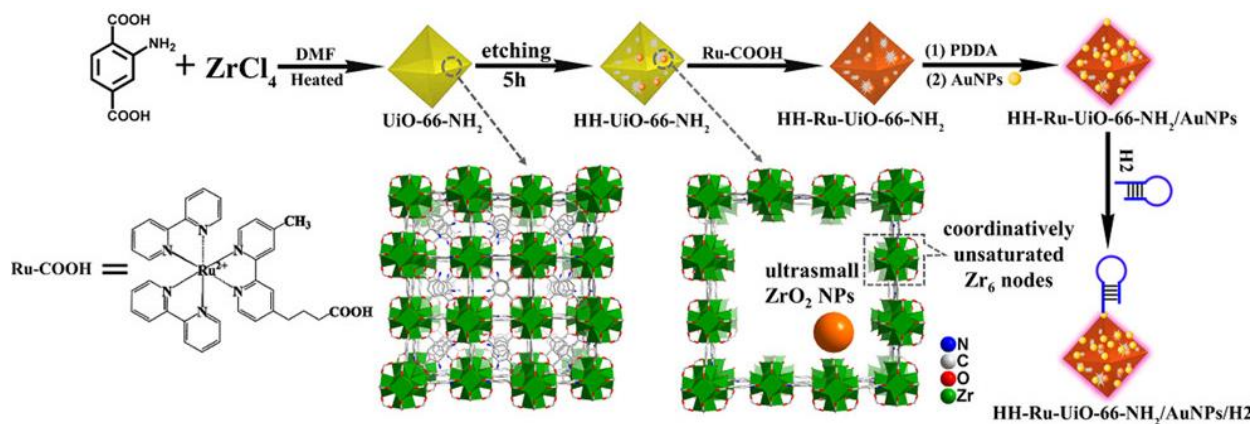


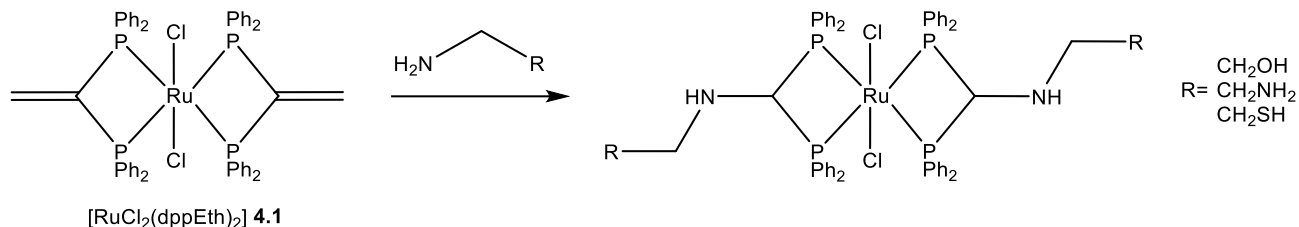
Figure 39: Method of immobilising carboxylate functionalised ruthenium complex onto etched UiO-66-NH₂ by Xiao *et al.*¹

Initially, UiO-66-NH₂ was synthesised from 2-aminoterephthalic acid and ZrCl₄, then an etching procedure was employed to make a hollow hierarchical analogue of UiO-66-NH₂ (HH-UiO-66-NH₂ Figure 39). This could be made by simply heating a water suspension of the pristine UiO-66-NH₂ in an autoclave at 200 °C, etching the framework to make a hollow MOF, where the size of the cavities made could be controlled through changing the etching duration.¹ This etching process created coordinatively unsaturated sites on the metal nodes of the HH-UiO-66-NH₂ framework, which were used to coordinate the 'Ru-COOH' complex described in Figure 39, within the etched pores (HH-Ru-UiO-66-NH₂, Figure 39).¹ The -COOH group present on the 4-(4'-methyl-[2,2'-bipyridin]-4-yl)butanoic acid ligand of the 'Ru-COOH' complex was used to strongly bond the complex to free coordination sites present on the etched MOF, thus immobilising the homogeneous complex within the framework.¹

The work of Xiao *et al.*¹ presented an interesting method to immobilise a homogeneous complex within a MOF and was identified as a potential method of immobilising a homogeneous transfer hydrogenation catalyst within a Lewis acidic MOF, to make a heterogeneous catalyst for the Guerbet upgrading of ethanol to butanol. The key functionality of the immobilised complex utilised by Xiao *et al.*¹ was the pendant -COOH group present on the 4-(4'-methyl-[2,2'-bipyridin]-4-yl)butanoic acid ligand (Ru-COOH, Figure 39). Transfer hydrogenation catalysts with pendant -COOH functionality could therefore theoretically be immobilised on the same class of etched UiO-66(Zr) frameworks, creating heterogeneous materials with the two distinct catalytic sites for the Guerbet synthesis of *n*-butanol. Developing new homogeneous complexes with pendant -COOH groups has been investigated here, with the aim of finding suitable transfer hydrogenation catalysts for immobilisation within UiO-66(Zr). Any suitably active catalysts could then be used in the synthesis of a heterogeneous Guerbet catalyst based on UiO-66(Zr) with a homogeneous transfer hydrogenation catalyst immobilised on the secondary building units of the Lewis acidic aldol catalyst framework.

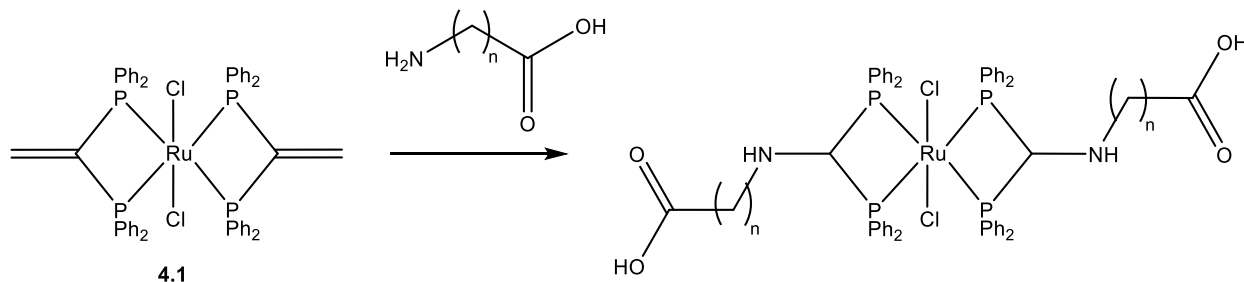
4.2 Complexes based on $[\text{RuCl}_2(\text{dppEth})_2]$

Previous work conducted by Josephine Sama in the Wass group investigated the nucleophilic addition of a variety of amine species across the ethylene groups present on the ligands of the complex $[\text{RuCl}_2(\text{dppEth})_2]$ (**4.1**) (dppEth = 1,1-bis(diphenylphosphino)ethylene) (Scheme 38).² This work was based on earlier studies by Higgins *et al.*^{3,4}



Scheme 38: Michael addition of amines across $[\text{RuCl}_2(\text{dppEth})_2]$ by Sama.²

The Michael addition of amines with varying functionalisation was demonstrated across $[\text{RuCl}_2(\text{dppEth})_2]$ (Scheme 38), forming complexes with good activity in the homogeneous Guerbet reaction using methanol and ethanol as substrates to form isobutanol (yields from 51-74% over 2 h).² It was theorised that the same principle could be applied to synthesise analogous ruthenium complexes to those shown in Scheme 38, functionalised with the desired -COOH group for coordination to the Zr_6 nodes of an etched variant of UiO-66(Zr). This would be achieved through the Michael addition of amino acids across the ethylene groups present on the dppEth ligands on $[\text{RuCl}_2(\text{dppEth})_2]$ (Scheme 39).



Scheme 39: Proposed Michael addition of amino acids across $[\text{RuCl}_2(\text{dppEth})_2]$.

The selective Michael addition of the amino group present on the amino acid over that of the alcohol was predicted. Previous work by Sama investigating the addition of ethanolamine to $[\text{RuCl}_2(\text{dppEth})_2]$ showed the selective addition of the amine group

Initially, the addition of glycine to $[\text{RuCl}_2(\text{dppEth})_2]$ in toluene was trialed at room temperature over 16 hours (reaction condition **i**, Scheme 41). When comparing the $^{31}\text{P}\{^1\text{H}\}$ NMR spectra of the starting complex (Figure 40, **A**) to that of the solution obtained after 16 h at room temp (Figure 40, **B**) the major product of the reaction was clearly the unreacted starting $[\text{RuCl}_2(\text{dppEth})_2]$ complex (14.7 ppm). The same lack of reactivity between $[\text{RuCl}_2(\text{dppEth})_2]$ and glycine was observed when the reaction duration was increased to 5 days at room temperature (reaction condition **ii**, Scheme 41), as the major peak observed in the $^{31}\text{P}\{^1\text{H}\}$ NMR spectrum was also 14.7 ppm (Figure 40, **C**), indicative of the $[\text{RuCl}_2(\text{dppEth})_2]$ starting complex. Interestingly, a second major peak is observed at -5.4 ppm (Figure 40, **C**) that is not observed in the spectra of any of the other reaction products. When considering the products of the previous Michael condition reactions across $[\text{RuCl}_2(\text{dppEth})_2]$ conducted by Sama, the desired product was expected to have a ^{31}P NMR resonance that was further downfield (10.6-16.0 ppm in CDCl_3),² hence this unknown peak at -5.4 ppm in the $^{31}\text{P}\{^1\text{H}\}$ NMR spectrum of the product of **ii** (Scheme 41) has not been attributed to the Michael addition product (**4.2**). This peak is indicative of triphenylphosphine, which may have been present in the system as residue from the $[\text{RuCl}_2(\text{dppEth})_2]$ synthesis.

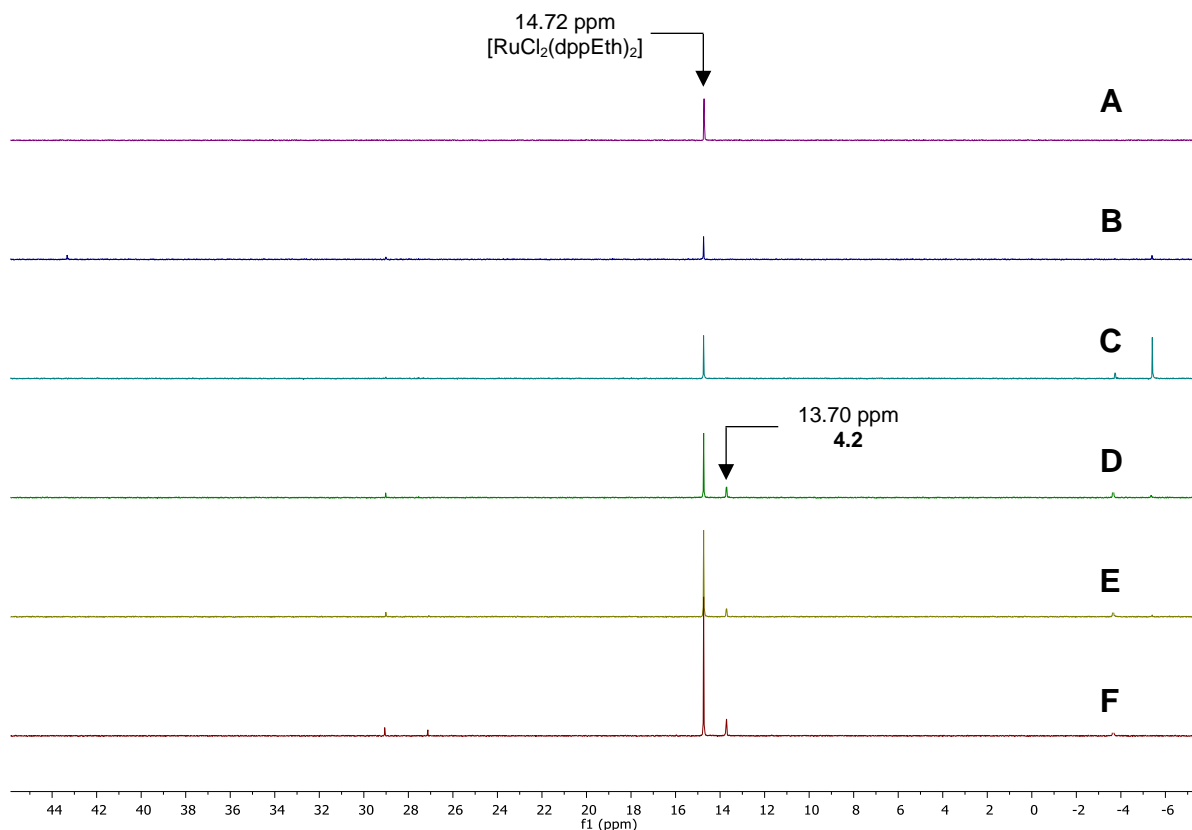
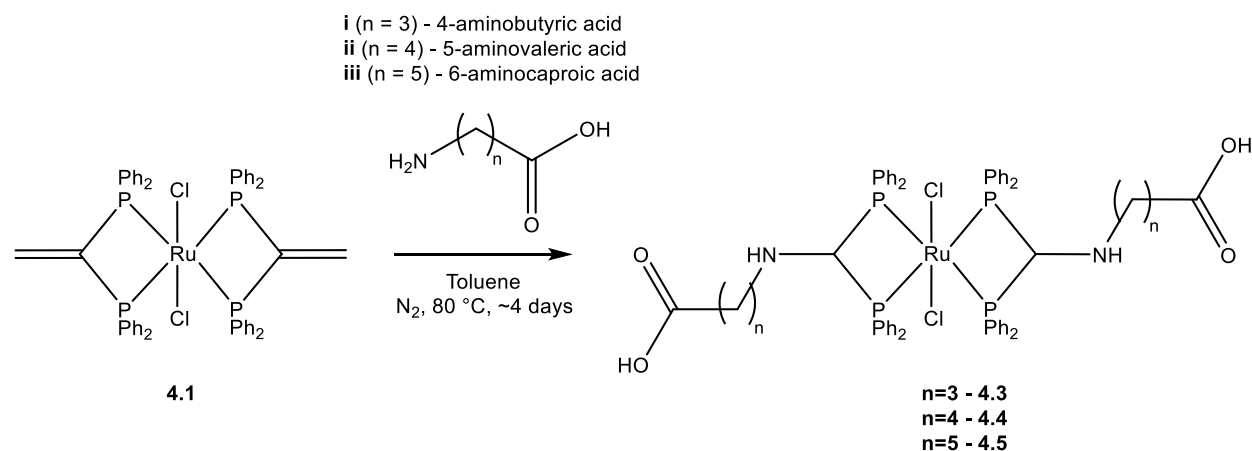


Figure 40: $^{31}\text{P}\{^1\text{H}\}$ NMR spectra of $[\text{RuCl}_2(\text{dppEth})_2]$ (**A**) and the products of the reaction of $[\text{RuCl}_2(\text{dppEth})_2]$ with glycine under various conditions in toluene as detailed in Scheme 41. Condition i (**B**) Condition ii (**C**) Condition iii (**D**) Condition iv (**E**) Condition v (**F**).

Increasing the reaction temperature to 80 °C (reaction conditions **iii** and **iv**, Scheme 41) appeared to result in a minor conversion of the starting $[\text{RuCl}_2(\text{dppEth})_2]$ complex to **4.2**. In the $^{31}\text{P}\{^1\text{H}\}$ NMR spectra (Figure 40, **D** and **E**), a minor peak slightly upfield of that of the starting complex was observed, at 13.7 ppm. While previous investigation by Sama indicates that these peaks are indicative of the product of the Michael addition of glycine across the dppEth ligands of $[\text{RuCl}_2(\text{dppEth})_2]$ (as Michael adduct complexes showed peaks slightly upfield to the 14.72 ppm singlet of $[\text{RuCl}_2(\text{dppEth})_2]$),² they are minor compared to that of the starting material, indicating that the reaction was inefficient. A final attempt to increase the yield of the Michael addition of glycine to $[\text{RuCl}_2(\text{dppEth})_2]$ was made through increasing the reaction temperature further to reflux, over a duration of ~16 hours (reaction condition **v**, Scheme 41). When considering the $^{31}\text{P}\{^1\text{H}\}$ NMR spectrum of the product of this reaction (Figure 40, **F**), the peak identified as **4.2** (13.7

ppm) is still minor compared to that of the starting complex (14.7 ppm). While the NMR data presented in Figure 40 suggested that higher reaction temperatures would partially facilitate the Michael addition of glycine across $[\text{RuCl}_2(\text{dppEth})_2]$, in toluene, the reaction was inefficient regarding product yield. The $^{31}\text{P}\{^1\text{H}\}$ NMR spectra presented in Figure 40 are from the product mixtures from the reactions in Scheme 41, which were isolated from the post-reaction solution. $^{31}\text{P}\{^1\text{H}\}$ NMR spectra were also recorded of residual solid present in the reactions, where the solid isolated from reactions **i-iv** (Scheme 41) showed the exclusive presence of the starting $[\text{RuCl}_2(\text{dppEth})_2]$ (**4.1**) complex. This highlighted that the starting complex was only partially soluble in toluene at room temperature and at 80 °C, while the $^{31}\text{P}\{^1\text{H}\}$ NMR spectrum of the post reaction solid of reaction **v** (Scheme 41) showed no trace of any phosphorus compound, indicating that $[\text{RuCl}_2(\text{dppEth})_2]$ was fully soluble in toluene at reflux. While the product mixtures of the reactions performed at 80 °C (**iii** and **iv**, Scheme 41) did show the presence of **4.2**, the trend in solubility of the $[\text{RuCl}_2(\text{dppEth})_2]$ complex is important to note, when considering further reaction optimisation.

To determine whether toluene was an ineffective solvent for the Michael addition of linear amino acids across $[\text{RuCl}_2(\text{dppEth})_2]$, or if glycine was a poor substrate in this system, the additions of 4-aminobutyric acid, 5-aminovaleric acid and 6-aminocaproic acid were attempted across $[\text{RuCl}_2(\text{dppEth})_2]$ in toluene at 80 °C over 4 days (Scheme 42).



Scheme 42: Attempted Michael addition of amino acids across $[\text{RuCl}_2(\text{dppEth})_2]$ in toluene at 80 °C over 4 days.

When considering the $^{31}\text{P}\{^1\text{H}\}$ NMR spectra of **4.3**, **4.4** and **4.5** (Figure 41), the same limited reactivity between the longer amino acids and $[\text{RuCl}_2(\text{dppEth})_2]$ that was previously demonstrated with glycine was observed.

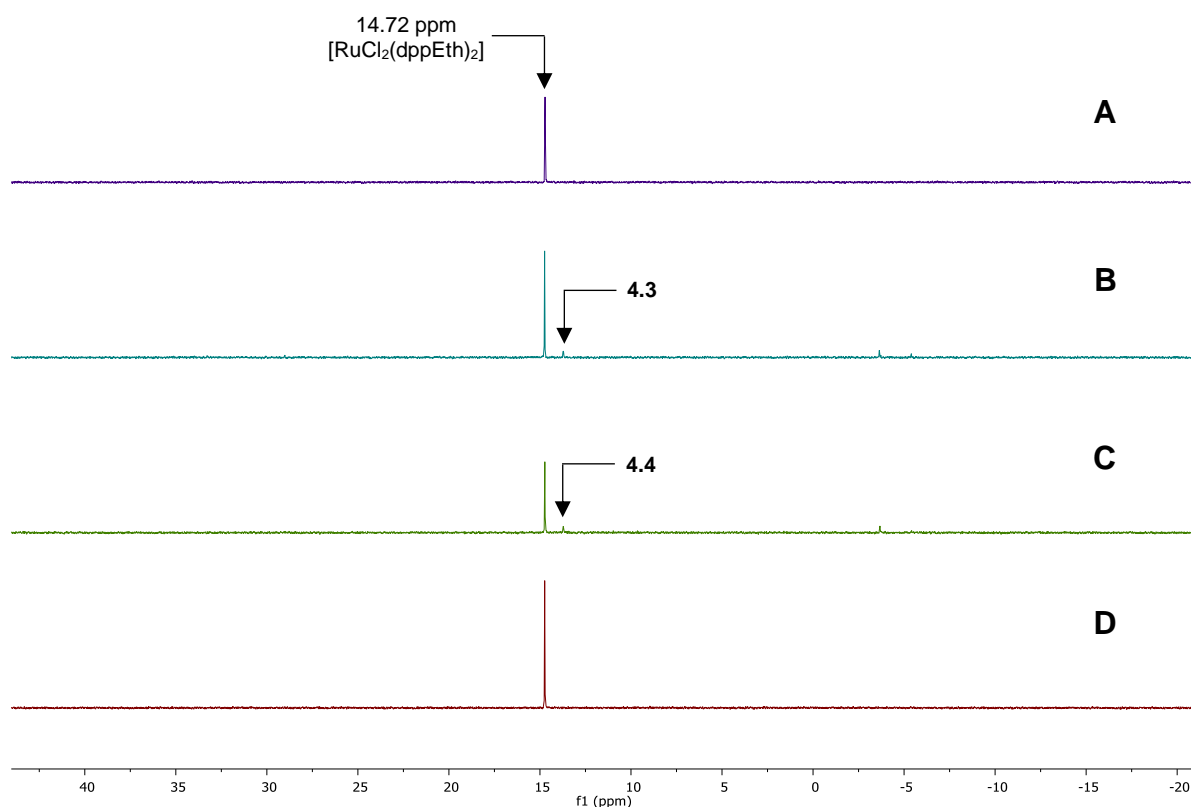
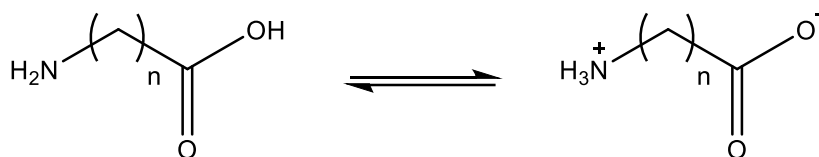


Figure 41: $^{31}\text{P}\{^1\text{H}\}$ NMR spectra of $[\text{RuCl}_2(\text{dppEth})_2]$ (A) and **4.3** (B), **4.4**(C) and **4.5** (D).

The $^{31}\text{P}\{^1\text{H}\}$ spectra of the products of the additions of 4-aminobutyric acid (Figure 41, **B**) and 5-aminovaleric acid (Figure 41, **C**) show minor traces of **4.3** and **4.4** respectively (peak at ~ 13.7 ppm), while that of the product of the addition of 6-aminocaproic acid (Figure 41, **D**) shows no trace of **4.5**. All three product reaction spectra shown in Figure 41 show that reaction product distribution is primarily composed of the starting $[\text{RuCl}_2(\text{dppEth})_2]$ complex. The spectra detailed in Figure 41, combined with those shown in Figure 40 highlight a lack of compatibility for the Michael additions of amino acids across $[\text{RuCl}_2(\text{dppEth})_2]$ in toluene. Hence further investigation was required to determine if other solvent systems were compatible for these reactions.

The addition of glycine across $[\text{RuCl}_2(\text{dppEth})_2]$ was attempted in different solvent systems; a 1:1 mixture of MeOH and toluene at room temperature over 16 hours, in MeOH

at reflux over 16 hours and in a 1:1 mixture of MeOH and DCM at room temperature over 16 hours. $^{31}\text{P}\{^1\text{H}\}$ NMR spectroscopy of the products of these reactions, like those shown in Figures 43 and 44, showed that the major species present was the unreacted starting $[\text{RuCl}_2(\text{dppEth})_2]$ complex. The trials conducted here on the Michael addition of amino acids directly across the ethylene groups of $[\text{RuCl}_2(\text{dppEth})_2]$ showed limited success in the synthesis of the desired product. Under each reaction trialed with different solvent systems and reaction conditions, $^{31}\text{P}\{^1\text{H}\}$ NMR spectroscopy showed that the major species in every reaction tested was the starting $[\text{RuCl}_2(\text{dppEth})_2]$ complex. Further optimisation experiments could be carried out to determine a solvent system that allows the facile Michael addition of amino acids across $[\text{RuCl}_2(\text{dppEth})_2]$, however, different routes were explored to overcome the lack of reactivity, which may have arisen due to the amino acid existing in equilibrium in the system.

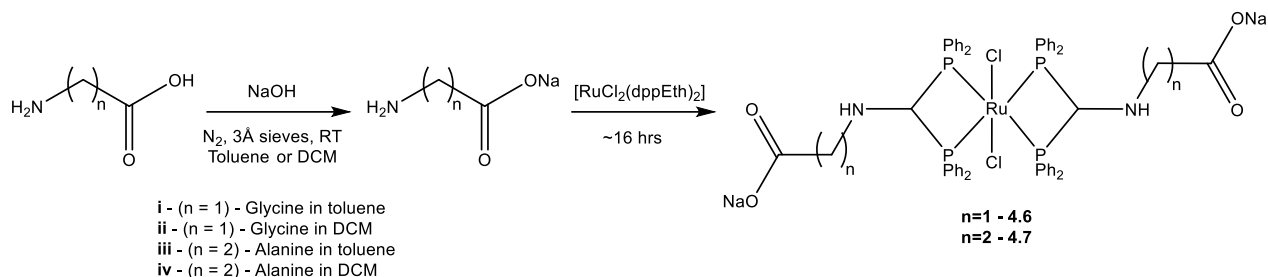


Scheme 43: Amino acid zwitterion formation equilibrium.

If the amino acids are present in the system in an equilibrium between the carboxylic acid and zwitterionic species described in scheme 43, then this would reduce the nucleophilicity of the amine and as a result, hinder its ability to function as a Michael adduct.

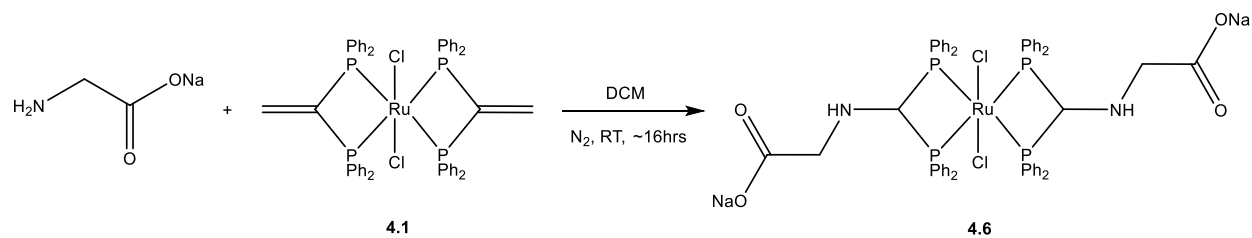
A method that was devised to attempt to overcome the lack of reactivity between $[\text{RuCl}_2(\text{dppEth})_2]$ and the amino acids was to convert the amino acid to the corresponding sodium salt before addition of the complex. This was theorised to prevent the formation of the zwitterionic species described in Scheme 43, and hence promote Michael addition across the dppEth ligands on $[\text{RuCl}_2(\text{dppEth})_2]$ by maintaining a more nucleophilic $-\text{NH}_2$ amine. Prior to the reaction, the amino acid would first be dried through stirring at room temperature in toluene and recovered through removal of the toluene-water azeotrope under vacuum. The dried amino acid would then be converted to the corresponding sodium salt through a reaction with sodium hydroxide in the presence of 3Å molecular sieves. The formation of the monosodium salt of the corresponding amino acid was

assumed, and $[\text{RuCl}_2(\text{dppEth})_2]$ would be added to the reaction mixture to determine whether the pre-formed sodium amino acid salt would react in a Michael addition across the complex (Scheme 44).



Scheme 44: Attempted Michael addition of amino acids across $[\text{RuCl}_2(\text{dppEth})_2]$ via pre-activation of the amino acids to their corresponding sodium salts.

As highlighted in Scheme 44, the Michael addition reactions conducted using the products of the reaction between amino acids and sodium hydroxide were performed in either toluene or DCM at room temperature and tested using glycine and alanine that had been previously dried in toluene. The $^{31}\text{P}\{^1\text{H}\}$ NMR spectra of the **4.6** and **4.7** solutions reactions conducted in toluene using the corresponding sodium salts formed *in situ* (i and iii, Scheme 44) showed no presence of any phosphorous signals (not even that of the starting complex). These results were curious and are potentially a result of the introduction of molecular sieves to the system preventing efficient stirring to dissolve the $[\text{RuCl}_2(\text{dppEth})_2]$ complex. Post reaction $^{31}\text{P}\{^1\text{H}\}$ NMR spectra were obtained from **4.6** and **4.7**, in the reactions between glycine and alanine with $[\text{RuCl}_2(\text{dppEth})_2]$ in DCM (ii and iv, Scheme 44), and exclusively showed the presence of the starting $[\text{RuCl}_2(\text{dppEth})_2]$ complex. Whether the failure of these reactions was a result of the lack of solubility of the sodium salts formed *in situ*, or whether the generation of the sodium salts of glycine and alanine was not forming in the first step of Scheme 44 was determined by testing the direct Michael addition of commercially obtained sodium glycinate across $[\text{RuCl}_2(\text{dppEth})_2]$ in DCM (Scheme 45).



Scheme 45: Attempted Michael addition of sodium glycinate across $[\text{RuCl}_2(\text{dppEth})_2]$ in DCM at room temperature.

A $^{31}\text{P}\{^1\text{H}\}$ NMR spectrum was recorded of the product of the direct addition of sodium glycinate across the ethyl groups of $[\text{RuCl}_2(\text{dppEth})_2]$, however as with the reaction described in Scheme 44 (ii), a single NMR resonance at 14.7 ppm was observed, that indicated unreacted $[\text{RuCl}_2(\text{dppEth})_2]$.

From the reactions trialed for the Michael addition of amino acids, and their sodium salt derivatives across the ethylene groups on $[\text{RuCl}_2(\text{dppEth})_2]$, there was very limited success in synthesising complexes with pendant $-\text{COOH}$ functionality. Only trace amounts of the glycine adduct complex were observed at high temperatures over long reaction times (conditions iii, iv and v, Scheme 41), when monitored by $^{31}\text{P}\{^1\text{H}\}$ NMR spectroscopy. The work presented here shows an incompatibility of amino acids and their sodium salt derivatives as reactants for the Michael addition across $[\text{RuCl}_2(\text{dppEth})_2]$ under the reaction conditions that were trialed.

4.3 Phosphino azomethinylate ligands

A new class of ligand was highlighted as a potential route to synthesising transfer hydrogenation catalysts with pendant carboxylate functionality for immobilisation on the nodes of UiO-66(Zr). Previous unpublished work by Adshead had shown that the PNO ligands detailed in Figure 42, when complexed to ruthenium, formed active transfer hydrogenation catalysts in the homogenous Guerbet synthesis of isobutanol from ethanol and methanol.⁶

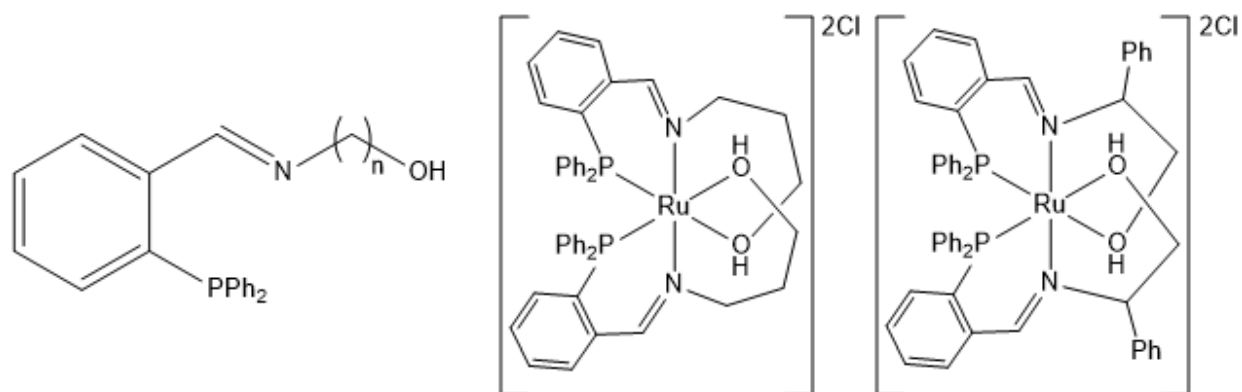


Figure 42: Ruthenium bischelate PNO Complexes Previously Synthesised by Adshead.⁶

From the research into the ligands detailed in Figure 42 conducted by Adshead,⁶ a new ligand set was identified to form ruthenium complexes with pendant carboxylate functionality. Phosphino azomethinylate ligands (Figure 43), if coordinated to a metal centre only through bidentate PN coordination, would form metal complexes with the pendant carboxylate functionality that was desired.

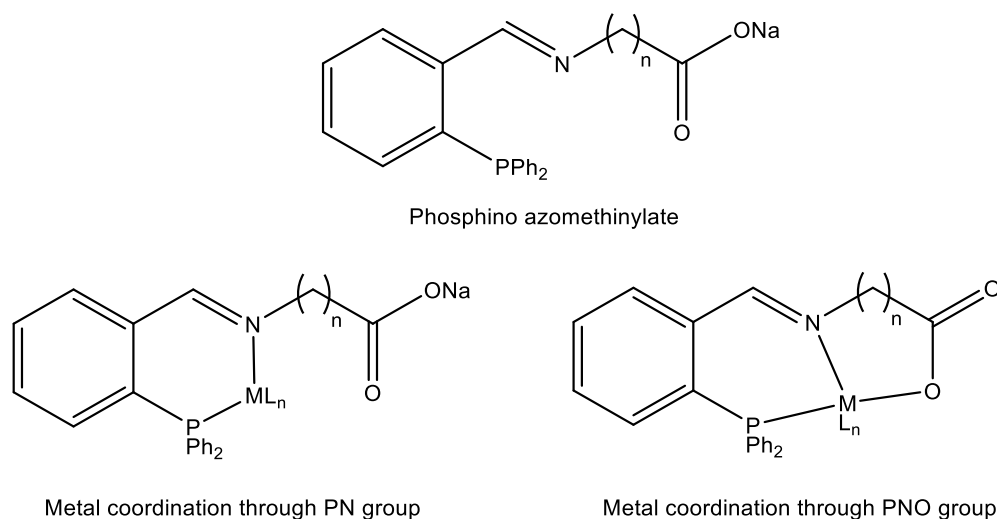
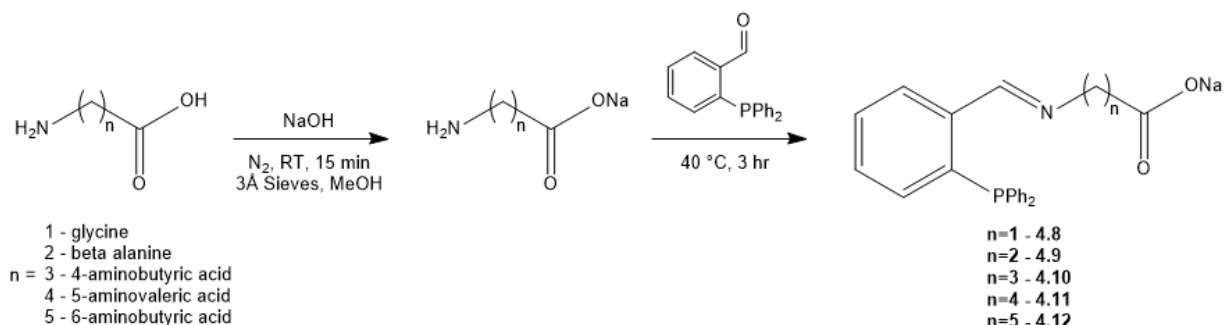


Figure 43: Targeted phosphino azomethinylate ligand set, and predicted binding modes of these ligands to ruthenium centres.

If the ligand coordinated through a tridentate PNO coordination, then the resulting complex would not possess the desired pendant carboxylate functionality for coordination to a MOF node (Figure 43). It was postulated that the nature of the coordination of the phosphino azomethinylate ligand to a ruthenium centre would depend on the chain length of the ligand, and that increasing the carbon chain length of the substituted imine

carboxylate would change the nature of the complexation to a metal centre. Phosphino azomethinylate ligands with shorter chains were predicted to bind to a metal centre through a tridentate PNO coordination, while longer chained ligands were predicted to coordinate *via* a bidentate PN coordination, leaving a pendant carboxylate group present on the complex.

Previous work in the Wass group had been conducted on the synthesis of phosphino azomethinylate ligands derived from valine, glycine, and phenyl glycine,⁶ where the synthesis of these ligands was previous work by Wencel *et al.*⁷ Initial work on the synthesis of phosphino azomethinylate ligands as precursors to transfer hydrogenation catalysts to be immobilised within MOFs was conducted by Cole, who studied the synthesis of different phosphino azomethinylate ligands (Scheme 46), and corresponding ruthenium complexes.⁸



*Scheme 46: Synthesis of phosphino azomethinylate ligands conducted by Cole.*⁸

Initially, pre-dried (stirred in toluene that was then removed in vacuo) amino acid was converted to the corresponding sodium salt through a reaction with sodium hydroxide in MeOH in the presence of 3 Å molecular sieves following a modified literature procedure.⁷ 2-(Diphenylphosphino)benzaldehyde was added to the reaction mixture, which was then heated to 40 °C and stirred for three hours (Scheme 46) to generate the phosphino azomethinylate sodium salt. Five different amino acid precursors were used to generate phosphino azomethinylate sodium salts with different carbon chain lengths of the imine carboxylate group. This was to enable an investigation into the effect of the chain length of these ligands with regards to the nature of their complexation to a ruthenium centre. Ruthenium complexes with sodium phosphino azomethinylate ligands bound through the

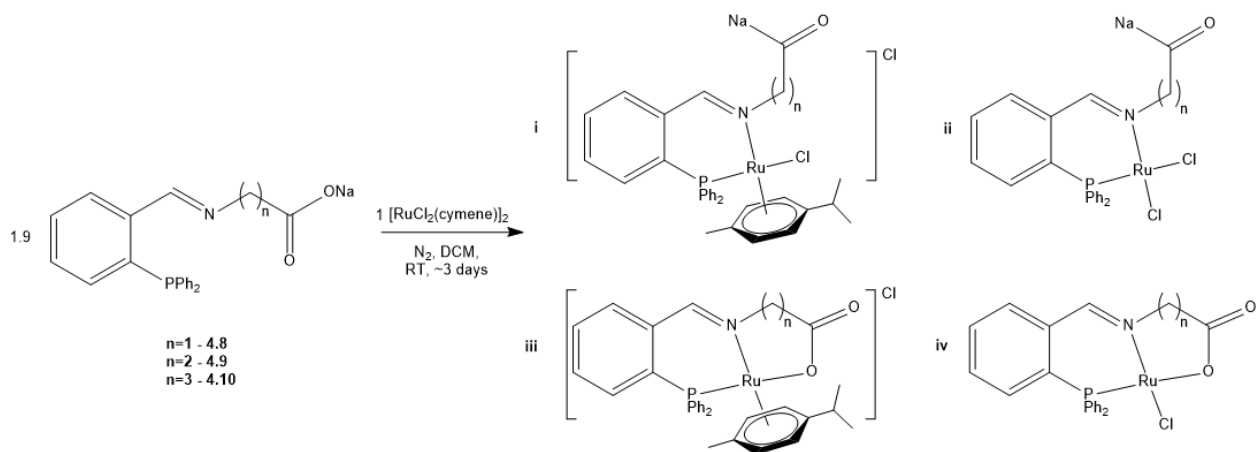
PN groups only of the ligand were desired (to leave pendant carboxylate groups), and that such complexes were also active for the transfer hydrogenation reaction in the Guerbet synthesis of *n*-butanol.

Preliminary work was also conducted by Cole into the formation of ruthenium complexes with phosphino azomethinylate ligands. The reaction of different phosphino azomethinylate ligands with $[\text{RuCl}_2(\text{PPh}_3)_3]$ and $[\text{RuCl}_2(\eta^6\text{-}p\text{-cymene})]_2$ precursors tended to give mixtures of different products, comprising of unknown complex species, starting materials and degraded ligand. While the formation of the sodium phosphino azomethinylate ligands was demonstrated, the work conducted by Cole into the formation of ruthenium catalysts using these ligands was still preliminary, as was investigation into the use of these ligands on ruthenium as catalysts for the transfer hydrogenation steps in the Guerbet upgrading of ethanol. Further study into both these areas was undertaken.

4.3.1 Homogeneous catalyst synthesis

The previous study into the formation of ruthenium-phosphino azomethinylate complexes conducted by Cole focused on the synthesis of monochelate complexes using $[\text{RuCl}_2(\text{PPh}_3)_3]$ as a precursor, and bischelate complexes using $[\text{RuCl}_2(\eta^6\text{-}p\text{-cymene})]_2$ as a precursor. Hence for this investigation monochelate ruthenium-phosphino azomethinylate complex formation using $[\text{RuCl}_2(\eta^6\text{-}p\text{-cymene})]_2$ as a precursor, and bischelate complex formation using $[\text{RuCl}_2(\text{PPh}_3)_3]$ as a precursor were targeted.

$[\text{RuCl}_2(\eta^6\text{-}p\text{-cymene})]_2$ was used a precursor complex to synthesise monochelate ruthenium-phosphino azomethinylate complexes, *via* reacting sodium phosphino azomethinylate ligands and $[\text{RuCl}_2(\text{cymene})]_2$ in DCM at room temperature under N_2 (Scheme 47).



Scheme 47: Attempted formation of monochelate sodium phosphino azomethinylate complexes with $[\text{RuCl}_2(\eta^6\text{-p-cymene})]_2$ as a precursor, and predicted possible binding modes of the ligand to the metal.

As $[\text{RuCl}_2(\eta^6\text{-p-cymene})]_2$ is a bimetallic complex, 1.9 equivalents of ligand was added to the reaction mixture to promote the formation of monochelate phosphino azomethinylate complexes (0.95 molar equivalents of ligand to one mole of ruthenium in the reaction). As detailed in Scheme 47, a number of different ruthenium complexes (**i-iv**) could potentially be formed as products of the complexation reaction. The phosphino azomethinylate ligand was predicted to bind to the ruthenium center in a bidentate fashion *via* PN coordination (**i-ii**, Scheme 47), or *via* tridentate PNO coordination. The reaction detailed in Scheme 47 was carried out using **4.8**, **4.9** and **4.10**, and $^{31}\text{P}\{^1\text{H}\}$ NMR spectra were recorded of the products of these reactions (Figure 44).

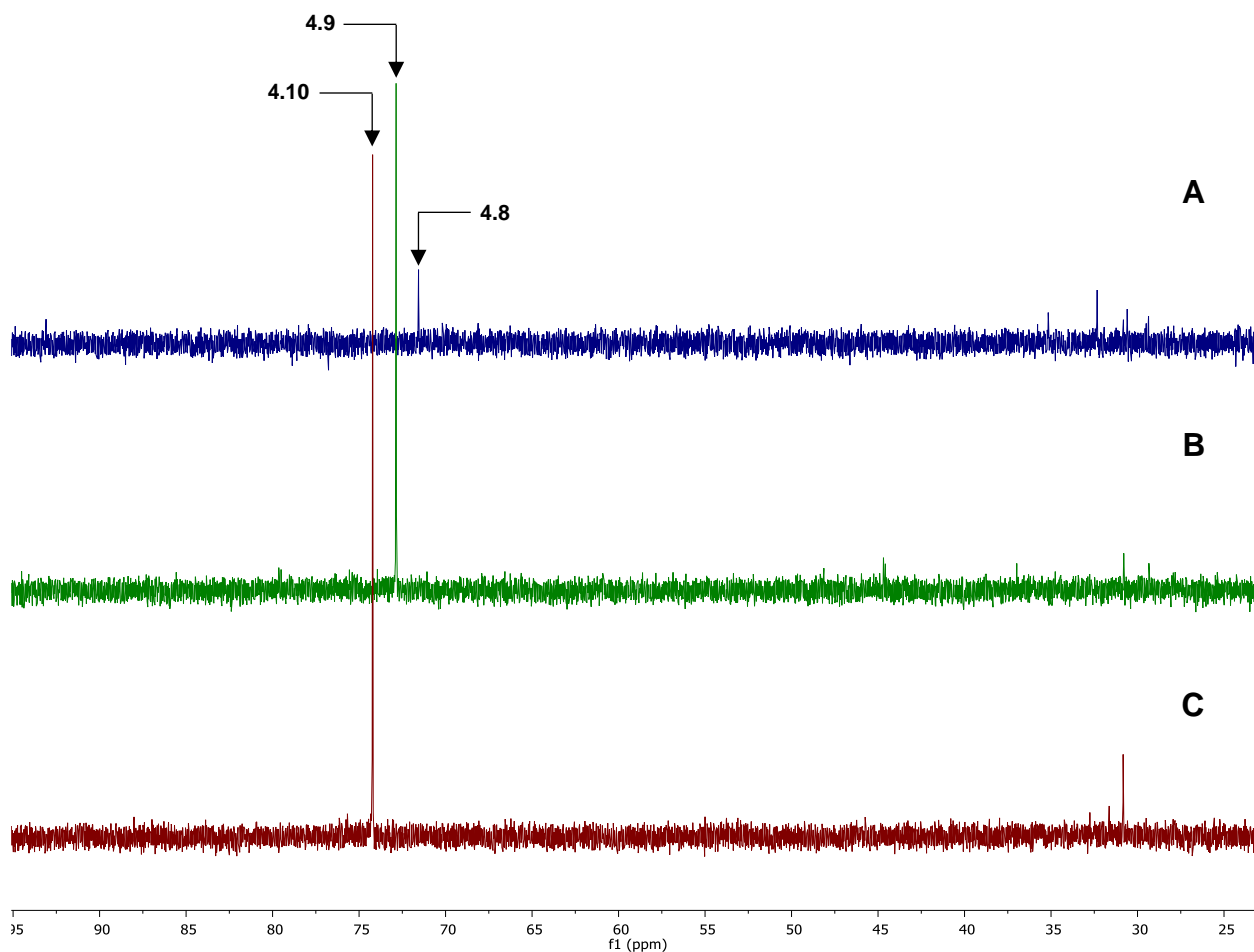


Figure 44: $^{31}\text{P}\{^1\text{H}\}$ NMR spectra of the products of the reactions of $[\text{RuCl}_2(\eta^6\text{-}p\text{-cymene})]_2$ with **4.8** (A), **4.9** (B) and **4.10** (C) to target monochelate complex formation

The $^{31}\text{P}\{^1\text{H}\}$ NMR spectra of the products from the reaction of $[\text{RuCl}_2(\eta^6\text{-}p\text{-cymene})]_2$ with phosphino azomethinylate ligands showed that in each reaction, a similar species was forming as a majority product. The product of the complexation of **4.8** showed a major peak at 71.6 ppm (Figure 44, A), while the products of the complexations of **4.9** (Figure 44, B) and **4.10** (Figure 44, C) exhibited a similar peak, moving more downfield as the chain length of the ligand increases. The structure of the complexes formed in the reactions detailed in Scheme 47 could not be rationalised through mass spectrometry, which gave a variety of peaks representing different ruthenium species. The major products of the reactions detailed in Scheme 47 were theorised to be tridentate PNO coordinated species (iii or iv, Scheme 47) due to the extent of the deshielding of the large singlet phosphorus signals >70 ppm present in the ^{31}P NMR spectra of the products of the complexation reactions (Figure 44). However, in each of the spectra shown in Figure 44, there are a number of upfield signals corresponding to a variety of unknown species

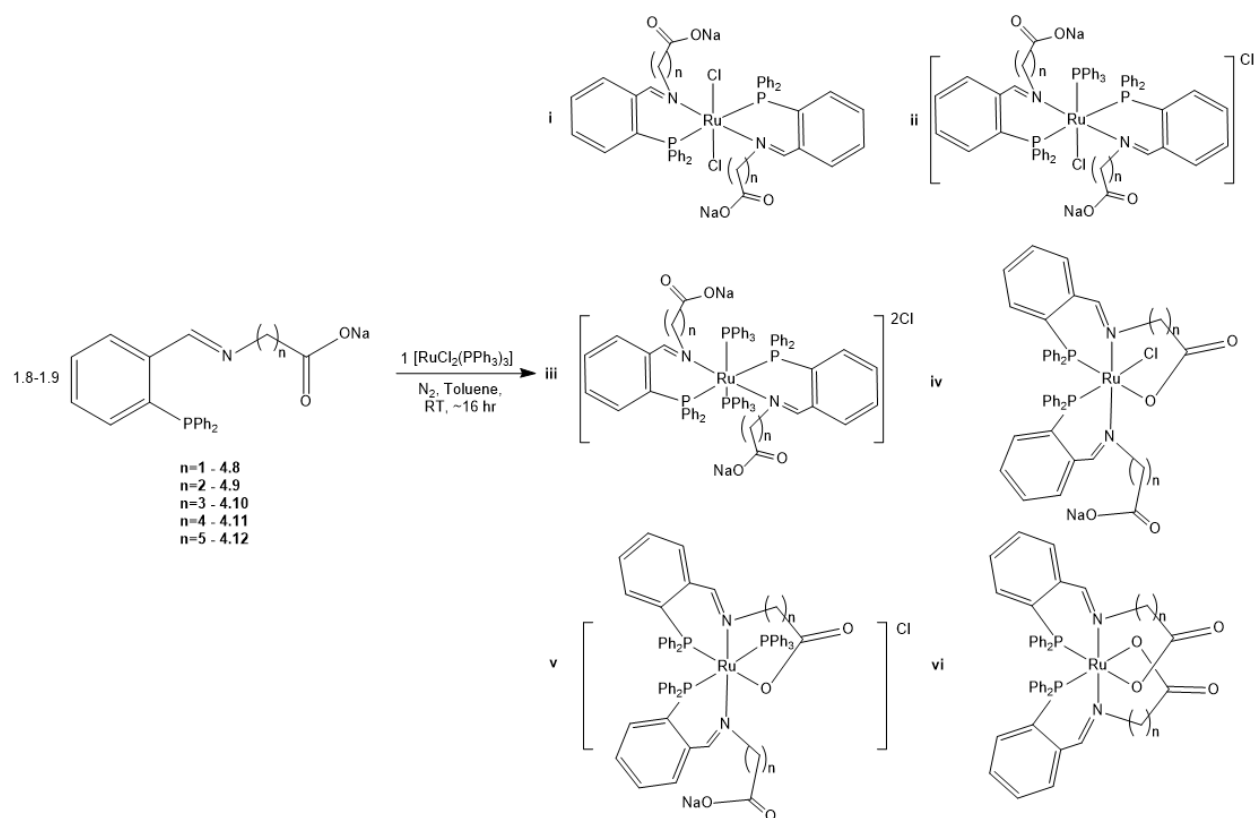
present in the product mixture, and mass spectrometry showed that in each of the products of the reactions detailed in Scheme 47, a mixture of products was forming. In each of the spectra presented in Appendix 7.2.1, Appendix 7.2.2 and Appendix 7.2.3, there are numerous peaks that display the characteristic isotopic splitting pattern of ruthenium (isotopic split of peak into 7 signals), hence it is known that when analysed by mass spectrometry, the products of the complexations of **4.8**, **4.9** and **4.10** (Scheme 47) split into numerous ruthenium containing fragments of different mass. For example, the spectra in Appendices 7.2.1, 7.2.2 and 7.2.3 all show a major peak at 270.98, indicative of the $[\text{RuCl}(\text{cymene})]^+$ fragment.

The mass spectrum of the product of the complexation of **4.8** shows a peak at 738.09 (Appendix 7.2.1), the mass spectrum of the product of the complexation of **4.9** shows a peak at 752.11 (Appendix 7.2.2) and the mass spectrum of the product of the complexation of **4.10** shows a peak at 766.12 (Appendix 7.2.3). Considering the chain lengths of ligands **4.8**, **4.9** and **4.10**, **4.9** contains an extra CH_2 group than **4.8**, and **4.10** contains an extra CH_2 group than **4.9**. Extra CH_2 groups mean that the mass of the ligand increases by 14 with every addition group present, hence these correspond to different m/z values of the 738.09, 752.11 and 766.12 peaks present in the spectrum in Appendix 7.2.1, Appendix 7.2.2 and Appendix 7.2.3 respectively. From this information, it is known that these peaks correspond to complexes of identical structure bearing the phosphinoazomethinylate ligands. The m/z peaks of 525.01 in Appendix 7.2.1, 539.02 in Appendix 7.2.2 and 553.04 in Appendix 7.2.3 show this same trend, hence these peaks can also be attributed to identical complex fragments bearing ligands **4.8**, **4.9** and **4.10** respectively. These peaks could theoretically belong to fragments of a single positive charge bearing one phosphinoazomethinylate ligand, or fragments of 2+ charge bearing two phosphinoazomethinylate ligands, but their presence highlights the successful complexation of **4.8**, **4.9** and **4.10** to ruthenium according to the procedure in Scheme 47.

Considering the mass spectra of product of the targeted formation of the monochelate complex of **4.8** (Appendix 7.2.1), the peak at 831.09 is indicative of the a bischelate complex fragment $[\text{Ru}(\text{4.8 H})_2\text{Cl}]^+$ where the sodium ions originally present on the phosphinoazomethinylate ligands have been substituted by protons. And in the same

spectrum (Appendix 7.2.1), the peak at 795.11 is indicative of the complex fragment $[\text{Ru}(\mathbf{4.8}^-)(\mathbf{4.8H})]^+$, where one ligand has been deprotonated, and on the other the substitution of sodium by hydrogen has proceeded. While when **4.10** was used in the same reaction (Scheme 47), the mass spectrum of the product (Appendix 7.2.3) shows a strong peak at 646.12, indicative of the formation of monochelate complex fragment $[\text{Ru}(\mathbf{4.10H})(\text{cymene})\text{Cl}]^+$, again where the sodium ion of the initial complex has been replaced by proton. In both these MS spectra however (Appendix 7.2.1 and Appendix 7.2.3), there are multiple peaks that are indicative of ruthenium species, hence what is being observed is a mixture of a variety of different ruthenium complexes being formed in the reactions described in Scheme 47.

The reaction of 2 equivalents of phosphino azomethinylate ligands with $[\text{RuCl}_2(\text{PPh}_3)_3]$ as a precursor was also investigated at room temperature under nitrogen in toluene with a view to synthesising bischelate complexes (Scheme 48).



Scheme 48: Attempted formation of bischelate sodium phosphino azomethinylate complexes with $[\text{RuCl}_2(\text{PPh}_3)_3]$ as a precursor, and predicted possible binding modes of the ligands to the metal.

Complexation of the five sodium phosphino azomethinylate ligands derived from amino acids of different carbon chain length were trialed according to the procedure shown in Scheme 48. A wide variety of ruthenium complex structures could possibly form in the reaction (**i-vi**, Scheme 48), where the carbon chain length of the phosphino azomethinylate was predicted to influence the topology of the ruthenium complex formed. The smaller ligands such as **4.8** and **4.9** were predicted to favour the formation of bischelate complexes where both ligands bind to the ruthenium center *via* $\kappa^3\text{-P,N,O}$ -coordination (**vi**, Scheme 48). As the chain length of the phosphino azomethinylate ligands increased, the resulting complex structure was theorised to favour ligand coordination through fewer donors (i.e. $\kappa^2\text{-P,N}$) due to the O- donor being further away from the ruthenium center. Structures **iv** and **v** (Scheme 48), where one phosphino azomethinylate ligand binds to the ruthenium center through a tridentate coordination, and the other through a bidentate coordination were predicted for medium sized ligands, while longer chained ligands were predicted to favour formation of the bidentate bis chelate complex structures **i**, **ii** or **iii** (Scheme 48). The reactions detailed in Scheme 48 were performed using the five specified sodium phosphino azomethinylate ligands derived from amino acids of increasing chain length, and $^{31}\text{P}\{^1\text{H}\}$ NMR spectra were recorded of the products of each of them (Figure 45).

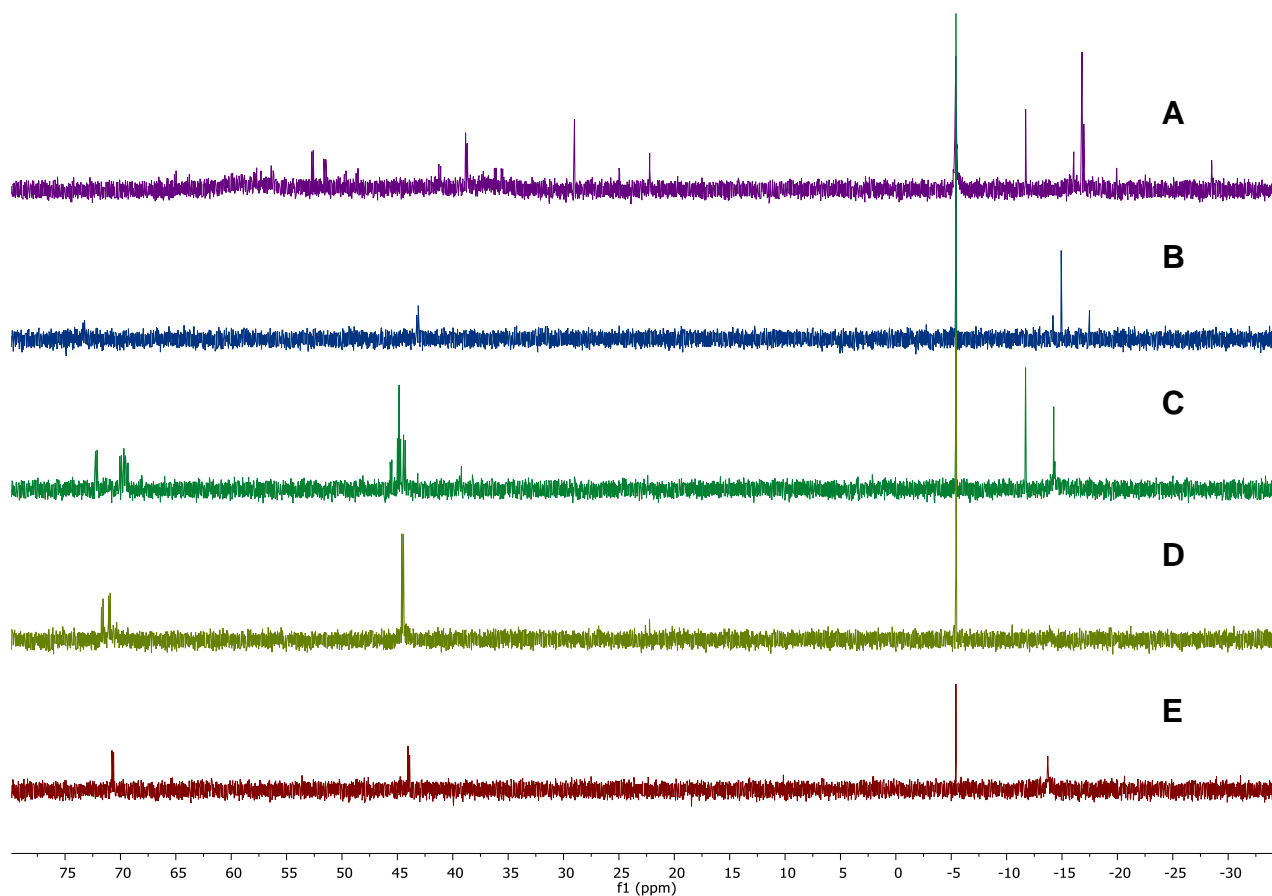


Figure 45: $^{31}\text{P}\{^1\text{H}\}$ NMR spectra of the products of the reactions of $[\text{RuCl}_2(\text{PPh}_3)_3]$ with **4.8** (A), **4.9** (B), **4.10** (C), **4.11** (D) and **4.12** (E) targeting bischelate complex formation.

When the $^{31}\text{P}\{^1\text{H}\}$ NMR spectra of the products of the reactions detailed in Scheme 48 were analysed, it appeared that the ligands of different chain length coordinated to ruthenium in different ways depending on the chain length. When analysing the product of the complexation reaction of **4.12** (Appendix 7.2.4), two mutually coupled doublets were observed at 44.0 ppm and 70.7 ppm ($^2J_{\text{PP}} = 29.6$ Hz). Considering the potential structures of the products of the bis chelate complexation reactions shown in Scheme 48, the only structure that would display such a pattern would be that of **iv** (Scheme 48), indicating that one **4.12** ligand coordinates to the ruthenium center *via* a tridentate coordination, and the other through a bidentate coordination. However, in the spectra presented in Figure 45 (E), free phosphino azomethinylate ligand is present, which would actually suggest that the product of the reaction described in Scheme 11 ($n=5$) is a monochelate complex, as no excess free ligand would be present if the only product was a bischelate complex. The presence of two mutually couple phosphorous signals could

very reasonably arise from phosphorus atoms bound to the ruthenium center from PPh₃ and bound P-N-O ligand, hence a monochelate κ^3 -P,N,O-coordination complex is the most likely product of the reaction detailed in Scheme 11 (n=5). A similar splitting pattern is observed in the ³¹P{¹H} NMR spectrum of the product observed from the reaction of **4.11** with [RuCl₂(PPh₃)₃], however, a further doublet is present in the spectra at 71.6 ppm (Appendix 7.2.5). This raises the possibility that the doublet signal at 44.0 ppm is in fact two coincidental doublet peaks that are stacked on top of each other, and that two similar structural isomers are forming in this reaction that result in the presence of an additional doublet at 71.6 ppm. The lack of free phosphino azomethinylate in the spectra detailed in Figure 45 (D) does give a strong indication that the product complex does possess bischelate P-N-O ligands. The ³¹P NMR spectrum of the product of the reaction between **4.10** and [RuCl₂(PPh₃)₃] (Scheme 48, n=3) also indicates that a mixture of species are forming in the reaction (Appendix 7.2.6). The downfield doublet present at 72.2 ppm suggests that the mixture of structural isomers with **4.10** ligands is forming, however there are other peaks that suggest the formation of other topologies. The triplet signal shown at 44.9 ppm (Appendix 7.2.6) is indicative of the formation of the bidentate bis chelate complex (iii, Scheme 48) with 4-aminobutyric acid derived ligands, however, numerous other mutually coupled doublet signals indicate the formation of other complex structures. A significant amount of free phosphino azomethinylate ligand is present in the spectra presented in Figure 45 (C), which also indicates that monochelate P-N-O complexes are also forming in the n=3 reaction (Scheme 11). Though weak, the ³¹P NMR spectrum of the product of the reaction between the **4.9** and [RuCl₂(PPh₃)₃] (Scheme 48, n=2) shows two mutually coupled doublet signals (Appendix 7.2.7), but also the presence of a significant amount of free β-alanine derived ligand in the spectra. Hence, as observed with the products of reactions n=5 (Scheme 48) and n=3 (Scheme 11), a mixture of products are forming, containing monochelate bound P-N-O ligands with coordinated PPh₃ to the ruthenium centre, with the possibility of bischelate complexes also making up the product mixture. The ³¹P NMR spectrum of the product of the reaction of **4.8** is complex and shows a variety of signals, indicating a highly complex mixture of species forming in the reaction (Appendix 7.2.8). When all the ³¹P NMR spectra of the reactions

detailed in Scheme 48 are considered (Figure 45), each spectrum shows a strong phosphorous signal at -5.4 ppm, that is indicative of free triphenylphosphine.

While the results of the complexation reactions detailed in 4.3.1 have been used to attempt to predict potential structures of monochelate and bischelate ruthenium-phosphino azomethinylate complexes, most of the reactions led to the formation of mixtures of different complex species. Whether or not the synthesis of single isomers of the other targeted ruthenium-phosphino azomethinylate complexes is possible requires further detailed reaction optimisation. Due to the difficulty in obtaining pure complexes, catalytic testing was performed using sodium phosphino azomethinylate ligands and a ruthenium precursor loaded into the reaction vessel separately, to generate ruthenium-phosphino azomethinylate complexes *in-situ*. Differences in catalytic activity of Guerbet systems utilising the different sodium phosphino azomethinylate ligands would be used to theorize differences in the structure of the transfer hydrogenation catalysts formed in the reaction, predominantly based on the chain length of the amino acid moiety of the ligands and predicted coordination to the ruthenium centre.

4.3.2 *In-situ* catalytic study – NaOEt base

As the nature of the interaction between the phosphino azomethinylate ligands and ruthenium precursors discussed in Section 4.3.1 could not yet be fully determined, an *in-situ* catalytic study was conducted. Guerbet reactions of ethanol were carried out, loading $[\text{RuCl}_2(\eta^6\text{-}p\text{-cymene})]_2$ and phosphino azomethinylate ligands separately into the reaction mixture with an aldol catalyst. This method was used to determine the efficacy of the resultant catalyst formed from the reaction between $[\text{RuCl}_2(\eta^6\text{-}p\text{-cymene})]_2$ and sodium phosphino azomethinylates *in-situ* for transfer hydrogenation in the Guerbet reaction under conditions harsher than those employed in Section 4.3.1. Initially, studies were conducted into the homogeneous Guerbet coupling of ethanol using sodium ethoxide as an aldol catalyst, at 150 °C. The fully homogeneous Guerbet upgrading of ethanol using ruthenium transfer hydrogenation catalysts previously tested in the Wass group typically takes place at 150 °C, a temperature that is less harsh than the 210 °C than in the UiO-66(Zr) temperature optimised reaction from Section 2.2.1. Although the ruthenium-phosphino azomethinylate complexes would ideally be coordinated to UiO-66(Zr) derived

heterogeneous aldol catalysts, as a new class of transfer hydrogenation catalyst, studies were initially conducted using NaOEt as an aldol mediator in the Guerbet reaction at 150 °C.

Initially, a 2:1 loading of sodium phosphino azomethinylate:[RuCl₂(η⁶-*p*-cymene)]₂ was added to the Guerbet reaction as precursor species. As [RuCl₂(η⁶-*p*-cymene)]₂ is a bimetallic species, using twice the loading of ligand to catalyst was carried out to promote the formation of monochelate species. The catalytic results of the Guerbet upgrading of ethanol conducted using sodium phosphino azomethinylates and [RuCl₂(*cymene*)]₂ in a 1:1 (ligand:Ru) ratio as transfer hydrogenation catalyst precursors with NaOEt at 150 °C are detailed in Table 22.

Table 22: Guerbet upgrading of ethanol using sodium phosphino azomethinylate ligands with [RuCl₂(η⁶-*p*-cymene)]₂ (2:1 ratio) as transfer hydrogen catalyst precursors

		Selectivity (%) ^b					
Entry	Ligand	EtOH Conversion (%) ^a	<i>n</i> -BuOH (yield %)	EtOAc	2-BuOH	Higher Alcohols ^c	Other ^d
1	4.8	15.4	70.1 (10.8)	1.9	1.3	20.1	6.6
2	4.9	11.2	50.0 (5.6)	21.4	-	9.8	18.8
3	4.10	11.1	35.1 (3.9)	19.8	-	4.5	40.6
4	4.11	24.1	61.4 (14.8)	7.9	0.4	24.9	5.4
5	4.12	24.0	55.8 (13.4)	2.1	-	27.1	15.0

^a Conversion of ethanol calculated based on total liquid products obtained determined *via* GC analysis. ^b Selectivity to Guerbet products in liquid fraction determined *via* GC analysis. ^c C₆ and C₈ alcohol products calibrated *via* GC analysis. ^d Products not characterised from GC calibration.

The system utilising **4.8** shows modest activity for ethanol conversion with [RuCl₂(η⁶-*p*-cymene)]₂ when a monochelate complex is targeted; however, the system shows high

selectivity towards *n*-BuOH formation (Entry 1, Table 22). As the chain length on the ligand increases to 2 (**4.9**) and 3 (**4.10**) carbons (Entries 2 and 3, Table 22), the Guerbet system becomes less active for ethanol conversion (and significantly more selective towards the formation of ethyl acetate), indicating that the longer chain length on **4.9** and **4.10** hinders the activity of the resulting complexes formed *in-situ* for the dehydrogenation of ethanol to acetaldehyde. However, when the ligand chain length is further increased, when **4.11** and **4.12** are used in the reaction with $[\text{RuCl}_2(\eta^6\text{-}p\text{-cymene})]_2$ (Entries 4 and 5, Table 22), the Guerbet systems with NaOEt are more active for ethanol conversion and higher yielding of *n*-BuOH than that using **4.8** (Entry 1, Table 22). This is an interesting observation and suggests a change in complex structure formation when the longer chained ligands are used in the *in situ* Guerbet reaction. A possible theory is that phosphino azomethinylate ligands derived from glycine, β -alanine and 4-aminobutyric acid are coordinated to the ruthenium *via* the phosphine, imine and carboxylate groups, as these smaller ligands are energetically favoured to bind to the ruthenium center *via* three atoms (Figure 46).

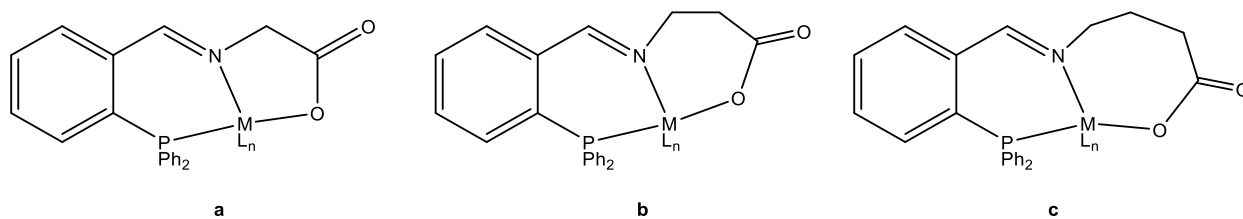


Figure 46: Proposed formation of tridentate bound phosphino azomethinylate complexes in the Guerbet reactions detailed in Table 22, Entries 1 (a), 2 (b) and 3 (c).

The longer chain phosphino azomethinylate ligands derived from 5-aminovaleric acid and 6-aminocaproic acid may not be able to bind to the metal center in the same way as the smaller analogues and may bind exclusively through the imine and the phosphine groups (Figure 47).

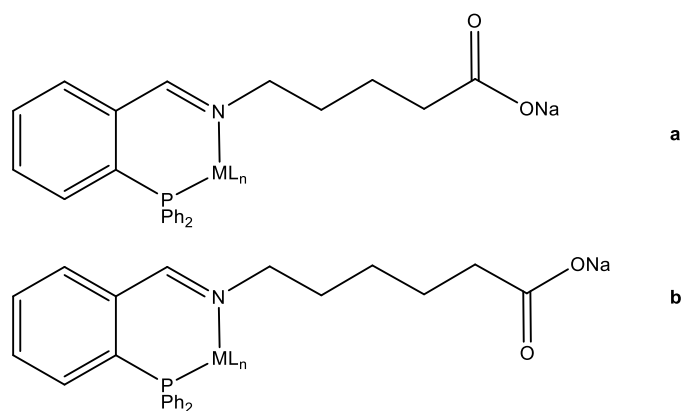
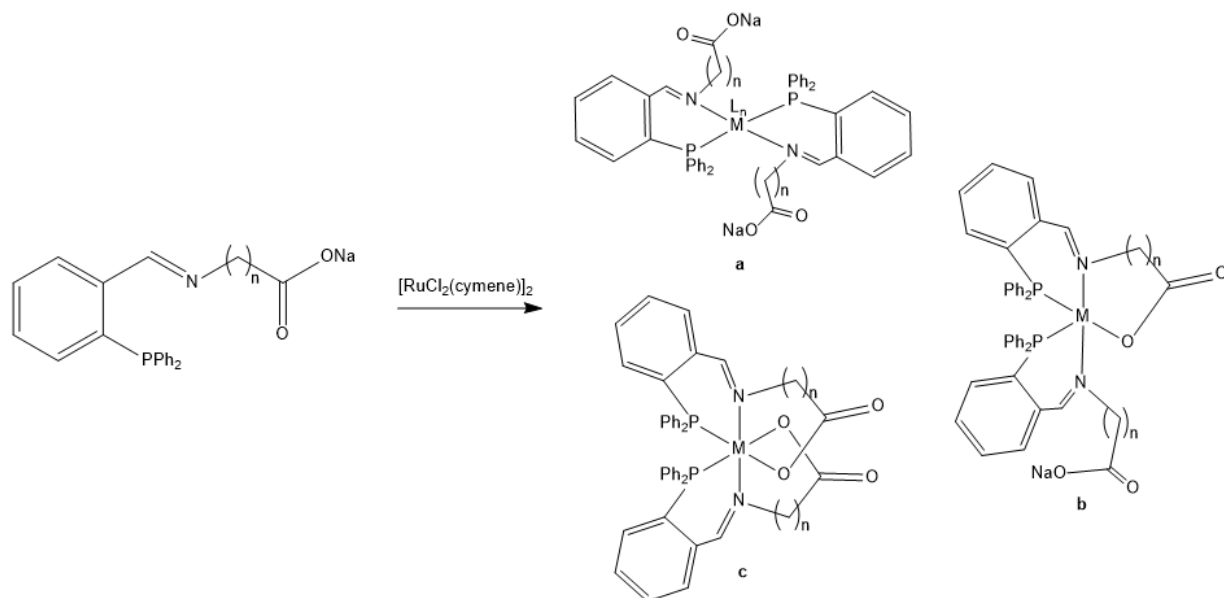


Figure 47: Proposed formation of bidentate bound phosphino azomethinylate complexes in the Guerbet reactions detailed in Table 22, Entries 4 (a) and 5 (b).

While these may not be the exact binding modes of the ligands to the resulting complexes formed in the *in-situ* Guerbet reactions, a phenomenon like this could explain the large increase in activity demonstrated by the longer chained phosphino azomethinylate ligands **4.11** and **4.12** compared to the shorter chained ligands, if the PN-coordinated complexes (Figure 47) were more active transfer hydrogenation catalysts than those favouring PNO coordination (Figure 46).

A further set of Guerbet catalytic runs were conducted, using $[\text{RuCl}_2(\eta^6\text{-}p\text{-cymene})]_2$ and phosphino azomethinylate ligands as transfer hydrogenation catalyst precursors, with NaOEt as an aldol mediator in a fully homogeneous system. While the previous set of reactions were conducted with 2:1 (ligand: $[\text{RuCl}_2(\eta^6\text{-}p\text{-cymene})]_2$) ratios to target the formation of monochelate species (Table 22), these Guerbet reactions were run with 4:1 (ligand: $[\text{RuCl}_2(\eta^6\text{-}p\text{-cymene})]_2$) to target the formation of bischelate complexes. Again, while the exact structure of the transfer hydrogenation catalysts formed *in-situ* in the reaction would not be able to be monitored, this set of experiments would give an insight into whether increasing the chain length of the phosphino azomethinylate ligands proved beneficial to transfer hydrogenation activity in the Guerbet reaction. The short chain (**4.8** and **4.9**) ligands were predicted to form tridentate bischelate ruthenium complexes (Scheme 49, c). The binding modes of the larger ligands (**4.10**, **4.11** and **4.12**) were predicted to be a mix of bidentate and tridentate bischelate complexes, with the bidentate complex ($\kappa^2\text{-}P,N$ binding ligands) favoured by the larger ligands (Scheme 49, a). The nature of the ancillary ligands present on bidentate bischelate complexes could not be

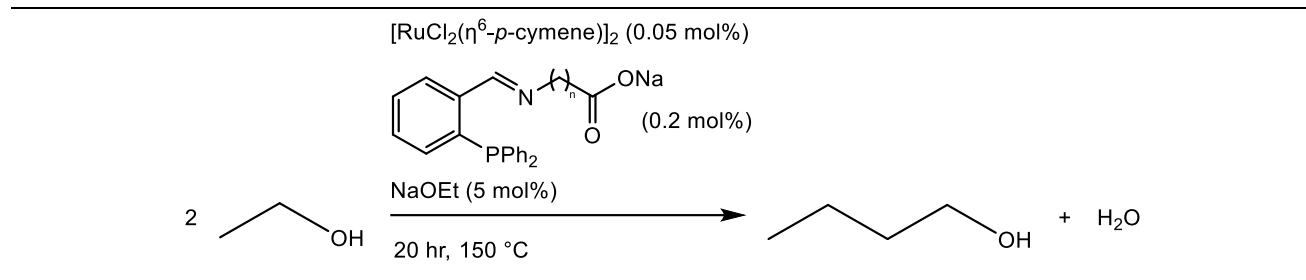
rationalised *in situ*, while an intermediate complex with one tridentate and one bidentate bound phosphino azomethinylate ligand was also a possible complex structural motif that could be formed in the *in-situ* Guerbet reaction with a 4:1 loading of phosphino azomethinylate ligand:[RuCl₂(η⁶-*p*-cymene)]₂ (Scheme 49, **b**).



Scheme 49: Predicted formation of bischelate phosphino azomethinylate ruthenium complexes in-situ in the Guerbet upgrading of ethanol - a) bischelate complex with bidentate ligands, b) bischelate complex with a bidentate and tridentate ligand, c) bischelate complex with tridentate ligands.

The 2:1 ligand:Ru Guerbet upgrading of ethanol was performed by adding one equivalent of $[\text{RuCl}_2(\eta^6\text{-}p\text{-cymene})]_2$ to four equivalents of the five different sodium phosphino azomethinylate ligands derived from amino acids of different chain length (transfer hydrogenation catalyst precursors), with NaOEt as an aldol mediator at 150 °C over 20 hours (Table 23).

Table 23: Guerbet upgrading of ethanol using sodium phosphino azomethinylate ligands with $[\text{RuCl}_2(\eta^6\text{-}p\text{-cymene})]_2$ (4:1) ratio) as transfer hydrogen catalyst precursors



Entry	Ligand	EtOH Conversion (%) ^a	Selectivity (%) ^b				
			<i>n</i> -BuOH	EtOAc	2-BuOH	Higher Alcohols ^c	Other ^d
1	4.8	14.3	54.5	2.8	1.4	13.3	28.0
2	4.9	12.3	39.0	22.8	0.8	7.3	30.1
3	4.10	15.7	63.7	11.5	1.3	15.9	7.6
4	4.11	20.7	56.5	1.4	1.0	15.9	25.2
5	4.12	22.0	68.6	1.8	0.9	22.7	6.0

^a Conversion of ethanol calculated based on total liquid products obtained determined *via* GC analysis. ^b Selectivity to Guerbet products in liquid fraction determined *via* GC analysis. ^c C₆ and C₈ alcohol products calibrated *via* GC analysis. ^d Products not characterised from GC calibration.

The Guerbet reactions of ethanol using **4.8** and **4.9** in the 4:1 (ligand: $[\text{RuCl}_2(\eta^6\text{-}p\text{-cymene})]_2$) system with NaOEt were the least active, and least selective towards *n*-BuOH formation of those tested with the different ligands (Entries 1 and 2, Table 23). While the identity of the transfer hydrogenation catalyst(s) in the reaction have not been identified, the reduced EtOH conversion activity compared to the other systems with larger phosphino azomethinylate ligands suggests that the transfer hydrogenation catalysts formed in these reactions have a different topology to those in the reactions conducted with longer carbon chain sodium phosphino azomethinylate ligands. The transfer hydrogenation catalysts formed in the reactions detailed in Entries 1 and 2 (Table 23) are predicted to possess a tridentate bischelate structure (Figure 48) and the Guerbet reactions using the 4:1 (ligand: $[\text{RuCl}_2(\eta^6\text{-}p\text{-cymene})]_2$) loadings were the least active and selective of those trialed. Potentially owing to a lack of availability for ethanol to

access the metal center complexes that are formed with two tridentate bound phosphino azomethinylate ligands.

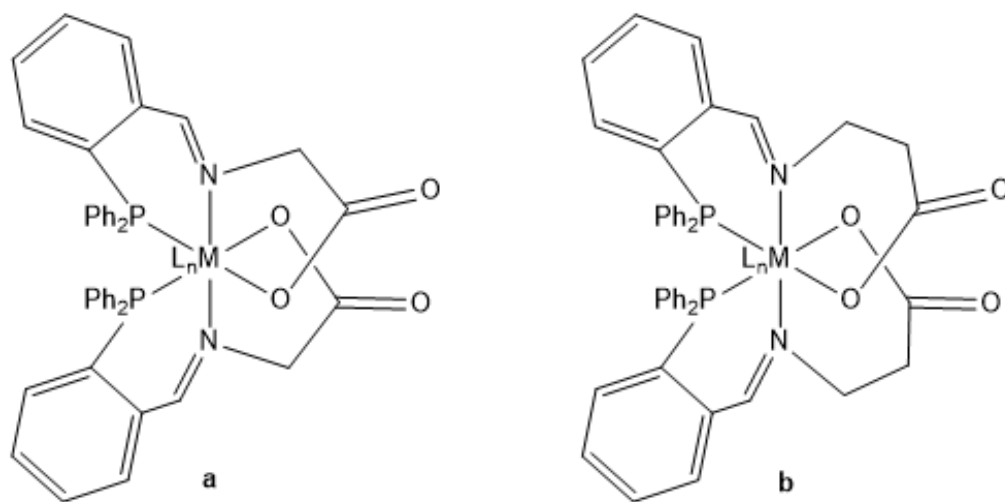


Figure 48: Predicted structures of ruthenium complexes formed in the reactions detailed in Table 23 Entries 1 (a) and 2 (b).

The Guerbet reaction detailed in Entry 3 (Table 23), using **4.10**, shows similar ethanol conversions to those conducted with the shorter chained ligands. However, reaction selectivity towards *n*-butanol (and *n*-butanol yield) of the reactions using this ligand is significantly higher than those using **4.8** (Table 23, Entry 1) and **4.9** (Table 23, Entry 2).

The Guerbet reactions of ethanol with NaOEt conducted using one equivalent of [RuCl₂(η⁶-*p*-cymene)]₂ to four equivalents of **4.11** and **4.12** as transfer hydrogenation catalyst precursors (Entries 4 and 5, Table 23) were the most active for ethanol conversion of those trialed. This increased activity suggests that the structure of the transfer hydrogenation catalysts formed *in-situ* using the longer chained ligands is more active for transfer hydrogenation than the complexes formed using **4.8**, **4.9** and **4.10**. As the most active transfer hydrogenation catalysts are formed using the longest ligands, it can be predicted that the then increased chain length hinders the formation of tridentate κ³-*P,N,O* bound ligands, and that the longer chain ligands favour the formation of bidentate bischelate κ²-*P,N* complexes (Figure 49).

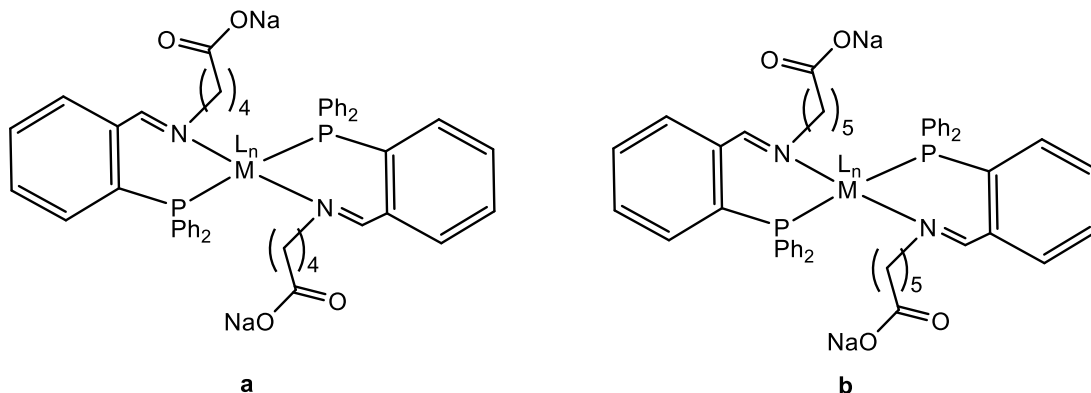


Figure 49: Predicted structures of ruthenium complexes formed in the reactions detailed in Table 23 Entries 4 (a) and 5 (b).

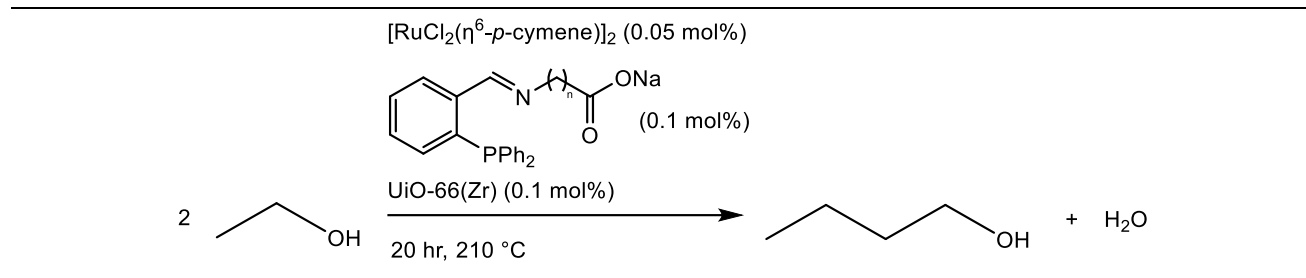
The transfer hydrogenation catalyst structures have been predicted for the reactions in Entries 1-5 (Table 23) (Figures 51 and 52) based on the differences in ethanol conversion (hence ethanol dehydrogenation activity) facilitated by the *in-situ* homogeneous catalyst formation Guerbet reactions (Table 23), combined with the different carbon chain lengths of the ligands that promoted the different activities. In reality, based on previous studies into the synthesis of the homogeneous ruthenium complexes using sodium phosphino azomethinylate ligands, there is likely to be a complex mixture of different ruthenium species forming in the Guerbet reactions with the complex precursors. However, a significant difference in EtOH conversion activity is observed when the longer chained 5-aminovaleric acid and 6-aminocaproic acid derived sodium phosphino azomethinylate ligands are used in the reaction detailed in Table 23, a trend that is also observed in the *in-situ* 1:1 (ligand:Ru) experiment described in Table 22. The significantly increased activity of the Guerbet systems utilising **4.11** and **4.12** in both the *in situ* 1:1 (ligand:Ru) experiment and *in-situ* 2:1 (ligand:Ru) experiment over those utilising the smaller chained ligands gives a strong indication that different complex structures are forming *in situ*. Structures of lower denticity (leaving a more accessible metal site for EtOH to react) reasonably explains the observations in catalytic activity, giving an early suggestion that bidentate P-N complex formation is favoured with the longer ligands.

4.3.3 *In-situ* catalytic study – UiO-66(Zr) aldol catalyst

While the Guerbet catalytic systems tested adding $[\text{RuCl}_2(\eta^6\text{-}p\text{-cymene})]_2$ and sodium phosphino azomethinylate ligands as transfer hydrogenation catalyst precursors showed modest ethanol conversions (Tables 22 and 23) with NaOEt, high product selectivities towards *n*-BuOH were achieved in most cases. In the *in-situ* 1:1 ligand:Ru experiments, use of the **4.11** facilitated an *n*-BuOH yield of 14.8 % with an EtOH conversion of only 24.1 % (selectivity towards *n*-BuOH of 61.4 %) (Table 22, Entry 4). While for the *in situ* 2:1 ligand:Ru experiments, the system using **4.12** demonstrated an *n*-BuOH yield of 15.1 % at an EtOH conversion of 22.0 % (selectivity towards *n*-BuOH of 68.6 %) (Table 23, Entry 5). The high selectivity towards *n*-BuOH achieved by these systems employing NaOEt as an aldol mediator showed that the $[\text{RuCl}_2(\eta^6\text{-}p\text{-cymene})]_2$ and sodium phosphino azomethinylate ligand transfer hydrogenation catalyst precursor mixture had potential to be effective in the Guerbet upgrading of ethanol using UiO-66(Zr) as a heterogeneous aldol catalyst in place of NaOEt. Hence, Guerbet reaction studies similar to those conducted in Section 4.3.2 were carried out, loading $[\text{RuCl}_2(\eta^6\text{-}p\text{-cymene})]_2$ and sodium phosphino azomethinylate ligands as transfer hydrogenation catalyst precursors with catalytic loadings of UiO-66(Zr) for the Guerbet upgrading of ethanol, under the conditions previously optimised for the UiO-66(Zr)/ $[\text{RuCl}_2(\text{dppm})_2]$ catalytic system in Section 2.2.1.

Initially, experiments were conducted with a loading of one equivalent of $[\text{RuCl}_2(\eta^6\text{-}p\text{-cymene})]_2$ to two equivalents of the five different sodium phosphino azomethinylate ligands of different chain length as transfer hydrogenation catalyst precursors, with a catalytic loading of UiO-66(Zr). The Guerbet upgrading of ethanol was then tested over a duration of 20 hours at 210 °C (Table 24).

Table 24: Guerbet upgrading of ethanol using sodium phosphino azomethinylate ligands with $[\text{RuCl}_2(\eta^6\text{-}p\text{-cymene})]_2$ (2:1) ratio) as transfer hydrogen catalyst precursors



Entry	Ligand	EtOH Conversion (%) ^a	Selectivity (%) ^b				
			<i>n</i> -BuOH	EtOAc	2-BuOH	Higher Alcohols ^c	Other ^d
1	4.8	26.1	11.1	65.9	0.8	-	22.2
2	4.9	23.6	9.7	80.2	0.8	0.4	8.9
3	4.10	18.5	9.2	70.3	-	0.5	20.0
4	4.11	25.6	5.1	82.8	0.4	-	11.7
5	4.12	22.6	8.4	77.9	0.4	0.4	12.9

^a Conversion of ethanol calculated based on total liquid products obtained determined *via* GC analysis. ^b Selectivity to Guerbet products in liquid fraction determined *via* GC analysis. ^c C₆ and C₈ alcohol products calibrated *via* GC analysis. ^d Products not characterised from GC calibration.

At the elevated temperature of 210 °C with UiO-66(Zr) as an aldol catalyst, the catalyst precursor mixture of $[\text{RuCl}_2(\eta^6\text{-}p\text{-cymene})]_2$ and sodium phosphino azomethinylate in a 2:1 (ligand:complex) ratio facilitates the formation of a very different product distribution when compared to the same transfer hydrogenation catalyst precursor mixture with NaOEt at 150 °C, in the Guerbet upgrading of ethanol. In the homogeneous Guerbet reaction with NaOEt at 150 °C, for each reaction that was conducted with sodium phosphino azomethinylate ligands of different chain length, the product distribution of the corresponding Guerbet reaction was always most selective towards the formation of *n*-BuOH (Table 22). However, when the reaction temperature was increased to 210 °C, and UiO-66(Zr) used as an aldol catalyst in place of NaOEt, the same loadings of transfer hydrogenation catalyst precursor resulted in highly selective transformations of ethanol to ethyl acetate (Table 24). The most selective reaction to *n*-BuOH was observed using **4.8** (Entry 1, Table 24); however, this reaction was still highly selective for the formation

of EtOAc (65.9 %), while use of the **4.11** facilitated a Guerbet reaction that was 82.8 % selective towards the formation of EtOAc (Entry 4, Table 24). Each of the Guerbet reactions using 1:1 ligand:Ru ratios with UiO-66(Zr) showed poor activity for *n*-BuOH formation, with a maximum yield observed using **4.8** (2.9 % yield of *n*-BuOH), with this ligand also facilitating the highest, but poor selectivity towards *n*-BuOH formation of 11.1 % (Entry 1, Table 24). Interestingly, there does not appear to be a correlation between the chain length of the phosphino azomethinylate ligand, and the EtOH conversion that the Guerbet reactions described in Table 24 demonstrate.

To further investigate the effect of the higher temperature UiO-66(Zr) aldol catalysed system, Guerbet reactions were conducted using a 2:1 ligand:Ru ratio with phosphino azomethinylate ligands and $[\text{RuCl}_2(\eta^6\text{-}p\text{-cymene})]_2$. Four equivalents of **4.9**, **4.10** and **4.11** were loaded into ethanol upgrading Guerbet reactions with one equivalent of $[\text{RuCl}_2(\eta^6\text{-}p\text{-cymene})]_2$. Mixtures of these transfer hydrogenation precursor catalysts were trialed in the Guerbet reaction with UiO-66(Zr) (0.1 mol%) at 210 °C, over 20 hours (Table 25).

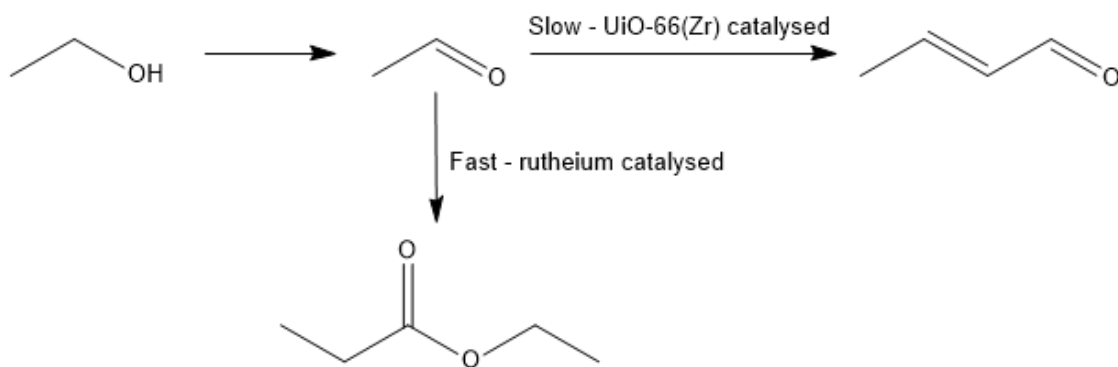
Table 25: Guerbet upgrading of ethanol using sodium phosphino azomethinylate ligands with $[\text{RuCl}_2(\eta^6\text{-}p\text{-cymene})]_2$ (4:1 ratio) as transfer hydrogen catalyst precursors

Entry	Ligand	EtOH Conversion (%) ^a	Selectivity (%) ^b				
			<i>n</i> -BuOH	EtOAc	2-BuOH	Higher Alcohols ^c	Other ^d
1	4.9	27.0	5.9	87.8	0.4	0.4	5.5
2	4.10	25.1	6.4	88.0	0.8	-	4.8
3	4.11	29.1	5.5	79.7	0.3	-	14.5

^a Conversion of ethanol calculated based on total liquid products obtained determined *via* GC analysis. ^b Selectivity to Guerbet products in liquid fraction determined *via* GC analysis. ^c C₆ and C₈ alcohol products calibrated *via* GC analysis. ^d Products not characterised from GC calibration.

Following the same trend as the Guerbet reactions conducted with a 1:1 ratio of phosphino azomethinylate:Ru (Table 24), the 2:1 ligand:Ru Guerbet reactions were also highly selective towards the formation of EtOAc (Table 25). EtOH conversion appears to be a factor that is not influenced greatly by varying the chain length of the sodium phosphino azomethinylate ligand added to the reaction mixture, while the maximum reaction selectivities towards EtOAc formation are even higher than those facilitated in the 1:1 ligand:Ru Guerbet reactions conducted in Table 24. Use of **4.10** in the Guerbet reaction described in Table 25 gave a very high product selectivity towards EtOAc of 88.0 % (Entry 3, Table 25). Regardless of the ratio of ligand:Ru, when using sodium phosphino azomethinylates and $[\text{RuCl}_2(\eta^6\text{-}p\text{-cymene})]_2$ in high temperature Guerbet reactions with UiO-66(Zr), the results in Tables 24 and 25 show that the resulting catalysts were inactive for *n*-BuOH formation, and highly active for the formation of EtOAc.

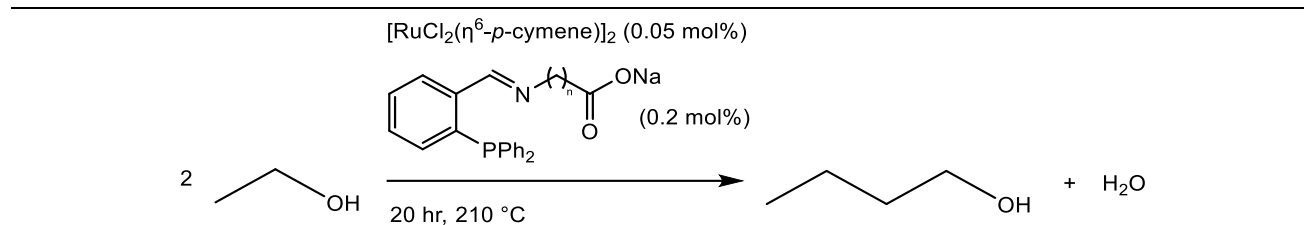
The high selectivities of the Guerbet reactions described in Table 24 and Table 25 towards EtOAc is curious. EtOH conversions facilitated by the Guerbet systems doesn't seem to be largely affected by the chain lengths of the sodium phosphino azomethinylate ligands, as the ethanol conversions shown in Tables 24 and 25 show no real relationship to ligand chain length. Ethanol conversions are moderate, however there is limited formation of unknown products in each of the reactions described in Tables 24 and 25, indicating that the UiO-66(Zr) isn't converting the ethanol to uncharacterised side products in these reactions, or longer chain alcohols (as *n*-BuOH yields are consistently low). It is unlikely that UiO-66(Zr) is promoting the Tishchenko coupling of acetaldehyde to ethyl acetate, as previous successful Guerbet reactions using the MOF aldol catalyst have shown low yields of EtOAc under the same reaction conditions, with much higher *n*-BuOH yields. These observations suggest that the ruthenium catalysts that are forming under the reaction conditions described in Table 24 and Table 25 are active ethanol dehydrogenation catalysts, while also being active catalysts for the Tishchenko coupling of acetaldehyde to ethyl acetate (Scheme 50).



Scheme 50: Potential difference in catalytic activity for the Guerbet reactions detailed in Tables 24 and Table 25.

To determine whether the ruthenium species being formed *in-situ* in Guerbet reactions employing sodium phosphino azomethinylate ligands and $[\text{RuCl}_2(\eta^6\text{-}p\text{-cymene})]_2$ were catalysing the Tishchenko coupling of acetaldehyde to ethyl acetate, Guerbet reactions were carried out under the conditions detailed in Table 25 in the absence of UiO-66(Zr). By adding only sodium phosphino azomethinylate ligands and $[\text{RuCl}_2(\eta^6\text{-}p\text{-cymene})]_2$ to ethanol as catalyst precursors, the absence of UiO-66(Zr) would allow for the determination of whether the ruthenium species was catalysing this undesired side reaction. These reactions were trialed using **4.8** and **4.10**, and the results of these reactions are shown in Table 26.

Table 26: Guerbet upgrading of ethanol using sodium phosphino azomethinylate ligands with $[\text{RuCl}_2(\eta^6\text{-}p\text{-cymene})]_2$ (4:1 ratio) as transfer hydrogen catalyst precursors



Entry	Ligand	EtOH Conversion (%) ^a	Selectivity (%) ^b				Other ^d
			<i>n</i> -BuOH	EtOAc	2-BuOH	Higher Alcohols ^c	
1	4.8	21.0	-	26.7	-	-	73.3
2	4.10	16.6	-	77.1	-	-	22.9

^a Conversion of ethanol calculated based on total liquid products obtained determined *via* GC analysis. ^b Selectivity to Guerbet products in liquid fraction determined *via* GC analysis. ^c C₆ and C₈ alcohol products calibrated *via* GC analysis. ^d Products not characterised from GC calibration.

When considering the results presented in Table 26, the combination of $[\text{RuCl}_2(\eta^6\text{-}p\text{-cymene})]_2$ and sodium phosphino azomethinylates are shown to catalyse ethanol dehydrogenation to acetaldehyde, and the subsequent Tishchenko coupling of acetaldehyde to ethyl acetate. When **4.8** and **4.10** were tested in the Guerbet reaction conditions described in Table 26, the only product observed *via* GC characterisation was ethyl acetate, with no Guerbet coupled product observed. The reaction using **4.8** was highly active for competing reactions which are currently unknown. If the ruthenium catalysts formed *in-situ* in the Guerbet reactions detailed in Table 26 thermally decompose to ruthenium nanoparticles and free phosphine azomethinylate ligand, then it is plausible that the free ligand could react with ethanol or acetaldehyde in the system to form unknown products, but this theory requires further investigation. While the current evolution of the ruthenium catalyst is unknown, the results presented in Table 26 do suggest that the ruthenium catalyst present in the reaction is a more active catalyst for the Tishchenko coupling of acetaldehyde to ethyl acetate, than the UiO-66(Zr) aldol catalyst is for the aldol coupling of acetaldehyde to crotonaldehyde (Scheme 50).

The Guerbet reactions of ethanol conducted with $[\text{RuCl}_2(\eta^6\text{-}p\text{-cymene})]_2$ and the sodium phosphino azomethinylate ligands as transfer hydrogenation catalyst precursors with UiO-66(Zr) as an aldol catalyst showed poor activity for *n*-BuOH production. Whether the reaction was performed with 1 (Table 24) or 2 equivalents (Table 25) of ligand to Ru centre, under the optimised UiO-66(Zr) aldol catalysed reaction conditions, high selectivity to ethyl acetate was observed. The nature of the evolution of the ruthenium catalyst in these reactions has not yet been identified, however, a practical theory is that any homogeneous complex species forming in the reaction may decompose to ruthenium nanoparticles that are active for the Tishchenko coupling of acetaldehyde. Further investigation into the evolution of the catalysts in these reactions is warranted, however, ruthenium-phosphino azomethinylate complexes do not appear to be a suitable class of transfer hydrogenation catalyst for immobilisation on a MOF to produce single, heterogeneous catalyst for the Guerbet upgrading of ethanol to *n*-butanol.

4.4 Conclusions

Based on the concept of immobilising homogeneous complexes on the nodes of etched UiO-66(Zr) introduced in 4.1, the work presented in Chapter 4 details the development of ruthenium complexes with pendant carboxylate functionality. The complexes that were targeted would have ideally acted as transfer hydrogenation catalysts in the Guerbet upgrading of ethanol with UiO-66(Zr), with the final aim being immobilisation on the nodes of an etched variant of UiO-66(Zr), to produce a single heterogeneous catalysts for the Guerbet synthesis of *n*-butanol.

The concept of using $[\text{RuCl}_2(\text{dppEth})_2]$ as a precursor for ruthenium complexes with pendant carboxylate functionality was explored. The Michael addition of amino acids of different carbon chain lengths across the ethylene groups present on the dppEth ligands of $[\text{RuCl}_2(\text{dppEth})_2]$ was attempted *via* a number of different methods, to synthesise $[\text{RuCl}_2(\text{dppEth})_2]$ analogues with pendant carboxylate groups (Scheme 39). Preliminary work on the Michael addition of glycine across $[\text{RuCl}_2(\text{dppEth})_2]$ in toluene showed the formation of small quantities of **4.2** under reaction conditions of elevated temperature,

however, the majority of complex present in the reaction product was that of the $[\text{RuCl}_2(\text{dppEth})_2]$ starting material (Figure 40). The Michael addition of longer chained amino acids across the ethylene functionalised ligands of $[\text{RuCl}_2(\text{dppEth})_2]$ was also attempted, however, as with the targeted glycine adduct complex, only small amounts of the Michael adduct complex were observed, or none at all. Different solvent systems were trialed for the Michael addition of glycine across $[\text{RuCl}_2(\text{dppEth})_2]$, however, none of these reactions showed the formation of the desired Michael adduct complex. Poor solubility was postulated to be an issue, preventing the dissolution of the amino acids, hence pre-activation of the amino acids was attempted by converting them to corresponding sodium salts *in-situ*, with subsequent addition of $[\text{RuCl}_2(\text{dppEth})_2]$ to promote the Michael addition of the sodium amino acid salts across the complex ligands (Scheme 44). These reactions also failed to produce any carboxylate functionalised amino acid adduct complex, while the attempted direct addition of sodium glycinate across $[\text{RuCl}_2(\text{dppEth})_2]$ (Scheme 45) also failed. While trace amounts of carboxylate functionalised amino acid adduct complexes were observed in Figure 40, the reaction systems trialed for the synthesis of -COOH functionalised complexes from $[\text{RuCl}_2(\text{dppEth})_2]$ through the Michael addition of amino acids were unsuccessful.

Phosphino azomethinylate ligands were identified as a class of ligand that could coordinate to ruthenium centers to form complexes with pendant carboxylate functionality, if bound *via* a bidentate $\kappa^2\text{-P,N}$ coordination. Initial work in this area was conducted by Cole (BSc student), into the synthesis of sodium phosphino azomethinylate ligands deriving from amino acids of differing carbon chain lengths, and the use of these ligands in synthesising ruthenium complexes.⁸ This work was continued, where further investigation into ruthenium complex formation was conducted, as well as an *in-situ* ruthenium transfer hydrogenation catalyst formation study in the Guerbet synthesis of *n*-butanol. The formation of mono- and bischelate complexes bearing phosphino azomethinylate ligands was attempted, using $[\text{RuCl}_2(\eta^6\text{-}p\text{-cymene})]_2$ and $[\text{RuCl}_2(\text{PPh}_3)_3]$ complexes respectively. The formation of monochelate ruthenium complexes bearing phosphino azomethinylate ligands derived from glycine, β -alanine and 4-aminocaproic acid was conducted using $[\text{RuCl}_2(\eta^6\text{-}p\text{-cymene})]_2$ as a precursor. The $^{31}\text{P}\{^1\text{H}\}$ NMR spectra of the products of these reactions showed the formation of a major species among

a number of minor complex structures (Figure 44). The major species were predicted to be monochelate ruthenium-phosphino azomethinylate complexes with the ligands binding through a tridentate $\kappa^3\text{-P,N,O}$ coordination, however this could not be confirmed through mass spectrometry, which showed a large variety of complexes forming in the reactions described in Scheme 47. The formation of bischelate ruthenium-phosphino azomethinylate complexes *via* the reaction of glycine, β -alanine, 4-aminobutyric acid, 5-aminovaleric acid and 6-aminocaproic acid derived sodium phosphino azomethinylate with $[\text{RuCl}_2(\text{PPh}_3)_3]$ were also trialed. $^{31}\text{P}\{^1\text{H}\}$ NMR spectroscopy was used to predict possible structure(s) of the ruthenium complex products forming in these reactions (Figure 45), where in most cases, a mixture of mono- and bischelate complex formation was predicted.

Guerbet reactions were conducted where sodium phosphino azomethinylate ligands and $[\text{RuCl}_2(\eta^6\text{-p-cymene})]_2$ were added to the reaction as transfer hydrogenation catalyst precursors, both with NaOEt and UiO-66(Zr) as aldol catalysts at 150 °C and 210 °C respectively. Under typical homogeneous Guerbet reaction conditions (NaOEt at 150 °C), the transfer hydrogenation catalyst precursor mixture of the longer chained ligands **4.11** and **4.12** with $[\text{RuCl}_2(\eta^6\text{-p-cymene})]_2$ resulted in the most active catalysts tested for EtOH conversion regardless of ligand:ruthenium stoichiometry (Tables 22 and 23). The longer chained ligand systems also showed the highest *n*-BuOH yields, and the catalytic results presented in Table 22 and Table 23 were used to predict the structures of the ruthenium catalysts that were forming *in situ* in the respective Guerbet reactions, using the chain length of the ligands as a major predicting factor. The use of sodium phosphino azomethinylate ligands and $[\text{RuCl}_2(\eta^6\text{-p-cymene})]_2$ as transfer hydrogenation catalyst precursors in the Guerbet synthesis of *n*-butanol using UiO-66(Zr) as an aldol catalyst at a reaction temperature of 210 °C was investigated. When both 1:1 and 2:1 ligand:ruthenium stoichiometries were used, the Guerbet reactions at the elevated temperature were highly selective for the formation of ethyl acetate, and poor catalytic systems for the production of *n*-butanol (Tables 24 and 25). The ruthenium catalyst precursor mixture was theorised to evolve under the elevated temperature conditions to an active Tishchenko catalyst for the coupling of acetaldehyde to ethyl acetate. Hence the reaction of ethanol with sodium phosphino azomethinylate ligands and $[\text{RuCl}_2(\eta^6\text{-p-$

cymene) $_2$ in the absence of UiO-66(Zr) was trialed at 210 °C. Under the Guerbet reaction conditions, in the absence of the aldol catalyst, sodium phosphino azomethinylate ligands and $[\text{RuCl}_2(\eta^6\text{-}p\text{-cymene})]_2$ were shown to still produce ethyl acetate (Table 26), through a predicted catalytic pathway of the dehydrogenation of ethanol to acetaldehyde, and the subsequent Tishchenko coupling of acetaldehyde to ethyl acetate. This result showed that under Guerbet reaction conditions employing UiO-66(Zr) as an aldol catalyst, the combination of sodium phosphino azomethinylates and $[\text{RuCl}_2(\eta^6\text{-}p\text{-cymene})]_2$ were incompatible catalyst precursors for effective Guerbet synthesis of *n*-butanol.

The complex NMR spectra in Figures 44 and 45 highlight the difficulty in controlling the formation of single isomers of ruthenium complexes bearing phosphino azomethinylate ligands, however, the demonstration that this class of ligand with $[\text{RuCl}_2(\eta^6\text{-}p\text{-cymene})]_2$ proved an active pre-catalyst mixture in the Guerbet synthesis of *n*-butanol with NaOEt was a success. Although when the same mixture of catalyst precursors were significantly less active for the synthesis of *n*-butanol with UiO-66(Zr) under the higher temperature conditions, the work conducted here opens up the pathway for further investigation towards the immobilisation of ruthenium phosphino azomethinylate complexes on MOFs as Guerbet catalysts. Although not-targeted, the highly selective synthesis of ethyl acetate from ethanol from the systems described in Tables 24 and 25 was an interesting observation, and this work may also prove useful in the field of heterogeneous catalysis towards the production of ethyl acetate.

4.5 Further work

There is scope for further research into the two areas of carboxylate functionalised complex chemistry that has been discussed here, as well as for different methods to synthesise complexes with this functionality, for use as potential transfer hydrogenation catalysts in the Guerbet synthesis of *n*-butanol.

4.5.1 [RuCl₂(dppEth)₂] work

The synthetic procedures trialed in Section 4.2 for the formation of ruthenium complexes with pendant carboxylate functionality deriving from [RuCl₂(dppEth)₂] were unsuccessful, where the ³¹P{¹H} NMR spectra detailed in Figure 40 showed the potential formation of trace amounts of desired Michael adduct complex. A potential reason for the lack of reactivity was poor solubility of the amino acids in the solvent systems that were tested, with potential zwitterion formation preventing dissolution of the amino acid substrates. Further work on the Michael addition of simple, linear amino acids to [RuCl₂(dppEth)₂] is warranted, with initial investigation into deducing a solvent system that is known to dissolve both the ruthenium complex and amino acid starting materials. The dissolution of amino acids in different solvents/solvent mixtures would initially be investigated, and solvent systems for the successful dissolution of the amino acids would then be tested for [RuCl₂(dppEth)₂]. Any solvent system that successfully dissolved both starting materials would then be used for the Michael addition of linear amino acids across to [RuCl₂(dppEth)₂] under different reaction temperatures and durations. Conducting the Michael addition reactions of amino acids across [RuCl₂(dppEth)₂] under basic conditions may prevent the formation of zwitterionic species (through deprotonation of NH₃⁺), aiding amino acid dissolution and potentially promoting Michael addition across [RuCl₂(dppEth)₂]. While the testing conducted in Section 4.2 focused on the Michael addition of linear amino acids with carbon chain lengths increasing from glycine to 6-aminocaproic acid, introduction of different functional groups onto the amino acid may also improve solubility and reactivity. Research into the area of using [RuCl₂(dppEth)₂] as a precursor complex for ruthenium species with pendant carboxylate functionality through the Michael addition of amino acids detailed in Section 4.2 is preliminary, in systems based on those previously conducted by Sama for the Michael addition of different amines across the complex.² Through a more detailed reaction optimisation, employing the ideas introduced in 4.5.1, the Michael addition of amino acids across [RuCl₂(dppEth)₂] would have a greater probability of success.

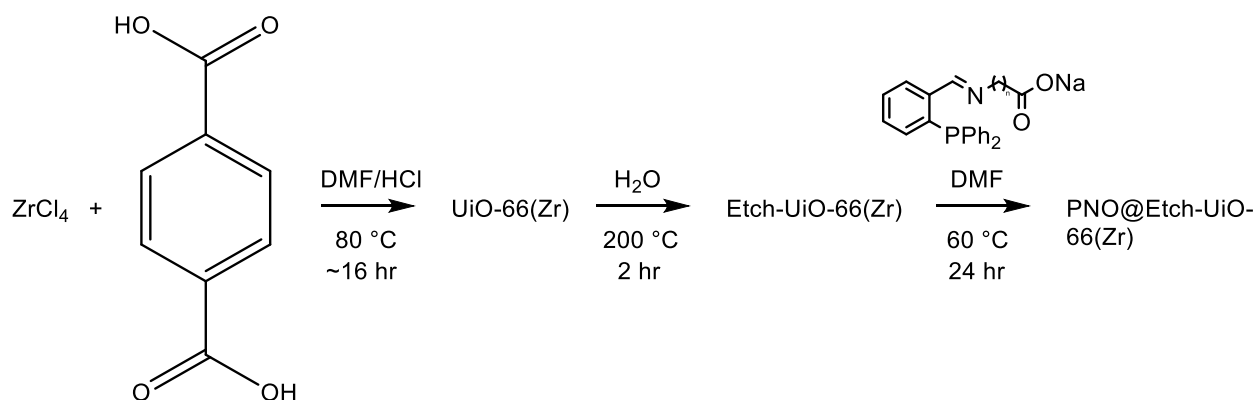
4.5.2 Phosphino azomethinylates

Initial work on ruthenium-phosphino azomethinylate complexes in the Guerbet synthesis of *n*-butanol detailed the synthesis of homogeneous complexes in 4.3.1. $^{31}\text{P}\{^1\text{H}\}$ NMR spectroscopy was used to predict structures of mono- and bischelate complexes that were formed in complexation reactions using $[\text{RuCl}_2(\eta^6\text{-}p\text{-cymene})]_2$ (monochelate complex) and $[\text{RuCl}_2(\text{PPh}_3)_3]$ (bischelate complex) precursors with sodium phosphino azomethinylate ligands. The formation of monochelate complexes was trialed with **4.8**, **4.9** and **4.10**, and $^{31}\text{P}\{^1\text{H}\}$ NMR spectrometry was used to predict the major product isomers in these reactions. Mass spectrometry, and the $^{31}\text{P}\{^1\text{H}\}$ NMR spectra of the products of these complexation reactions (Figure 44) showed a number of different ruthenium species being formed in the monochelate complex formation experiments trialed, hence further reaction optimisation is warranted with the aim of promoting a complex topology. Tridentate ($\kappa^3\text{-}P,N,O$) coordination monochelate complexes were the major isomers predicted to have formed in the monochelate complex formation experiments using the smaller chained sodium phosphino azomethinylate ligands (Scheme 47), which would not possess the desired pendant carboxylate functionality. Further study is warranted on monochelate complex formation using longer chained ligands **4.11** and **4.12**, to promote the formation of bidentate ($\kappa^2\text{-}P,N$) coordinated monochelate ruthenium-phosphino azomethinylate complexes.

$^{31}\text{P}\{^1\text{H}\}$ NMR spectroscopy was used to predict the structure of bischelate complexes with phosphino azomethinylate ligands of increasing carbon chain length (**4.8**, **4.9**, **4.10**, **4.11**, **4.12**) (Figure 45). The formation of single ruthenium complex isomers has been theorised for the reactions described in Scheme 48 with certain sodium phosphino azomethinylate ligands, hence the growth of crystals of these complexes is desired to rationalise whether a single complex topology is forming, *via* X-ray crystallography. As with the monochelate complex formation experiments described previously (Scheme 47), the formation of bischelate ruthenium-phosphino azomethinylate complexes was only trialed under the one set of reaction conditions (Scheme 48). Extensive further work could be conducted into the formation of monochelate and bischelate ruthenium-phosphino azomethinylate complexes, with a variety of changeable reaction parameters (e.g.

temperature, solvent, ruthenium precursor) to promote the formation of single complex isomers.

The work presented in Chapter 4 focused on the synthesis of ruthenium complexes with pendant carboxylate functionality, as previous work from Xiao *et al.* had shown that a ruthenium complex with a ligand bearing this functional group had been immobilised on the nodes of an etched variant of UiO-66(Zr) (Figure 39).¹ If these complexes were active transfer hydrogenation catalysts in the Guerbet synthesis of *n*-butanol, then their immobilisation on a Lewis acidic UiO-66(Zr) framework may form a single heterogeneous catalyst for the upgrading of ethanol. Due to the difficulties encountered with synthesising pure ruthenium-phosphino azomethinylate complexes, further work could be conducted into immobilising the free ligands on the etched nodes of UiO-66(Zr) and forming homogeneous ruthenium complexes directly on the MOF (Scheme 51).



Scheme 51: Potential route to immobilising phosphino azomethinylate ligands on etched UiO-66(Zr).

This study would begin with synthesis of the etched variant of UiO-66(Zr) according to the procedure reported by Xiao *et al.*,¹ and the immobilisation sodium phosphino azomethinylates on the nodes of the MOF would be attempted. Successful immobilisation of the ligands would be confirmed by solid state NMR spectroscopy and FTIR, and the modified MOFs would then be used to co-ordinate ruthenium precursor complexes to form node-immobilised complexes. These complex-functionalised MOFs would then be examined for their catalytic activity in the Guerbet upgrading of ethanol. Under Guerbet reaction conditions optimised for UiO-66(Zr) aldol catalysis, the combination of sodium phosphino azomethinylate ligands and $[\text{RuCl}_2(\eta^6\text{-}p\text{-cymene})]_2$ as transfer hydrogenation

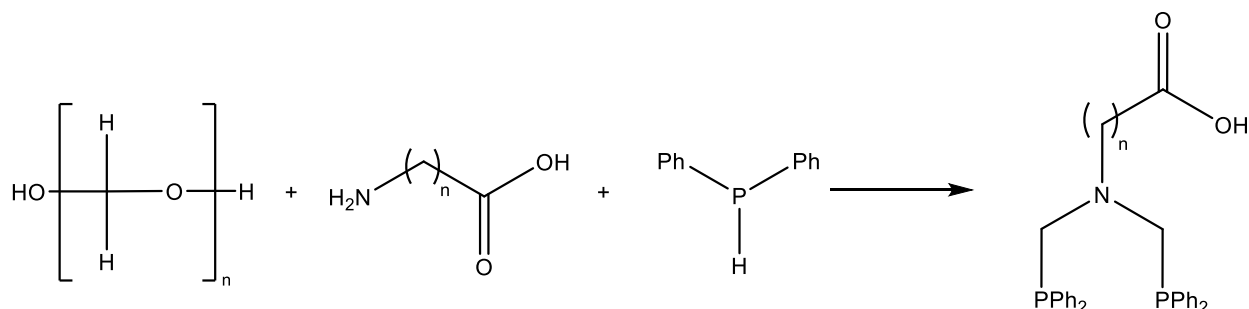
catalyst precursors resulted in catalytic systems that were highly selective for the formation of ethyl acetate, instead of the desired *n*-BuOH (Tables 24 and 25). If a set of immobilised phosphino azomethinylate ligands on UiO-66(Zr) (PNO@Etch-UiO-66(Zr)) were shown to be synthesised, it would be interesting to determine whether the combination of these ligand@UiO-66(Zr) frameworks with $[\text{RuCl}_2(\eta^6\text{-}p\text{-cymene})]_2$ in the Guerbet reaction also promoted the selective conversion of ethanol to ethyl acetate; or if the phosphino azomethinylate ligands immobilised on UiO-66(Zr) interacted with $[\text{RuCl}_2(\text{cymene})]_2$ to produce a catalyst that was active for the production of aldol products like *n*-BuOH.

Considering the Guerbet reaction study of the *in-situ* formation of ruthenium catalysts with sodium phosphino azomethinylate and $[\text{RuCl}_2(\eta^6\text{-}p\text{-cymene})]_2$ precursors, with UiO-66(Zr) (Section 4.3.3), further study on the development of the ruthenium catalyst in the reaction is warranted. The ruthenium catalysts formed in the Guerbet reactions detailed in Table 24 and Table 25 are active catalysts for the dehydrogenation of ethanol to acetaldehyde, and the Tishchenko coupling of acetaldehyde to ethyl acetate. The nature of the evolution of the ruthenium catalyst in these reactions is currently unknown. There is a possibility that any ruthenium-phosphino azomethinylate complexes formed *in-situ* are unstable at the elevated reaction temperature of 210 °C and decompose to nanoparticles that are active for the Tishchenko coupling of acetaldehyde. However, this theory is yet to be proven, and homogeneous ruthenium-phosphino azomethinylate catalysts that are active for this reaction may be forming that are stable under these conditions. $^{31}\text{P}\{^1\text{H}\}$ NMR spectroscopy of the product mixtures of the reactions detailed in Table 24 and Table 25 would give insight into whether stable complexes, or nanoparticles were forming in the reaction. It would also be of interest to utilise ruthenium nanoparticle catalysts in the Guerbet upgrading of ethanol with UiO-66(Zr), to rationalise whether this system is also active for the conversion of ethanol to ethyl acetate.

4.5.3 Other further work

The concept of synthesising transfer hydrogenation catalysts with pendant carboxylate functionality has been discussed here, focusing on the Michael addition of amino acids across $[\text{RuCl}_2(\text{dppEth})_2]$, and the use of phosphino azomethinylate ligands to synthesise

ruthenium complexes with the desired carboxylate functionality. However, there are other options that could be explored to synthesise this class of complex, for example, through the synthesis of PCNCP ligands (Scheme 52).



Scheme 52: Formation of PCNCP ligands as Demonstrated by Shaw et al.⁹

This class of ligand had previously been reported by Shaw *et al.*,⁹ who synthesised PCNCP ligands bearing carboxylate functionality by reacting amino acids with paraformaldehyde and diphenylphosphine as shown in Scheme 52. The synthesis of PCNCP ligands using glycine and β -alanine according to the methodology shown in Scheme 52 was unsuccessfully attempted, however, further work on this ligand set towards homogeneous complex immobilisation within a MOF is warranted. On successful synthesis, investigation into the formation of ruthenium complexes bearing these ligands as transfer hydrogenation catalysts in the Guerbet reaction could be carried out. Similar to the Guerbet reactions where sodium-phosphino azomethinylate and $[\text{RuCl}_2(\eta^6\text{-}p\text{-cymene})]_2$ were added as transfer hydrogenation catalyst precursors (4.3.2 and 4.3.3), PCNCP ligands could be loaded with ruthenium precursors in the Guerbet upgrading of ethanol to *n*-butanol.

4.6 References

- 1 W. Huang, G. B. Hu, W. bin Liang, J. M. Wang, M. L. Lu, R. Yuan and D. R. Xiao, *Anal. Chem.*, 2021, **93**, 6239–6245.
- 2 F. J. Sama, PhD Thesis, Cardiff University, 2020.
- 3 S. J. Higgins, H. L. Jones, M. K. McCart and T. J. Pounds, *Chem. Commun.*, 1997, 1907–1908.
- 4 S. J. Higgins, M. K. McCart, M. McElhinney, D. C. Nugent and T. J. Pounds, *J. Chem. Soc., Chem. Commun.*, 1995, **96**, 2129–2130.
- 5 J. V. Barkley, S. J. Higgins, M. K. McCart and T. J. Pounds, *Inorg. Chem.*, 1997, **36**, 6188–6196.
- 6 D. W. Adshead, A. Ma, W. Wingad, R. L. Wass, *Unpublished work*, .
- 7 J. Wencel, D. Rix, T. Jennequin, S. Labat, C. Crévisy and M. Mauduit, *Tetrahedron: Asymmetry*, 2008, **19**, 1804–1809.
- 8 Jess Cole, BSC Thesis, Cardiff University, 2022.
- 9 N. Priyadarshani, B. Ginovska, J. T. Bays, J. C. Linehan and W. J. Shaw, *Dalton Trans.*, 2015, **44**, 14854–14864.

Chapter 5 - Final Conclusions

5.1 Conclusions

The combination of MOF and homogeneous ruthenium complex catalysis has been explored in developing a heterogeneous catalysed system for the upgrading of ethanol to *n*-butanol *via* the Guerbet reaction.

Initially, the use of UiO-66(Zr) as an aldol catalyst in place of NaOEt in the Guerbet upgrading of ethanol with $[\text{RuCl}_2(\text{dppm})_2]$ was extensively studied, to find optimal reaction conditions and loadings for the catalysed reaction. Changing the nature of the UiO-66(Zr) in the reaction was investigated, by testing analogues with more and less acetic acid modulator present in their syntheses, while UiO-66(Zr)-NH₂ and UiO-66(Hf) were also tested as heterogeneous aldol catalysts in the reaction. UiO-66(Zr) was tested as an aldol catalyst in the Guerbet reaction with a variety of homogeneous ruthenium complexes in further attempts to improve the catalytic activity systems utilising the MOF, and extensive study was conducted on the recyclability of catalytic systems employing UiO-66(Zr) and $[\text{RuCl}_2(\text{dppm})_2]$ for the Guerbet upgrading of ethanol.

As the combination of zirconium derived MOF and ruthenium transfer hydrogenation catalyst had been shown to be an active combination of catalysts for the Guerbet synthesis of *n*-butanol, focus turned to immobilising ruthenium complexes within zirconium MOFs, in search of a single, heterogeneous catalyst for the reaction. Initially, the concept of immobilising ruthenium complexes within the linkers of MOFs was explored, with complexes bearing dicarboxylate bipyridine and phenanthroline ligands targeted for immobilisation within the linkers of UiO-67(Zr). Preliminary work conducted by Elliot Rogers (Master's student) on the topic examined the catalytic activity of $[\text{RuCl}(\text{cymene})(\text{bipy})]\text{Cl}$ and $[\text{RuCl}(\text{cymene})(\text{phen})]\text{Cl}$ (complexes with non-carboxylated ligands) as homogeneous transfer hydrogenation catalysts with UiO-66(Zr) as an aldol catalyst, as well as the activity of $[\text{RuCl}(\text{cymene})(\text{bipy-COOH})]\text{Cl}$ in the Guerbet upgrading of ethanol. The activity of UiO-67(Zr) as an aldol catalyst in the Guerbet upgrading of ethanol was shown (with $[\text{RuCl}_2(\text{dppm})_2]$ as a transfer hydrogenation catalyst), hence attention turned to the immobilisation of $[\text{RuCl}(\text{cymene})(\text{bipy-COOH})]\text{Cl}$

on UiO-67(Zr), in search of a heterogeneous Guerbet catalyst. Various synthetic procedures were attempted to immobilise homogeneous ruthenium complexes within the structure of UiO-67(Zr), however, when analysed by SEM/EDX, the products of these reactions did not show the formation of immobilised complex.

Ruthenium complexes bearing complexes with pendant ligand carboxylate functionality were also targeted, as potential transfer hydrogenation catalysts that could be immobilised on the nodes of etched variants of UiO-66(Zr), as an alternate route to a heterogeneous catalyst for the production of *n*-butanol from ethanol. Initially, the addition of amino acids across $[\text{RuCl}_2(\text{dppEth})_2]$ was tested (Schemes 41 and 42), however, under the reaction conditions that were attempted for these additions, limited quantities of target product were observed through $^{31}\text{P}\{^1\text{H}\}$ NMR spectroscopy (Figures 43 and 44). Addition of sodium salt derivatives of amino acids across $[\text{RuCl}_2(\text{dppEth})_2]$ was also unsuccessful. Following this work, sodium phosphino azomethinylate ligands were targeted as another avenue to synthesising ruthenium complexes with pendant carboxylate functionality. Initially Jess Cole (BSc Student) synthesised 5 phosphino azomethinylate ligands deriving from different amino acids (Scheme 46) and attempted to synthesise ruthenium complexes using these ligands. This work was continued, through the attempted synthesis of monochelate complexes using $[\text{RuCl}_2(\text{cymene})]_2$ as a precursor, and bischelate complexes using $[\text{RuCl}_2(\text{PPh}_3)_3]$ as a precursor. $^{31}\text{P}\{^1\text{H}\}$ NMR spectroscopy showed, in most cases the formation of several different species forming in these complexation reactions, hence an *in-situ* study was conducted, loading $[\text{RuCl}_2(\text{cymene})]_2$ and phosphino azomethinylate ligands as transfer hydrogenation catalyst precursors in the Guerbet synthesis of *n*-butanol with both NaOEt (at 150 °C) and UiO-66(Zr) (at 210 °C). Active transfer hydrogenation catalysts were formed with NaOEt (at 150 °C) while the higher temperature Guerbet reaction with UiO-66(Zr) was detrimental to the catalytic activity of the systems using $[\text{RuCl}_2(\text{cymene})]_2$ and phosphino azomethinylate ligands as transfer hydrogenation catalyst precursors. The main success of the research presented in this thesis is from the work conducted in Section 2.6, where a recyclable catalytic system for the Guerbet upgrading of ethanol to *n*-butanol was demonstrated utilising UiO-66(Zr) as an aldol catalyst. This discovery proved one the key hypotheses outlined in the reasoning towards the investigation of MOFs as aldol catalysts in the Guerbet reaction,

in that they could be re-used over successive catalytic cycles. The development of the system detailed in Section 2.6, where the mixture of catalysts evolved to increase *n*-butanol yield after 6 cycles compared to the initial cycle paved the way for the research conducted in Chapters 3 and 4.

While the work conducted in Chapter 3 was largely unsuccessful, insight into the interaction of solid supports and ruthenium complexes under different reaction conditions was obtained. For example, the post synthetic exchange of UiO-67(Zr) linkers and carboxylate functionalised complexes was determined to be favoured using MOFs prepared with modulation to introduce defect sites for complex binding. While the formation of ruthenium nanoparticles on ZrO₂ when reacted with [RuCl₂(cymene)]₂ also appeared to proceed.

The key findings from the research conducted in Chapter 4 surrounded the investigation into the development of ruthenium complexes bearing phosphino azomethinylate ligands in the Guerbet upgrading of ethanol. The complexation of this class of ligand to ruthenium was shown to proceed, albeit to a mixture of product isomers that were difficult to rationalise from NMR and MS analysis. While this ligand set was shown to form active transfer hydrogenation catalysts when added to NaOEt mediated Guerbet reactions (150 °C) with [RuCl₂(cymene)]₂, under elevated temperatures (210 °C) with UiO-66(Zr), the ethanol substrate favored conversion to ethyl acetate. This was an interesting observation, and if this reaction system can't be further optimised to favour *n*-butanol formation, then it may well be of interest in the field of ethyl acetate production through homogeneous and heterogeneous catalysis.

5.2 Key Further Work

While the main key further study associated with the work presented here is associated with homogeneous complex immobilisation within MOFs, there are still important studies to conduct on the combined homogeneous/heterogeneous catalysed upgrading of ethanol. For example, focus on MOF Lewis acid catalysis in the Guerbet upgrading of ethanol with [RuCl₂(dppm)]₂ was on UiO-66 derivatives as catalysts, however, there may

be other MOFs that are more active aldol catalysts. Hence further study into MOFs with SBUs composed of metals that are alternative to zirconium as Lewis acid catalysts in the Guerbet upgrading of ethanol, in combination with homogeneous ruthenium transfer hydrogenation catalysts is warranted. Further study on the recycling of $[\text{RuCl}_2(\text{dppm})_2]$ and UiO-66(Zr) as catalysts in the Guerbet reaction are also required, to determine whether the increased activity of the system shown in Scheme 27 is stable over further catalytic cycles, or whether the combination of these catalysts is applicable in a flow-type system.

Considering the work presented in Chapter 3 on the immobilisation of homogeneous complexes within the linkers of UiO-67, primary further study would be on investigation post-synthetic exchange of ligands of UiO-67 prepared according to different procedures. The reported preparation of immobilised $[\text{RuCl}(\text{cymene})(\text{bipy-COOH})]$ within UiO-67(Zr) that was adapted in 3.5.1 used UiO-67(Zr) that had been prepared with acetic acid as a modulator, while the synthesis employed according to Scheme 33 was conducted using non-modulated UiO-67(Zr). Missing linkers in the MOF support would theoretically promote the formation of immobilised complex within the linkers of UiO-67(Zr), hence further study on $[\text{RuCl}(\text{cymene})(\text{bipy-COOH})]$ immobilisation on modulated UiO-67(Zr) is warranted.

There is a precedent for further investigation into the formation homogeneous ruthenium complexes with pendant carboxylate functionality, to immobilise on the nodes of UiO-derived MOFs. While significant work went into investigating the synthesis of amino acid Michael adduct complexes using $[\text{RuCl}_2(\text{dppEth})_2]$ as a starting material, and trace amounts of target complex were detected through $^{31}\text{P}\{^1\text{H}\}$ NMR spectroscopy, formation of carboxylate functionalised complex through this route was largely unsuccessful. Further investigation into the synthesis of this class of homogeneous ruthenium complex could be conducted, where reaction conditions like increased temperature could be investigated to drive the formation of Michael adduct complex. Functionalisation of the alcohol of the amino acid to prevent zwitterion formation would also be an interesting area to study with an aim to regenerate the carboxylic acid after successful Michael addition. The formation of ruthenium complexes bearing phosphino

azomethinylate complexes was also studied, however, synthesis of these complexes resulted in the formation of a variety of products, with predicted isomers present in a number of complex species. Varying reaction parameters like a reduction in reaction duration may allow for the formation of a single ruthenium complex isomer bearing phosphino azomethinylate ligands. On successful synthesis of ruthenium complexes with pendant carboxylate functionality, further work could be conducted on probing their catalytic transfer hydrogenation activity in the Guerbet synthesis of *n*-butanol, and their immobilisation on the nodes of UiO-derived MOFs. The immobilisation of phosphino azomethinylate ligands directly onto UiO-derived MOFs could also be investigated, with a view to forming immobilised transfer hydrogenation complexes on Lewis acidic MOFs using ligand that is already present on the heterogeneous support.

Chapter 6 – Experimental

6.1 General experimental

6.1.1 General considerations

Chemicals were purchased from commercial supplies (Sigma-Aldrich/Merck, Fluorochem, Alfa Aesar, Acros Scientific) and used without further purification. Air and moisture sensitive solid reagents were stored in an MBraun glovebox under an Ar atmosphere. Air and moisture sensitive liquid reagents were transferred from the container received from the supplier to an evacuated Young's flask and stored under N₂.

Reactions carried out under inert conditions were done so under N₂ employing standard Schlenk line techniques. Dry/degassed DCM, hexane, toluene and THF were purified with an anhydrous engineering Grubbs-type solvent system, and subsequently degassed. Dry/degassed pentane was obtained through drying commercial pentane over 3 Å molecular sieves, and subsequently degassing it. Dry/degassed MeOH and EtOH were obtained through purchasing anhydrous MeOH and EtOH from Sigma-Aldrich/Merck, transferring to an evacuated flask loaded with 3 Å molecular sieves, then degassing the solvent. Air sensitive reagents were stored in an MBraun glovebox, under an inert atmosphere of argon.

NMR Spectra were recorded on Bruker 400 or 500 Hz spectrometers (specified for each reaction). ¹H NMR Spectra were referenced against residual solvent peaks in the deuterated solvents used to make the NMR sample, and ³¹P{¹H} NMR spectra were referenced against an 85% H₃PO₄ external standard. DMSO-d₆ was used as received from a commercial source. Air sensitive materials were analysed by NMR spectroscopy using dry/degassed solvents (CDCl₃, MeOD) that were made from drying commercial wet solvent over 3 Å molecular sieves, then degassing the solvent.

Powder X-ray diffraction patterns (PXRD) were recorded with an PANalytical X'Pert diffractometer with a Ni-filtered Cu-K α radiation source that was operating at 40 mA and 40 kV. Diffraction patterns were recorded within a 2 θ range of 5 - 80 ° at a step size of 0.0167 ° employing a back filled sample holder.

GC-FID analysis of products of Guerbet synthesis of *n*-butanol reactions were conducted on an Agilent 782-A GC fitted with a CARBOWAX/20M column. 30m x 320 μ m. Film 0.25 μ m. Method: oven start temperature at 60 °C (held for 5 minutes), then heated to 220 °C at a rate of 40 °C min⁻¹ and then held at 220 °C for 5 minutes.

6.1.2 Guerbet reaction procedure

Reactions for the catalytic Guerbet upgrading of ethanol to *n*-butanol were conducted in a 100 mL Parr autoclave, with substrate and catalyst loaded in a PTFE sleeve equipped with a stirrer bar. The catalysts were loaded into the PTFE sleeve in air, and subsequently sealed inside the autoclave and evacuated. Dried and degassed ethanol (10 mL, 171 mmol) was loaded into the autoclave, which was sealed under nitrogen (flowing from Schlenk line). The closed reaction mixture was heated and stirred in a heating block for a pre-determined reaction duration. After the reaction duration was complete, the hot autoclave was removed from the heating block, and immediately inserted into an ice bath to cool. Once cooled, the reaction products were decanted into a sample vial, which was stored in a freezer, for further analysis. All Guerbet reactions were conducted according to this general procedure unless stated, with reaction conditions and catalyst loadings for the Guerbet reactions detailed in Chapters 2, 3 and 4 described in Sections 6.2, 6.3 and 6.4 respectively.

6.1.3 Post Guerbet reaction analysis

A sample of the Guerbet reaction product was filtered through acidic alumina to remove any residual solid, and sealed inside a vial. 100 μ L of the filtered liquid product was added to a GC vial using a micro syringe and hexadecane (10 μ L) was added to the same vial, as a standard. Et₂O (~1.6 mL) was added the previously prepared sample in the GC vial to make up the sample, which was filtered through a glass microfilter into a new GC vial. This sample was analysed *via* GC analysis, according to the procedure detailed in Section 6.1.1

6.1.4 Guerbet reaction EtOH conversion and product selectivity calculation

Ethanol conversions and product selectivity towards known products were calculated from the liquid fraction of Guerbet reaction products. As described in Section 6.1.3, hexadecane was added to the GC sample of liquid Guerbet reaction product, to act as an internal standard. Calibration curves of known concentrations of ethanol, as well as the Guerbet reaction products: *n*-butanol, ethyl acetate, 2-butanol, 1-hexanol, 2-ethylbutanol, 1-octanol and 2-ethylhexanol were plotted against hexadecane. The ratios of the areas of the peaks in the gas chromatograms of increasing volumes of these species against a consistent volume of hexadecane were used to plot the calibration curves used to calculate ethanol conversion and product yields of the Guerbet reactions that were conducted.

Calibration curves were obtained with 5 data points, where increasing quantities of Guerbet reaction product were added to vials that were also filled with 10 μL of hexadecane standard and 1.7 mL Et_2O . For each of the 5 samples, the ratio of product peak/hexadecane peak was plotted against the molar amount of product/molar amount of hexadecane. An example calibration curve for *n*-butanol is shown in Figure 50.

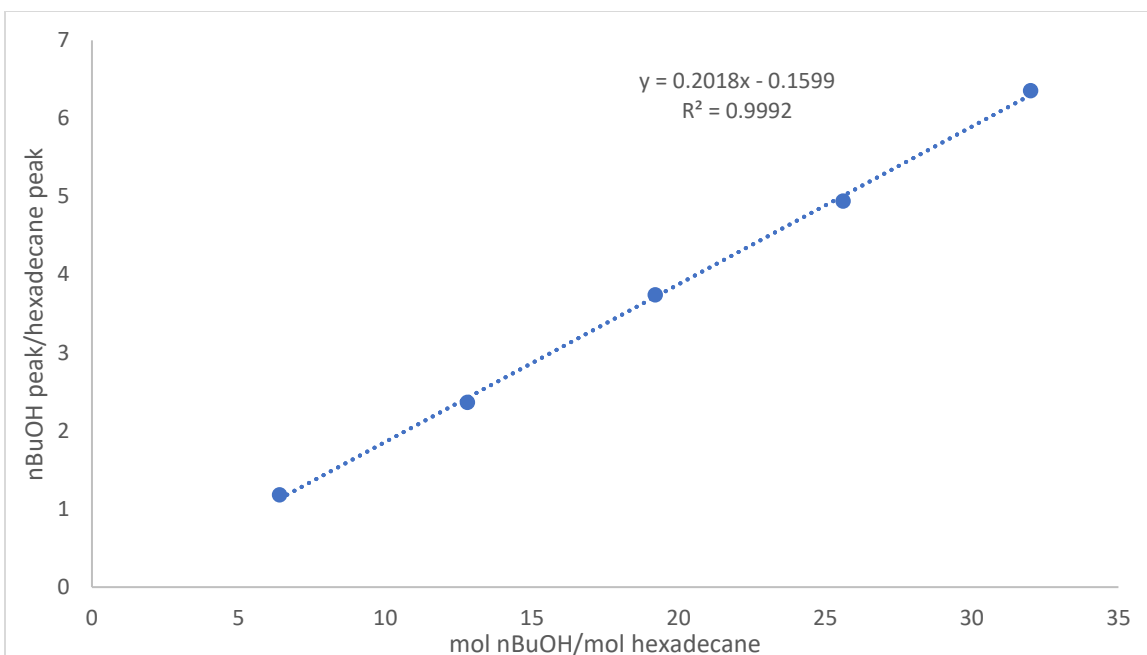


Figure 50: *n*-BuOH calibration curve

This calibration curve gave a gradient that could be used to calculate the number of moles of any given product in a post-Guerbet reaction sample. In the case of *n*-BuOH, the chromatogram obtained from a sample prepared according to Section 6.1.3 gave peak areas that could be used to ascertain the moles of *n*-BuOH in the sample according to:

$$\frac{nBuOH \text{ Peak Area}}{\text{Hexadecane Peak Area}} \times \frac{1}{nBuOH \text{ calibration curve gradient}} \times \text{mol hexadecane} = \text{mol } nBuOH$$

As the number of moles of hexadecane in a GC sample was known (10 μ L – 0.0341 mMol), chromatogram peak areas could be used in combination with calibration curve data for a specific product fraction to calculate the number of moles of that product in the sample. The molar amount of product was converted to a percentage yield (as the starting quantity of ethanol in the sample was known).

The same principal above was also applied in the calculation of ethanol conversion, where an ethanol calibration curve was plotted, and the peak areas of ethanol and hexadecane in a post-Guerbet reaction GC sample could be used to calculate the amount of ethanol left in the product sample. The difference between the known quantity of

ethanol loaded in the initial Guerbet reaction, and the quantity of ethanol left in the sample were used to calculate ethanol conversion percentage:

$$\frac{100 - \text{mol EtOH (product)}}{\text{mol EtOH (starting)}} \times 100 = \text{EtOH Conversion Percentage}$$

Reaction selectivity to a known product (in this case nBuOH) was calculated according to:

$$\text{EtOH Conversion Percentage} * \text{nBuOH Yield} = \text{nBuOH selectivity}$$

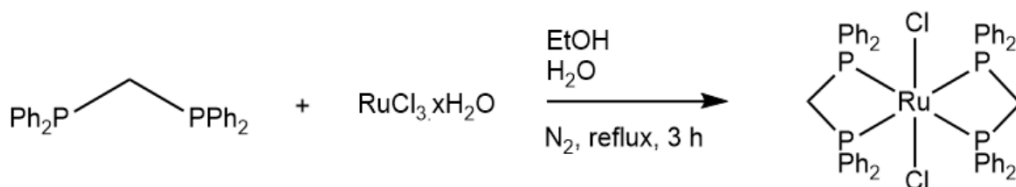
The sum of selectivities to known products calibrated according the curve method described in Figure 50 was calculated, where selectivity to unknown 'other products' was calculated according to

$$100 - \text{sum of known product selectivities} = \text{other product selectivity}$$

6.2 Chapter 2 experimental

6.2.1 Homogeneous ruthenium complexes

6.2.1.1 [RuCl₂(dppm)₂] Synthesis



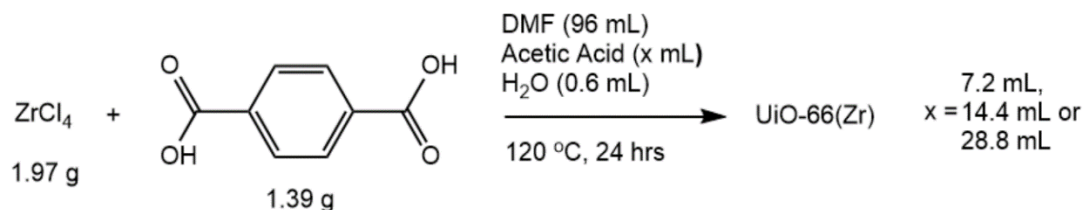
Prepared according to literature procedure reported from Chatt and Hayter.¹

¹H NMR (CDCl₃, 500 MHz) δ 7.18 – 7.11 (m, 10H), 7.02 (t, *J* = 7.6 Hz, 15H), 4.93 (p, *J* = 4.3 Hz, 4H) ³¹P{¹H} NMR (CDCl₃, 202 MHz) δ -7.82 (s)

6.2.2 MOF Synthesis

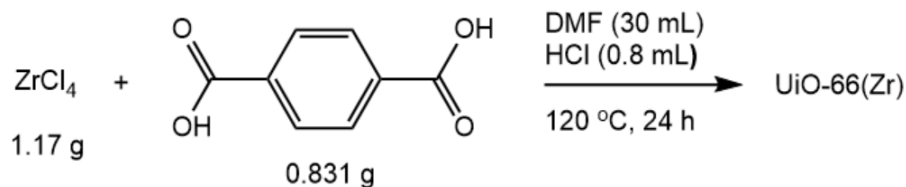
6.2.2.1 UiO-66(Zr) Synthesis – acetic acid modulated – modified from Jiang *et al.*²

2.1 (x = 14.4 mL), 2.3 (x = 7.2 mL), 2.4 (x = 28.8 mL)



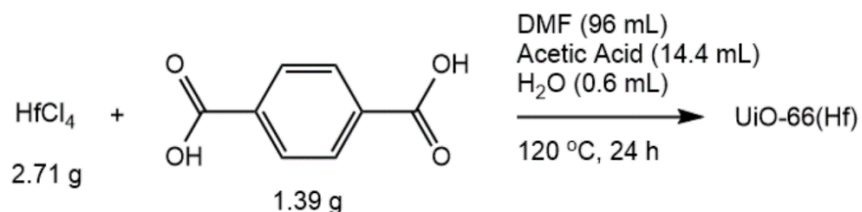
ZrCl_4 (1.97 g, 8.5 mmol) and terephthalic acid (1.39 g, 8.4 mmol) were suspended in DMF (96 mL). Acetic acid (7.2, 14.4 or 28.8 mL) and H_2O (0.6 mL) were added, and the reaction mixture was stirred to achieve dissolution. The reaction mixture was transferred to a 300 mL Teflon sleeve that was sealed in an autoclave, that was then heated at 120 °C under static conditions for 24 hours. The post-reaction solid was isolated *via* centrifugation, then washed twice with DMF/MeOH (4:1) and twice with MeOH *via* centrifugation. The final product was activated at 150 °C under vacuum overnight.

6.2.2.2 UiO-66(Zr) (2.2) Synthesis – non-modulated – modified from Xu *et al.*³



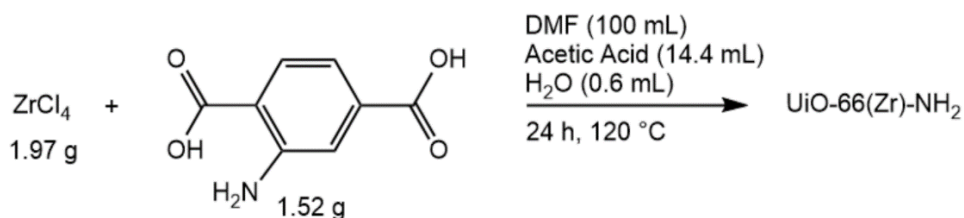
ZrCl_4 (1.17 g, 5.0 mmol) and terephthalic acid (0.83 g, 5.0 mmol) were suspended in DMF (30 mL) and HCl (0.8 mL). The reaction mixture was sonicated for 30 minutes and transferred to a 100 mL Teflon sleeve that was sealed inside an autoclave. The autoclave was heated at 120 °C under static conditions for 24 hours. The post-reaction solid was isolated *via* centrifugation, then washed three times with DMF and once with MeOH *via* centrifugation. The product was then activated at 100 °C under vacuum overnight.

6.2.2.3 UiO-66(Hf) (2.5) Synthesis



HfCl₄ (2.71 g, 8.5 mmol) and terephthalic acid (1.39 g, 8.4 mmol) were suspended in DMF (96 mL). Acetic acid (14.4 mL) and H₂O (0.6 mL) were added, and the reaction mixture was stirred to achieve dissolution. The reaction mixture was transferred to a 300 mL Teflon sleeve that was sealed in an autoclave, that was then heated under static conditions for 24 hours. The post-reaction solid was isolated *via* centrifugation, then washed twice with DMF/MeOH (4:1) and twice with MeOH *via* centrifugation. The final product was activated at 150 °C under vacuum overnight.

6.2.2.4 UiO-66(Zr)-NH₂ (2.6) Synthesis



ZrCl₄ (1.97 g, 8.5 mmol) and 2-aminoterephthalic acid (1.52 g, 8.4 mmol) were suspended in DMF (100 mL). Acetic acid (14.4 mL) and H₂O (0.6 mL) were added, and the reaction mixture was stirred to achieve dissolution. The reaction mixture was transferred to a 300 mL Teflon sleeve that was sealed in an autoclave, that was then heated at 120 °C under static conditions for 24 hours. The post-reaction solid was isolated *via* Buchner filtration and washed with DMF/MeOH (4:1, 2 x 50 mL) and MeOH (2 x 50 mL). The final product was activated at 150 °C under vacuum overnight.

6.2.3 Guerbet reaction procedures - conditions screen

6.2.3.1 Homogeneous Lewis acid screen

Guerbet reactions of ethanol detailed in Section 2.1 (Table 3) were conducted according to the general Guerbet reaction procedure detailed in Section 6.1.2 at a reaction temperature of 210 °C, over a duration of 20 hours at a stirring rate of 500 rpm. The following catalysts and loadings were added to the PTFE sleeve in the reactions: [RuCl₂(dppm)₂] (0.161 g, 0.17 mmol, 0.1 mol%) and Lewis acid (1.7 mmol, 1 mol%) (Cu(OTf)₂ – 0.618 g, Zn(OTf)₂ – 0.622 g, Al(OTf)₂ – 0.812 g, B(C₆F₅)₃ – 0.875 g, Zr(OEt)₂ – 0.464 g).

6.2.3.2 Reaction temperature screen

Guerbet reactions of ethanol detailed in Section 2.2.1 (Table 4, Entries 1-6) were conducted according to the general Guerbet reaction procedure detailed in Section 6.1.2 over a reaction duration of 20 hours at a stirring rate of 500 rpm, with reaction temperature being changed as a variable (150, 180, 190, 200, 210, 220 °C). The following catalysts and loadings were added to the PTFE sleeve in each reaction: [RuCl₂(dppm)₂] (0.161 g, 0.17 mmol, 0.1 mol%) and UiO-66(Zr) (0.285 g, 0.17 mmol, 0.1 mol%).

The Guerbet reaction of ethanol detailed in Table 4 Entry 7 was conducted according to the general Guerbet reaction procedure detailed in Section 6.1.2 over a reaction duration of 20 hours with stirring rate of 500 rpm at 150 °C. The following catalyst loading was added to the PTFE sleeve in the reaction: UiO-66(Zr) (0.285 g, 0.17 mmol, 0.1 mol%).

Guerbet reactions of ethanol detailed in Table 5 (Entries 1 and 2) were conducted according to the general Guerbet reaction procedure detailed in Section 6.1.2 over a reaction duration of 20 hours at a stirring rate of 500 rpm, with reaction temperature being changed as a variable (150 and 210 °C). The following catalysts and loadings were added to the PTFE sleeve in each reaction: [RuCl₂(dppm)₂] (0.161 g, 0.17 mmol, 0.1 mol%) and NaOEt (0.582 g, 0.855 mmol, 5 mol%).

6.2.3.3 Reaction duration screen

Guerbet reactions of ethanol detailed in Section 2.2.2 (Table 6) were conducted according to the general Guerbet reaction procedure detailed in Section 6.1.2 at a reaction temperature of 210 °C with a stirring rate of 500 rpm, at varied reaction durations (2, 4, 20, 65 hours). The following catalysts and loadings were added to the PTFE sleeve in each reaction: $[\text{RuCl}_2(\text{dppm})_2]$ (0.161 g, 0.17 mmol, 0.1 mol%) and UiO-66(Zr) (0.285 g, 0.17 mmol, 0.1 mol%).

6.2.3.4 UiO-66(Zr) Loading screen

Guerbet reactions of ethanol detailed in Table 7 were conducted according to the general Guerbet reaction procedure detailed in Section 6.1.2 at a reaction temperature of 210 °C, over a duration of 20 hours at a stirring rate of 500 rpm. The following catalysts and loadings were added to the PTFE sleeve in each reaction: $[\text{RuCl}_2(\text{dppm})_2]$ (0.161 g, 0.17 mmol, 0.1 mol%) and UiO-66(Zr) (varied loadings) (0.05, 0.10 or 0.20 mol%) (0.143, 0.285 or 0.570 g).

6.2.3.5 Stirring rate screen

Guerbet reactions of ethanol detailed in Table 8 were conducted according to the general Guerbet reaction procedure detailed in Section 6.1.2 at a reaction temperature of 210 °C over a duration of 20 hours, with varied stirring rates (500, 750, 1000 rpm). The following catalyst loading was added to the PTFE sleeve in the reaction: $[\text{RuCl}_2(\text{dppm})_2]$ (0.161 g, 0.17 mmol, 0.1 mol%) and UiO-66(Zr) (0.285 g, 0.17 mmol, 0.1 mol%).

6.2.3.6 Water loading screen

Guerbet reactions of ethanol detailed in Table 9 (Entries 2-4) were conducted according to a slightly modified procedure to that detailed in Section 6.1.2. The reactions were trialed at a reaction temperature of 210 °C, over a duration of 20 hours at a stirring rate of 500 rpm. The following catalysts and loadings were added to the PTFE sleeve in each reaction: $[\text{RuCl}_2(\text{dppm})_2]$ (0.161 g, 0.17 mmol, 0.1 mol%) and UiO-66(Zr) (0.285 g, 0.17 mmol, 0.1 mol%). In addition, H₂O (degassed) was also added to the reaction mixture, with different water loadings tested (10, 20, 30 wt% relative to EtOH).

6.2.4 Guerbet reaction procedures - changing the MOF

6.2.4.1 UiO-66(Zr) Modulation screen

Guerbet reactions of ethanol detailed in Table 10 were conducted according to the general Guerbet reaction procedure detailed in Section 6.1.2 at a reaction temperature of 210 °C, over a duration of 20 hours at a stirring rate of 500 rpm. The following catalysts and loadings were added to the PTFE sleeve in the reactions: $[\text{RuCl}_2(\text{dppm})_2]$ (0.161 g, 0.17 mmol, 0.1 mol%) and UiO-66(Zr)-(x) (0.285 g, 0.17 mmol, 0.1 mol%) (either UiO-66-(i), UiO-66-(ii), UiO-66-(iii) or UiO-66-(iv) from Scheme 23).

6.2.4.2 UiO-66(Zr) Analogue screen

Guerbet reactions of ethanol detailed in Table 11 were conducted according to the general Guerbet reaction procedure detailed in Section 6.1.2 at a reaction temperature of 210 °C, over a duration of 20 hours at a stirring rate of 500 rpm. The following catalysts and loadings were added to the PTFE sleeve in the reactions: $[\text{RuCl}_2(\text{dppm})_2]$ (0.161 g, 0.17 mmol, 0.1 mol%) and UiO-66 analogue (0.17 mmol, 0.1 mol%) (UiO-66(Zr) - 0.285 g, UiO-66(Hf) - 0.375 g) or UiO-66-NH₂ (0.285 g, 0.16 mmol, 0.1 mol%)

6.2.5 Guerbet reaction procedures - changing the ruthenium catalyst

Of the homogeneous ruthenium catalysts used in the Guerbet reactions detailed in Table 12, $[\text{RuCl}_2(\text{dppe})_2]$ and $[\text{RuCl}_2(\text{dppp})_2]$ and $[\text{RuCl}(\text{cymene})(\text{dppp})]\text{Cl}$ were sourced from legacy samples that were synthesised from previous members of the Wass group. $[\text{RuCl}_2(\text{dppm})_2]$ was used from the synthesis detailed in Section 6.2.1.1 and Ru-MACHO was purchased from a commercial supplier. $[\text{RuCl}(\text{cymene})(\text{dppm})]\text{Cl}$, $[\text{RuCl}(\text{cymene})(\text{dppe})]\text{Cl}$ and $[\text{RuCl}(\text{cymene})(2\text{-(Diphenylphosphino)-3-methyl-1H-indole})]\text{Cl}$ were synthesised *in situ* in the Guerbet reactions by loading catalyst precursors.

Guerbet reactions of ethanol detailed in Table 12 (entries 1,2,3,6 and 7) were conducted according to the general Guerbet reaction procedure detailed in Section 6.1.2 at a reaction temperature of 210 °C, over a duration of 20 hours at a stirring rate of 500 rpm. The following catalysts and loadings were added to the PTFE sleeve in the reactions:

UiO-66(Zr) (0.285 g, 0.17 mmol, 0.1 mol%) and [Ru] (0.17 mmol, 0.1 mol%) ([RuCl₂(dppm)₂] - 0.161 g, [RuCl₂(dppe)₂] - 0.167 g, [RuCl₂(dppp)₂] - 0.170 g, [RuCl(cymene)(dppp)]Cl - 0.117 g, Ru-MACHO - 0.104 g).

Guerbet reactions of ethanol detailed in Table 12 (entries 4,5 and 8) were conducted according to the general Guerbet reaction procedure detailed in Section 6.1.2 at a reaction temperature of 210 °C, over a duration of 20 hours at a stirring rate of 500 rpm. The following transfer hydrogenation catalyst precursors and aldol catalyst were added to the PTFE sleeve in each reaction: [RuCl₂(cymene)]₂ (0.053 g, 0.087 mmol, 0.05 mol%), UiO-66(Zr) (0.285 g, 0.17 mmol, 0.1 mol%) and Ligand (0.17 mmol, 0.1 mol%) (dppm - 0.066 g, dppe - 0.069 g, 2-(Diphenylphosphino)-3-methyl-1H-indole - 0.054 g).

6.2.6 Guerbet reaction catalyst recycling studies

6.2.6.1 UiO-66(Zr) recycling procedure (Scheme 26)

UiO-66(Zr) (0.285 g, 0.17 mmol) and [RuCl₂(dppm)₂] (0.161 g, 0.17 mmol) were added to a 100 mL Teflon sleeve that was sealed in an autoclave. The autoclave was evacuated and dry/degassed EtOH (10 mL, 171 mmol) was added. The autoclave was sealed under N₂ and heated at 210 °C for 20 hours while stirring at 500 rpm. The post reaction mixture was filtered to isolate the solid, and solid that passed through the filter was isolated *via* centrifugation. All solid products from the reaction were washed with acetone, then twice with DMF/MeOH (4:1) and twice with MeOH *via* centrifugation. The solid (recycled UiO-66(Zr)) was then activated at 150 °C under vacuum overnight. The recycled UiO-66(Zr) (2.04 g, 0.12 mmol) was added to a 100 mL Teflon sleeve with [RuCl₂(dppm)₂] (0.161 g, 0.17 mmol). The autoclave was evacuated, dry/degassed EtOH (10 mL, 171 mmol) was added, and the autoclave was sealed under N₂ and heated at 210 °C for 20 hours while stirring. The post reaction liquid product fraction was analysed by gas chromatography.

6.2.6.2 UiO-66(Zr) and [RuCl₂(dppm)₂] recycling procedure (Scheme 27)

UiO-66(Zr) (1.14 g, 0.69 mmol) and [RuCl₂(dppm)₂] (0.161 g, 0.17 mmol) were added to a 100 mL Teflon sleeve that was sealed in an autoclave. The autoclave was evacuated and dry/degassed EtOH (10 mL, 171 mmol) was added. The autoclave was sealed under N₂ and heated at 210 °C for 20 hours while stirring at 500 rpm. Once cooled, the sealed

autoclave was connected to an external solvent trap, and the system was evacuated at room temperature. Residual pressure from the autoclave was released, the external solvent trap was inserted into a dewar of liquid nitrogen, and the liquid product fraction of the previous Guerbet reaction was isolated by heating the autoclave at 130 °C for 150 minutes under vacuum. The cold trap was removed from the liquid nitrogen dewar, the system was purged with nitrogen, and the autoclave was sealed under an N₂ atmosphere and left to cool to room temperature. Once melted, the liquid product fraction from the Guerbet reaction was analysed by gas chromatography.

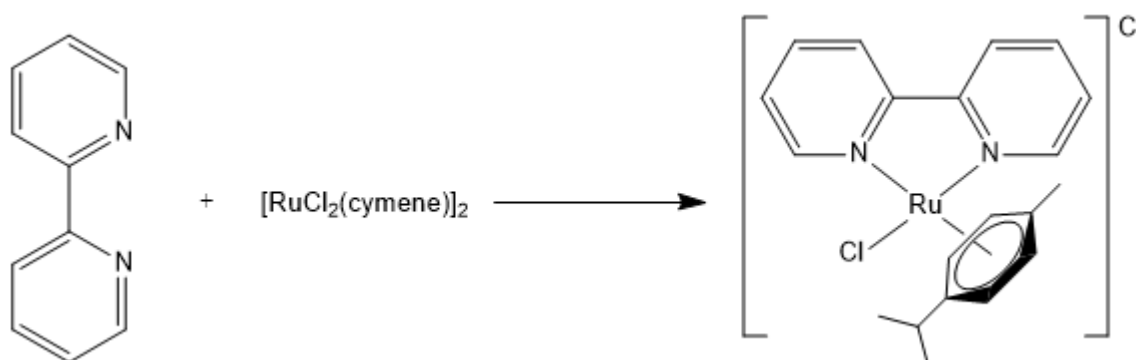
Under N₂, dry/degassed EtOH (10 mL, 171 mmol) was added to the autoclave containing the residual solid catalyst from the previous reaction. The autoclave was sealed under N₂ and heated at 210 °C for 20 hours while stirring at 500 rpm. The work up procedure described above was repeated, where 5 sequential Guerbet reactions were conducted using recycled UiO-66(Zr) and [RuCl₂(dppm)₂] catalyst.

6.3 Chapter 3 experimental

6.3.1 Preliminary work (conducted by Elliot Rogers)⁴

6.3.1.1 Homogeneous complex synthesis

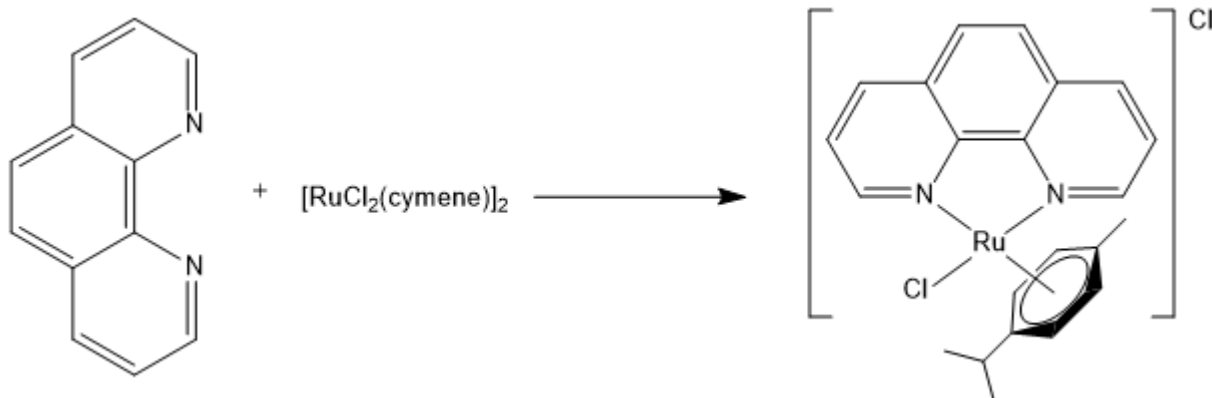
6.3.1.1.1 Synthesis of [RuCl(cymene)(bipy)]Cl (3.3)



Prepared by Rogers ⁴ according to a literature procedure reported from Dykeman *et al.*⁵

$^1\text{H NMR}$ (CDCl_3 , 400 MHz) δ 9.72 (s, 2H), 8.34 (d, 2H, $J = 6.9$ Hz), 8.01 (d, 2H, $J = 6.0$ Hz), 7.66 (d, 2H, $J = 5.8$ Hz), 6.10 (dd, 4H, $J = 51.5, 5.8$ Hz), 2.63 (m, 1H, 6.5 Hz), 2.23 (s, 3H), 0.98 (d, 6H, $J = 6.3$ Hz).

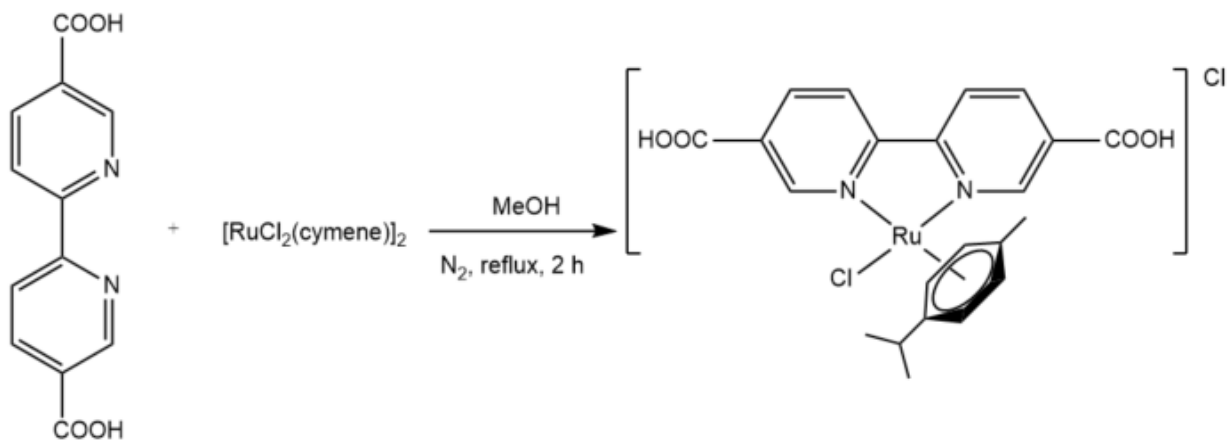
6.3.1.1.2 Synthesis of $[\text{RuCl}(\text{cymene})(\text{phen})]\text{Cl}$ (3.4)



Prepared by Rogers ⁴ according to a literature procedure modified from Dykeman *et al.*⁵

$^1\text{H NMR}$ (CDCl_3 , 400 MHz) δ 8.48 (d, 2H, $J = 8.0$ Hz), 7.92 (s, 2H), 6.34 (dd, 4H, $J = 49.6, 6.9$ Hz), 2.68 (m, 1H, $J = 7.0$ Hz), 2.21 (s, 3H), 0.95 (d, 6H, $J = 6.9$ Hz)

6.3.1.1.3 Synthesis of $[\text{RuCl}(\text{cymene})(\text{bipy-COOH})]\text{Cl}$ (3.1)



2,2-Bipyridine dicarboxylic acid (0.200 g, 0.82 mmol) and $[\text{RuCl}_2(\text{cymene})]_2$ (0.251 g, 0.41 mmol) were added to a Schlenk flask that was subsequently evacuated. Dry/degassed MeOH (145 mL) was added to the reaction mixture, that was stirred under reflux for 2

hours under N₂. The reaction solution was reduced in vacuo to afford the product as a solid powder.

6.3.1.2 Guerbet reactions - benchmarking homogeneous ruthenium catalysts

6.3.1.2.1 [RuCl(cymene)(bipy)]Cl and [RuCl(cymene)(phen)]Cl screen – with NaOEt

Guerbet reactions of ethanol detailed in Section 3.1 (Table 17) were conducted according to the general Guerbet reaction procedure detailed in Section 6.1.2 at a reaction temperature of 150 °C, over a duration of 20 hours at a stirring rate of 500 rpm. The following transfer hydrogenation catalyst and aldol mediator were added to the PTFE sleeve in each reaction: NaOEt (0.582 g, 0.855 mmol, 5.0 mol%), [Ru] (0.17 mmol, 0.1 mol%) ([RuCl(cymene)(bipy)]Cl - 0.073 g, [RuCl(cymene)(phen)]Cl - 0.077 g).

6.3.1.2.2 [RuCl(cymene)(bipy)]Cl and [RuCl(cymene)(phen)]Cl screen – with UiO-66(Zr)

Guerbet reactions of ethanol detailed in Section 3.1 (Table 18) were conducted according to the general Guerbet reaction procedure detailed in Section 6.1.2 at a reaction temperature of 210 °C, over a duration of 20 hours at a stirring rate of 500 rpm. The following transfer hydrogenation catalyst and aldol mediator were added to the PTFE sleeve in each reaction: UiO-66(Zr) (0.285 g, 0.017 mmol, 0.1 mol%), [Ru] (0.17 mmol, 0.1 mol%) ([RuCl(cymene)(bipy)]Cl - 0.073 g, [RuCl(cymene)(phen)]Cl - 0.077 g).

6.3.1.2.3 [RuCl(cymene)(bipy-COOH)]Cl Screen

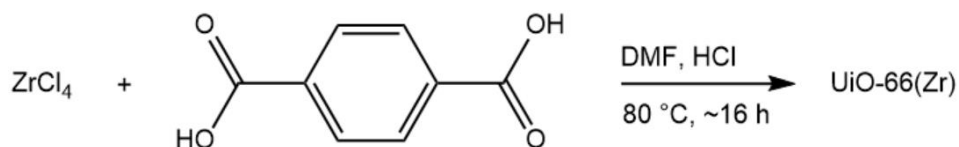
The Guerbet reaction of ethanol detailed in Entry 1 of Table 19 in Section 3.1 was conducted according to the general Guerbet reaction procedure detailed in Section 6.1.2 at a reaction temperature of 150 °C, over a duration of 20 hours at a stirring rate of 500 rpm. The following transfer hydrogenation catalyst and aldol mediator were added to the PTFE sleeve in the reaction: NaOEt (0.582 g, 0.855 mmol, 5.0 mol%), RuCl(cymene)(bipy-COOH)]Cl (0.088 g, 0.017 mmol, 0.1 mol%).

The Guerbet reaction of ethanol detailed in Entry 2 of Table 19 in 3.1 was conducted according to the general Guerbet reaction procedure detailed in 6.1.2 at a reaction temperature of 210 °C, over a duration of 20 hours at a stirring rate of 500 rpm. The

following catalysts and loadings were added to the PTFE sleeve in the reaction: UiO-66(Zr) (0.285 g, 0.017 mmol, 0.1 mol%), RuCl(cymene)(bipy-COOH)]Cl (0.088 g, 0.017 mmol, 0.1 mol%)

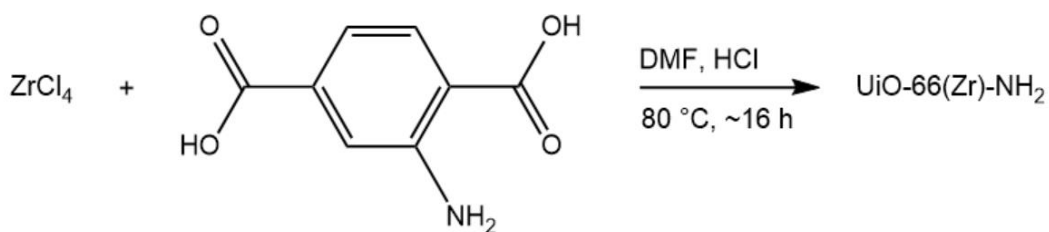
6.3.2 MOF Synthesis

6.3.2.1 UiO-66(Zr) (3.5) Synthesis – prepared according to Katz *et al.*⁶



ZrCl₄ (2.08 g, 8.9 mmol) was added to a Schott bottle in a glovebox. On removal, DMF (80 mL) and HCl (16.6 mL) were added, and the reaction mixture was sonicated for 20 minutes. DMF (170 mL) and terephthalic acid (2.05 g, 12.3 mmol) were added to the reaction mixture in the Schott bottle, which was sonicated for a further 30 minutes to achieve dissolution. The reaction mixture inside the sealed Schott Bottle was heated at 80 °C under static conditions for ~16 hours. A solid precipitate had formed in the reaction mixture, that was isolated *via* centrifugation, then washed twice with DMF and twice with EtOH by centrifugation. The solid product was then activated by heating under vacuum at 150 °C for ~3 hours.

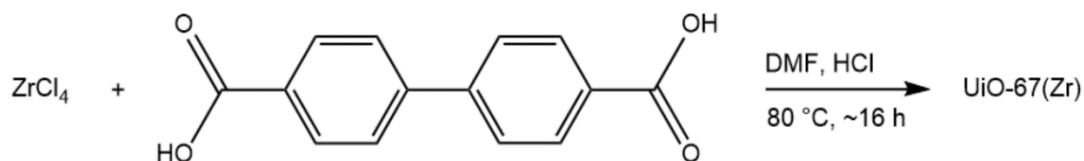
6.3.2.2 UiO-66(Zr)-NH₂ (3.6) Synthesis - prepared according to Katz *et al.*⁶



ZrCl₄ (2.08 g, 8.9 mmol) was added to a Schott bottle in a glovebox. On removal, DMF (80 mL) and HCl (16.6 mL) were added, and the reaction mixture was sonicated for 20 minutes. DMF (170 mL) and 2-amino terephthalic acid were added to the reaction mixture in the Schott bottle, which was sonicated for a further 40 minutes to achieve dissolution.

The reaction mixture inside the sealed Schott Bottle was heated at 80 °C under static conditions for ~16 hours. A solid precipitate had formed in the reaction mixture, that was isolated *via* centrifugation, then washed twice with DMF and twice with EtOH by centrifugation. The solid product was then activated by heating under vacuum at 150 °C for ~3 hours.

6.3.2.3 UiO-67(Zr) (3.7) Synthesis - prepared according to Katz *et al.*⁶



ZrCl₄ (1.12 g, 4.8 mmol) was added to a Schott bottle in a glovebox. On removal, DMF (80 mL) and HCl (8.4 mL) were added, and the reaction mixture was sonicated for 20 minutes. DMF (170 mL) and biphenyl-4,4'-dicarboxylic acid (1.50 g, 6.2 mmol) were added to the reaction mixture in the Schott bottle, which was sonicated for a further 30 minutes to achieve dissolution. The reaction mixture inside the sealed Schott Bottle was heated at 80 °C under static conditions for ~16 hours. A solid precipitate had formed in the reaction mixture, that was isolated *via* centrifugation, then washed twice with DMF and twice with EtOH by centrifugation. The solid product was then activated by heating under vacuum at 150 °C for ~3 hours.

6.3.3 Guerbet reactions - benchmarking heterogeneous UiO-derived catalysts

6.3.3.1 UiO-Derived MOF screen

Guerbet reactions of ethanol detailed in Section 3.2 (Table 20) were conducted according to the general Guerbet reaction procedure detailed in Section 6.1.2 at a reaction temperature of 210 °C, over a duration of 20 hours at a stirring rate of 500 rpm. The following catalysts and loadings were added to the PTFE sleeve in the reactions: [RuCl₂(dppm)₂] (0.161 g, 0.17 mmol, 0.1 mol%) and MOF (0.17 mmol, 0.1 mol%) (UiO-66(Zr) - 0.285 g, UiO-66(Zr)-NH₂ - 0.301 g, UiO-67(Zr) - 0.365 g).

6.3.4 Post synthetic modification of UiO-67(Zr) - exchanging [RuCl(cymene)(bipy-COOH)]Cl with UiO-67(Zr) linkers

6.3.4.1 Post synthetic exchange reaction - replacing biphenyl-4,4'-dicarboxylic acid with [RuCl(cymene)(bipy-COOH)]Cl in UiO-67(Zr) – modified from Liao *et al.*⁷ (3.8, 3.9, 3.10)

UiO-67(Zr) (400 mg) and [RuCl(cymene)(bipy-COOH)] (20, 60 or 80 mg) were dissolved/suspended in a mixture of H₂O (33 mL) and DMF (33 mL). The reaction mixture was stirred at room temperature overnight, where the solid product was isolated *via* centrifugation. The product was washed twice with DMF/MeOH (1:1) and twice with DMF *via* centrifugation. The final product was activated at 150 °C under vacuum for 3 hours.

6.3.5 Post synthetic modification of UiO-67(Zr) - immobilisation of [RuCl₂(cymene)]₂ on the linkers of UiO-67(Zr)-Bipy

6.3.5.1 Attempted synthesis of UiO-67(Zr)-Bipy (3.11)

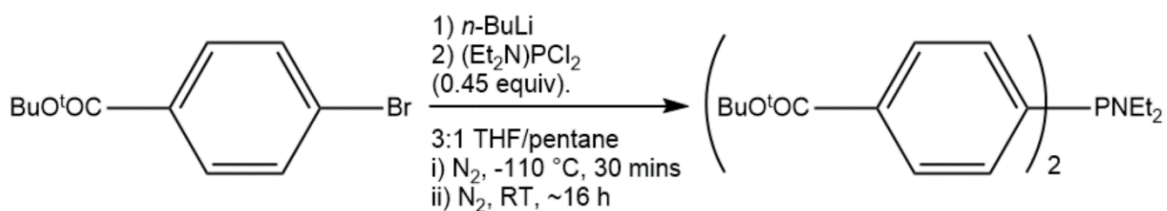
ZrCl₄ (1.12 g) was weighed into a Schott bottle in a glove box. DMF (80 mL) and HCl (8.4 mL) were added, and the mixture was sonicated for 20 minutes. DMF (80 mL) and 2,2'-bipyridine-5,5'-dicarboxylic acid (1.51 g) were added to the reaction mixture, which was sonicated for a further hour. The sealed reaction mixture was heated at 80 °C under static conditions overnight. A solid precipitate formed in the reaction mixture, that was isolated *via* centrifugation, and subsequently washed twice with DMF and twice with EtOH by centrifugation. The solid product was then activated by heating under vacuum at 150 °C for ~3 hours.

6.3.5.2 Attempted immobilisation of [RuCl₂(cymene)]₂ on the assumed UiO-67(Zr)-Bipy (prepared according to Section 6.3.5.1) (3.12, 3.13, 3.14)

[RuCl₂(cymene)]₂ (29, 58 or 87 mg) was dissolved in MeCN (20 mL). To this solution, UiO-67(Zr)-bipy (200 mg, prepared according to Section 6.3.5.1) was added, and the reaction mixture was stirred at room temperature for 24 hours. The solid product was isolated by centrifugation, and subsequently washed three times *via* centrifugation in MeCN, then dried under vacuum at 50 °C for 3 hours.

6.3.6 Immobilisation of pincer complexes on MOFs – preliminary study

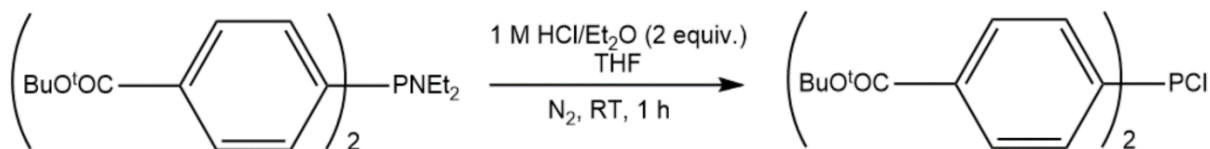
6.3.6.1 Synthesis of (3.19) – prepared according to Burgess *et al.*⁸



4-Bromobenzoic acid *tert*-butyl ester (2.2 mL, 11.4 mmol) was added to a 3-necked round bottomed, that was subsequently evacuated. Dry/degassed THF (45 mL) and dry/degassed pentane (15 mL) were added to dissolve the ester, and the reaction mixture was cooled to -110 °C, using an ethanol/liquid N₂ bath. ⁿBuLi (2.15 M in hexanes, 5.3 mL, 11.4 mmol) was added to the reaction mixture, that was stirred at -110 °C for 30 minutes. While the reaction mixture was stirring, (Et₂N)PCl₂ (0.75 mL, 5.2 mmol) was added to an evacuated Schlenk flask with dry/degassed THF (5 mL) to dissolve it. The THF solution of (Et₂N)PCl₂ was added to the reaction mixture at -110 °C, and the Schlenk flask containing the (Et₂N)PCl₂ was washed with ~1 mL of dry/degassed THF, which was also added to the reaction mixture at -110 °C. The reaction mixture was allowed to warm to room temperature, and then stirred at room temperature for ~ 16 hours. The reaction mixture was reduced in vacuo to afford a gum, that was dissolved in a mixture of dry/degassed pentane (100 mL) and dry/degassed hexane (~8 mL). The crude product solution was then filtered through celite under N₂, and the filtrate solution was reduced in vacuo to afford a gum which was dried in vacuo. The isolated gum was precipitated from dry/degassed pentane (2 x ~10 mL) to afford the product.

³¹P{¹H} NMR (CDCl₃, 202 MHz) δ 60.37 (s)

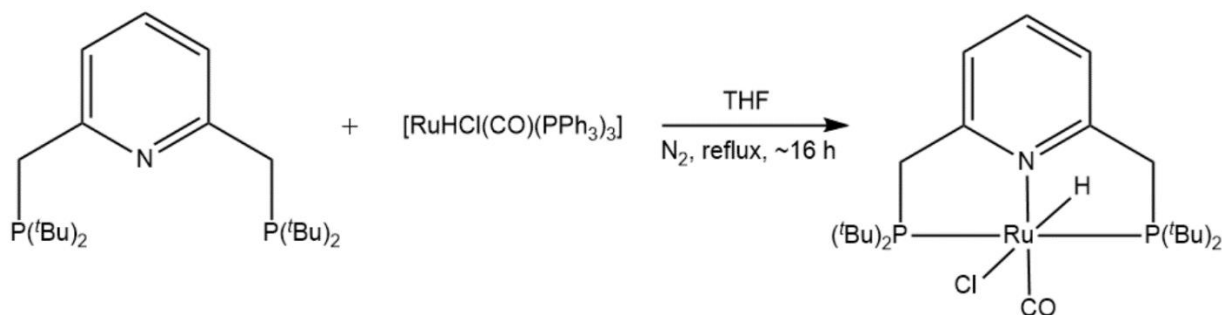
6.3.6.2 Synthesis of (3.20) - prepared according to Burgess *et al.*⁸



((Diethylamino)phosphanediy)bis(4,1-phenylene) bis(2,2-dimethylpropanoate) (1.075 g, 2.35 mmol) was weighed into a Schlenk flask in a glovebox. Once removed, dry/degassed THF (11.2 mL) was added to dissolve the ester. To this solution HCl in Et₂O (2M, 2.35 mL, 4.7 mmol) was added dropwise under N₂ and the reaction was stirred at room temperature under N₂ for one hour. The reaction solution was isolated *via* cannular filtration and reduced in vacuo to afford a gum. The gum was dissolved in hexane and filtered through a pad of celite. The filtrate solution was reduced in vacuo to afford the product as a gum.

³¹P{¹H} NMR (CDCl₃, 202 MHz) δ 78.26 (s), trace impurities at -15.39 (s), -23.92 (s) and -25.29 (s)

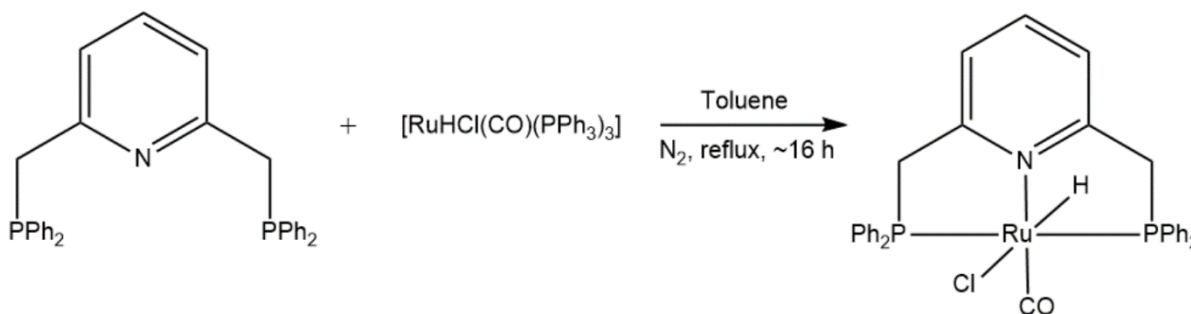
6.3.6.3 Synthesis of [RuHCl(CO)(PCNCP-^tBu)] (3.21)



Prepared according to literature procedure reported by Gnanaprakasam *et al.*⁹

³¹P{¹H} NMR (CDCl₃, 202 MHz) δ 89.32

6.3.6.4 Synthesis of [RuHCl(CO)(PCNCP-Ph)] (3.22)



Prepared according to literature procedure reported by Jia *et al.*¹⁰

³¹P{¹H} NMR (CDCl₃, 202 MHz) δ 50.89 (s)

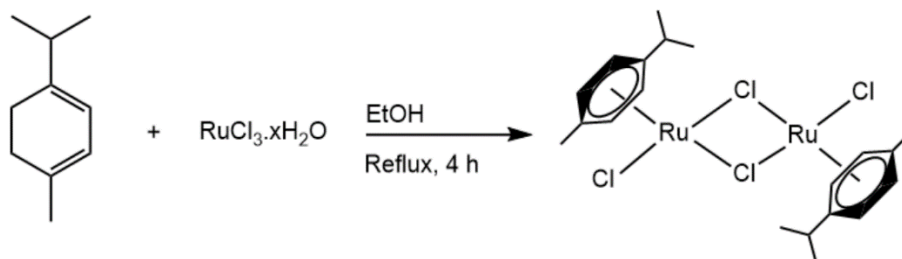
6.3.6.5 Guerbet reactions - screening [RuHCl(CO)(PCNCP-^tBu)] and [RuHCl(CO)(PCNCP-Ph)]

Guerbet reactions of ethanol detailed in section 3.5.2 (Table 21) were conducted according to the general Guerbet reaction procedure detailed in 6.1.2 at a reaction temperature of 210 °C, over a duration of 20 hours at a stirring rate of 500 rpm. The following catalysts and loadings were added to the PTFE sleeve in the reactions: UiO-66(Zr) (0.285 g, 0.17 mmol, 0.1 mol%), [Ru] (0.17 mmol, 0.1 mol%) ([RuHCl(CO)(PCNCP-^tBu)] - 0.096 g, [RuHCl(CO)(PCNCP-Ph)] - 0.110 g).

6.4 Chapter 4 experimental

6.4.1 [RuCl₂(dppEth)₂] and attempted complexations in Section 4.2.1

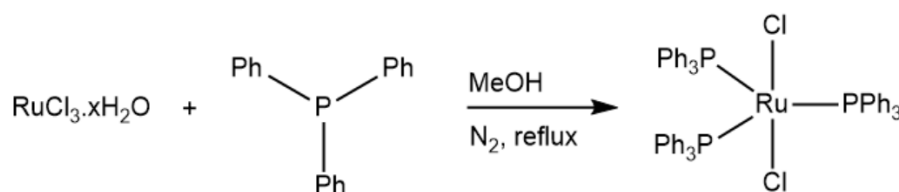
6.4.1.1 Synthesis of [RuCl₂(cymene)]₂



Prepared according to a modified literature procedure reported from Giuffredi *et al.*¹¹

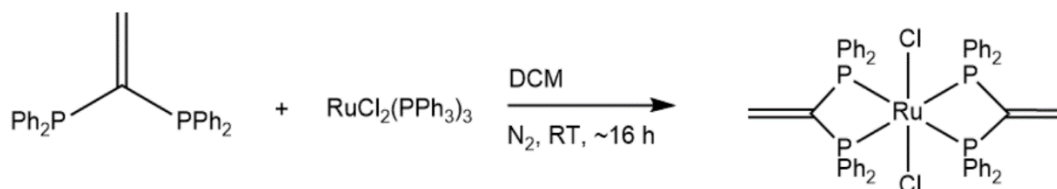
¹H NMR (DMSO-d₆, 400 MHz) δ 5.80 (dd, *J* = 17.5, 6.5 Hz, 8H), 2.83 (hept, *J* = 6.9 Hz, 2H), 2.08 (s, 6H), 1.19 (d, *J* = 7.0 Hz, 11H)

6.4.1.2 Synthesis of [RuCl₂(PPh₃)₃]



Prepared according to literature procedure reported from Samouei *et al.*¹²

6.4.1.3 Synthesis of [RuCl₂(dppEth)₂] (4.1) – prepared according to Barkley *et al.*¹³

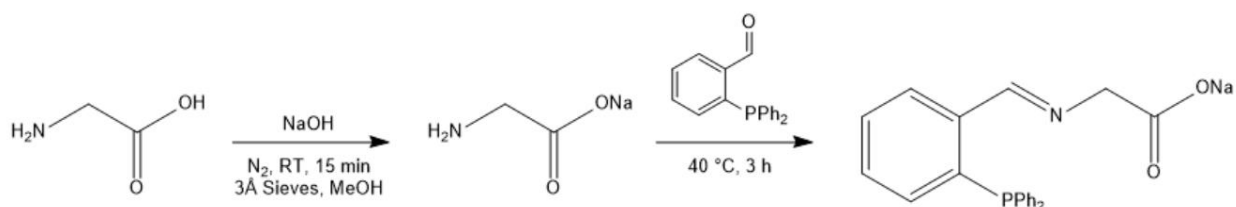


A Schlenk flask was charged with [RuCl₂(PPh₃)₃] (590 mg, 0.62 mmol) and evacuated. DCM (dry/degassed, 10 mL) was added to dissolve the complex. In a separate Schlenk flask, 1,1-Bis(diphenylphosphino)ethylene (500 mg, 1.3 mmol) was added, the flask was

evacuated, and DCM (dry/degassed (10 mL) was added to dissolve the ligand. The ligand solution was added to the complex solution *via* syringe, and the reaction mixture was stirred at room temperature under N₂ overnight. The post-reaction solution was isolated *via* cannular filtration, and residual solid in the reaction flask was washed with DCM (dry/degassed), that was added to the isolated reaction solution *via* cannular filtration. The DCM product fraction was reduced in vacuo, and the residual solid was triturated with hexane (dry/degassed) to afford a solid powder that was isolated *via* cannular filtration and dried under vacuum. ¹H NMR (CDCl₃, 500 MHz) δ 7.45 – 7.38 (m, 17H), 7.13 (t, *J* = 7.6 Hz, 16H), 6.15 (p, *J* = 12.7 Hz, 4H), 2.37 (s, 1H), 2.35 (s, 1H), 2.31 (s, 1H), 2.17 (s, 2H), 1.32 – 1.19 (m, 12H), 0.93 – 0.85 (m, 7H); ³¹P{¹H} NMR (CDCl₃, 202 MHz) δ 14.72 (s)

6.4.2 Phosphino azomethinylate ligand synthesis – performed by Cole¹⁴

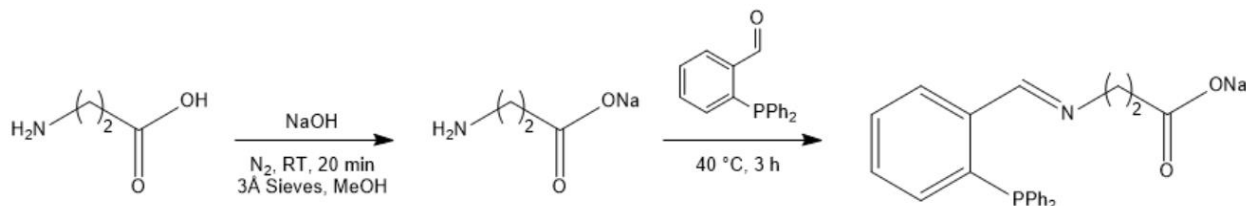
6.4.2.1 Sodium 2-((2-(diphenylphosphaneyl)benzylidene)amino)acetate – adapted from Wencel *et al.*¹⁵ (4.8)



A Schlenk flask was charged with 3 Å molecular sieves, glycine (165 mg, 2.2 mmol) and NaOH (88 mg, 2.2 mmol), and the flask was evacuated. MeOH (dry/degassed, 10 mL) was added to the reaction mixture, that was stirred for 15 minutes under N₂ at room temperature. 2-Diphenylphosphino benzaldehyde (594 mg, 2.0 mmol) was added to the reaction mixture, that was stirred for 3 hours under N₂ at 40 °C. The reaction solution was isolated *via* cannular filtration, and the residual molecular sieves were washed with MeOH (dry/degassed), which was added to the post-reaction solution *via* cannular filtration. The isolated MeOH solution was reduced in vacuo, and the resulting gum was triturated with hexane (dry/degassed) to afford a powder. The residual hexane was removed, *via* cannular filtration, and the product powder was dried in vacuo. ¹H NMR (MeOD, 500 MHz)

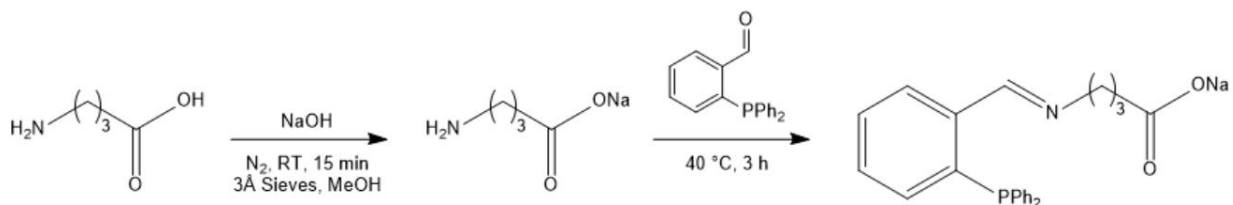
δ 8.97 (d, $J = 5.3$ Hz, 1H), 8.13 (ddd, $J = 7.9, 4.1, 1.4$ Hz, 1H), 7.44 (t, $J = 6.7$ Hz, 1H), 7.40 – 7.32 (m, 6H), 7.30 – 7.21 (m, 4H), 6.91 (ddd, $J = 7.9, 4.8, 1.3$ Hz, 1H), 4.09 (s, 2H), 3.36 (s, 1H), 1.37 – 1.27 (m, 2H), 0.91 (t, $J = 7.0$ Hz, 1H); $^{31}\text{P}\{^1\text{H}\}$ NMR (MeOD, 202 MHz) δ -15.96 (s)

6.4.2.2 Sodium 3-((2-(diphenylphosphaneyl)benzylidene)amino)propanoate – adapted from Wencel *et al.*¹⁵ (4.9)



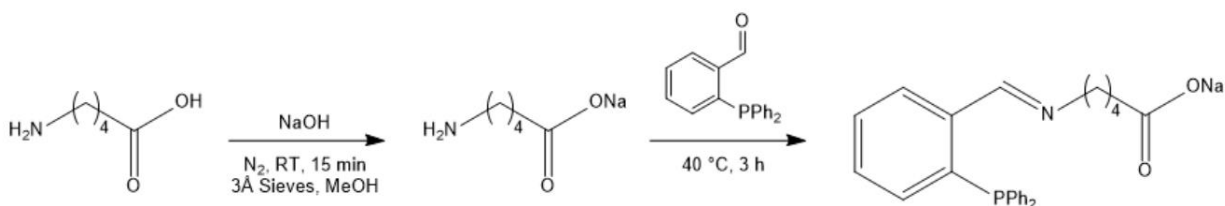
A Schlenk flask was charged with 3 Å molecular sieves, beta alanine (196 mg, 2.2 mmol) and NaOH (88 mg, 2.2 mmol), and the flask was evacuated. MeOH (dry/degassed, 10 mL) was added to the reaction mixture, that was stirred for 20 minutes under N₂ at room temperature. 2-Diphenylphosphino benzaldehyde (594 mg, 2.0 mmol) was added to the reaction mixture, that was stirred for 3 hours under N₂ at 40 °C. The reaction solution was isolated *via* cannular filtration, and the residual molecular sieves were washed with MeOH (dry/degassed), which was added to the post-reaction solution *via* cannular filtration. The isolated MeOH solution was reduced in vacuo, and the resulting gum was triturated with hexane (dry/degassed) to afford a powder. The residual hexane was removed, *via* cannular filtration, and the product powder was dried in vacuo. ^1H NMR (MeOD, 500 MHz) δ 8.99 (d, $J = 4.8$ Hz, 1H), 7.92 – 7.86 (m, 1H), 7.42 (t, $J = 7.7$ Hz, 1H), 7.39 – 7.30 (m, 8H), 7.28 – 7.22 (m, 5H), 6.92 – 6.86 (m, 1H), 3.69 (t, $J = 7.8$ Hz, 2H), 3.36 (s, 1H), 2.35 (t, $J = 7.8$ Hz, 2H); $^{31}\text{P}\{^1\text{H}\}$ NMR (MeOD, 202 MHz) δ -14.91 (s)

6.4.2.3 Sodium 4-((2-(diphenylphosphaneyl)benzylidene)amino)butanoate – adapted from Wencel *et al.*¹⁵ (4.10)



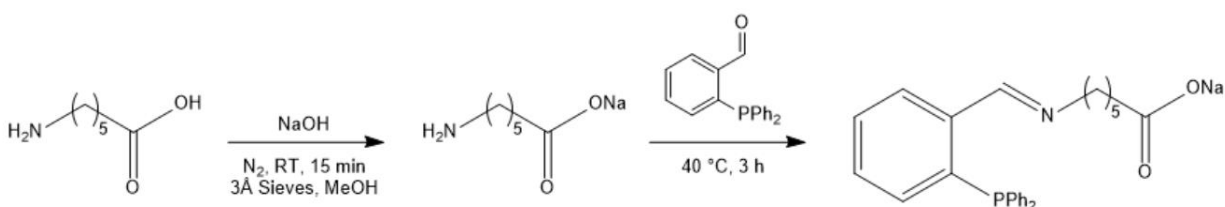
A Schlenk flask was charged with 3 Å molecular sieves, 4-aminobutyric acid (227 mg, 2.2 mmol) and NaOH (88 mg, 2.2 mmol), and the flask was evacuated. MeOH (dry/degassed, 10 mL) was added to the reaction mixture, that was stirred for 15 minutes under N₂ at room temperature. 2-Diphenylphosphino benzaldehyde (594 mg, 2.0 mmol) was added to the reaction mixture, that was stirred for 3 hours under N₂ at 40 °C. The reaction solution was isolated *via* cannular filtration, and the residual molecular sieves were washed with MeOH (dry/degassed), which was added to the post-reaction solution *via* cannular filtration. The isolated MeOH solution was reduced in vacuo, and the resulting gum was triturated with hexane (dry/degassed) to afford a powder. The residual hexane was removed, *via* cannular filtration, and the product powder was dried in vacuo. **¹H NMR** (MeOD, 500 MHz) δ 8.94 (d, *J* = 4.7 Hz, 1H), 7.90 (ddd, *J* = 7.8, 4.0, 1.4 Hz, 1H), 7.43 (d, *J* = 7.7 Hz, 1H), 7.40 – 7.29 (m, 9H), 7.29 – 7.16 (m, 7H), 6.89 (dddd, *J* = 7.7, 4.7, 1.3, 0.6 Hz, 1H), 3.47 (t, *J* = 7.4 Hz, 2H), 3.36 (s, 1H), 2.10 (t, *J* = 7.6 Hz, 2H), 1.91 – 1.74 (m, 2H), 1.39 – 1.26 (m, 2H), 0.91 (t, *J* = 7.0 Hz, 1H); **³¹P{¹H} NMR** (MeOD, 202 MHz) δ -14.64 (s)

6.4.2.4 Sodium 5-((2-(diphenylphosphanyl)benzylidene)amino)pentanoate – adapted from Wencel *et al.*¹⁵ (4.11)



A Schlenk flask was charged with 3 Å molecular sieves, 5-aminovaleric acid (258mg, 2.2 mmol) and NaOH (88 mg, 2.2 mmol), and the flask was evacuated. MeOH (dry/degassed, 10 mL) was added to the reaction mixture, that was stirred for 15 minutes under N₂ at room temperature. 2-Diphenylphosphino benzaldehyde (594 mg, 2.0 mmol) was added to the reaction mixture, that was stirred for 3 hours under N₂ at 40 °C. The reaction solution was isolated *via* cannular filtration, and the residual molecular sieves were washed with MeOH (dry/degassed), which was added to the post-reaction solution *via* cannular filtration. The isolated MeOH solution was reduced in vacuo, and the resulting gum was triturated with hexane (dry/degassed) to afford a powder. The residual hexane was removed, *via* cannular filtration, and the product powder was dried in vacuo. ¹H NMR (MeOD, 500 MHz) δ 8.90 (d, *J* = 4.9 Hz, 1H), 7.86 (ddd, *J* = 7.8, 4.0, 1.3 Hz, 1H), 7.42 (t, *J* = 7.6 Hz, 1H), 7.38 – 7.30 (m, 6H), 7.27 – 7.20 (m, 4H), 6.87 (dddd, *J* = 8.6, 5.5, 1.4, 0.8 Hz, 1H), 3.45 (t, *J* = 6.3 Hz, 2H), 2.76 – 2.71 (m, 1H), 2.18 (t, *J* = 7.2 Hz, 1H), 2.12 – 2.07 (m, 2H), 1.66 – 1.59 (m, 1H), 1.59 – 1.53 (m, 1H), 1.52 – 1.40 (m, 5H); ³¹P{¹H} NMR (MeOD, 202 MHz) δ -14.37 (s)

6.4.2.5 Sodium 6-((2-(diphenylphosphanyl)benzylidene)amino)hexanoate – adapted from Wencel *et al.*¹⁵ (4.12)



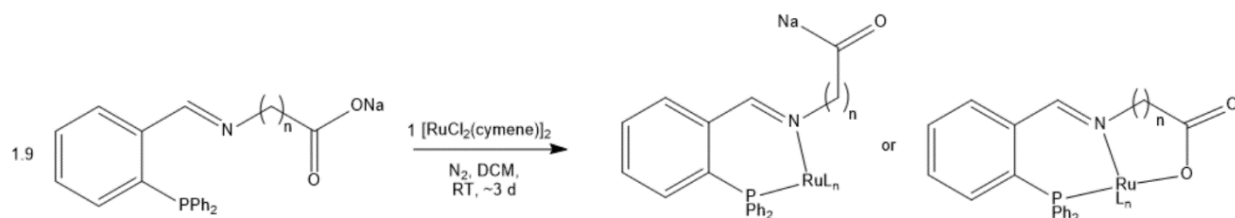
A Schlenk flask was charged with 3 Å molecular sieves, 6-aminocaproic acid (289 mg, 2.2 mmol) and NaOH (88 mg, 2.2 mmol), and the flask was evacuated. MeOH

(dry/degassed, 10 mL) was added to the reaction mixture, that was stirred for 15 minutes under N₂ at room temperature. 2-Diphenylphosphino benzaldehyde (594 mg, 2.0 mmol) was added to the reaction mixture, that was stirred for 3 hours under N₂ at 40 °C. The reaction solution was isolated *via* cannular filtration, and the residual molecular sieves were washed with MeOH (dry/degassed), which was added to the post-reaction solution *via* cannular filtration. The isolated MeOH solution was reduced in vacuo, and the resulting gum was triturated with hexane (dry/degassed) to afford a powder. The residual hexane was removed, *via* cannular filtration, and the product powder was dried in vacuo.

¹H NMR (MeOD, 500 MHz) δ 8.89 (d, *J* = 4.8 Hz, 1H), 7.86 (dd, *J* = 7.8, 3.9 Hz, 1H), 7.43 (t, *J* = 7.6 Hz, 1H), 7.40 – 7.31 (m, 7H), 7.29 – 7.21 (m, 4H), 6.89 – 6.83 (m, 1H), 3.44 (t, *J* = 7.0 Hz, 2H), 2.88 (t, *J* = 7.4 Hz, 1H), 2.19 (t, *J* = 7.1 Hz, 1H), 2.11 (t, *J* = 7.5 Hz, 2H), 1.64 (h, *J* = 7.1 Hz, 1H), 1.54 (p, *J* = 7.7 Hz, 2H), 1.50 – 1.37 (m, 2H), 1.35 – 1.27 (m, 2H), 1.16 (p, *J* = 7.8 Hz, 2H), 0.95 – 0.85 (m, 1H); **³¹P{¹H} NMR** (MeOD, 202 MHz) δ -14.25 (s)

6.4.3 Complexation reactions with ligands prepared in 6.4.2

6.4.3.1 Monochelate complex formation



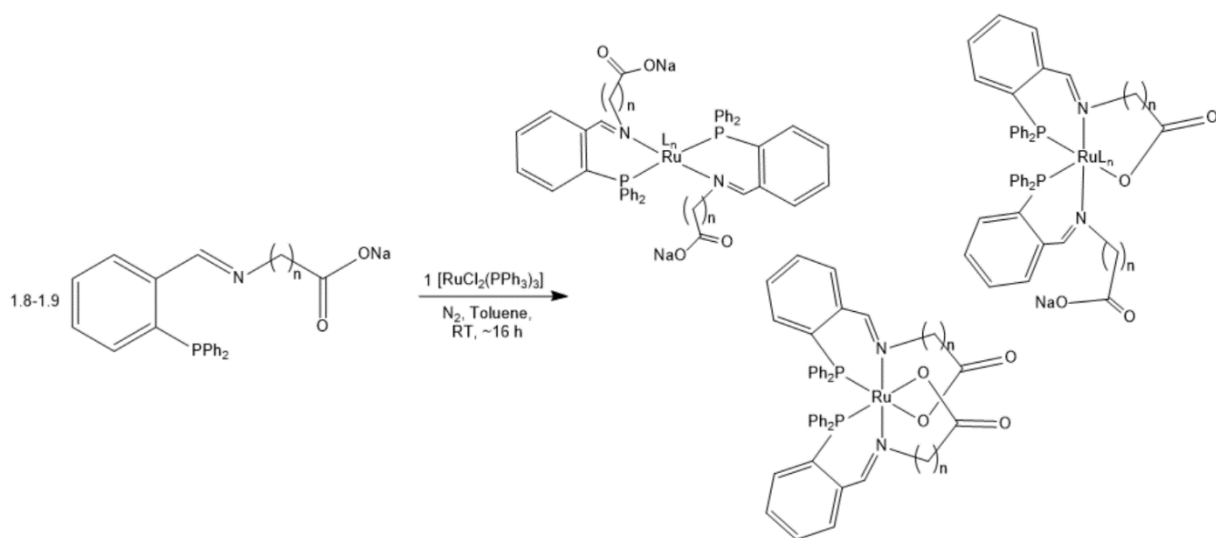
[RuCl₂(cymene)]₂ (50 mg, 0.082 mmol) and the phosphino azomethinylate ligand (1.9 eqvs - sodium 2-((2-(diphenylphosphaneyl)benzylidene)amino)acetate = 57 mg, sodium 3-((2-(diphenylphosphaneyl)benzylidene)amino)propanoate = 59 mg, sodium 4-((2-(diphenylphosphaneyl)benzylidene)amino)butanoate = 61 mg) were added to a Schlenk flask that was evacuated. DCM (dry/degassed, 10 mL) was added to the reaction mixture, that was subsequently stirred under N₂ at room temperature for approximately 3 days. The post-reaction solution was isolated *via* cannular filtration and reduced to dryness to afford a gum. The gum was triturated with Et₂O (dry/degassed) to afford a solid, that was isolated *via* cannular filtration and dried in vacuo.

Sodium 2-((2-(diphenylphosphaneyl)benzylidene)amino)acetate complexation $^{31}\text{P}\{^1\text{H}\}$ NMR (CDCl_3 , 202 MHz) δ 71.56 (s), 32.33 (s), 30.59 (s)

Sodium 3-((2-(diphenylphosphaneyl)benzylidene)amino)propanoate complexation $^{31}\text{P}\{^1\text{H}\}$ NMR (CDCl_3 , 202 MHz) δ 72.85 (s), 44.69 (s), 36.98 (s), 30.80 (s)

Sodium 4-((2-(diphenylphosphaneyl)benzylidene)amino)butanoate complexation $^{31}\text{P}\{^1\text{H}\}$ NMR (CDCl_3 , 202 MHz) δ 74.22 (s), 30.83 (s)

6.4.3.2 Bis chelate complex formation



[RuCl₂(PPh₃)₃] (100 mg, 0.10 mmol) and the phosphino azomethinylate ligand (1.8-1.9 eqvs - sodium 2-((2-(diphenylphosphaneyl)benzylidene)amino)acetate = 72 mg, sodium 3-((2-(diphenylphosphaneyl)benzylidene)amino)propanoate = 72 mg, sodium 4-((2-(diphenylphosphaneyl)benzylidene)amino)butanoate = 80 mg, sodium 5-((2-(diphenylphosphaneyl)benzylidene)amino)pentanoate = 80 mg, sodium 6-((2-(diphenylphosphaneyl)benzylidene)amino)hexanoate = 87 mg) were added to a Schlenk flask that was evacuated. Toluene (dry/degassed, 20 mL) was added to the reaction mixture, that was subsequently stirred at room temperature under N₂ overnight. The reaction solution was isolated *via* cannular filtration and reduced in vacuo to afford a gum. The gum was triturated with hexane (dry/degassed) to afford a solid that was isolated *via* cannular filtration and dried in vacuo.

Sodium 2-((2-(diphenylphosphaneyl)benzylidene)amino)acetate complexation $^{31}\text{P}\{^1\text{H}\}$ NMR (CDCl_3 , 202 MHz) δ 52.66 (d, $J = 28.5$ Hz), 51.54 (d, $J = 34.9$ Hz), 41.25 (s), 38.84 (s), 38.70 (s), 29.01 (s), 24.99 (s), 22.22 (s), -5.41 (s), -11.72 (s), -16.06 (s), -16.78 (d, $J = 9.7$ Hz), -16.97 (s), -19.94 (s), -28.51 (s)

Sodium 3-((2-(diphenylphosphaneyl)benzylidene)amino)propanoate complexation $^{31}\text{P}\{^1\text{H}\}$ NMR (CDCl_3 , 202 MHz) δ 43.12 (s), -5.42 (s), -14.18 (s), -14.93 (s), -17.48 (s)

Sodium 4-((2-(diphenylphosphaneyl)benzylidene)amino)butanoate complexation $^{31}\text{P}\{^1\text{H}\}$ NMR (CDCl_3 , 202 MHz) δ 72.18 (d, $J = 29.2$ Hz), 69.98 (d, $J = 29.7$ Hz), 69.62 (d, $J = 29.4$ Hz), 69.32 (s), 45.57 (d, $J = 30.4$ Hz), 44.85 (t, $J = 29.5$ Hz), 44.37 (d, $J = 29.7$ Hz), -5.42 (s), -11.71 (s), -14.26 (s)

Sodium 5-((2-(diphenylphosphaneyl)benzylidene)amino)pentanoate complexation $^{31}\text{P}\{^1\text{H}\}$ NMR (CDCl_3 , 202 MHz) δ 71.64 (d, $J = 29.7$ Hz), 70.99 (d, $J = 29.7$ Hz), 44.52 (d, $J = 29.4$ Hz), -5.42 (s)

Sodium 6-((2-(diphenylphosphaneyl)benzylidene)amino)hexanoate complexation $^{31}\text{P}\{^1\text{H}\}$ NMR (CDCl_3 , 202 MHz) δ 70.69 (d, $J = 29.6$ Hz), 43.97 (d, $J = 29.6$ Hz), -5.42 (s), -13.72 (s)

6.4.4 Guerbet reactions – forming transfer hydrogenation catalyst *in situ*

Guerbet reactions of ethanol detailed in Table 22 were conducted according to the general Guerbet reaction procedure detailed in 6.1.2 at a reaction temperature of 150 °C, over a duration of 20 hours at a stirring rate of 500 rpm. The following transfer hydrogenation catalyst precursors and aldol mediator were added to the PTFE sleeve in each reaction: $[\text{RuCl}_2(\text{cymene})]_2$ (0.053 g, 0.087 mmol, 0.05 mol%), phosphino azomethinylate ligand (2 eqvs, 0.17 mmol, 0.1 mol%) and NaOEt (0.582 g, 0.855 mmol, 5 mol%)

Guerbet reactions of ethanol detailed in Table 23 were conducted according to the general Guerbet reaction procedure detailed in 6.1.2 at a reaction temperature of 150 °C, over a duration of 20 hours at a stirring rate of 500 rpm. The following transfer

hydrogenation catalyst precursors and aldol mediator were added to the PTFE sleeve in each reaction: $[\text{RuCl}_2(\text{cymene})]_2$ (0.053 g, 0.087 mmol, 0.05 mol%), phosphino azomethinylate ligand (4 eqvs, 0.34 mmol, 0.2 mol%) and NaOEt (0.582 g, 0.855 mmol, 5 mol%)

Guerbet reactions of ethanol detailed in Table 24 were conducted according to the general Guerbet reaction procedure detailed in 6.1.2 at a reaction temperature of 210 °C, over a duration of 20 hours at a stirring rate of 500 rpm. The following transfer hydrogenation catalyst precursors and aldol catalyst were added to the PTFE sleeve in each reaction: $[\text{RuCl}_2(\text{cymene})]_2$ (0.053 g, 0.087 mmol, 0.05 mol%), phosphino azomethinylate ligand (2 eqvs, 0.17 mmol, 0.1 mol%) and UiO-66(Zr) (0.285 g, 0.17 mmol, 0.1 mol%)

Guerbet reactions of ethanol detailed in Table 25 were conducted according to the general Guerbet reaction procedure detailed in 6.1.2 at a reaction temperature of 210 °C, over a duration of 20 hours at a stirring rate of 500 rpm. The following transfer hydrogenation catalyst precursors and aldol catalyst were added to the PTFE sleeve in each reaction: $[\text{RuCl}_2(\text{cymene})]_2$ (0.053 g, 0.087 mmol, 0.05 mol%), phosphino azomethinylate ligand (4 eqvs, 0.34 mmol, 0.2 mol%) and UiO-66(Zr) (0.285 g, 0.17 mmol, 0.1 mol%)

6.4.5 Reactions of ethanol under Guerbet conditions in absence of aldol catalyst

Guerbet reactions of ethanol detailed in Table 26 were conducted according to the general Guerbet reaction procedure detailed in 6.1.2 at a reaction temperature of 210 °C, over a duration of 20 hours at a stirring rate of 500 rpm. The following transfer hydrogenation catalyst precursors were added to the PTFE sleeve in each reaction: $[\text{RuCl}_2(\text{cymene})]_2$ (0.053 g, 0.087 mmol, 0.05 mol%), phosphino azomethinylate ligand (4 eqvs, 0.34 mmol, 0.2 mol%)

6.5 References

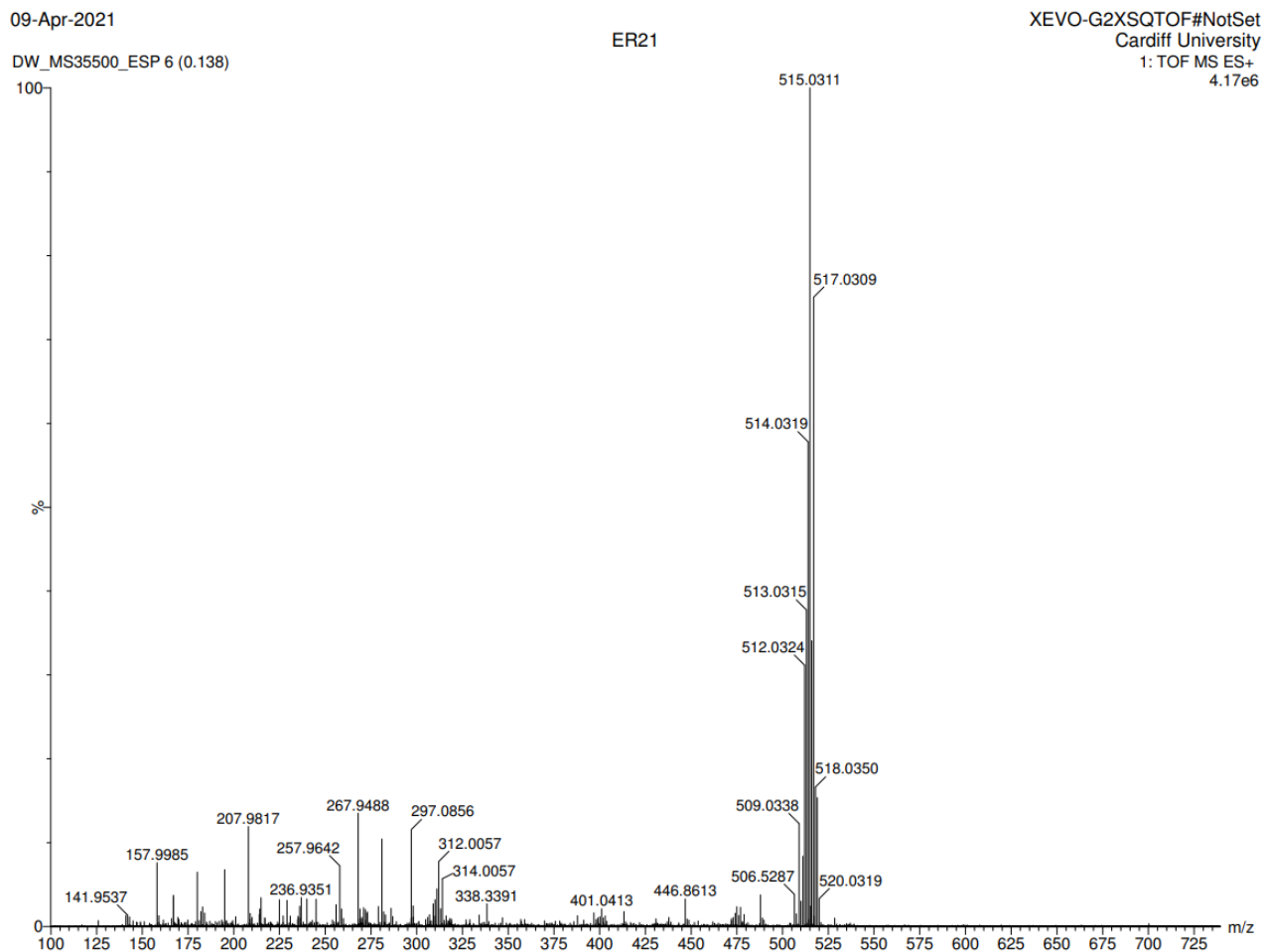
- 1 J. Chatt and R. G. Hayter, *J. Chem. Soc.*, 1961, 896-904
- 2 D. Jiang, G. Fang, Y. Tong, X. Wu, Y. Wang, D. Hong, W. Leng, Z. Liang, P. Tu, L. Liu, K. Xu, J. Ni and X. Li, *ACS Catal.*, 2018, **8**, 11973–11978.
- 3 W. Xu, M. Dong, L. Di and X. Zhang, *Nanomaterials*, 2019, **9**, 10–13.
- 4 Elliot Rogers, MChem Thesis, Cardiff University, 2021.
- 5 R. R. Dykeman, K. L. Luska, M. E. Thibault, M. D. Jones, M. Schlaf, M. Khanfar, N. J. Taylor, J. F. Britten and L. Harrington, *Journal of Molecular Catalysis A: Chemical*, 2007, **277**, 233–251.
- 6 M. J. Katz, Z. J. Brown, Y. J. Colón, P. W. Siu, K. A. Scheidt, R. Q. Snurr, J. T. Hupp and O. K. Farha, *Chem. Commun.*, 2013, **49**, 9449–9451.
- 7 W. M. Liao, J. H. Zhang, Z. Wang, S. Y. Yin, M. Pan, H. P. Wang and C. Y. Su, *J. Mater. Chem. A*, 2018, **6**, 11337–11345.
- 8 S. A. Burgess, A. Kassie, S. A. Baranowski, K. J. Fritzsching, K. Schmidt-Rohr, C. M. Brown and C. R. Wade, *J. Am. Chem. Soc.*, 2016, **138**, 1780–1783.
- 9 B. Gnanaprakasam, J. Zhang and D. Milstein, *Angew. Chem. Int. Ed.*, 2010, **49**, 1468–1471.
- 10 G. Jia, H. M. Lee, I. D. Williams, C. P. Lau and Y. Chen, *Organometallics*, 1997, **16**, 3941–3949.
- 11 G. T. Giuffredi, S. Purser, M. Sawicki, A. L. Thompson and V. Gouverneur, *Tetrahedron: Asymmetry*, 2009, **20**, 910–920.
- 12 H. Samouei and V. V Grushin, *Organometallics*, 2013, **32**, 4440–4443.
- 13 J. V. Barkley, S. J. Higgins, M. K. McCart and T. J. Pounds, *Inorg Chem.*, 1997, **36**, 6188–6196.
- 14 Jess Cole, BSC Thesis, Cardiff University, 2022.

15 J. Wencel, D. Rix, T. Jennequin, S. Labat, C. Crévisy and M. Mauduit,
Tetrahedron: Asymmetry, 2008, **19**, 1804–1809.

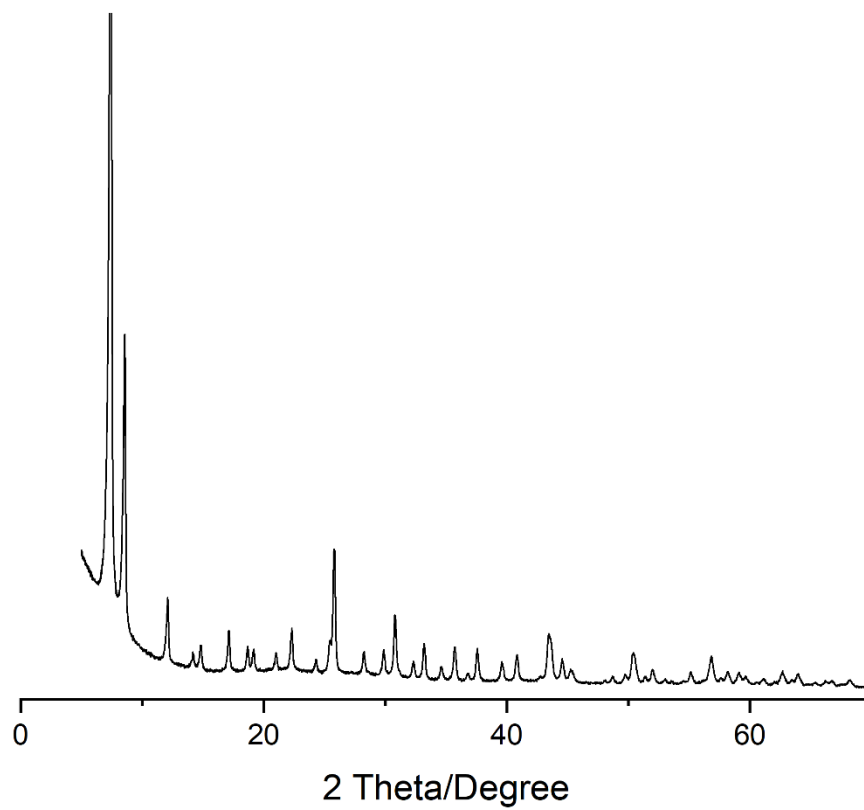
Chapter 7 - Appendix

7.1 - Chapter 3 Appendix

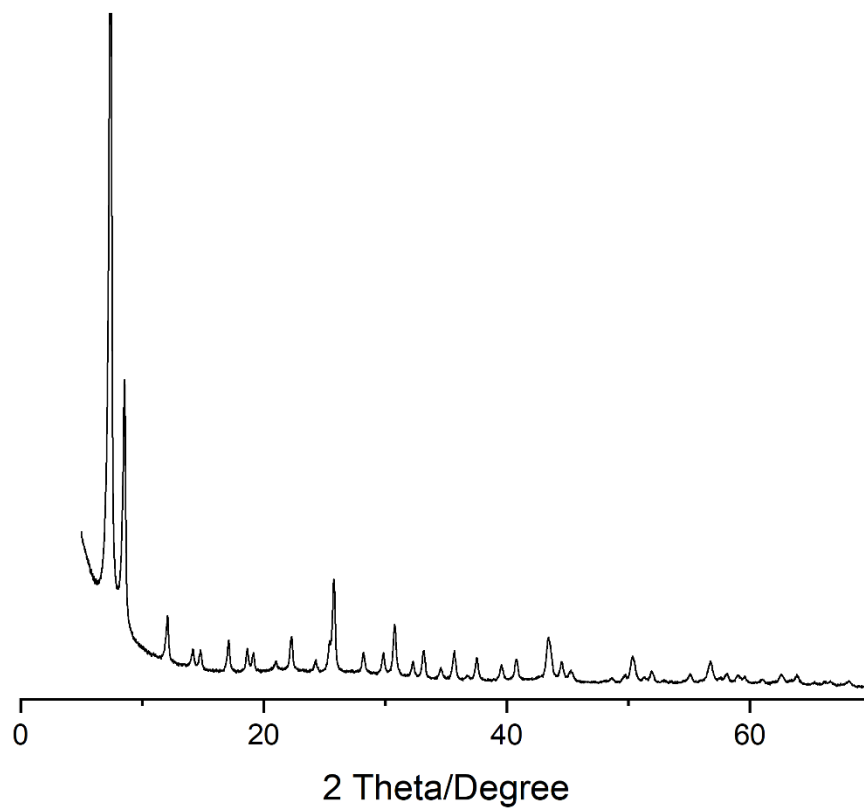
7.1.1 Mass spectrum of [RuCl(cymene)(bipy-COOH)]Cl (3.1) synthesised by Elliot Rogers



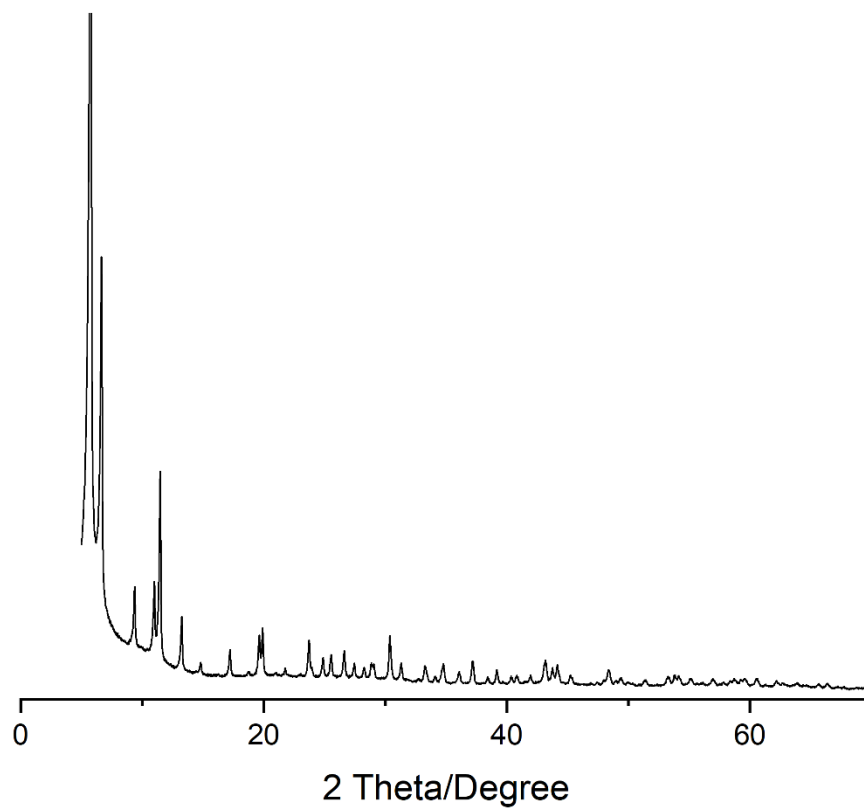
7.1.2 PXRD pattern of UiO-66(Zr) (3.5)



7.1.3 PXRD pattern of UiO-66-(Zr)NH₂ (3.6)



7.1.4 PXRD pattern of UiO-67(Zr) (3.7)



7.1.5 Elemental breakdown of EDX analysis of 3.10

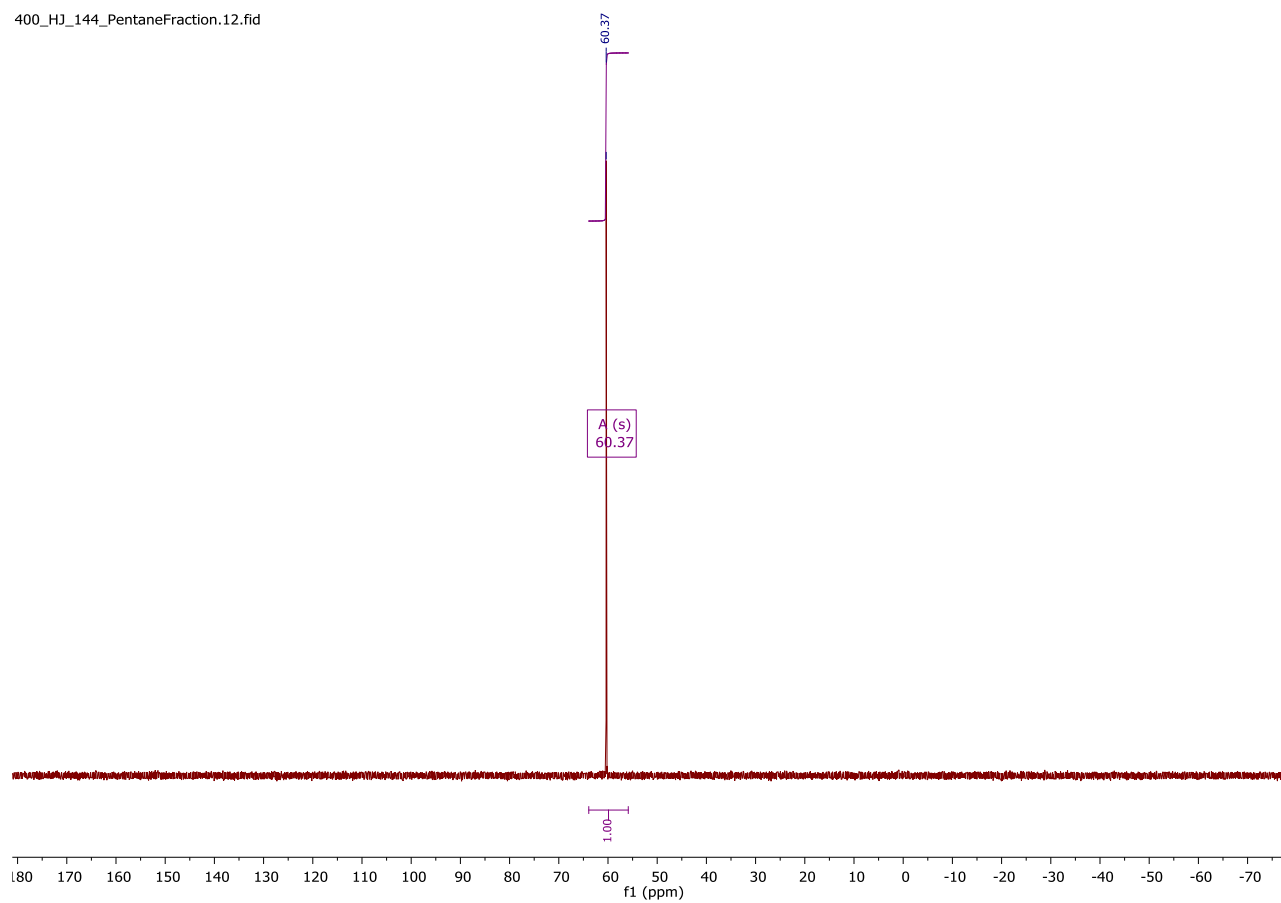
Map Sum Spectrum								
Element	Line Type	Apparent Concentration	k Ratio	Wt%	Wt% Sigma	Standard Label	Factory Standard	Standard Calibration Date
C	K series	102.80	1.02795	76.34	0.21	C Vit	Yes	
O	K series	27.96	0.09409	18.55	0.20	SiO2	Yes	
Na	K series	1.04	0.00437	0.22	0.03	Albite	Yes	
Zr	L series	17.32	0.17323	4.89	0.10	Zr	Yes	
Total:				100.00				

7.1.6 Elemental breakdown of EDX analysis of 3.9

Map Sum Spectrum								
Element	Line Type	Apparent Concentration	k Ratio	Wt%	Wt% Sigma	Standard Label	Factory Standard	Standard Calibration Date
N	K series	0.00	0.00000	0.00	0.70	BN	Yes	
O	K series	40.79	0.13726	48.44	0.23	SiO2	Yes	
Cl	K series	1.85	0.01612	2.14	0.07	NaCl	Yes	
Ti	K series	1.76	0.01755	1.93	0.08	Ti	Yes	
Zr	L series	42.24	0.42237	47.48	0.23	Zr	Yes	
Total:				100.00				

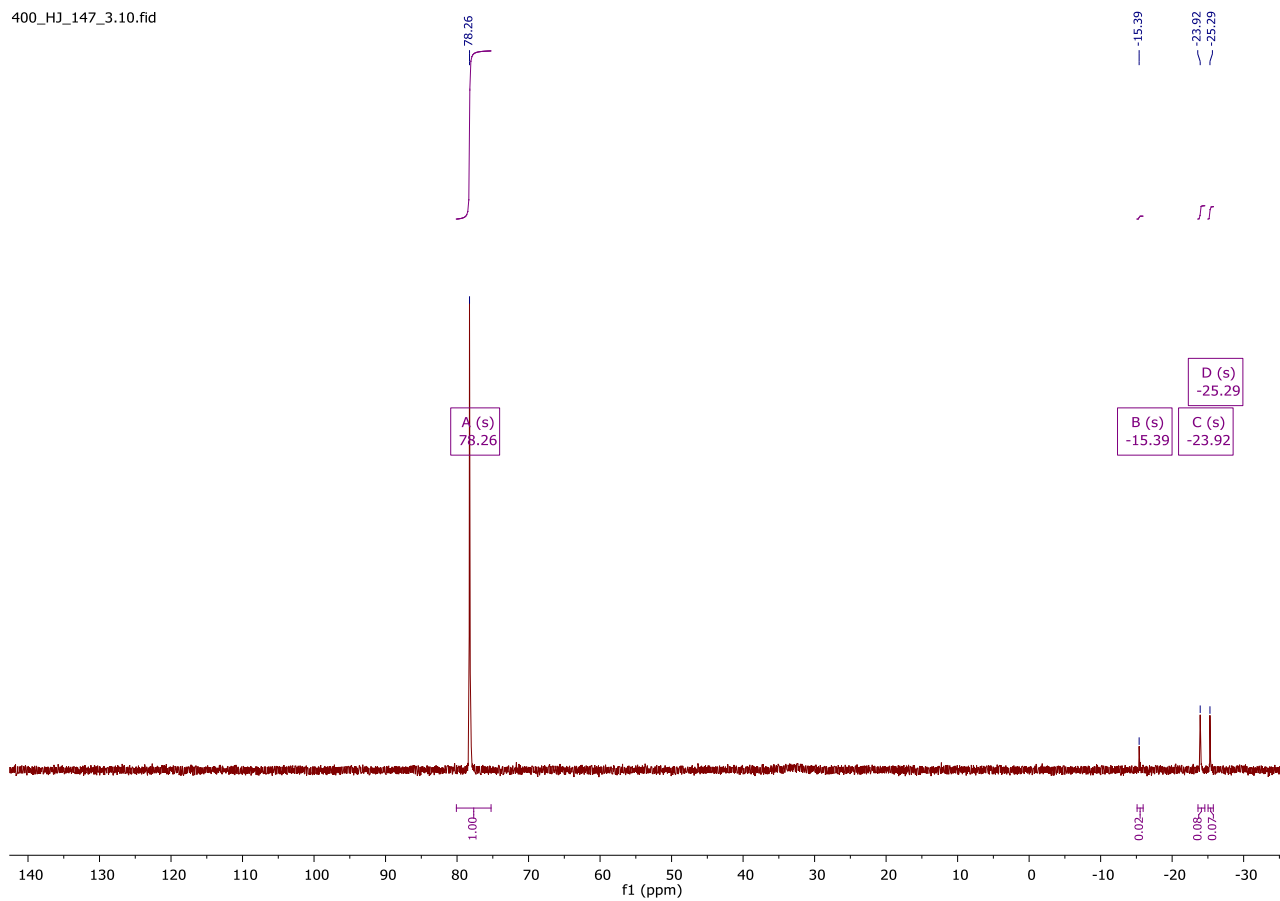
7.1.7 $^{31}\text{P}\{^1\text{H}\}$ NMR Spectrum of 3.19

400_HJ_144_PentaneFraction.12.fid



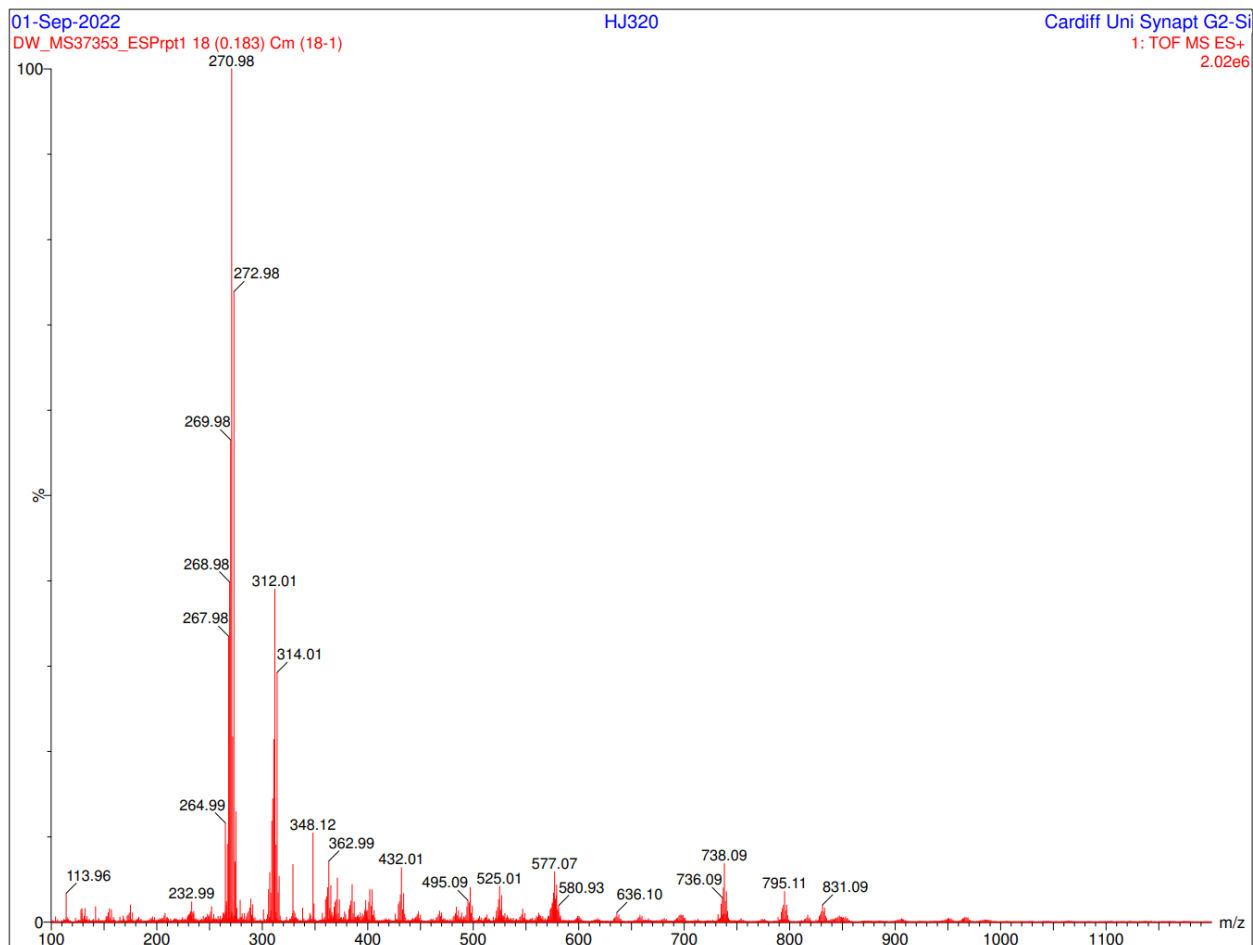
7.1.8 $^{31}\text{P}\{^1\text{H}\}$ NMR Spectrum of 3.20

400_HJ_147_3.10.fid

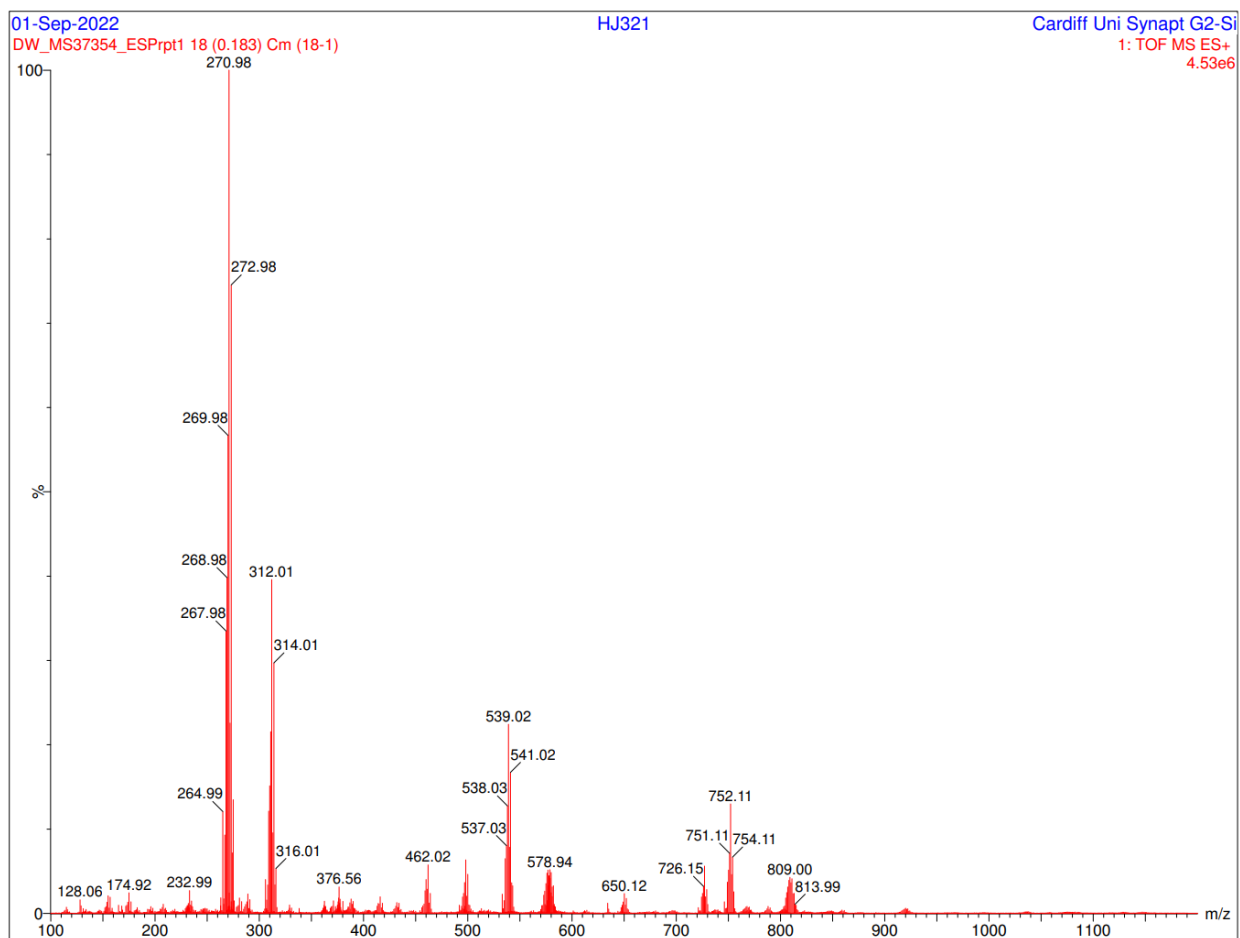


7.2 - Chapter 4 Appendix

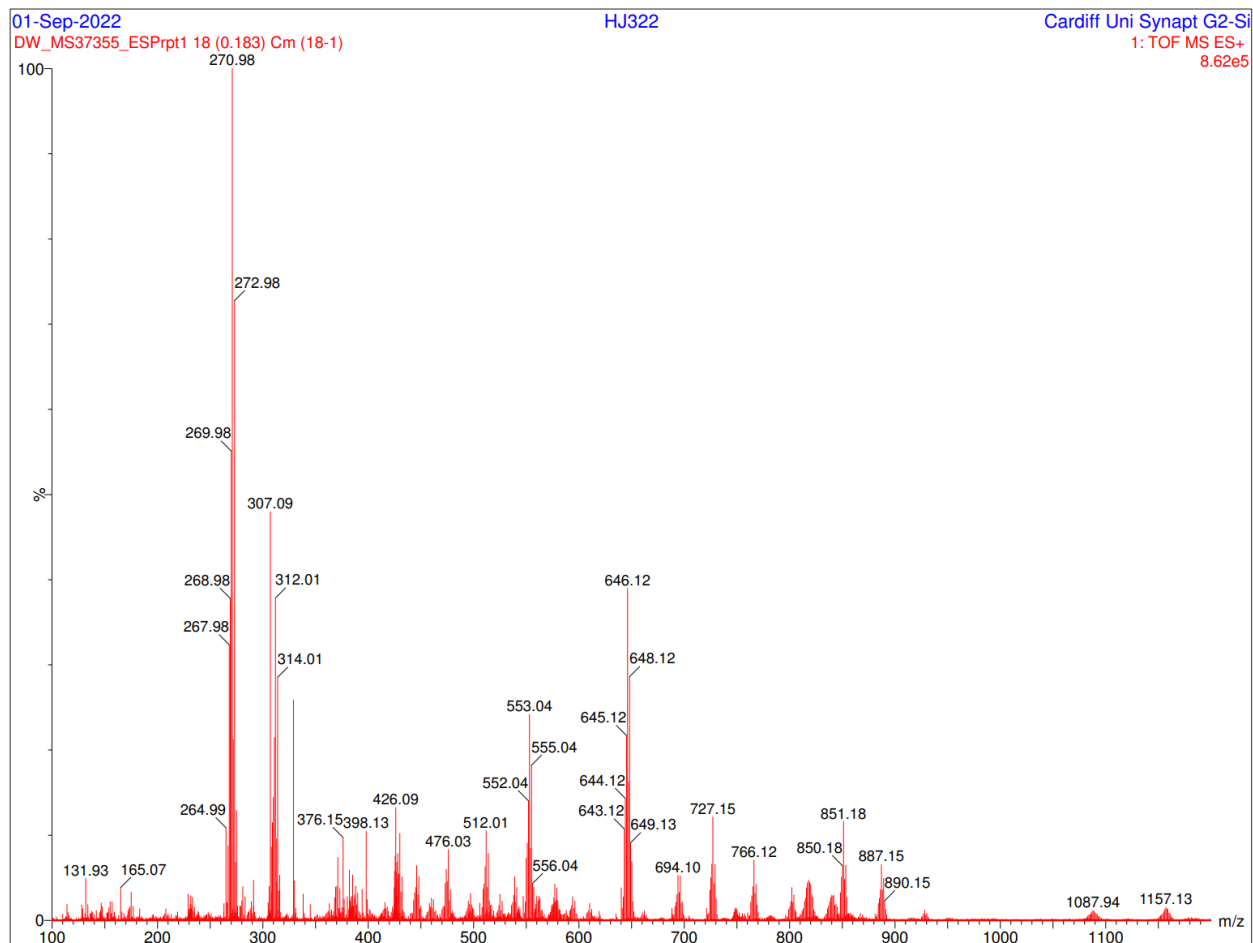
7.2.1 Mass spectrum of the product mixture 4.8 of the reaction between $[\text{RuCl}_2(\text{cymene})]_2$ and 4.8



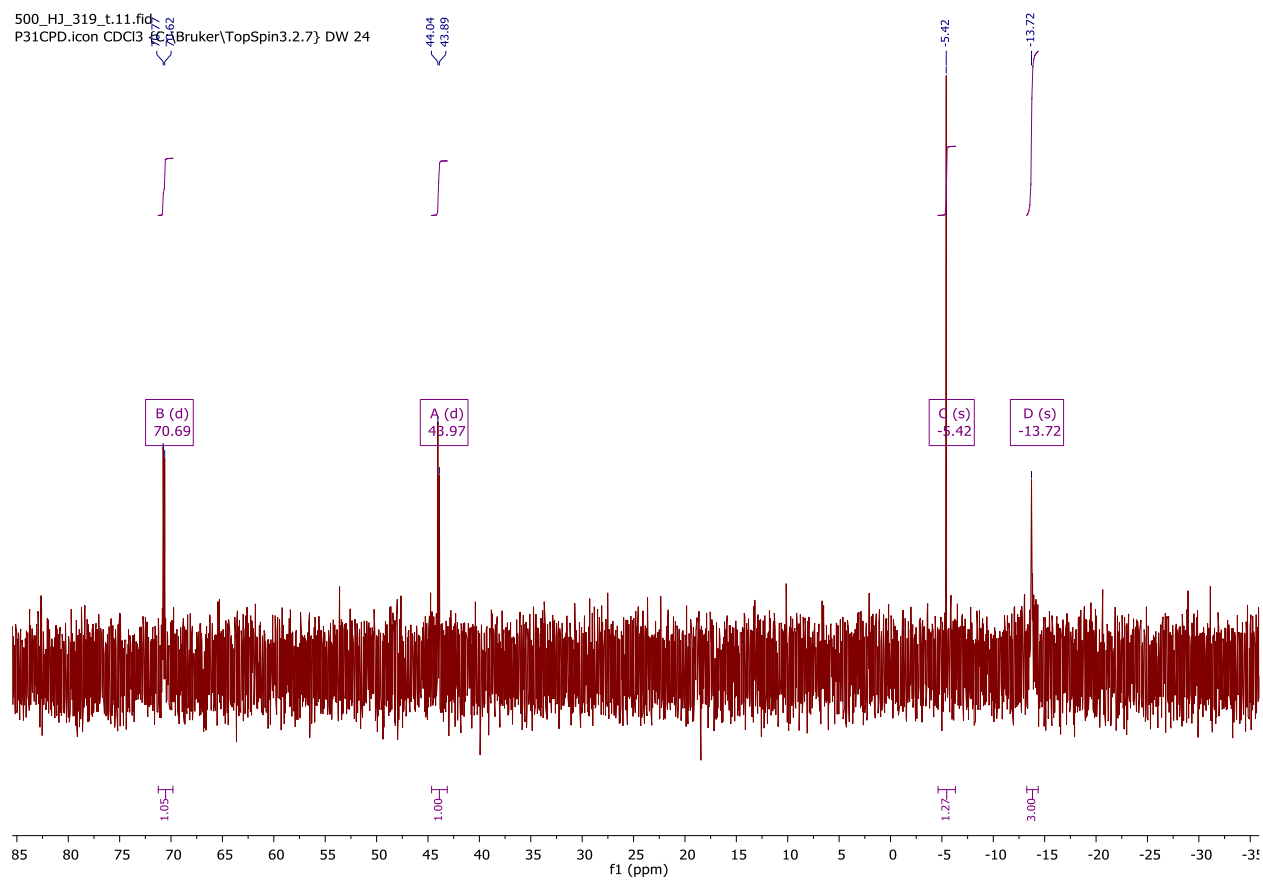
7.2.2 Mass spectrum of the product mixture of the reaction between $[\text{RuCl}_2(\text{cymene})]_2$ and 4.94.9



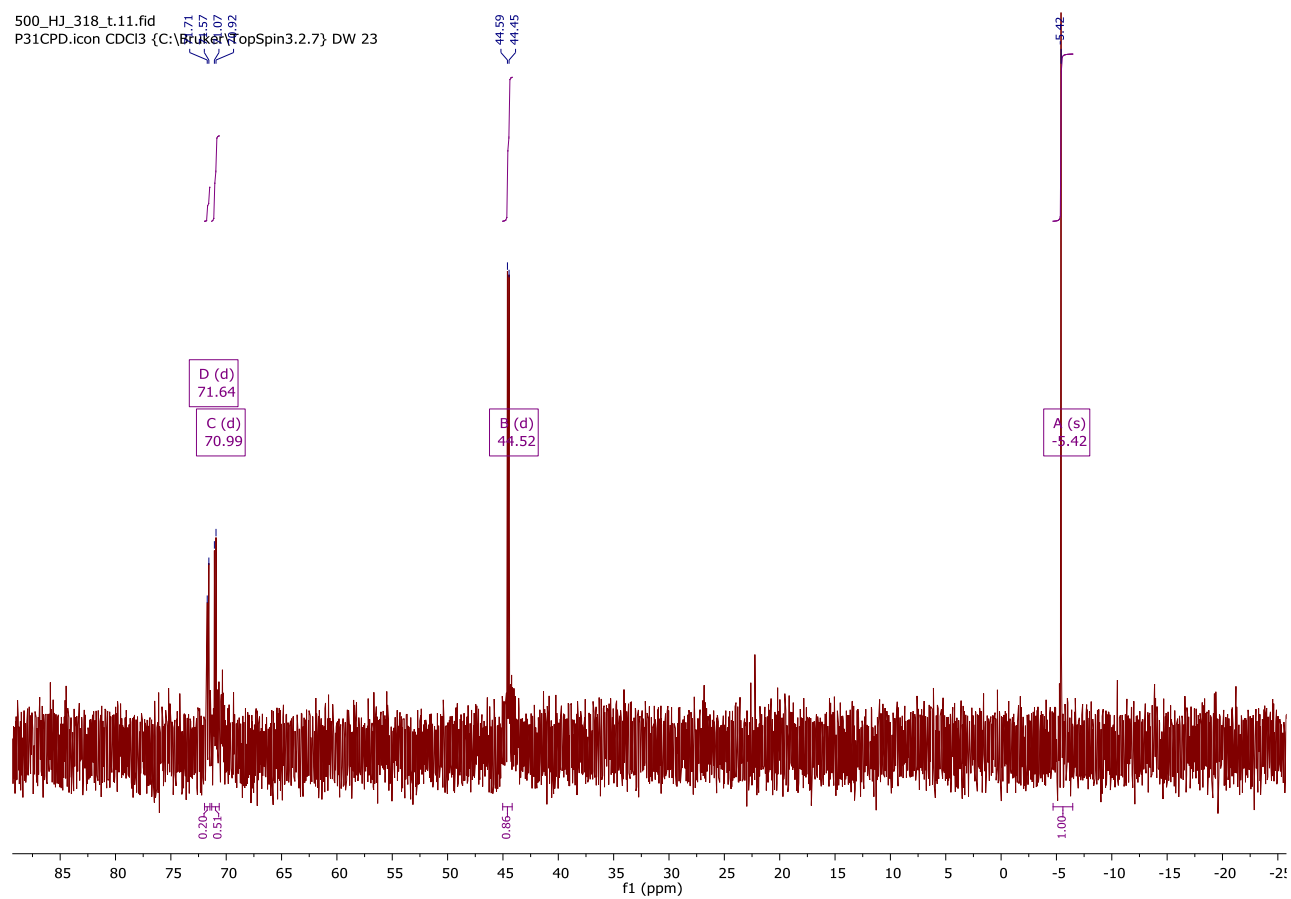
7.2.3 Mass spectrum of the product mixture of the reaction between $[\text{RuCl}_2(\text{cymene})]_2$ and 4.104.10



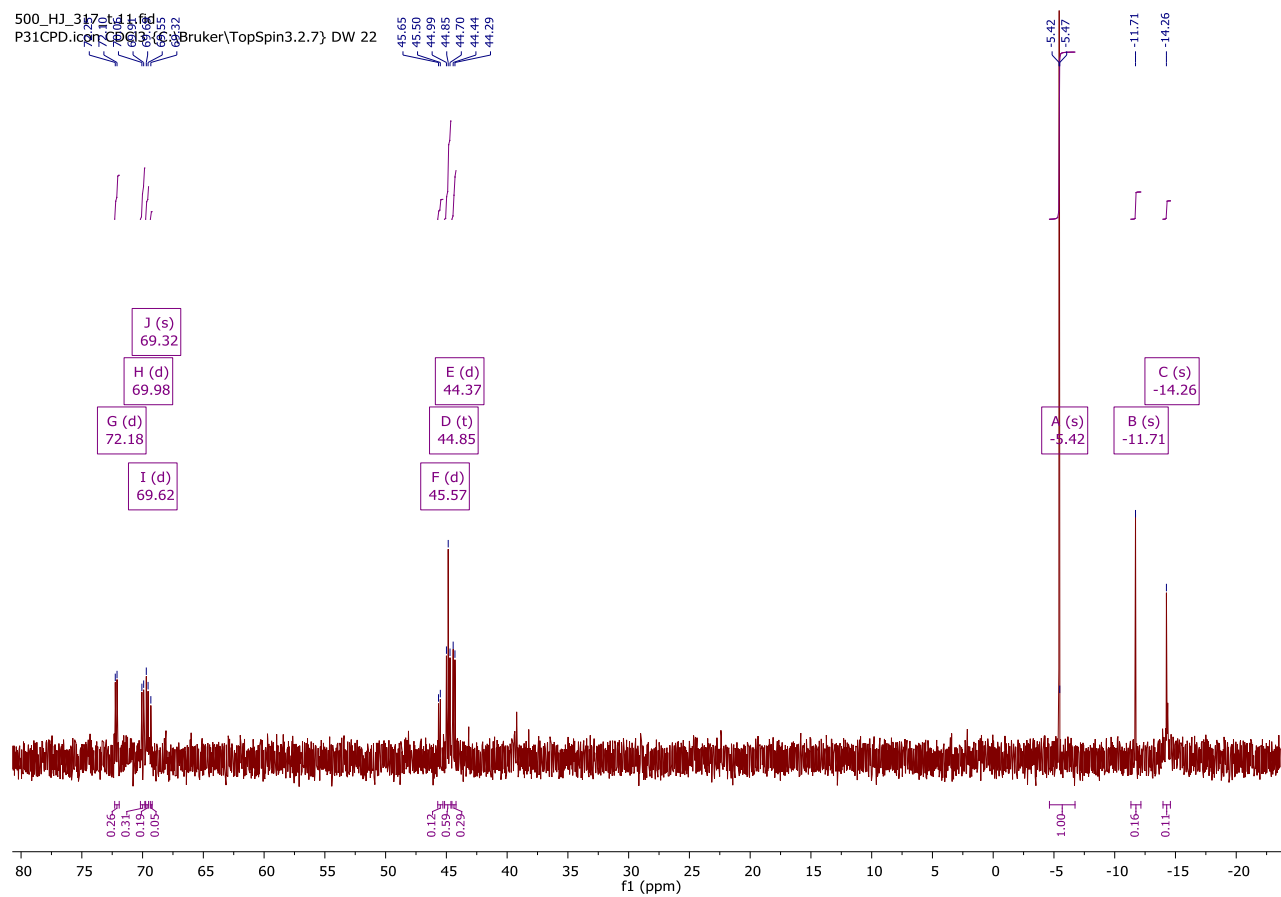
7.2.4 $^{31}\text{P}\{^1\text{H}\}$ NMR spectrum of the product mixture of the reaction between 4.12 and $[\text{RuCl}_2(\text{PPh}_3)_3]$ 4.12



7.2.5 $^{31}\text{P}\{^1\text{H}\}$ NMR spectrum of the product mixture of the reaction between 4.11 and $[\text{RuCl}_2(\text{PPh}_3)_3]$ 4.11

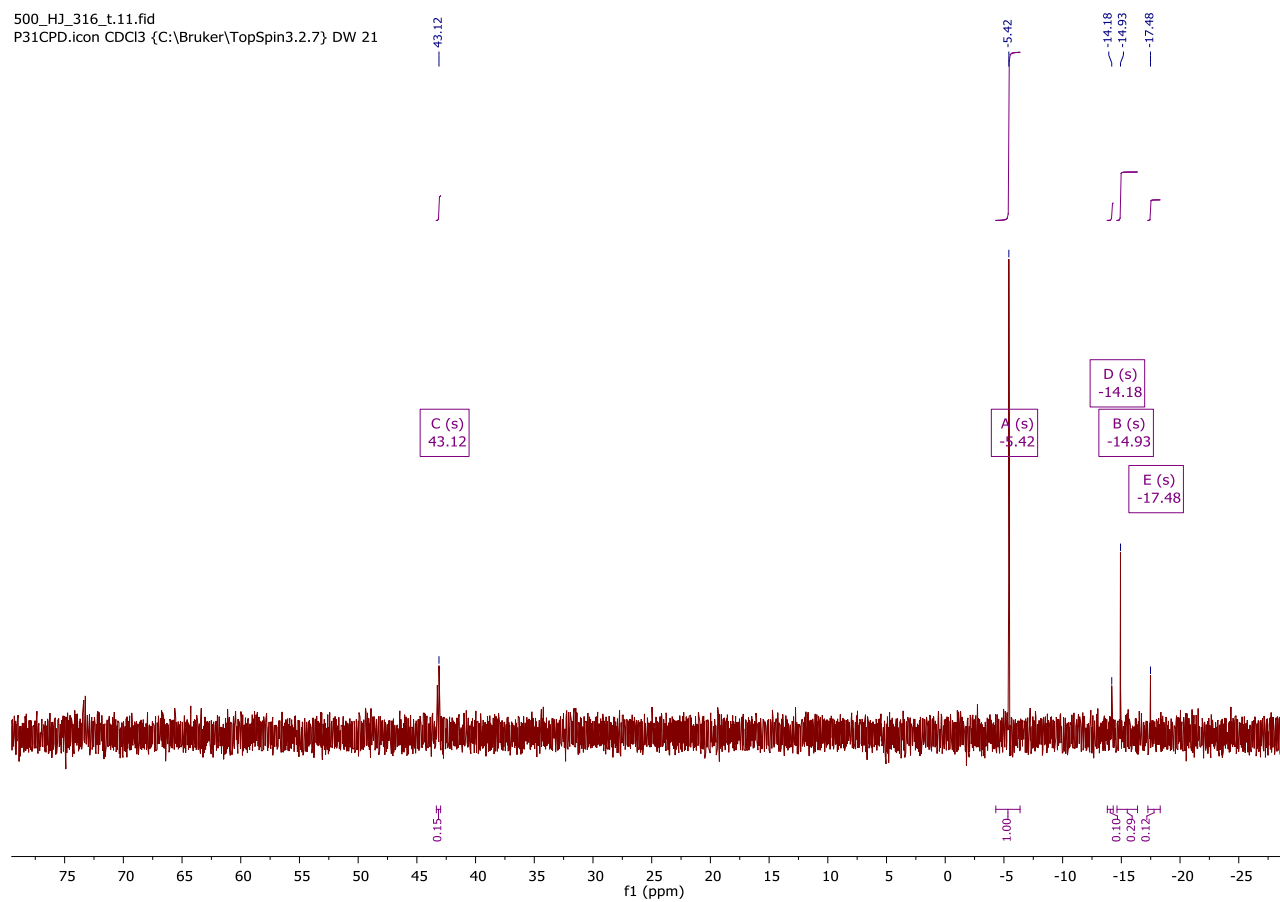


7.2.6 $^{31}\text{P}\{^1\text{H}\}$ NMR spectrum of the product mixture of the reaction between 4.10 and $[\text{RuCl}_2(\text{PPh}_3)_3]$ 4.10



7.2.7 $^{31}\text{P}\{^1\text{H}\}$ NMR spectrum of the product mixture of the reaction between 4.9 and $[\text{RuCl}_2(\text{PPh}_3)_3]4.9$

500_HJ_316_t.11.fid
P31CPD.icon CDCI3 {C:\Bruker\TopSpin3.2.7} DW 21



7.2.8 $^{31}\text{P}\{^1\text{H}\}$ NMR spectrum of the product mixture of the reaction between 4.8 and $[\text{RuCl}_2(\text{PPh}_3)_3]4.8$

